A decorative graphic at the top of the page features a dark purple background with a large, light purple circle and a smaller, light purple circle below it. A vertical pink bar is positioned on the right side of the graphic. The text is overlaid on the dark purple background.

Uukuniemi virus as a tick-borne virus model  
to characterize the vector-host switch *in vitro*

Magalie Mazelier

Dissertation submitted to the  
Combined Faculties for the Natural Sciences and for Mathematics  
of the Ruperto-Carola University of Heidelberg, Germany  
for the degree of  
Doctor of Natural Sciences

presented by

M. Sc Magalie Mazelier

Born in Tulle, France  
Oral-examination: 17<sup>th</sup> of July 2017



Uukuniemi virus as a tick-borne virus model  
to characterize the vector-host switch *in vitro*

Referees:

Prof. Dr. Hans-Georg **Kräusslich**

Dr. Pierre-Yves **Lozach**

*U2's best work has always been when he didn't know what he was doing.*

*Adapted from Bono*

## Acknowledgement

The present work was carried out at the Virology Unit, Department of Infectious Diseases Heidelberg University Hospital and it was supported by the CellNetworks cluster of excellence.

First of all I would like to acknowledge the departmental head director Prof. Dr. Hans-Georg Kräusslich for providing excellent facilities, stimulating research environment, and for the time he took to follow my work during the whole project.

I am grateful to PY for giving me the opportunity to work in his laboratory. Such a fulfilled professional life would not have been possible in another laboratory than in the Bunya Lab. It was an amazing time working for you. I appreciated your energy and enthusiasm, the “human” management behind the stress of being a (young) group leader, the constant positive thoughts and the fruitful (but sometimes too long) meetings discussing results (or birds, or house, or gardening...). Because you love la langue de Molière : Je suis ravie d’être ta première thésarde! La tâche n’était pas facile mais “plus grand est l’obstacle, et plus grande est la gloire de le surmonter” (Jean Baptiste Poquelin).

I warmly thank PD Dr. Jacomine Krijnse-Locker and Dr. Steeve Boulant for agreeing to be part of my PhD Defense Committee and Dr. Amanda Chase for her precious time to review my thesis.

---

They are two, they are highly talented, they are funny, and I spent a LOT of good time with them: Psylvia and Anja. Pipette and Pistache meow for you; they still remember your (food) visits. I don’t forget NicolE (pronounce the E as a German/French, she loves it) who shared with us, for a while, the pleasure to be part of The Lozach’ girls. The team that I’ll never forget. My head is full of good memories. I would like to thank also all the students who visited us and brought happiness in the lab, specially Julia Wegner, a talented student whose work contributed to move forward my project.

I also want to thank my office-mates because our office was the best of all PhD and PostDocs' offices, no doubt about it! Thanks Amanda and Birthe, you brought me into running, I cannot live without it anymore. I won't forget my first half marathon. Thank you Volkan to have been my dance partner, it was just AWESOME. I loved it. I also liked the coffee breaks and our discussions, but I have to highlight the coffee partner number one: Mr. Obr. Thanks Martin for the fruitful discussions and for trusting me. I was glad to share some movie nights, beach volley game and the Wurstmarkt festival with you. I also warmly thank Robin to make me laugh so many times, Annica, Mia, Bojana, Niko, Miguel, Johanna, Maud, Chiara, and Margarida. You are all so great people, so smart, so kind, so funny, so happy... I wish to all of you the best for your personal and professional life.

I want to express my gratitude to all the past and present workers in the department, they contributed to my happiness working here. My life was a *tutti frutti* sweet in Heidelberg, I enjoyed it so much.

GBMA forever and friends for 10 years, I would like to say thanks to Elise, Marie, Marine, Fanny, Chloé, Maguelonne, Maud, Julie, Daminou, Charlou, Benji, Fifi, Didou, and Loic, Roro, Romain, Nils, and Clément. I am already looking forward to our next weekends together, they make me feel strong and optimistic. C'est à chaque fois un bain de jouvence.

---

My sincere appreciation goes to my family for giving me the opportunity to explore the world. Thank you for letting me live (leave) the life I chose, a life far from you. Thank you for your unconditional and continuous support. Merci papi René pour ton aide financière qui m'a permis de débiter ma carrière ; et merci à papi Lulu de m'avoir toujours soutenu, tu me manques beaucoup.

Last but not least, le meilleur pour la fin, I thank the person who always trusted me, always encouraged me, and pushed me. His unlimited patience, his good mood and optimism were valuable and outstanding. Thank you for being part of my life, for supporting my ambitions and my personality. Benjamin, without your help I would not have accomplished all of this. I hope the road with you will be long.

## Abstract

Ticks are harmful vectors responsible for emerging disease outbreaks caused by bacteria, parasites, and viruses worldwide. Recently, novel tick-borne pathogenic phleboviruses, from the *Phenuiviridae* family (formerly *Bunyaviridae*), have emerged through distinct continents. Examples include Heartland virus (HRTV) in North America and severe fever with thrombocytopenia syndrome virus (SFTSV) in Asia, associated with a fatality rate up to 30%. So far, no vaccines or treatments have been approved for human use. Although these viruses are transmitted to human via ticks, studies mainly rely on virus stocks produced in mammalian cells. In contrast, viruses originating from tick cells are poorly characterized and transmission and infectious entry in humans remain largely uncovered.

The overall goal of this PhD project is to understand early host cell-virus interactions following virus transmission by infected ticks. The central hypothesis is that viruses derived from tick cells present a higher infectivity in mammalian hosts than those produced in mammalian cells. I proposed to recapitulate the tick-mammal switch *in vitro* and to characterize the molecular differences between tick and mammalian cell-derived viruses. To this end, I used the nonpathogenic Uukuniemi virus (UUKV), closely related to HRTV and SFTSV, as a tick-borne phlebovirus model.

A reverse genetics system was first developed to rescue UUKV from cDNAs with a genome identical to that of the virus isolated from the tick *Ixodes ricinus*. Using this system, it was shown that tick cells were persistently infected after few months. The folding, maturation, and nature of glycans of the viral envelope glycoprotein G<sub>N</sub>, but not G<sub>C</sub>, differed whether virions were produced from vector tick cells or host mammalian cells. However, tick cell-derived viruses still rely on endosomal acidification for infection and are still able to use the UUKV receptor on human dendritic cells, DC-SIGN. Moreover, results suggest that the lipid composition differs between tick and mammalian cell-derived viruses. In addition, the size of the particles varies, with those from the tick cells being smaller. Results also point out that the amount of structural proteins in viral particles derived from tick cells differ from those of mammalian cell-derived viral particles, which might contribute to a higher infectivity for tick cell-derived progenies. Finally, the nonstructural protein NSs was shown to be dispensable for replication in and infection of mammalian cells, whereas it was essential for the virus life cycle in tick cells.

Altogether, this work emphasizes that arthropod vectors leave an imprint on viruses that arguably affects their infectivity in mammalian host cells. This study, therefore, highlights the importance of working with viruses originating from arthropod vector cells when investigating the cell biology of arbovirus transmission and entry. It opens large avenues for future investigations into the virus life cycle in tick cells, the transmission of tick-borne viruses and the associated pathogenesis, elucidating the basis of which should help to develop new therapeutic targets and vaccines.

## Zusammenfassung

Zecken sind Vektoren gefährlicher Krankheiten und verantwortlich für Ausbrüche neu auftretender Infektionskrankheiten weltweit, die durch Bakterien, Parasiten und Viren ausgelöst werden. Jüngst sind neuartige, durch Zecken übertragene pathogene Phleboviren aus der Familie der *Phenuiviridae* (ehemals *Bunyaviridae*) auf mehreren Kontinenten aufgetreten. Beispiele hierfür sind unter anderem der Ausbruch des Heartland-Virus (HRTV) in Nordamerika und des Severe fever with thrombocytopenia syndrome virus (SFTSV) in Asien mit Fatalitätsraten von bis zu 30%. Bislang sind keine Impfstoffe oder Medikamente für den menschlichen Gebrauch zugelassen. Obwohl diese Viren durch Zecken auf den Menschen übertragen werden, werden für die meisten Studien Viruspartikel verwendet, die in Säugerzellen produziert wurden. In Zeckenzellen hergestellte Viruspartikel dagegen sind kaum charakterisiert und die Übertragung sowie der Eintrittsweg für eine produktive Infektion humaner Zellen bleiben bis heute größtenteils unerforscht.

Das Ziel der vorliegenden Dissertation ist es, frühe Interaktionen zwischen Wirtszelle und Virus zu verstehen, die unmittelbar nach der Übertragung der Viruspartikel auf Wirtszellen durch infizierte Zecken erfolgen. Die zentrale Hypothese hierbei ist, dass in Zeckenzellen produzierte Viren für Säugerzellen eine höhere Infektiosität aufweisen als solche, die aus Säugerzellen stammen. Aus diesem Grund wurde die Übertragung von Zecken- auf Säugerzellen *in vitro* rekapituliert und die Unterschiede zwischen in Zecken- und Säugerzellen produzierten Viren charakterisiert. Zu diesem Zweck wurde das nicht-pathogene Uukuniemi-Virus (UUKV), welches eng mit den human pathogenen HRTV und SFTSV verwandt ist, als Modell für durch Zecken übertragene Phlebovirus Infektionen genutzt.

Für diese Untersuchungen wurde ein revers-genetisches System etabliert, um UUKV aus cDNAs zu gewinnen, deren Genom identisch zu dem aus der Zecke *Ixodes ricinus* isolierten Virus ist. Unter Verwendung dieses Systems konnte gezeigt werden, dass Zeckenzellen über mehrere Monate produktiv infiziert sein können. Des Weiteren unterscheiden sich Faltung, Reifung und das Glykosylierungsmuster der  $G_N$ -Proteine der Virushülle abhängig davon ob die Viruspartikel in Vektorzellen (Zeckenzellen) oder Wirtszellen (Säugerzellen) hergestellt wurden. Interessanterweise wurden diese Unterschiede jedoch nicht für das  $G_C$ -Protein der Virushülle festgestellt. Außerdem sind in Zeckenzellen produzierte Viruspartikel ebenso wie in Säugerzellen hergestellte Partikel auf die Ansäuerung von Endosomen angewiesen um eine produktive Infektion zu etablieren und können den gleichen Rezeptor auf humanen dendritischen Zellen, DC-SIGN, für den Viruseintritt nutzen. Zudem lassen weitere Ergebnisse vermuten, dass sich sowohl die Lipidzusammensetzung als auch die Größe von in Zecken- oder Säugerzellen produzierten Viruspartikeln unterscheidet, wobei Viruspartikel aus Zeckenzellen kleiner sind. Weitere Ergebnisse weisen außerdem darauf hin, dass sich die Anzahl der Strukturproteine in Viruspartikeln aus Zeckenzellen von der aus Säugerzellen unterscheidet, was bei in Zeckenzellen entstandenen Viruspartikeln möglicherweise zu einer

höheren Infektiosität beiträgt. Zudem konnte gezeigt werden, dass das Nichtstrukturprotein NSs für die Infektion von und Replikation in Säugerzellen entbehrlich ist, wohingegen es essentiell für den Lebenszyklus in Zeckenzellen ist.

Insgesamt macht diese Arbeit deutlich, dass Arthropoden als Vektoren Auswirkungen auf mehrere Charakteristiken von Viruspartikeln haben und somit deren Infektiosität in Säugerzellen beeinflussen könnten. Diese Ergebnisse unterstreichen die Wichtigkeit des Arbeitens mit aus Arthropoden stammenden Viruspartikeln für die Analyse der Zellbiologie von Arbovirus-Transmission oder –zelleintritt. Außerdem eröffnet diese Studie neue Wege für zukünftige Untersuchungen des viralen Lebenszyklus in Zeckenzellen, um die Übertragung und Pathogenese von durch Zecken übertragenen Viren besser zu verstehen. Dies könnte helfen neue therapeutische Ansatzpunkte für Vakzine oder anti-virale Wirkstoffe zu identifizieren.



## Table of content

Acknowledgement .....	i
Abstract .....	iii
Zusammenfassung .....	iv
Table of content .....	vii
Figures .....	x
Tables.....	xi
Abbreviations .....	xii
Introduction .....	1
1. The biological significance of studying arboviruses.....	1
2. The <i>Bunyaviridae</i> family.....	2
a. Overview.....	2
i. Taxonomy .....	2
ii. Genomic organization of phleboviruses.....	5
iii. Virion structure of phleboviruses.....	8
b. Reverse Genetics System .....	9
c. Entry into mammalian cells.....	10
i. Receptor for tick-borne bunyaviruses .....	10
ii. Uptake of tick-borne bunyaviruses .....	11
iii. The Journey of tick-borne phleboviruses in the endocytic pathway: from EE to the ER.....	13
d. Replication cycle .....	15
i. Transcription and replication.....	15
ii. Assembly and release of viral particles.....	16
iii. Post-translational modifications .....	17
3. The vector-host switch in the context of tick-borne bunyaviruses.....	18
a. Ticks and tick-borne viruses.....	18
i. Biology and ecology of ticks.....	18
ii. Tick-borne diseases.....	19
iii. Tick-borne virus transmission .....	20
iv. Viral development cycle in ticks .....	21
b. Release of the tick-borne bunyavirus into mammalian skin dermis.....	23
4. Tick-borne phlebovirus and the host-cell antiviral response: the role of NSs protein .....	26
a. Interferon signaling pathway upon viral infection.....	26
b. NSs antagonizes interferon response in mammalian cells.....	28

c.	RNA interference in vector cells .....	30
i.	RNAi mechanism.....	31
ii.	Viruses counteract arthropod immune system.....	32
Results.....		37
1.	Reverse genetics system of UUKV.....	37
a.	The system used for this study.....	37
b.	The recovery viruses from Pol-I driven plasmid DNA .....	39
c.	rUUKV and rUUKV S23 characterization.....	40
d.	rUUKV behave like UUKV in mammalian cells.....	42
2.	Tick cell lines IRE/CTVM19 and IRE/CTVM20: the proof of concept .....	45
a.	Tick cells are persistently infected.....	45
b.	The glycosylation profile of tick cell-derived rUUKV S23 is unique.....	49
c.	A distinct pattern for the tick cell-derived G <sub>N</sub> .....	52
d.	Tick cell-derived rUUKV S23 is more infectious than mammalian cell-derived rUUKV S23.....	54
e.	Genetic evolution of wild-type UUKV originating from Swedish ticks .....	57
3.	Towards the characterization of tick cell-derived UUKV viral particles .....	59
a.	<i>Ixodes scapularis</i> cell lines are persistently infected by UUKV.....	59
b.	IDE8 cells as tick cell culture model.....	61
c.	Development of a high scale virus production in IDE8 cells and purification .....	62
d.	Tick cell-derived rUUKV: a unique fingerprint .....	66
4.	Early steps of UUKV infection.....	73
a.	DC-SIGN mediates infection by tick cell derived rUUKV S23 .....	73
b.	pH dependency .....	75
5.	Replication of rUUKV: the role of the nonstructural protein NSs.....	77
a.	Generation of recombinant viruses .....	77
b.	Stability of recombinant viruses .....	80
c.	Further characterization of recombinant viruses.....	81
d.	Growth properties of rescued recombinant viruses in tick cells .....	84
Discussion .....		89
Conclusion – Perspective .....		102
Material and Methods .....		105
1.	Material .....	105
2.	Methods.....	115
a.	Cellular culture .....	115
i.	Mammalian cell culture.....	115
ii.	Tick cell culture.....	115

iii.	Medium preparation for tick cells.....	115
iv.	Long term storage of cell lines .....	116
b.	Molecular biology methods.....	117
i.	RNA extraction.....	117
ii.	Reverse Transcription .....	117
iii.	Polymerase chain reaction.....	117
iv.	Gel extraction .....	118
v.	Cloning procedure.....	119
c.	Production and purification of plasmids DNA .....	119
d.	Sequencing .....	120
i.	DNA for cloning procedure.....	120
ii.	Full-length S or M segment.....	120
iii.	Full-length M segment isolated from UUKV-infected ticks .....	120
e.	Virus production and virology assay.....	121
i.	Rescue of UUKV from plasmid DNAs.....	121
ii.	Passaging of rescued viruses .....	121
iii.	Virus production .....	121
iv.	Virus purification.....	122
f.	Virus titration by focus-forming assay.....	123
g.	Infection assays.....	123
h.	Biochemistry .....	124
i.	Luciferase assay.....	124
ii.	Deglycosylation.....	124
iii.	Protein analysis by SDS-PAGE.....	125
i.	Flow cytometry.....	126
j.	Microscopy.....	126
i.	Wide-field fluorescence microscopy.....	126
ii.	Electron Microscopy.....	126
iii.	Cryo- electron microscopy .....	127
k.	Mass spectrometry of lipids.....	127
l.	Statistical Analysis.....	128
	Supplementary Material .....	129
	References.....	136
	Scientific Knowledge Dissemination.....	153

## Figures

Figure 1: <i>Bunyaviridae</i> family.....	3
Figure 2: Schematic representation of arbo-bunyavirus particles and genome.....	7
Figure 3: Replication cycle of bunyaviruses in mammalian cells.....	12
Figure 4: Structure of phleboviral glycoprotein G <sub>C</sub> .....	15
Figure 5: Biological tick life cycle and transmission of a tick-borne viruses.....	19
Figure 6: Distribution of representative human and veterinary diseases transmitted by ticks.....	20
Figure 7: The journey of tick-borne pathogens inside the tick: from acquisition to release inside the skin. .....	23
Figure 8: Release of tick-borne viruses into the host skin dermis.....	25
Figure 9: Representation of type I interferon response in mammalian host cells.....	28
Figure 10: Schematic representation of type I IFN inhibition by the nonstructural protein NSs of phleboviruses.....	30
Figure 11: Proposed RNA interference mechanism in ticks.....	33
Figure 12: Alternation of hosts during a tick-borne virus life cycle.....	35
Figure 13: Representation of mutations found in the laboratory strain UUKV compared to the reference strain UUKV S23.....	37
Figure 14: Schematic representation of the polymerase I driven reverse genetics used to rescue UUKV from plasmids.....	38
Figure 15: Recovery of UUKV from plasmid DNA.....	40
Figure 16: Genetic stability of rescued viruses.....	41
Figure 17: Characterization of UUKV rescued from plasmids.....	44
Figure 18: Infection of IRE/CTVM19 cells by rUUKV and rUUKV S23 is persistent.....	47
Figure 19: Tick-cell derived rUUKV S23 infect BHK-21 cells.....	48
Figure 20: N-linked glycosylation on UUKV glycoproteins.....	50
Figure 21: N-linked glycosylation harbored by the envelop proteins G <sub>N</sub> and G <sub>C</sub> on virions produced in tick or mammalian cells.....	51
Figure 22: Glycosylation specificity of tick-cell derived rUUKV S23.....	52
Figure 23: rUUKV S23 glycoproteins G <sub>N</sub> and G <sub>C</sub> from IRE/CTVM19 and BHK-21 cells.....	54
Figure 24: Tick and mammalian cell-derived structural viral proteins.....	56
Figure 25: Quantification of the structural rUUKV S23 proteins G <sub>N</sub> , G <sub>C</sub> , and N in infectious viral particles. .....	57
Figure 26: I. scapularis cell lines are persistently infected by rUUKV.....	60
Figure 27: rUUKV production in IDE8 cells without FBS.....	62
Figure 28: Purification of viral particles through an OptiPrep gradient.....	64
Figure 29: High scale production of rUUKV in vector tick cells.....	65
Figure 30: Lipid composition of IRE/CTVM19-derived Uukuniemi viral particles.....	67
Figure 31: Lipid composition of mammalian cell-derived Uukuniemi viral particles.....	68
Figure 32: Size of tick or mammalian cell-derived rUUKV.....	71
Figure 33: Tick cell-derived viral particle morphology.....	72
Figure 34: DC-SIGN is required for the tick cell-derived rUUKV S23 infection.....	74
Figure 35: rUUKV S23 requires low pH for infection.....	77
Figure 36: Schematic representation of the recovery of recombinant UUKV.....	78

Figure 37: Recovery of recombinant viruses.....	80
Figure 38: Passaging of recombinant viruses in BHK-21 cells.....	82
Figure 39: Characterization of recombinant rescued viruses. ....	83
Figure 40: Infection of tick cells with rUUKV eGFP. ....	84
Figure 41: Early replication of rUUKV $\Delta$ NSs in tick cells. ....	86
Figure 42: Production and replication of rUUKV $\Delta$ NSs in tick cells. ....	88
Figure 43: Proposed model of viral particles coming from vector tick cells and host mammalian cells....	97
Figure 44: Culture of tick cells in 3 mL flat glass tubes. ....	116

## Tables

Table 1: The new taxonomy of the Bunyavirales order.....	4
Table 2: Sequences of tick cell-derived rescued viruses.....	48
Table 3: Analysis of the M amino acid sequence from UUKV-infected field <i>I. ricinus</i> ticks.....	59
Table 4: Chemicals and reagents.....	105
Table 5: Components used for DNA analysis.....	106
Table 6: Buffers and their composition.....	106
Table 7: Commercial kits.....	107
Table 8: Compounds used for cellular culture.....	107
Table 9: Media used for mammalian cell culture.....	108
Table 10: Media used for tick cell culture.....	108
Table 11: Mammalian cell line and seeding.....	109
Table 12: Tick cells.....	109
Table 13: Primary antibodies.....	110
Table 14: Secondary antibodies.....	110
Table 15: Plasmids list.....	111
Table 16: Primers used to generate plasmids for the reverse genetics system.....	111
Table 17: Primers used to sequence the M segment.....	112
Table 18: primers for S or S- $\Delta$ NSs segment amplification.....	113
Table 19: Equipment.....	113

## Abbreviations

aa	Amino acid
aPC	Acyl-linked phosphatidylcholine
aPE	Acyl-linked phosphatidylethanolamine
BHK-21	Baby Hamster Kidney (cells)
bp	Base pair
BUNV	Bunyamwera virus
CCHFV	Crimean-Congo hemorrhagic fever virus
cDNA	Complementary DNA
CE	Cholesteryl ester
Cer	Ceramide
Chol	Cholesterol
CME	Clathrin mediated endocytosis
CMV	Cytomegalovirus
CPE	Cytopathic effect
CRD	Carbohydrate recognition domain
DAG	Diacylglycerol
DCs	Dendritic cells
DC-SIGN	Dendritic cell-specific intercellular adhesion molecule 3-grabbing non integrin
DENV	Dengue virus
DI	Domain I
DII	Domain II
DIII	Domain III
DNA	Deoxyribonucleic acid
dsRNA	Double stranded RNA
DUGV	Dugbe virus
EE	Early endosome
eGFP	Enhancer green fluorescent protein
eIF2	Eukaryotic initiation factor 2
EM	Electron microscopy
Endo H	Endoglycosidase H
ePC	Ether-linked phosphatidylcholine
ePE	Ether-linked phosphatidylethanolamine
ER	Endoplasmic reticulum
FBXO3	F-box 3 protein
FFA	Foci-forming assay
FFU	Focus-forming unit
FKBP	FK506 binding protein
Gau	Gaussia luciferase
G <sub>C</sub>	Glycoprotein C
G <sub>N</sub>	Glycoprotein N
gRNA	Genomic RNA
GTPase	Guanosine triphosphate hydrolase protein
HAZV	Hazara virus
HexCer	Hexosylceramide

HIV	Human Immunodeficiency virus
HRTV	Heartland virus
HSP	Heat shock protein
IFN	Interferon
IFNAR	IFN $\alpha/\beta$ receptor
IKK $\epsilon$	Inhibitor of kappa B kinase epsilon protein
IRF3	IFN regulatory factor 3
ISG	IFN stimulated gene
kDa	Kilo Dalton
LACV	La Cross virus
LE	Late endosome
LGTV	Langat virus
LIV	Louping Ill virus
LPC	Lysophosphatidylcholine
L-SIGN	Liver cell-specific intercellular adhesion molecule 3-grabbing non integrin
MAVs	Mitochondrial antiviral-signaling protein
MDA5	Melanoma differentiation-associated protein 5
MOI	Multiplicity of infection
mRNA	Messenger RNA
MS	Mass spectrometry
MVBs	Multivesicular bodies
NF- $\kappa$ B	Nuclear factor kappa-light-chain-enhancer of activated B cells protein
NSDV	Nairobi sheep disease virus
NSm	Nonstructural protein on the M transcript
NSs	Nonstructural protein on the S transcript
NTR	Nontranslated region
ORF	Open reading frame
OROV	Oropouche virus
PA	Phosphatidic acid
PAMP	Pathogen-associated molecular patterns
PCR	Polymerase chain reaction
PG	Phosphatidylglycerol
PI	Phosphatidylinositol
PKR	Protein kinase R
PI-PE	Plasmalogen phosphatidylethanolamine
PNGase F	Peptide – N glycosidase F
Pol I	Polymerase I
PRR	Pattern-recognition receptors
PS	Phosphatidylserine
PTV	Punta Toro virus
RdRp	RNA dependent RNA polymerase
Ren	Renilla luciferase
RGS	Reverse genetics system
RIG-I	Retinoic acid-induced gene 1
RISC	RNA-induced silencing complex
RLR	RIG-I-like receptor
RLU	Relative light unit

RNA	Ribonucleic acid
RNAi	RNA interference
RNP	Ribonucleoprotein
RSS	RNA silencing suppressor
RVFV	Rift Valley fever virus
SAP30	Sin3A associated protein 30
SBV	Schmallenberg virus
SCRV	St Croix river virus
SDS-PAGE	Sodium dodecyl sulfate polyacrylamide gel electrophoresis
SFTSV	Sever fever with thrombocytopenia syndrome virus
SFV	Semliki Forest virus
shRNA	Short hairpin RNA
siRNA	Small interfering RNA
SM	Sphingomyelin
TAG	Triacylglycerol
TBEV	Tick-borne encephalitis virus
TBK1	Tank-binding kinase 1
TBVs	Tick-borne viruses
TFIIH	Transcription factor II H
TIR	Toll-interleukin 1 receptor
TLR	Toll-like receptor
TOSV	Toscana virus
TRIF	TIR domain-containing adapter-inducing IFN- $\beta$
TRIM25	Tripartite motif-containing protein 25
UUKV	Uukuniemi virus
viRNA	Virus-derived small interfering RNA
VSV	Vesicular stomatitis virus
XBP1	X-box binding protein 1

## Introduction

### 1. The biological significance of studying arboviruses

Arboviruses are defined as arthropod-borne viruses; viruses that are transmitted by mosquitoes, ticks, midges or sand flies (invertebrates) to mammalian hosts and other vertebrates. They are maintained in a complex life cycle that engages the vector, the virus and the host. Arboviruses are unique in a sense that they replicate both in invertebrates' vectors and vertebrates' hosts <sup>1</sup>. Currently, more than 500 arboviruses are known, many are responsible for outbreak globally; 80 are known to infect humans <sup>2</sup> and livestock. Arboviruses are described in seven families namely *Asfar-*, *Bunya-*, *Flavi-*, *Orthomyxo-*, *Reo-*, *Rhabdo-*, and *Togaviridae*. Except for the African swine fever virus (*Asfaviridae*), all arboviruses possess an RNA genome <sup>3</sup>. The human overpopulation, global warming, trade globalization, and travels are parameters that facilitate the spread of vectors and are responsible for emerging or re-emerging arboviral diseases. One of the best example is the recent Zika disease outbreak that started in the Pacific Islands and spread rapidly to Americas where the virus encountered non immunized population. Zika virus is a member of the *Flaviviridae* family as dengue virus (DENV) that is the most widespread arbovirus in the world. Within the vast group of arbovirus, bunya-, flavi-, reo-, rhabdo-, and togaviruses are the main pathogenic viruses that represent a global threat for agricultural economy, livestock, travelers and public health.

Currently, treatments or vaccines are available for only few arboviral diseases. Part of the reasons are arguably that the cell biology of arboviruses are not completely understood and under investigated. Regarding bunyaviruses, a lot remains to be uncovered to understand virus transmission, life cycle in arthropod vectors and vertebrate hosts, and tropism. The overall aim of my PhD project is to improve our knowledge about the vector-host transition from a cell biology and virology perspective. To this end, I used the tick-borne bunyavirus Uukuniemi (UUKV) as tick-borne virus model.

## 2. The *Bunyaviridae* family

### a. Overview

#### i. Taxonomy

UUKV is a bunyavirus from the *phlebovirus* genus. The *Bunyaviridae* family is the largest family of RNA viruses with more than 350 members divided in five genera *Hantavirus*, *Orthobunyavirus*, *Phlebovirus*, *Nairovirus* and *Tospovirus* based on serological, morphological and biochemical characteristics <sup>4</sup>. With the exception of tospoviruses that are plant specific and hantaviruses that are transmitted to humans via aerosols from urine, feces or saliva of infected rodents <sup>5</sup>, all the other bunyavirus isolates are arthropod-borne viruses, which will be designated elsewhere as arbo-bunyaviruses for convenience. Orthobunyaviruses, phleboviruses and nairoviruses replicate in, and are transmitted by, blood feeding arthropods such as mosquitoes, ticks or phlebotomine flies <sup>6-8</sup>. This work is focused on arbo-bunyaviruses that represent a threat for the veterinary and public health. This excludes *de facto* tospoviruses and hantaviruses (**figure 1**).

Genus	Hosts	Vectors	Representative arbovirus members
<i>Orthobunyavirus</i>	M A M	 <b>Mosquitoes</b> Culicoid flies	BUNV SBV LACV OROV
<i>Phlebovirus</i>	M A L	 <b>Phlebotomine flies</b> Mosquitoes Ticks	RVFV SFTSV HRTV UUKV
<i>Nairovirus</i>	S	 <b>Ticks</b> Culicoid flies Mosquitoes	CCHFV DUGV NSDV HAZV

**Figure 1: *Bunyaviridae* family.**

The *Bunyaviridae* family is composed of more than 350 members distributed in five genera and are depicted here according to their hosts and vectors. Main vector are in bold. Only arthropod-borne bunyaviruses are highlighted in grey with examples of representative members. Abbreviations: BUNV: Bunyamwera virus, SBV: Schmallenberg virus, LACV: La Crosse virus, OROV: Oropouche virus, RVFV: Rift Valley fever virus, SFTSV: Sever fever with thrombocytopenia virus, HRTV: Heartland virus, UUKV: Uukuniemi virus, CCHFV: Crimean-Congo hemorrhagic fever virus, DUGV: Dugbe virus, NSDV: Nairobi sheep disease virus, HAZV: Hazara virus.

The taxonomy has very recently changed for multiple reasons. First, a lot of members of the *Bunyaviridae* family were not assigned to a genus and could not be assigned with this classification. Then, newly discovered viruses assigned to this family were bisegmented and not three segmented. Finally, plant viruses, which encode more than three segments were described as “bunyavirus-like”, and their proteins clustered with those of bunyaviruses. Thus, the order *Bunyavirales* was created (International Committee on Taxonomy of Viruses) <sup>9–12</sup>. The new taxonomy is explained in the **table 1**. However, for convenience with the work presented here and recently published, I have chosen to keep the previous taxonomy nomenclature.

The number of outbreaks caused by arbo-bunyaviruses have increased worldwide over the last decade. These viruses must be seriously taken as emerging and re-emerging viruses. Recent examples are the two new phleboviruses namely sever fever with thrombocytopenia syndrome virus (SFTSV) and Heartland virus (HRTV) discovered in China and the U.S.A, respectively <sup>13,14</sup>. Both infect humans and can be highly pathogenic. They cause mild symptoms to hemorrhagic fever with a fatality rate between 10 and 30% <sup>15,16</sup>. In November 2011, cattle with fever and reduced milk yield production were diagnosed with a virus closely related to the orthobunyavirus Akabane <sup>17</sup>. This new virus, named Schmallenberg virus (SBV), has rapidly spread from Germany through Europe causing outbreak in sheep, cattle, and goats <sup>18,19</sup>. The disease lead to reduction of milk production in adult cows and mild symptoms in adults. Nevertheless, female can transmit the virus to fetuses that lead to high-rate abortions and malformations in progenies <sup>17–19</sup>.

**Table 1: The new taxonomy of the Bunyavirales order.**

Order	Family	Genus (number of species)	Example names
<i>Bunyavirales</i>	<i>Feraviridae</i>	<i>Orthoferavirus</i> (1)	
	<i>Fimoviridae</i>	<i>Emaravirus</i> (9)	
	<i>Hantaviridae</i>	<i>Orthohantavirus</i> (41)	Hantaan orthohantavirus
	<i>Jonviridae</i>	<i>Orthojonvirus</i> (1)	
	<i>Nairoviridae</i>	<i>Orthonairovirus</i> (12)	Crimean-Congo hemorrhagic fever orthonairovirus
	<i>Peribunyaviridae</i>	<i>Herbevirus</i> (4)	
		<i>Orthobunyavirus</i> (48)	Bunyamwera orthobunyavirus
	<i>Phasmaviridae</i>	<i>Orthophasmavirus</i> (6)	
	<i>Phenuiviridae</i>	<i>Goukovirus</i> (3)	
		<i>Phasivirus</i> (4)	
<i>Phlebovirus</i> (10)		Rift Valley fever phlebovirus Uukuniemi phlebovirus	
<i>Tenuivirus</i> (7)			
<i>Tospoviridae</i>	<i>Orthotospovirus</i> (11)	Tomato spotted wilt orthotospovirus	

Arbo-bunyaviruses cause a wide range of syndromes, from febrile illness to hemorrhagic fever in infected humans and animals and many arbo-bunyaviruses are teratogenic for gestating livestock <sup>20–22</sup>. Infected humans with Oropouche virus (*Orthobunyavirus* genus) develop febrile illness while La Cross virus (LACV - *Orthobunyavirus* genus) infection might lead to encephalitis <sup>7</sup>. In the *nairovirus* genus, Nairobi sheep disease virus and Crimean-Congo hemorrhagic fever virus (CCHFV) are the most threatening viruses from a public and veterinary point of view. CCHFV is the most widespread tick-borne virus, the second arboviral disease after the dengue fever disease <sup>23</sup>. They both lead to hemorrhagic diseases, the first affecting sheep and goat, the second infecting also humans <sup>23</sup>. In the *Phlebovirus* genus, the prototype Rift Valley fever virus (RVFV) is highly pathogenic for livestock, it causes abortion in sheep, cattle and goat. During outbreak, it can be transmitted to human via infected mosquitoes and can lead to a hemorrhagic fever in 1% of cases <sup>24</sup>. Arbo-bunyaviruses are responsible for agricultural productivity decrease, and are a public health

concern. Some of the arbo-bunyaviruses are classified as potential biological weapons (category A) by US authorities and listed as high-priority pathogens by the World Health Organization.

## ii. Genomic organization of phleboviruses

UUKV has never been associated with any diseases in humans. Thus, UUKV can be handled in biosafety laboratory of class 2, a major difference with SFTSV, HRTV or other highly pathogenic phleboviruses that have to be handled in a higher confinement level (3 or 4). Therefore UUKV has been used as a surrogate for phleboviruses and especially tick-borne phleboviruses during the last decades. The genus *Phlebovirus* is composed of 70 members that are mainly transmitted by phlebotomine flies, hence the name of the genus<sup>25</sup>, even though some viruses like RVFV and UUKV are transmitted by mosquitoes and ticks, respectively. The *Phlebovirus* genus can be divided into two groups: the Uukuniemi-like virus group and the sandfly fever virus group<sup>6,25</sup>. While viruses of the first group (UUKV, SFTSV and HRTV for instance) are all transmitted by ticks, viruses of the sandfly fever group (RVFV and Toscana virus) are transmitted by dipteran, i.e. phlebotomines and mosquitoes<sup>25</sup>. Genomic and metagenomics analysis reported that UUKV and SFTSV or HRTV are closely related, though UUKV shares up to 40% genetic similarity with the mosquito borne RVFV<sup>6,14,26–29</sup>.

As all other bunyaviruses, phleboviruses and UUKV are enveloped and spherical viruses with a diameter approximately 80 – 140 nm<sup>25,30</sup> (**figure 2A**). They replicate exclusively in the cytoplasm of infected cells. Phleboviruses share the same genome organization than other bunyaviruses with three single-stranded negative sense RNA segments named according to their size: a small (S), a medium (M) and a large (L) segment<sup>4</sup>. The largest RNA segment encodes for the viral RNA-dependent RNA polymerase (RdRp), the protein L, in a negative sense orientation. The bunyavirus RdRps usually exceed 200 kDa and have two functions. First it perform mRNA transcription and RNA replication<sup>31</sup>, second it recognizes highly conserved 3' and 5' extremity of each segment to perform RNA synthesis<sup>32</sup> as explain in the section **2. a. iii**.

The medium (M) segment that has a negative sense polarity codes for a polyprotein precursor that is cleaved into two glycoproteins in the endoplasmic reticulum (ER) by host-cell proteases. The cleavage results in the formation of a glycoprotein N and a glycoprotein C, G<sub>N</sub> and

G<sub>C</sub>, respectively (**figure 2A &B**). The role of the glycoproteins will be explained more into details later throughout the introduction. Some members of the *Phlebovirus*, *Orthobunyavirus*, *Tospovirus* and *Nairovirus* genera present a nonstructural protein NSm. Very little is known about the NSm proteins. Curiously, it appears that the presence of NSm is one main distinction between tick- and dipteran-borne phleboviruses<sup>6</sup>. It has been suggested for RVFV that NSm is not important for viral replication but could be one of the factor of pathogenesis<sup>33,34</sup>. Better investigation are needed for those of nairoviruses. However, it is interesting to notice that the overall organization of the nairoviruses M segment is more complex than other bunyaviruses. CCHFV glycoprotein precursor is first cleaved by a peptidase signal as a PreG<sub>N</sub>, which will be further processed as a mucin-like, GP38, G<sub>N</sub> and NSm protein, and a PreG<sub>C</sub> glycoprotein<sup>8,35,36</sup> (**figure 2B**). Moreover, two nairoviruses (Hazara virus and Clo Mor virus) have been shown to produce a third glycoprotein, the function of which remains unknown<sup>37,38</sup>.

The small (S) segment encodes for the nucleoprotein N whose major function is to protect the viral genomic RNA, thus forming ribonucleoprotein (RNP) complexes. The N protein is the most abundant protein found in the cytoplasm<sup>39</sup> and therefore is often use as a read out for infection or viral replication in many experiments. For some bunyaviruses, the S segment also encodes a nonstructural protein NSs. Phleboviruses use an ambisense strategy with non-overlapping open reading frame (ORF) to encode N (negative sense) and NSs (sense) proteins<sup>21,40,41</sup>. In contrast, orthobunyaviruses have a single overlapping ORF that codes for both N and NSs in a negative-sense orientation<sup>42</sup> (**figure 2B**). Nairoviruses do not encode for a nonstructural protein NSs. The function of the NSs protein of tick-borne phleboviruses is unknown whereas it appears to be the main virulent factor for RVFV and other dipteran-borne phleboviruses. RVFV NSs interacts with numerous promoters, including many regulating genes involved in innate-immunity, coagulation and neurological functions<sup>43</sup>. The function of NSs in the context of SFTSV infection remains unclear. Some reports suggested a role of SFTSV NSs in the replication by forming a scaffold platform<sup>44</sup>. The protein might also be implicated in the interferon (IFN) signaling inhibition<sup>45,46</sup>. For further information, a detailed overview of the NSs function and its role in innate immunity is described in **4.b**.

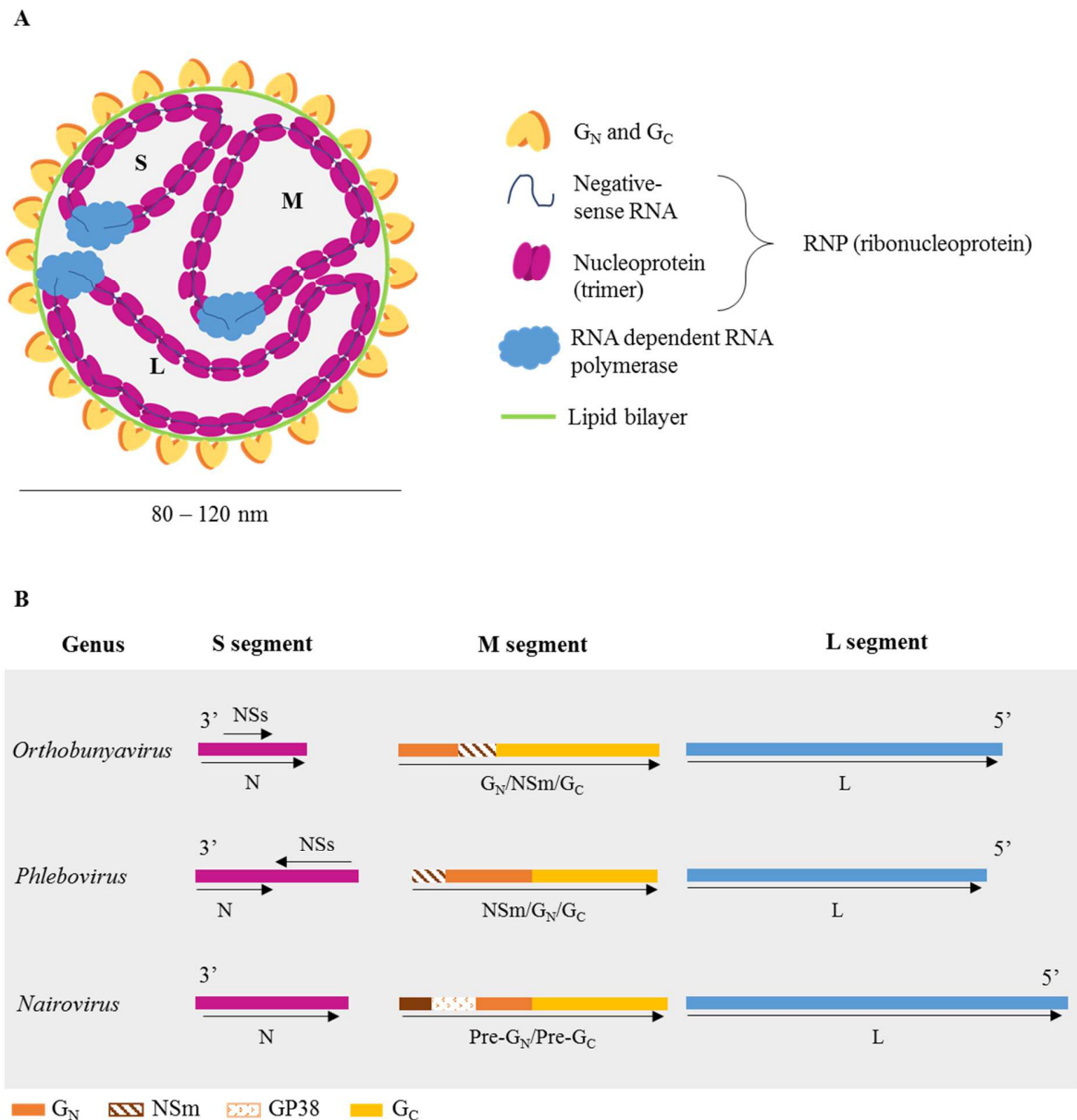


**Figure 2: Schematic representation of arbo-bunyavirus particles and genome.**

(A) Bunyavirus particles are generally spherical, enveloped with spike-like glycoproteins  $G_N$  and  $G_C$  heterodimers. They are three segmented (S, M and L segments), negative-sense RNA viruses. (B) Genomic representation of each segment for the five genera. Size of the segments are shown. Arrows indicate open reading frames (ORFs) expressed using a negative sense orientation, except for NSs ORFs of Phleboviruses.

### iii. Virion structure of phleboviruses

Inside viral particles, the RdRp L tightly interacts with RNPs. In fact, each strand of RNA molecules possesses 3' and 5' non-translated region (NTR) extremities that are highly conserved and genus specific<sup>32,40,47</sup>. The 3' and 5' extremity sequences are complementary to each other<sup>32,48</sup> and it has first been proposed that this complementarity forms panhandle structures that circularize the viral RNA, thus RNPs<sup>49–51</sup>. Recently, Gerlach et al., have shown that the polymerase of LACV had a highly specific and distinct sites for the 3' and 5' ends of viral RNA, which do not allow panhandle structures<sup>52</sup>. Nevertheless, the polymerase protects the 3' and 5' ends, essential to initiate the transcription into mRNA and positive sense anti-genome RNA that will in turn be used as template to increase the copies of viral negative genomic RNA strands<sup>52,53</sup>. The same authors argue that the function of the polymerase is conserved for numerous (if not all) negative sense RNA viruses, the phleboviruses being part of them.

Unlike other negative-sense RNA viruses, phleboviruses neither encode a matrix nor capsid proteins. Thus, the N protein that surrounds viral RNA has a major importance to protect the viral genome. Co-immunoprecipitation assays suggest that Uukuniemi virus G<sub>N</sub> and G<sub>C</sub> proteins interact with the N proteins. This interaction is believed to occur before the complex glycoproteins/N reaches the ER<sup>54</sup>. More specifically, the cytosolic tail of UUKV glycoprotein N has been shown to be essential for RNP packaging<sup>55–57</sup>. Interaction between UUKV RNPs and viral membrane has also been observed by cryotomography suggesting an interaction between the cytoplasmic tails of the G<sub>N</sub> and the N protein<sup>30</sup> (**figure 2A**). Whether one copy of each segment is packed inside one viral particle remains still unclear. Recently, a report suggests that packaging of RVFV genome occurs randomly<sup>58</sup>.

The structure of viral particles were first obtained for orthobunyaviruses while phleboviral particles have been described using UUKV and RVFV. Indeed, electron microscopy pictures of phlebo- and orthobunyaviruses show pleomorphic particles with a diameter mentioned above and spikes projections<sup>7,30,59–61</sup>. Recent advanced microscopy data confirmed the degree of pleomorphism previously observed for bunyaviruses particles. While UUKV and RVFV exhibit icosahedral arrangement of glycoproteins (with a triangulation of T=12), Bunyamwera virus (BUNV – *Orthobunyavirus*) glycoproteins form tripod-like arrangements<sup>62</sup>. Despite the biological significance of the glycoproteins in the bunyavirus life cycle, their function during viral entry, their

biogenesis and their role during assembly of new virions are not completely understood. They are however critical steps and further discussed in the following sections.

### **b. Reverse Genetics System**

Relatively few tools were initially available to study bunyaviruses. Within the last 10 years, many reverse genetics systems (RGS) have emerged to recover bunyavirus isolates from cDNAs. RGS allows the genome manipulation of segmented, negative strand RNA viruses. This technology was first described for influenza virus<sup>63</sup> whose the 8 segments were entirely recovered from cDNA in 1999 by Neumann and colleagues<sup>64</sup>. Since then, a lot of systems have been developed; the first of the *Bunyaviridae* members being Bunyamwera virus (BUNV). It is arguably a major advance for bunyavirus research, which has revolutionized our knowledge and understanding of these viruses. Indeed, it has been a useful tool to investigate the molecular biology of infection, replication and pathogenicity of these viruses<sup>65,66</sup>, while it remains under used to study transmission and entry.

Whereas several orthobunyaviruses have been recovered from cDNA<sup>67-69</sup>, such system are still missing for numerous phleboviruses and nairoviruses. First attempts to develop a reverse genetics system for UUKV was done by Ramon Flick and Ralf F. Pettersson<sup>70</sup>. Authors used the strategy based on the polymerase I promoter that successfully rescued influenza virus<sup>64,71</sup>. Using this technique, they showed that reporter genes flanked by the 5' and 3' ends of the M segment of UUKV were synthesized in mammalian cells and translocated to the cytoplasm. Some years later, Billecocq et al., followed the work of Flick and Pettersson to establish a full five plasmid system for RVFV<sup>72</sup>. Many bunyavirus RGS have been added to the list, including SFTSV that can be now rescued from double stranded DNA<sup>29</sup>.

**c. Entry into mammalian cells**

**i. Receptor for tick-borne bunyaviruses**

The first step that a virus accomplishes to infect a target cell is to enter this cell to deliver its viral genome. The receptors, cellular partners, factors or pathways used by tick-borne bunyaviruses are largely uncharacterized. However, few of them have been described in the literature. Interestingly, interactions between the virus and the host factors or receptors are mainly glycan-protein interactions. For instance, the mosquito-borne phlebovirus RVFV has been shown to make use of heparan sulfate for efficient cellular entry<sup>73,74</sup>. Heparan sulfate is a glycosaminoglycan, a polysaccharide containing repetition of disaccharide units, which can be linked to proteins, thus forming a proteoglycan. This glycosaminoglycan is found on a wide variety of cell types and tissues. Other arbo-bunyaviruses like CCHFV and Toscana virus (TOSV) seem to also use heparan sulfate for viral entry<sup>74-76</sup>. Recently, SFTSV has been shown to depend on the non-muscle myosin heavy chain IIA and CCHFV to require cell surface nucleolin<sup>76-78</sup>. Whether these macromolecules are attachment factors or receptors is unclear. Their interactions with viral proteins is also not well understood.

In 2011, the dendritic cell-specific intercellular adhesion molecule 3-grabbin nonintegrin (DC-SIGN) was identified as an authentic viral receptor for UUKV<sup>79</sup> (**figure 3**). DC-SIGN has first been described to bind HIV gp120<sup>80,81</sup>. Since then, numerous unrelated arboviruses (dengue virus, Japanese encephalitis, West Nile virus for instance) were shown to make use of this lectin to enter target cells<sup>82-86</sup>. DC-SIGN is a calcium dependent lectin that is specifically expressed on immature dermal dendritic cells (DCs)<sup>87</sup>, which are located at the anatomical site of arbovirus transmission (**see 3.b**). DC-SIGN is specialized in the capture of foreign antigens with *N*-linked mannosylated glycans, typical of insect-derived viruses<sup>88</sup>.

DC-SIGN is also required for entry of the phleboviruses RVFV, Punta Toro virus (PTV), TOSV<sup>79</sup>, and SFTSV<sup>89</sup>. More specifically, in addition to high mannose glycans, DC-SIGN also recognizes terminal fucose groups and thus covering a wide variety of ligands expressed by lots of pathogens. Evidences also confirmed the lectin specific of liver endothelial cells (L-SIGN) as a receptor for RVFV, UUKV, and TOSV phleboviruses<sup>90</sup>. L-SIGN shares 77% homology with DC-SIGN, binds to the same ligands, but is expressed at the surface of liver endothelial cells. Together,

the different localizations of these receptors might explain the large tropism of arbo-bunyaviruses and their spread throughout the organism.

## ii. Uptake of tick-borne bunyaviruses

As discussed previously, few viral receptors or co factors for attachment and internalization have been described for bunyaviruses. After binding to a receptor, phlebo- and other bunyaviruses are physically taken up by endocytic cellular machinery (**figure 3**). This process is referred as receptor-mediated endocytosis<sup>91</sup> and leads to the internalization of viral particles. Attachment of UUKV to DC-SIGN has been shown to induce intracellular signaling pathways<sup>79</sup> and endocytosis of the virus via the di-leucine motif (LL) in the cytosolic tail of the lectine. When DC-SIGN mutant that does not contain the di-leucine motif is expressed, UUKV binds the receptor but is no longer able to enter the cells<sup>79,92</sup>. This was not the case for L-SIGN whose endocytic-defective LL mutant does not impact infection<sup>90</sup>. Together these results indicate that DC-SIGN acts as a true endocytic receptor for UUKV and other phleboviruses whereas L-SIGN rather acts as an attachment factor. In addition to the LL motif, DC-SIGN carries several motifs involved in signaling, recycling and internalization of ligands. The nature of glycan on antigens recognized by DC-SIGN has been shown to trigger different signaling pathways<sup>93,94</sup>, highlighting the importance of the glycosylation on viral glycoproteins and the impact on innate immune response.

Several endocytic pathways have been proposed for enveloped viruses to enter their host cells such as clathrin-mediated endocytosis (CME), macropinocytosis, and lipid raft-mediated endocytosis<sup>91,95</sup>. Silencing of clathrin does not result in a significant decrease of UUKV infection and the virus was rarely observed in clathrin-coated pits at the plasma membrane and in clathrin-coated vesicles after internalization. It is, thus, rather unclear whether the virus relies on clathrin (Lozach et al., 2010). The situation remains uncovered for most phlebo and arbo-bunyaviruses. RVFV has been proposed to use the CME<sup>96,97</sup> like the nairo CCHFV and the orthobunya LACV<sup>98,99</sup>. Overall, the endocytic pathways used by arbo-bunyaviruses to enter host cells remain to be clarified.

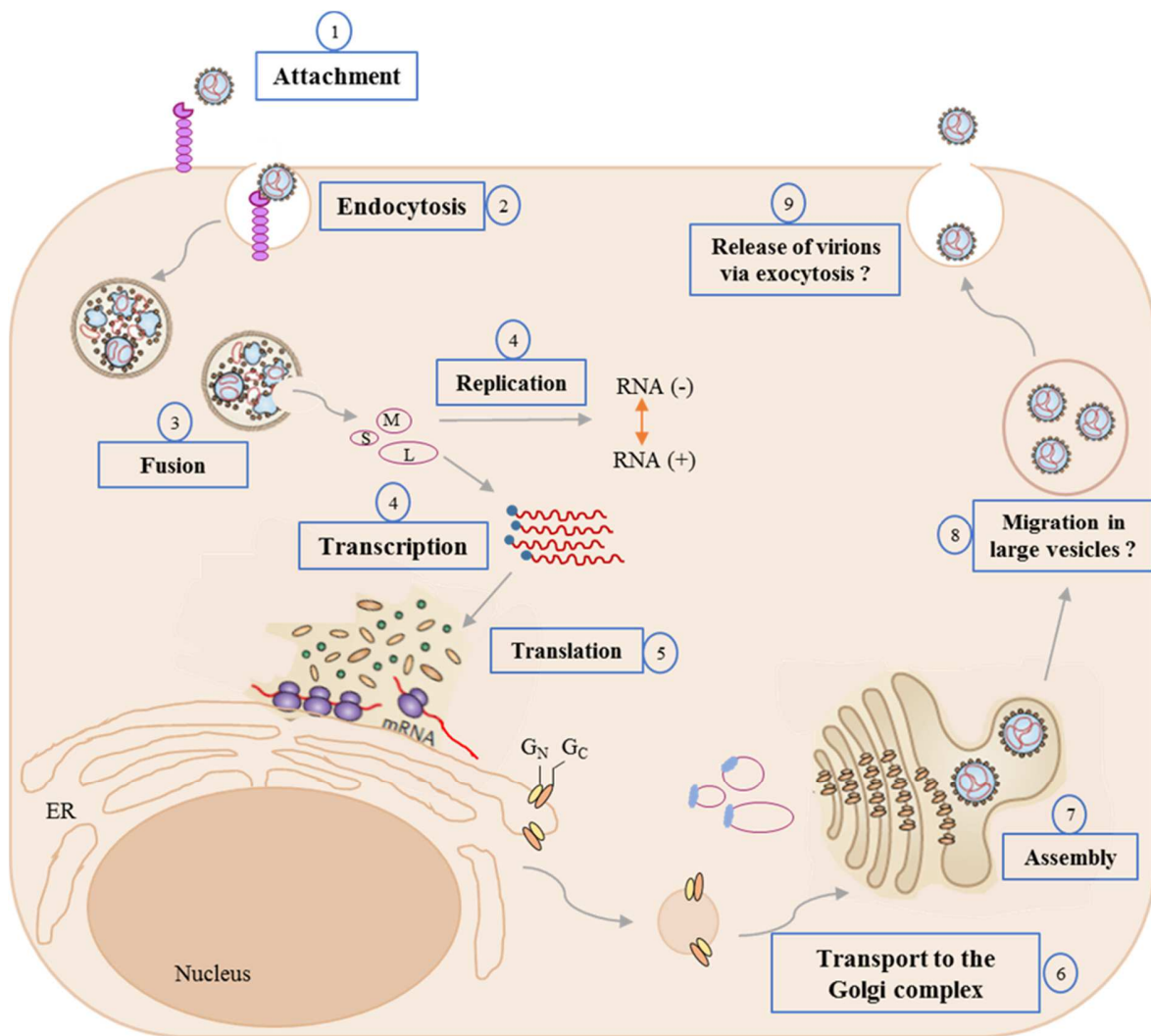


**Figure 3: Replication cycle of bunyaviruses in mammalian cells.**

(1) Viral particles bind to a receptor and (2) are internalized by endocytosis. Viruses travel through the endocytic machinery and (3) the genome is released into the cytoplasm via fusion between the viral and endosomal membranes. (4) The primary transcription of viral-complementary mRNA occurs using cap snatching mechanisms and then the replication of genomic RNA (RNA<sup>-</sup>) into anti-genomic RNA (RNA<sup>+</sup>) takes place. (5) mRNA are translated into proteins in the ER proximity where the glycoproteins G<sub>N</sub> and G<sub>C</sub> dimerize. (6) Viral proteins, viral genomes, and dimers of glycoproteins are transported to the Golgi complex where (7) they assemble into viral particles. (8) Virions travel to the plasma membrane, likely inside large vesicles, from the Golgi complex and (9) are probably released in the extracellular space via exocytosis. Scheme adapted from <sup>7</sup>.

### iii. The Journey of tick-borne phleboviruses in the endocytic pathway: from EE to the ER

After attachment and uptake, arbo-bunyaviruses need to enter into the cytoplasm to replicate. Like a large majority of enveloped viruses, they travel through the endocytic machinery to reach the appropriate endosomal compartment from where they penetrate cells.

Early endosomes (EE) are a prerequisite for the journey of bunyaviruses. Indeed, the inhibition of endogenous Rab5a, a small GTPase that regulates trafficking and maturation of EE, by expressing dominant negative or constitutively active mutants, blocks UUKV, CCHFV and LACV infection<sup>99-101</sup>. Most bunyaviruses belong to the group of late penetrating viruses that require late endosomal maturation for membrane fusion<sup>102</sup>. While Rab5a is a hallmark for EE, Rab7a decorate multivesicular bodies (MVBs) and late endosomes (LE). Not all tick-borne bunyaviruses rely on Rab7a for viral infection. For instance, the transient expression of dominant negative mutant of Rab7 has no impact on CCHFV<sup>98,101</sup>. Although a dominant negative form of Rab7a was not deleterious for UUKV infection, a constitutively active form of Rab7a resulted in the increase of UUKV infection<sup>100</sup>. Disrupting microtubules network, which is important for maturation of endosomes, also impaired UUKV infection<sup>100</sup>. These results suggest that UUKV relies on intact cell cytoskeleton and might also reach MVBs to deliver its RNA into the cytoplasm as CCHFV<sup>101</sup>. So far, early steps of SFTSV infection have not been characterized.

The last step for productive viral infection is the fusion between viral envelope and endosomal membrane that results in the release of viral genome into the cytoplasm (**figure 3**). For instance, UUKV and RVFV infectious entry occurs at pH below 6 and takes place after 20 to 40 minutes intracellular trafficking<sup>73,100,103</sup>. The vacuolar H<sup>+</sup>-ATPase (V-ATPases) are essential pumps that regulate the pH in intracellular vesicles. Ammonium chloride and bafilomycin A1 are two weak bases that inhibit V-ATPases<sup>104</sup>, resulting in the neutralization of endosomal pH. The low pH in endosomal compartments has been documented to be critical for the infection by several bunyaviruses. The use of ammonium chloride or bafilomycin A1 results in a block in UUKV, CCHFV and SFTSV infection<sup>98,100,105</sup>. While the pH decreases with the maturation of the endosomes, the glycoproteins G<sub>N</sub> and G<sub>C</sub> undergo conformational modifications. Phlebovirus membrane fusion is most likely mediated by the envelope glycoprotein G<sub>C</sub><sup>106</sup>.

Viral fusion proteins are classified into three classes (classes I-III) based on their structural and functional features <sup>107-109</sup>. In 2004, Garry & Garry postulated that the glycoprotein G<sub>C</sub> of the bunyavirus Sandfly fever virus could be a class II fusion protein base on proteomics computational analyses <sup>110</sup>. Followed by computational modeling analysis of RVFV glycoproteins, the role of G<sub>C</sub> in the fusion mechanism was reinforced <sup>111</sup>. More recently, the crystal structure of the ectodomain of RVFV G<sub>C</sub> was solved in the pre-fusion step <sup>112</sup> as well as the post-fusion step of SFTSV G<sub>C</sub> <sup>113</sup> supporting the hypothesis that G<sub>C</sub> of bunyaviruses is a class II fusion protein.

Class II fusion proteins are typically composed of three domains, namely domain I (DI), domain II (DII) and domain III (DIII). As shown for RVFV and SFTSV, DI is the central domain that links DII via a flexible hinge, or stem region, and DIII with a linker region (**figure 4**) <sup>112,113</sup>. While DII has a hydrophobic fusion loop that is important for the membrane fusion, DIII makes numerous protein-protein contacts with DI <sup>109,113</sup>. Interestingly, it has been shown that synthesized peptides that correspond to the DIII or to the stem region of alpha- and flaviviruses G<sub>C</sub> inhibited infection of those viruses <sup>114,115</sup>. Similarly, exogenous peptides against stem region of RVFV G<sub>C</sub> was recently observed for inhibiting RVFV infection as well as infection of Andes virus (class II fusion protein), Ebola virus (class I fusion protein), and Vesicular stomatitis virus (class III fusion protein) <sup>116</sup>. This suggests a conserved stem region among distinct viral fusion proteins.

The optimal pH that determines the viral fusion is related to specific histidine residues. Indeed, exposed histidine residues of alpha- and flaviviruses are protonated during maturation of endosomes, which leads to the fusion <sup>117,118</sup>. Essential histidine residues have also been described for RVFV G<sub>C</sub> and SFTSV G<sub>C</sub> proteins. Interestingly, such residues are not conserved among RVFV and SFTSV glycoproteins C. While the low pH (5,4 – 5,6) triggers the fusion of UUKV and RVFV <sup>97,100</sup>, recent data showed that other factors such as the phospholipid bis(monoacylglycero) phosphate enhanced UUKV fusion to liposomes <sup>119</sup>. Altogether, the results tend to present the endosomal pH as the major cue for phlebovirus fusion mechanisms although it is not the only element implicated. Though our understanding of phlebovirus fusion mechanisms has significantly increased in recent years, our knowledge of the process remains largely to be elucidated for other tick-borne bunyaviruses such as CCHFV or UUKV, for which crystal structures of G<sub>C</sub> are still missing. In addition, the structure of G<sub>N</sub> and its potential role in fusion remains unknown for all bunyaviruses.

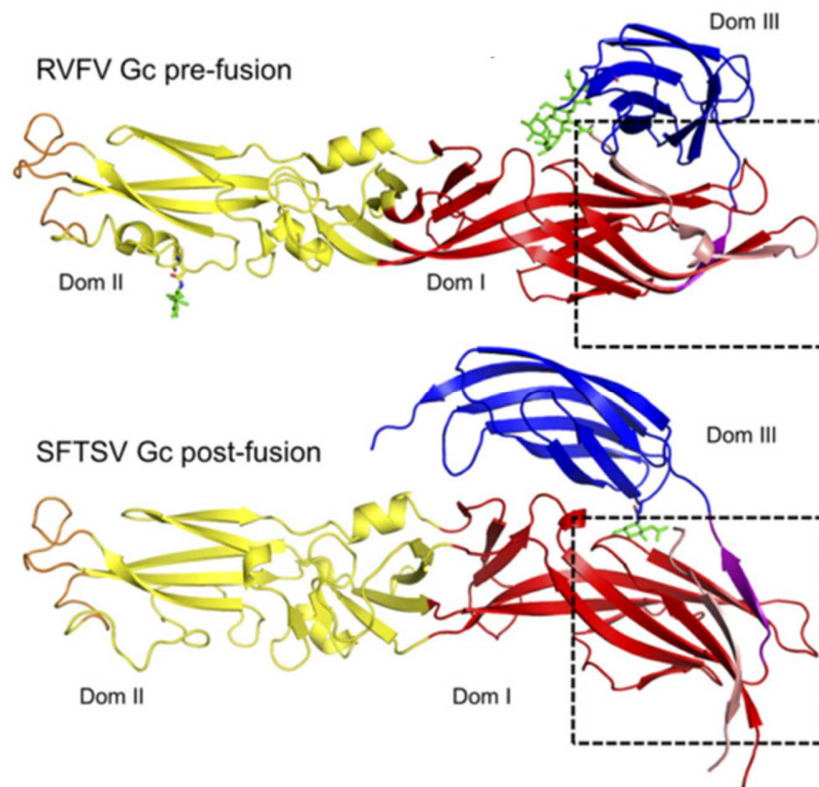


**Figure 4: Structure of phleboviral glycoprotein G<sub>C</sub>.**

Domain I is in red (Dom I), domain II is in yellow (Dom II) with the fusion loop in orange, domain III is in blue (Dom III), and glycans are shown in green. The scare (dash lines) in the domain I highlights the change between pre- and post-fusion steps with two strands (pink and purple) of the  $\beta$ -barrel that are reoriented. Adapted from <sup>113</sup>.

#### d. Replication cycle

##### i. Transcription and replication

Once the viral envelope and the endosomal membrane have fused, the RNPs are released into the cytoplasm. Like all negative sense viruses, phlebo- and bunyaviruses carry all the components they require for their replication cycle, the RNPs. Together with the N protein, the phlebovirus polymerase starts the transcription of negative-strand genomic RNA (gRNA) into mRNA by a cap snatching mechanism <sup>120</sup> that was first described for the influenza virus <sup>31,121,122</sup>. Briefly, the 5' cap of host cellular mRNA is cleaved by the endonuclease activity of the bunyavirus RdRp, translocated to the viral RNP to prime the synthesis of the viral mRNA. 12 to 18 nucleotides are needed to prime the transcription, which probably occurs via a “prime and realign” mechanism proposed for orthobunya- <sup>123</sup>. The transcription of gRNA into functional mRNA has been described

to require on-going translation. This phenomenon was shown for the S segments of RVFV<sup>124</sup> and LACV<sup>125,126</sup>. A common feature of bunyaviruses is that mRNAs lack a polyadenylated tail and are shorter than viral RNA by about 100 nucleotides<sup>4,127</sup>, therefore preventing 5' and 3' base pairing<sup>128</sup>.

While transcription results in shorter mRNA (**figure 3**), replication of the negative sense gRNA (RNA<sup>-</sup>) involves a full-length positive sense RNA copy (RNA<sup>+</sup>) that is used by the RdRp as a template in a primer-independent manner (**figure 3**). The difference probably comes from different termination signals for the transcription and the replication<sup>128</sup>. The replication mechanism has been recently elucidated by crystallization and cryo-electron microscopy of the LACV L protein together with viral RNA. The authors propose that the polymerase of, most probably, all bunyaviruses has different entry and exit tunnels for the RNA template (i.e, negative sense RNA) and product (i.e, the positive sense genome)<sup>52</sup>. However they do not comment on the switch from transcription to replication.

### ii. Assembly and release of viral particles

In mammalian cells, the assembly of tick-borne phlebovirion progenies takes place in the Golgi compartment (**figure 3**). It is driven by the folding and maturation of the glycoproteins and has been intensively characterized using UUKV as a system model. The following section is therefore mainly focused on UUKV since only few reports are available for other tick-borne bunyaviruses (CCHFV or SFTSV).

The two phleboviral glycoproteins are synthesized as a precursor of 110 kDa<sup>129</sup> that is co-translationally inserted in the membrane of the ER where it is cleaved into G<sub>N</sub> and G<sub>C</sub> by the host ER signal peptidase<sup>129-132</sup>. The proteins are then glycosylated and matured. While G<sub>N</sub> is folded in less than 10 min, G<sub>C</sub> requires an additional 35 to 50 min<sup>133</sup>. Both glycoproteins are considered as a type I transmembrane protein, the N-terminal part faces the lumen of the ER while the C-terminal part is in the cytoplasm<sup>134,135</sup>. The mature glycoproteins quickly heterodimerized in the ER, in less than 5 min for RVFV<sup>132</sup>. UUKV G<sub>N</sub> carries a targeting & retention signal for the Golgi apparatus located between amino acid (aa) 10 and 40 of the 98 aa long cytosolic tail<sup>135,136</sup>. Due to this signal, the heterodimer is transported to and accumulates in the Golgi<sup>135,137,138</sup>.

The cytosolic tail of  $G_C$  appears relatively small compare to that of  $G_N$ , with only 5 aa, but both of them are important for interaction with RNPs and for budding in the Golgi membrane<sup>56,57</sup>. Indeed, Uukuniemi viral glycoproteins accumulate in the Golgi from where newly particles are assembled<sup>139</sup>. More recently, the glycoproteins have been proposed to initiate budding by themselves, suggesting that a high concentration of  $G_N$  and  $G_C$  in the Golgi complex is required<sup>55</sup>. Though it remains matter of debate, it has been suggested that the particles reach then the plasma membrane within exocytic vesicles to exit cells<sup>139,140</sup> (**figure 3**). These steps of the life cycle of bunyaviruses remain to be thoroughly investigated.

### iii. Post-translational modifications

Both  $G_N$  and  $G_C$  are subjected to post-translational modifications that are important for the proper folding of the proteins. Cysteine residues represent approximately 4 to 7% of the amino acids in bunyavirus M segment. The number and the position of these residues are highly conserved among phleboviruses<sup>4</sup>. The number of disulfide-bond is therefore expected to be important and the formation of disulfide-bonds crucial for the proper folding of  $G_N$  and  $G_C$ . Both were found to precipitate with the disulfide isomerase, an enzyme that controls whether protein in the ER are correctly folded<sup>133</sup>. Furthermore, the two glycoproteins have been shown to interact with the chaperone binding immunoglobulin protein (BiP), the calnexin, and the calreticulin proteins, two proteins involved in protein folding in the ER<sup>133,141</sup>. These interactions highlight the importance of the folding quality control machinery in the  $G_N$  and  $G_C$  trafficking through the Golgi.

*N*-glycosylation occurs in the lumen of the ER, typically on asparagine residues of glycoproteins within a specific motif, i.e. Asn – X – Ser/Thr<sup>142</sup>. A number of reports demonstrated that *N*-glycosylations are important for both folding and function of phlebovirus glycoproteins<sup>54,79,143–145</sup>. *N*-glycosylation sites are found along the M segment of arbo-bunyaviruses although the number varies among bunyavirus isolates. SFTSV that shares 20% identity sequence with the M segment of UUKV<sup>28</sup>, is predicted to harbor two *N*-linked glycosylation sites on  $G_N$  and three on  $G_C$ <sup>89,113</sup> while four are found in both UUKV  $G_N$  and  $G_C$ <sup>54,130,146</sup>. The glycoprotein  $G_N$  of CCHFV carries *N*-linked glycans on a single asparagine residue<sup>145</sup>. Furthermore, the M segment of tick-borne nairoviruses encodes a mucin like domain that is enriched in *O*-glycosylation through the Golgi<sup>147</sup>. Overall it appears that the type of glycan is important for several steps of the phlebovirus

life cycle, including among others folding of  $G_N$  and  $G_C$ , particle assembly and interactions with receptors (e.g. DC-SIGN and L-SIGN).

### 3. The vector-host switch in the context of tick-borne bunyaviruses

The continuous expansion of CCHFV to new geographical area, together with the newly discovered human pathogen SFTSV, has raised the interest to use UUKV as a model for studying tick-borne bunyaviruses. Tick-borne viruses (TBVs) are unique in the sense they replicate in both their vector ticks and their vertebrate hosts. They developed strategies to take advantage of the cellular machinery of two different systems with diverse consequences for the vector and the host. This section will bring further knowledge to understand the alternation of organisms that a tick-borne virus will infect during its entire life cycle.

#### a. Ticks and tick-borne viruses

##### i. Biology and ecology of ticks

Ticks are not insects. They are arthropods (phylum *Arthropoda*) classified as arachnids (class *Arachnida*, subclass *Acari*). They belong to the order *Ixodida* that comprise three families: *Argasidae* or “soft ticks” and *Ixodidae* also referred as “hard ticks” because of their dorsal (hard) plate. The third family *Nuttalliellidae* is composed of a unique species, *Nuttalliella namaqua*<sup>148</sup>. Ticks are obligate hematophagous parasites present in almost every region of the world. Their life cycle is composed of several stages. After the egg molt, hard ticks undergo a three-stage life cycle - larvae, nymph and adult. Each stage requires a blood meal on host followed by the molt on the ground (**figure 5**)<sup>148–151</sup>. While some ticks are host specific, i.e., they bite the same host species for each blood meal, others can feed on distinct host species during their life time. The time of the tick life cycle is highly variable between ticks species<sup>152</sup>.

*Ixodes ricinus* (*I. ricinus*) is the most important vector of diseases in Europe <sup>153</sup> and *Ixodes scapularis* (*I. scapularis*) the most important in North America <sup>154</sup>. Their large distribution throughout the world, their ability to feed on multiple hosts and the variety of hosts make these parasites/vectors a main threat for humans and animals.

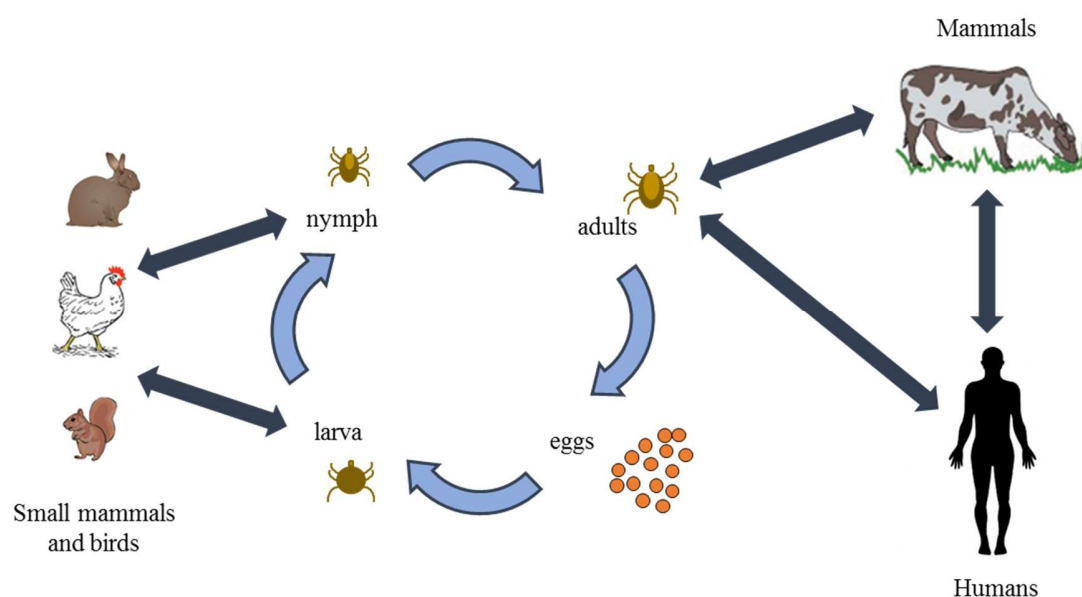


**Figure 5: Biological tick life cycle and transmission of a tick-borne viruses.**

The tick life cycle (light blue arrows) and tick-borne virus transmission based on CCHFV (dark blue arrows) are schematized. Tick-borne viruses can be transmitted at any stage of the tick life cycle. Larva and nymph preferably feed on small and adults on larger mammals. Viruses can be transmitted from the ticks to the mammals or vice-versa. Humans are infected by pathogens transmitted during tick bite or under specific circumstances by exposure to infected animals. In rare cases, human-to-human transmission (not depicted) is possible.

## ii. Tick-borne diseases

Ticks are arthropods that transmit the largest variety of human pathogens such as parasites, bacteria or viruses <sup>155,156</sup>, most of them threatening people and causing veterinary loss. Approximately 90 species of ticks are of medical or veterinary importance. These arthropods are distributed worldwide and cause a wide range of diseases <sup>157</sup>. Among them is the human granulocytic anaplasmosis, which is emerging in the United States of America (**figure 6**). The disease is caused by the obligate intracellular Gram-negative bacterium *Anaplasma phagocytophilum* (*A. phagocytophilum*). It is also transmitted to diverse domestic animals, and infects mainly neutrophils <sup>157,158</sup>. The most infamous human disease is probably the Lyme disease,

## Introduction

also identified as borreliosis. It is caused by the bacterium *Borrelia burgdorferi*, which is transmitted by tick nymphs or larvae since there is no transovarial transmission<sup>159</sup>. Following transmission to humans, which usually occurs after a long blood meal (>72hours), bacteria either remain at the bite site proximity or disseminate to different parts of the host body. The dissemination can concern many organs, causing severe complications<sup>159</sup>. Ticks also transmit the protozoa *Babesia* spp. that infect livestock in the tropical and sub-tropical areas causing a drastic reduction of milk production. *Babesia bovis* and *Babesia bigemina*, which are transmitted by *Rhipicephalus* tick species, are the main species of *Babesia* responsible for an important negative economic impact in the cattle industry<sup>157,160</sup>. TBVs and their transmission are further described in the next section.

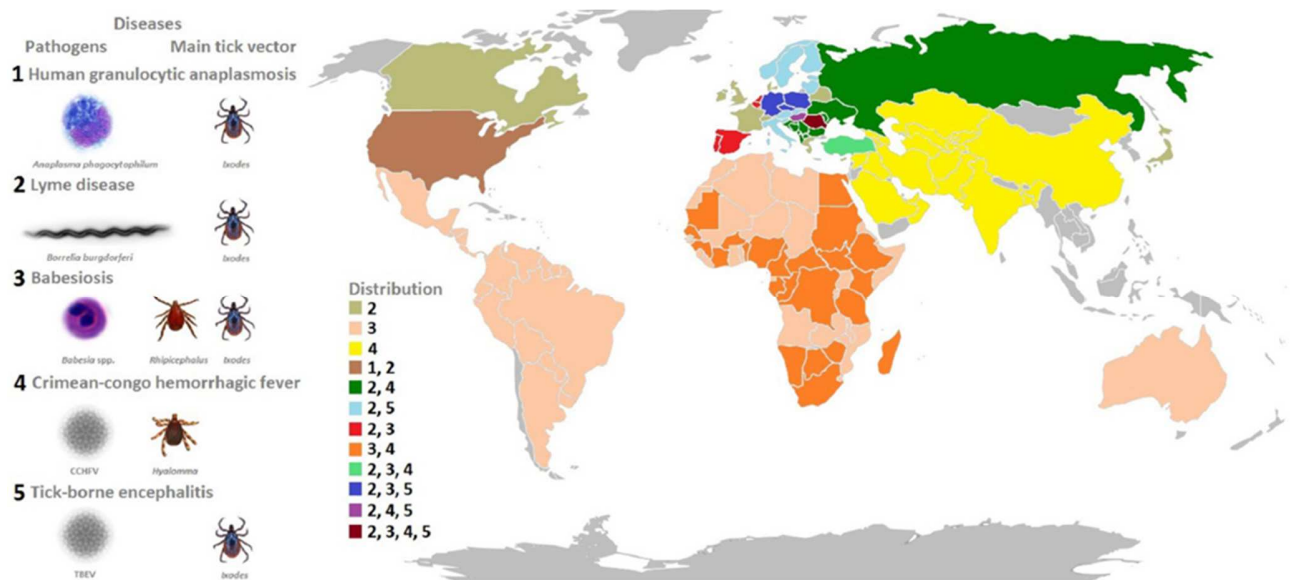


**Figure 6: Distribution of representative human and veterinary diseases transmitted by ticks.**

Bacteria *Anaplasma phagocytophilum* and *Borrelia burgdorferi* are responsible of the human granulocytic anaplasmosis and the lyme disease, respectively. Babesiosis, transmitted by the protozoa *Babesia* spp., and viral diseases such as Crimean-Congo hemorrhagic fever and tick-borne encephalitis are represented on the map as well as the main tick vectors. Map published by<sup>157</sup>.

### iii. Tick-borne virus transmission

TBVs are found in six virus families: *Asfarviridae*, *Bunyaviridae*, *Flaviviridae*, *Orthomyxoviridae*, *Reoviridae* and *Rhabdoviridae*. Except the African Swine fever virus (ASFV - reovirus), which is a double stranded DNA virus transmitted by soft ticks, all other TBVs are RNA

viruses transmitted by hard ticks <sup>150,151</sup>. The most characterized TBVs are those within the *Flaviviridae* (Tick-borne encephalitis virus: TBEV, Langat virus: LGTV, Louping ill virus: LIV) and *Bunyaviridae* (CCHFV, Nairobi sheep disease virus) families undoubtedly because of their medical and veterinary relevance.

In one hand, viruses are transmitted vertically. They can infect ticks independently on the stage of the tick development, i.e. larvae, nymph, or adult. Once infected, viruses remain in the tick animal for life meaning that the virus is transmitted from one stage to the other (**figure 5**). In the other hand, viruses can either be transmitted from infected ticks to uninfected vertebrates hosts or from infected vertebrates to naïve ticks. This is called horizontal transmission <sup>151</sup> (**figure 5**).

Viruses, such as TBEV notably, have a preferred tropism for salivary glands and oocytes. This preference results in transovarial transmission of the virus to the next progeny. Because the virus is present in the entire tick body it is spread from one stage to the other. Evidences also support a co-feeding transmission of viruses during blood meal <sup>151,161</sup>. This mode of transmission, within a same tick species, is poorly characterized.

In general, TBVs amplify in non-human vertebrates. Human-to-human horizontal transmission was thought to be rare but exists under certain circumstances like nosocomial transmission, which has been often reported for CCHFV for instance <sup>162</sup>. However, an accumulation of data suggests that human-to-human transmission of SFTSV is possible via aerosol or through contact with infected blood <sup>163-165</sup>. Transmission of TBVs from livestock to human has also been observed. This mostly happens during veterinary procedures or manipulation of dead animals contaminated by CCHFV or RVFV.

#### iv. Viral development cycle in ticks

It is commonly accepted that ticks, unlike mammals, do not show any sign of sickness or pathology following infection. This could be, at least in part, related to the inhibition of the tick apoptotic pathway in midgut and salivary gland cells as shown for *A. phagocytophilum* infection in *I. scapularis* ticks <sup>166</sup>. The inhibition of apoptosis has also been shown in *I. scapularis* ISE6 tick cells infected with *A. phagocytophilum* and in *I. ricinus* IRE/CTVM20 tick cells infected with TBEV, LIV, or *A. phagocytophilum* <sup>157,158,167</sup>. The apoptotic inhibition was demonstrated by

proteomic and/or transcriptomic analysis coupled with *in vitro* experiments. It has been suggested that TBVs use it as a strategy to enhance infection in the tick, thus survival of the pathogen. In spite of the absence of pathology in the vector, some studies have shown that the behavior of infected mosquitoes (both feeding and flying) was changed under dengue virus infection<sup>168,169</sup>. To my knowledge, whether the behavior of a tick change after infection by a pathogen has never been reported.

How a tick-borne virus replicates inside the tick is not clear, a lot need to be achieve to understand the replication cycle in tick cells and animals. The mechanisms involved, the proteins required or the pathways that viruses used to reach the salivary glands are still poorly characterized. Most of the information available so far on pathogen development cycle in ticks are coming from studies on the bacteria *Anaplasma* and *Borrelia*. The known proteins, the role of the tick cytoskeleton and tick endosymbionts as well as the inhibition of cell apoptosis during bacterial tick infections are reviewed in<sup>157</sup>. In line with the results obtained for anaplasmosis and borreliosis, one study on CCHFV suggested that after ingestion of the virus, the latter migrates to the midgut of ticks where it replicates. It subsequently disseminates in the hemolymph from where it infects several tissues<sup>170</sup>. The tick salivary gland protein (salp) 15, salp 20 and salp16 have been described as important proteins for infection of the salivary glands by *Borrelia* and *Anaplsma ssp*, respectively<sup>171</sup>. It remains unknown whether such proteins are also involved for virus spread in ticks. However, salivary glands are highly infected by TBVs. This seems to ensure the transmission and spread of the pathogen<sup>157</sup> (**figure 7**).

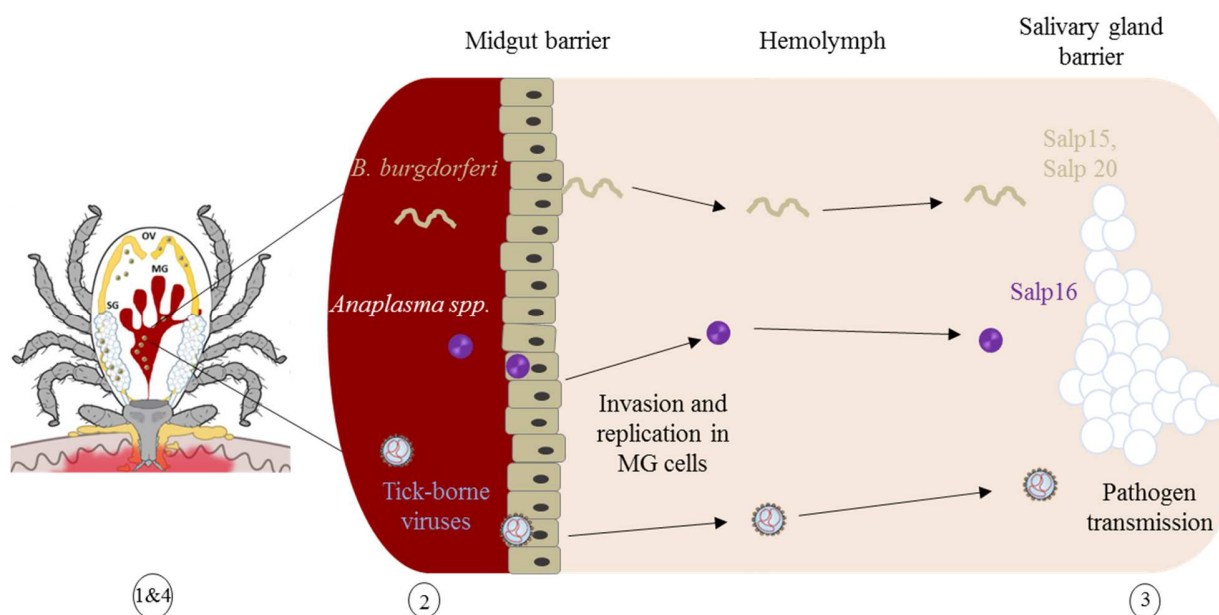


**Figure 7: The journey of tick-borne pathogens inside the tick: from acquisition to release inside the skin.**

1-Viruses and other pathogens are acquired during blood meal. 2- They replicate in the midgut (MG) that they cross to go to the hemolymph and 3- reach the salivary glands from where they are transmitted 4- to the host during the blood meal. The proteins Salp15, Salp20 and Salp16 promote bacteria entry into salivary glands. Adapted from <sup>157,171</sup>.

### b. Release of the tick-borne bunyavirus into mammalian skin dermis

Humans are usually dead-end hosts for arboviruses <sup>40</sup>. As mentioned previously, TBVs, like all arboviruses, have established a global life cycle based on host alternation in which they are maintained in their arthropod vectors and transmitted to vertebrate hosts. Viruses reach different organs in ticks, including the salivary glands from where they are injected into the mammalian skin.

The tick cell biology differs from that of mammalian cells by growing temperature, for instance. Mammalian cells grow at 37°C whereas most of the tick cells grow at 28°C, with some tolerating 32°C. Just this difference in temperature for cell culturing can impact a lot of biological processes. Unfortunately, the tick physiology and cell biology are poorly characterized. However, viruses critically depend on the cell biology of the tick to replicate, assemble the viral particles and bud from the cells. These events might leave imprint on the virions. Those characteristics are important for the infection of subsequent human target cells. One can easily imagine that different types of glycans on virion glycoproteins can result in the use of alternative human receptors, thus

changing the tropism of the virus. Similarly, the metabolism and composition in lipids and glycans may differ in ticks and mammals. This warrants to better understand the cell biology of tick-borne viruses and the host switch.

Concerning the glycosylation, “the viral particles coming from insect cells are well known to be essentially composed of mannose residues”<sup>21</sup>, whereas those produced in tick cells remain unknown. Yet, the glycosylation might impact at large the early steps of infection by vector-derived viruses in vertebrate hosts. A recent study on the non-related bunyavirus DENV has shown that depending on the producer cells (insect cells or tumor cell lines), the glycan patterns were different, which changed also the identity of targeted cells in subsequent rounds of infection<sup>172</sup>. This highlights the gap between our knowledge of the mammalian-derived and vector-derived arboviruses and reinforce the need to characterize these viruses in their vector species.

Ticks parasite their host for a much longer period of time than mosquitoes. They remain attached to the skin of vertebrate hosts for several days by firmly anchoring their mouthparts into the skin and producing a cement like structure (**figure 8**)<sup>173</sup>. During this event, two different organisms with their own characteristics enter in contact, the parasite and the host. In one hand the parasite, which creates skin damage and inflammation by invading the skin and injecting saliva; in the other hand the host that fights against it and activates immune responses. In order to complete their blood meal, ticks have developed strategies to encounter host defenses<sup>174</sup>.

Tick saliva is composed of pharmacologically active substances that have anticoagulants, immunosuppressors or anti-inflammatory effects<sup>175,176</sup>. Next generation sequencing on tick saliva have suggested that the proteome changes during the life cycle of the tick and the feeding process<sup>176</sup>. The naïve saliva of different tick species (*Ixodes* or *Richestes* ssp) has been shown to inhibit couple of immune system mechanisms. It inhibits for instance the phagocytosis of pathogens by macrophages<sup>177,178</sup>, natural killer and T cells<sup>178–180</sup>. A recent study showed that naive tick saliva inhibited DC maturation and migration *in vivo*<sup>178</sup>. The maturation of DC leads to their migration to the lymph node where the immune system gets activated<sup>181</sup>. Inhibition of the maturation and the migration of DCs by tick saliva suggest that specific immune responses are altered upon feeding of ticks.

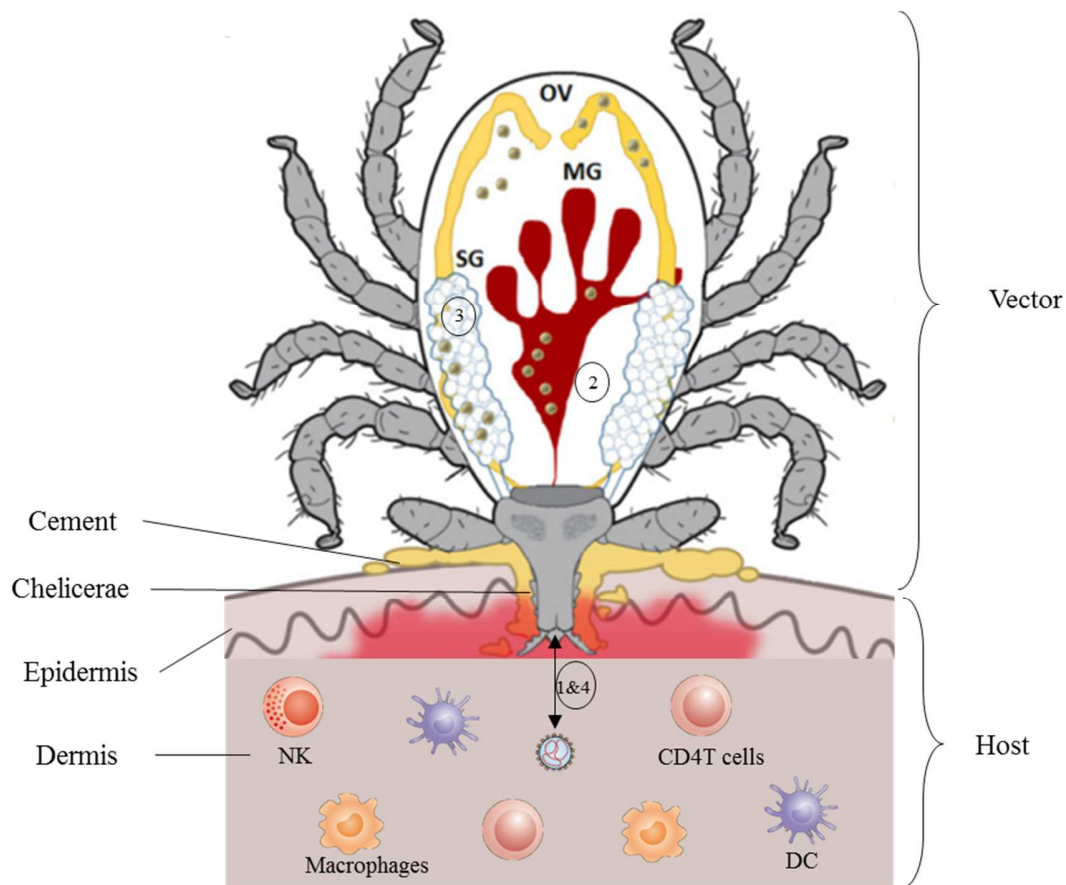


**Figure 8: Release of tick-borne viruses into the host skin dermis.**

Ticks insert their chelicerae into the skin and produce a cement like structure to firmly attach to the host. The steps 1 to 4 are described in figure 6. Viruses are delivered into the skin dermis during blood feeding where they encounter host immune cells. OV: ovaries, MG: midgut, SG: salivary gland, DC: dendritic cells, NK: natural killer cells. Adapted from <sup>157,182</sup>

While taking a blood meal, the tick does not continuously inject saliva. Yet, infected ticks introduce viruses along with saliva. TBEV has been shown to be preferentially transmitted within one hour <sup>183</sup> and Powassan virus (unrelated flavivirus) within the first three hours of feeding <sup>184</sup>. Viruses are released at the bite site in the dermis of the skin where immune cells like DCs, macrophages and T cells are located <sup>185</sup>. These cells are most likely to be the first cells to encounter the incoming viruses (**figure 8**). CCHFV has been reported to productively infect monocyte-derived DCs and monocyte-derived macrophages but not natural killers, T and B cells <sup>186,187</sup>. In addition, the tick-borne phlebovirus SFTSV might infect macrophages and monocyte-derived DCs, but the study has been conducted with rhabdoviral particles pseudotyped with the glycoproteins of the virus and not with a relevant wild type virus strain <sup>89</sup>. Phleboviruses such as UUKV and RVFV

infect human monocyte-derived DCs<sup>22,79,188,189</sup>. Finally, macrophages and DCs were involved in RVFV dissemination in mice but the animals were deficient for the interferon receptor<sup>190</sup>. Finally, studies on mosquito-borne flaviviruses DENV and WNV also support the role of DCs in the spread of arboviruses throughout the host<sup>191</sup>. Together these observations suggest a role of immune cells in arbo-bunyavirus spread throughout vertebrate hosts. However, the identity of the skin dermal cells and whether MPs or DCs are the first target cells following transmission remains to be clarified *in vivo*.

#### **4. Tick-borne phlebovirus and the host-cell antiviral response: the role of NSs protein**

Many arbo-bunyaviruses have developed strategies to evade host immune system. The arbo-bunyavirus nonstructural protein NSs has been described to interact with the vector /host immune system and to contribute to the pathogenesis in mammals. The best characterized NSs protein is that of RVFV. The NSs of tick-borne phleboviruses like UUKV has not been, yet, characterized and only few reports are available for SFTSV NSs.

Upon infection, NSs of SFTSV forms “inclusion bodies”<sup>44,192</sup> in the cytoplasm of infected cells, and that of BUNV was also found as aggregates in the nucleus<sup>193</sup>. In contrast, NSs of the mosquito-borne RVFV is found in the cytoplasm and in the nucleus where it forms filaments in both mammalian and mosquito cells<sup>194</sup>. To my knowledge, this phenotype has not been described for any other bunyaviruses. The function and formation of the RVFV NSs filaments remain unclear. The amino acid sequences similarity of NSs is low among phleboviruses, ranging from 7,5 to 28,6% when comparing the amino acid sequence identity of the Sicilian, Naples, Punta Toro, Icoaraci, and Frijoles serocomplexes with RVFV<sup>195,196</sup>. However, it seems that they all play a role in the virus escape of antiviral host cell responses that are briefly discussed in the following section.

##### **a. Interferon signaling pathway upon viral infection**

The mechanisms that regulate mammalian host defense against viral infection are complex and involve hundreds of cellular factors and pathways. One of the first line of defense against viral infection is the type I interferon response, the activation of which results in production of cytokines

such as IFN $\alpha$  and IFN $\beta$  that in turn promote the expression of IFN-stimulated genes (ISGs). Briefly, type I IFN antiviral response is initiated upon recognition of pathogen-associated molecular patterns (PAMPs), which are typically foreign antigens originating from bacteria, parasites, and viruses. They include among others bacterial lipopolysaccharides or viral DNA and RNA, such as double stranded RNAs (dsRNAs) that are produced during virus replication. PAMPs are recognized by cells via pattern-recognition receptors (PRR). There are two type of PRR: the membrane associated and the cytosolic PRR. For instance, the Toll-like receptors (TLR) are PRRs associated with plasma and organelle membranes whilst the protein kinase R (PKR), a serine-threonine kinase that senses dsRNAs, and the retinoic acid-induced gene 1 (RIG-I)-like receptor (RLR) are cytosolic PRRs. RIG-I and the melanoma differentiation-associated protein 5 (MDA5) are arguably the best documented cytosolic PRRs<sup>197,198</sup>. Membrane-associated and cytosolic PRRs together trigger the innate immune response against virus infections. The signaling cascade involves the recognition of the IFN  $\alpha/\beta$  receptor (IFNAR) 1 and IFNAR 2 that subsequently activates the phosphorylation of STAT1 and STAT2 proteins. This step is critical for the transcription of ISGs<sup>198–200</sup>. An illustration of antiviral process initiated by TLR3, RIG-I and PKR and resulting in the IFN response is shown in **figure 9**. For a more complete picture on host defense mechanisms and IFN response, I recommend the book Cellular and Molecular Immunology<sup>201</sup>.

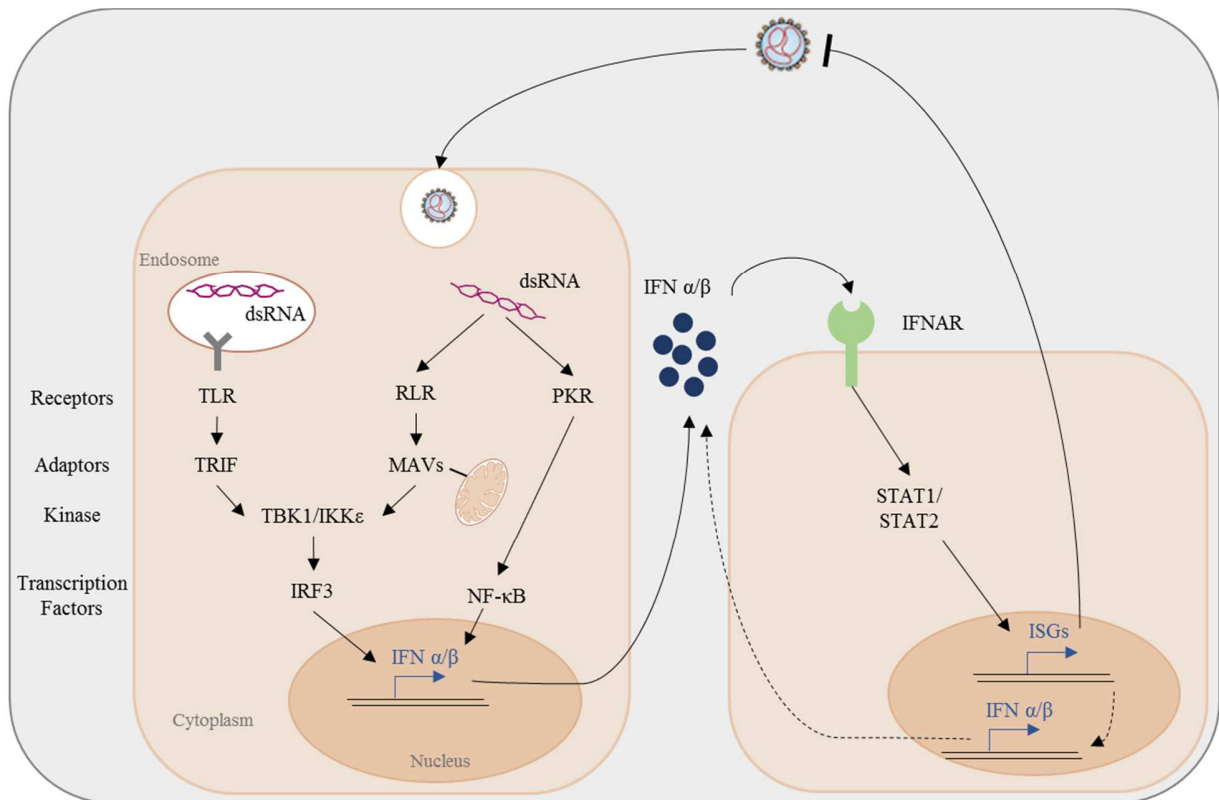


**Figure 9: Representation of type I interferon response in mammalian host cells.**

RNA viruses produce double stranded RNA (dsRNA), an intermediate of the virus replication process. These dsRNA are recognized by different receptors such as the Toll-like receptors (TLR), RIG-I-like receptor (RLR), and the protein kinase R (PKR). The recognition by the receptors TLR and RLR activates adaptor proteins such as the Toll-interleukin 1 receptor domain-containing adapter-inducing IFN- $\beta$  (TRIF) or the mitochondrial antiviral signaling (MAVs). Both TRIF and MAVs activate the Tank-binding kinase 1 (TBK1) and the inhibitor of kappa B kinase epsilon (IKK $\epsilon$ ). These kinases mediate activation of the IFN regulatory factor 3 (IRF3) while PKR mediates activation of the nuclear factor kappa-light-chain-enhancer of activated B cells (NF- $\kappa$ B). These two transcription factors induce the production of IFN that bind to the IFN receptor (IFNAR). Then the activation of STAT1 and STAT2 follows and results in an increase of IFN and ISG expression. Altogether the type I response aims to inhibit viral infection.

### b. NSs antagonizes interferon response in mammalian cells

While RVFV innate immune response has been extensively studied, a limited number of information is available for tick-borne bunyaviruses. Nevertheless, several groups have shown that SFTSV NSs inhibits INF- $\beta$  promoter<sup>192,199,202,203</sup>. SFTSV NSs forms “viroplasm-like structures”<sup>44</sup> in which multiple components of the RIG-I signaling pathway are sequestered. Indeed, TBK1 and IKK $\epsilon$  were shown to interact with NSs and relocate in inclusion bodies<sup>192,202</sup> first described as “viroplasm-like structures”<sup>44</sup>. Others showed that NSs also interacts with TRIM25, RIG-I, and IRF3 to inhibit the INF response<sup>203</sup>. Moreover, SFTSV NSs has been shown to hijack the

transcription factors STAT1 and STAT2 that are also relocated in inclusion bodies. In turn this inhibits the entire signaling pathway of IFN response<sup>204</sup>. While any biological function has thus far been reported for HRTV NSs, UUKV NSs might also inhibit IFN response, though this remains a matter of debate<sup>205</sup>. It is apparent that many bunyaviruses interfere with the IFN response targeting and blocking the activity of PKR. When activated, PKR phosphorylates the  $\alpha$  subunit of the eukaryotic initiation factor 2 (eIF-2), thereby preventing the translation of mRNA<sup>198</sup>. Unlike PTV, RVFV and TOSV induce the degradation of PKR<sup>206</sup>. The degradation of the kinase was first shown to be NSs dependent<sup>207</sup>. Recently, the F-box protein 11 FBXW11 was identified as a cellular partner of NSs that mediates PKR degradation<sup>208</sup>.

RVFV NSs protein is the best documented among arbo-bunyaviruses. NSs is believed to be the main viral determinant of RVFV virulence. RVFV Clone 13, a naturally-attenuated strain that has a deletion of approximately 70% of the NSs ORF, presents a strong attenuation for the virulence. This mutant induced INF  $\alpha/\beta$  production whereas wild-type RVFV (e.g. strain ZH548) was shown to block it<sup>209,210</sup>. In agreement with these results, mice infected with NSs Clone 13 strain survive to infection but not those injected with RVFV strain ZH548<sup>207,211</sup>. Although it was shown in this study that NSs repressed the type I IFN promoter, transcription factors that regulate IFN production (including IRF-3, NF- $\kappa$ B and AP-1) were not inhibited<sup>210</sup> (**figure 10**). In addition other studies have demonstrated that RVFV, through NSs, modulates the general host transcription machinery<sup>43,198</sup>. Indeed, NSs prevents the formation of the transcription factor II H (TFIIH) complex through interactions with the subunit p44, which leads to a decrease of cellular mRNA synthesis<sup>212</sup>.

RVFV NSs also targets and binds to the p62 subunit of the TFIIH complex, through a  $\Omega$ XaV motif located in the C terminal region of the nonstructural protein. This interaction, together with the F-box protein FBXO3, results in the proteasomal degradation of p62 and consequently in a general block of cellular transcription<sup>213–215</sup>. The NSs protein of RVFV has also been shown (1) to inhibit IFN  $\beta$  promoter by interacting with a transcriptional suppressor complex [that contains Sin3A associated protein 30 (SAP30)<sup>216</sup>] and (2) to block nuclear mRNA export in infected cells<sup>198</sup>. It has been proposed that other dipteran-borne phleboviruses, PTV and sandfly fever Sicilian virus, are able to inhibit host transcription but the mechanisms still remain to be uncovered<sup>206</sup>. In

## Introduction

contrast, the NSs protein of TOSV, which also antagonizes INF response, has not been shown to perturb host transcription<sup>217,218</sup>.

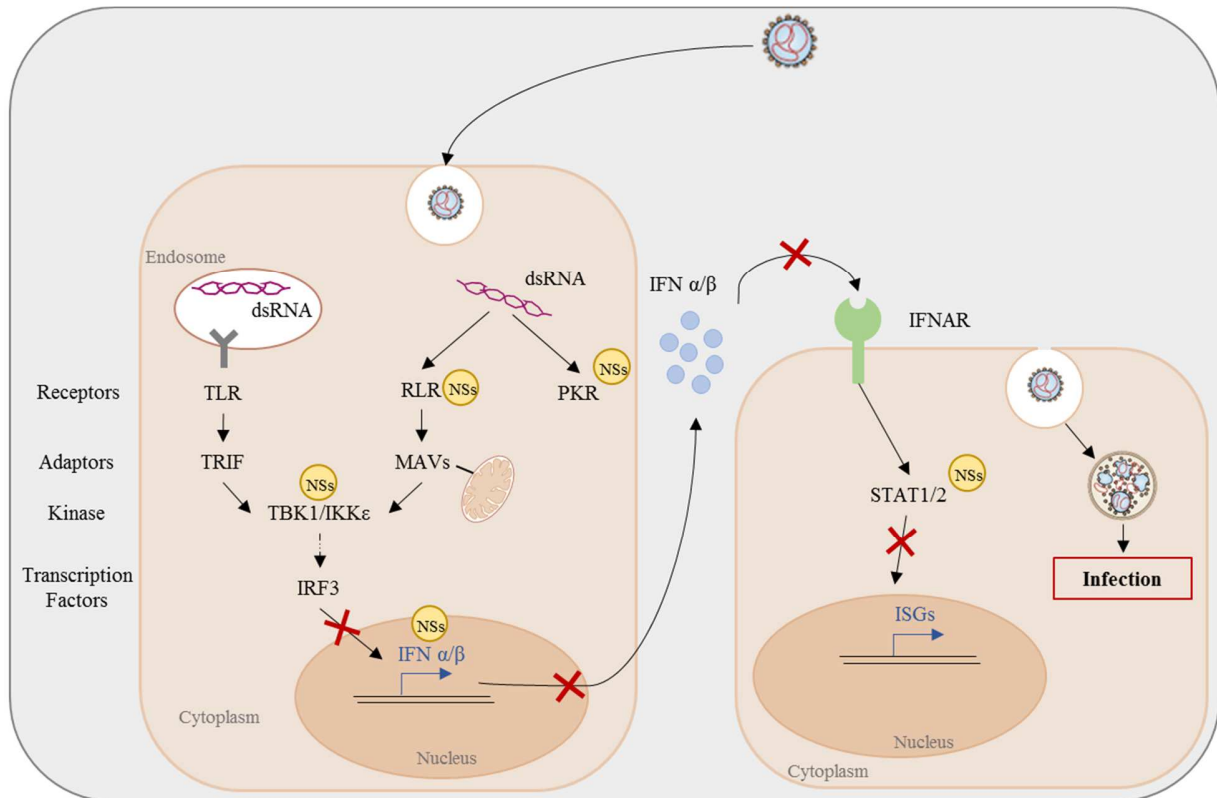


**Figure 10: Schematic representation of type I IFN inhibition by the nonstructural protein NSs of phleboviruses.** NSs acts at different levels both in the cytoplasm and in the nucleus. It binds to receptors, kinases or directly on the IFN promoter to inhibit the production of cytokines and signaling.

Despite a low conservation of its amino acid sequence, the overall function of the nonstructural protein NSs remains similar among phleboviruses, i.e. mainly consisting in antagonizing the IFN response.

### c. RNA interference in vector cells

In stark contrast to mammalian hosts, arthropod vectors do not have IFN-based immune response. Mosquitoes and flies mainly rely on RNA interference (RNAi) as antiviral response<sup>219</sup>. However, vertebrates also use RNAi as a defense mechanism. RNAi is a regulatory process

conserved among eukaryotes, which has first been identified in plants [recent review <sup>220</sup>] and well characterized in *Drosophila* <sup>221</sup>.

### i. RNAi mechanism

RNAi is, in fact, a mechanism that involves 3 pathways, all mediated by small RNAs (20 to 30 nucleotides in length) <sup>222</sup>. The best characterized pathway relies on small interfering RNAs (siRNA), the two others rely on microRNA (miRNA) and piwi-interacting RNA (piRNA) <sup>222</sup>. Mosquitoes and other insects such as *Drosophila* make use of all the three pathways. In ticks, only siRNA-mediated silencing of viral genes have been assessed. While this suggests that RNAi exists in tick cells, the details of the mechanisms and cellular players behind remain to be uncovered.

Briefly, RNAi targets dsRNA structures that are generated by secondary structures of viral RNA genome or intermediates of replication, for instance. In *Drosophila* and mosquitoes, dsRNA are recognized by the dsRNA-specific endoribonuclease III, Dicer-2, that cleaves them into virus-derived small interfering RNA (viRNA) of 21 nucleotides in length (**figure 11**). viRNA are then taken up by the RNA-induced silencing complex (RISC) whose the Ago-2 protein initiate mRNA degradation and protein downregulation <sup>220,222–224</sup>. A deletion of RNAi pathway has been shown to increase viral production in mosquito cells <sup>225</sup> and lethality rate in mosquitoes <sup>226</sup>. To counteract this pathway, plant-infecting viruses express an RNA silencing suppressor (RSS) proteins. Insect-specific viruses have developed similar strategy, though the viral protein responsible for silencing suppressor are not well characterized <sup>223</sup>. For more details about the molecular mechanisms and cellular factors that regulates and promotes RNAi, I recommend recent review <sup>222</sup>.

In 2016, Gulia-Nuss and colleagues have identified and annotated a number of genes in *I. scapularis* with functions related to immune defense mechanisms (Gulia-Nuss et al. 2016, supplementary table 17). A recent study indicates that RNAi-mediated response exists in ticks but shows differences with that in mosquitoes <sup>227</sup>. Hazara virus, a tick-borne nairovirus closely related to CCHFV, induces a RNAi response in *I. scapularis*-derived cells <sup>228</sup>. However it appears that siRNAs in mosquitoes and ticks differ in length, 21 versus 22 nucleotides respectively (**figure 11**). Others studies suggest that RNAi mechanisms are conserved in tick cells, involving proteins

analogous to those previously described in insects, vertebrates, and plants<sup>229,230</sup>. The molecular mechanisms of RNAi remain to be firmly uncovered.

Our knowledge of bunyavirus-arthropod immune system interactions is better documented for non-tick-borne bunyaviruses. RVFV has been shown to trigger mosquito immune response through the RNAi pathway. Indeed, in mosquito cell line that are competent for RNAi, NSs protein is targeted and lead to the clearance of nuclear NSs filaments. However, in incompetent RNAi mosquito cell line (C6/36 cells)<sup>231</sup> NSs is still expressed and filaments visible in the nucleus<sup>194</sup>. That NSs is targeted by arthropod RNAi immune response most likely allows the virus to develop persistent infection in arthropod cells as suggested by Léger et al.<sup>194</sup>. Similarly, BUNV and SBV have been shown to induce a RNAi response in mosquito and *Culicoides*-derived cells<sup>232</sup>.

### **ii. Viruses counteract arthropod immune system**

Though arthropods possess antiviral response mechanisms, it is established that arbovirus infection in arthropods is persistent and nonpathogenic. Thus, arboviruses must have built a strategy to replicate in the vector without killing it by developing tools to evade vector immune system; as a balance between arthropod survival and arbovirus replication<sup>222,224</sup>.

A recent report suggests that LIV infection, but not TBEV infection in IRE/CTVM20 cells (*I. ricinus* species), induces the upregulation of genes encoding the FK506 binding proteins (FKBP) and the X-box binding protein 1 (XBP1)<sup>167</sup>. FKBP are a large family of proteins that trigger immunosuppression; their detailed functions are described in the following review<sup>233</sup>. XBP1 is a transcription factor that regulates the transcription of multiple genes and is involved in B cells differentiation of antibody-secreted plasma cells<sup>234,235</sup>. Together this supports the view that LIV infection might trigger an antiviral response in tick IRE/CTVM20 cells<sup>167</sup>. Moreover, silencing of the tick heat-shock protein HSP70 and HSP90 increased both the mRNA level and the production of LGTV particles in IDE8 cells<sup>236</sup>, suggesting that HSP70 and HSP90 could be implicated in the siRNA pathway and are restriction factors of LGTV infection in tick cells<sup>236</sup>. The silencing of these proteins was however not efficient in another tick cell line (IRE/CTVM19).

While few is known about the RNAi antiviral mechanisms in tick cells, more and more reports use the power of siRNA or short hairpin RNA (shRNA) to study the role of proteins during

viral infection in tick cells<sup>227,237</sup> and correlate the phenotype with the sequence to annotate the genome of ticks<sup>171,237,238</sup>. Whether bunyaviral proteins, such as NSs, play a role in the antiviral mechanism in ticks is still an open question; to my knowledge, it has never been mentioned.

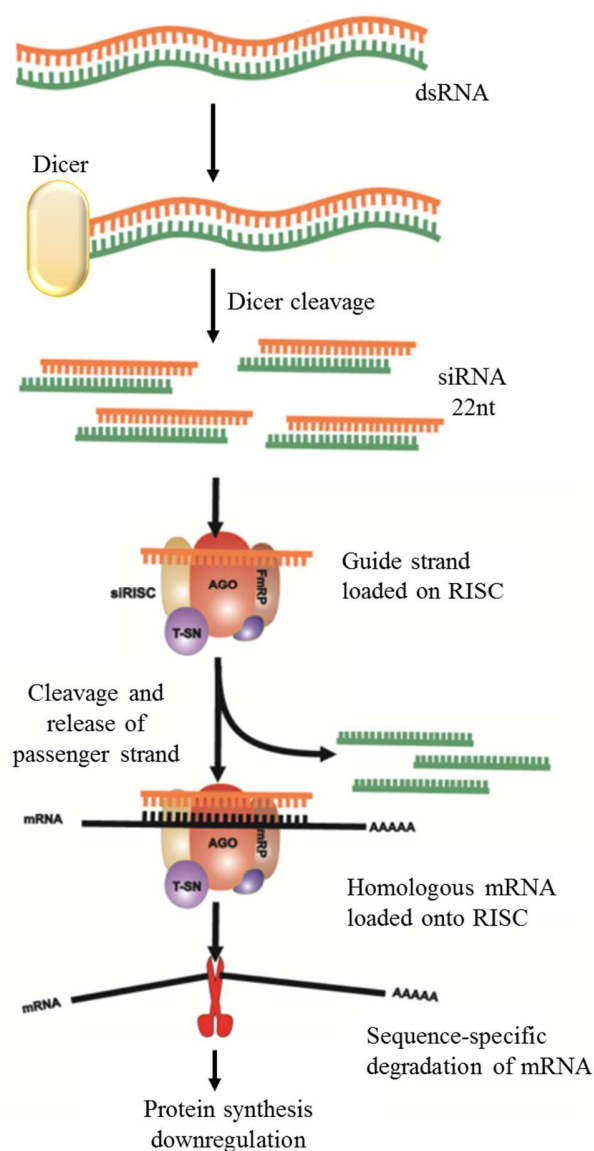


**Figure 11: Proposed RNA interference mechanism in ticks.**

Viral dsRNA are processed in siRNA of 22 nucleotides in length by a Dicer homologue protein. siRNA are incorporated into the RISC complex that mediates cleavage of the two strands. The guide strand allows recognition of cytoplasmic mRNA that are then degraded. This leads to the downregulation of encoded proteins. Adapted from<sup>238</sup>.

## Aim of the project

Bunyaviruses are emerging viruses causing worldwide outbreaks in humans and livestock. In 2009, new tick-borne viruses related to Uukuniemi virus were discovered in the United States of America and China, namely Heartland virus and severe fever with thrombocytopenia syndrome virus (SFTSV). The latter is highly pathogenic for humans, causing thrombocytopenia, gastrointestinal symptom or central nervous system manifestation. The fatality rate reaches 30%, and, during outbreaks, human-to-human transmission has been reported. No vaccines are available and no treatment allow the cure of the associated diseases. Transmission, cell entry as well as tropism and propagation within human hosts are poorly characterized and remain largely uncovered.

Previous studies on early tick-borne bunyavirus-host cell interactions have been carried out with viruses produced in mammalian cells. The molecular characteristics of arthropod-derived viruses are, so far, still missing to understand the first interactions between vector-derived viruses and mammalian host cells (**figure 12**). Dendritic cells are believed to be the first target cells after arbovirus infection, albeit it has not been formally established *in vivo*. Most of the studies are based on *in vitro* models, out of the physiological context. Moreover, the biology of tick and tick cells is poorly characterized although it can impact at large the lipidome and glycome of viruses.

The overall goal of my PhD project is to understand early tick cell-derived virus-mammalian host-cell interactions. My central hypothesis is that mammalian host cells are more sensitive to infection by viruses originating from tick cells than those produced in mammalian cells. To this end, I used the tick-borne phlebovirus UUKV as a model system to 1) investigate the molecular differences between tick and mammalian cell-derived viruses and to 2) recapitulate the tick-mammal switch *in vitro* presented in **figure 12**.

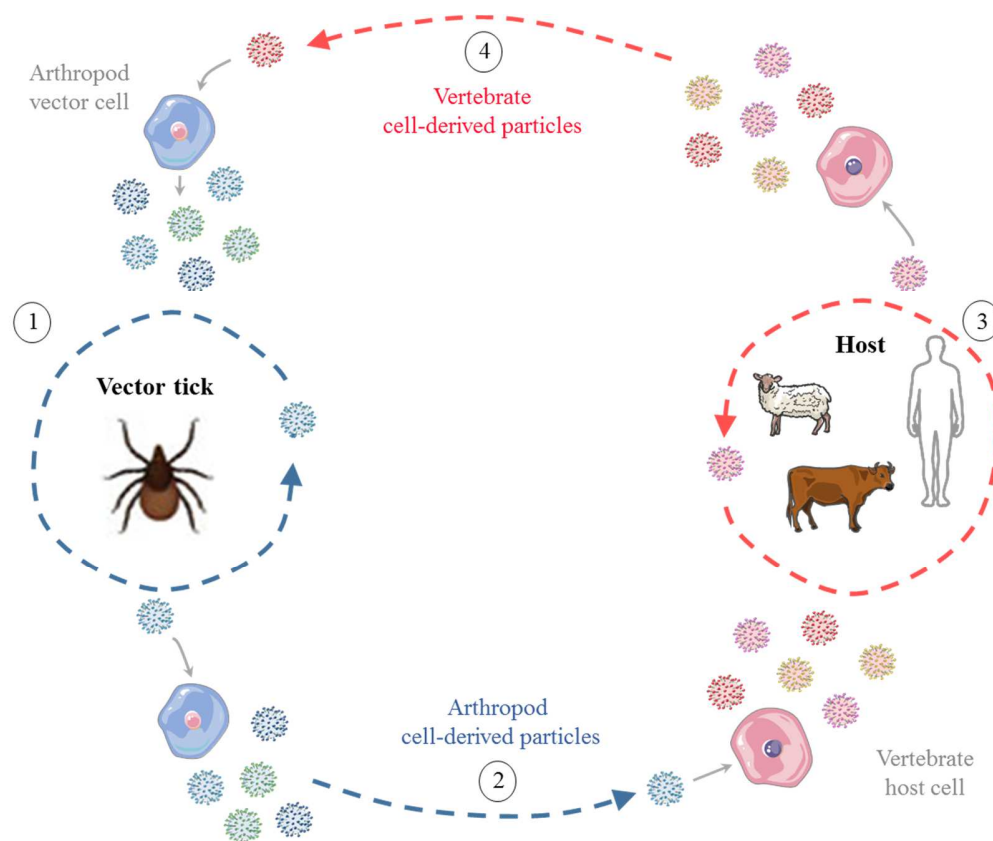


**Figure 12: Alternation of hosts during a tick-borne virus life cycle.**

Tick-borne viruses are amplified in ticks (1) in which they acquire specific molecular features before the transmission to mammals (2). Viruses then replicate in mammals (3) and acquire new features. They are eventually transmitted to ticks (4). The diversity and differences acquired in arthropod vectors and mammalian hosts are represented by blue and red colors respectively. Adapted from <sup>21</sup>.



## Results

### 1. Reverse genetics system of UUKV

#### a. The system used for this study

The UUKV used in our laboratory is derived from the prototype tick isolate UUKV strain 23 (UUKV S23), a virus isolated in 1959 from the tick *Ixodes ricinus*. UUKV S23 was plaque-purified five times in chicken embryo fibroblasts and then amplified in BHK-21 cells<sup>239,240</sup>. The S, M, and L segments of UUKV were sequenced prior to the development of the reverse genetics system. The nucleotide sequences of the S, M and L segments were then compared between the lab stain UUKV and UUKV S23 (NCBI reference sequences NC\_005221.1, NC\_005220.1, and NC\_005214.1 respectively). Few mutations were found in the L and M segments of UUKV; none in the S segment. The only mutation that was conserved over the entire genome is a non-silenced substitution (A2386G) located in the M transcript of the virus (**figure 13**)  
49,146,241.

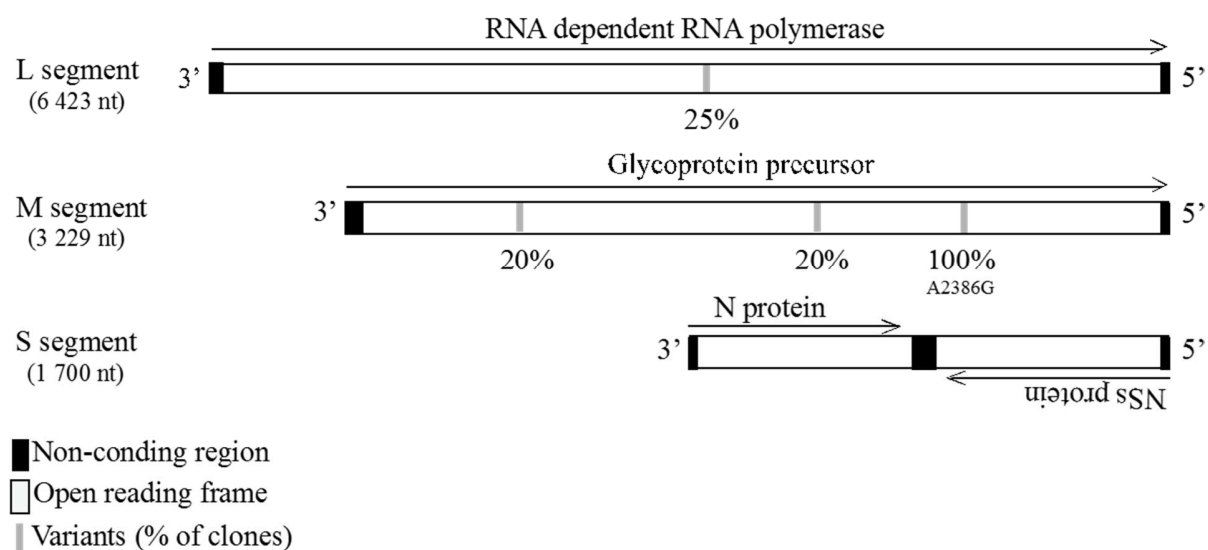


**Figure 13: Representation of mutations found in the laboratory strain UUKV compared to the reference strain UUKV S23.**

Clones of UUKV passaged several times in mammalian cell culture were sequenced, and each segment was compared to those of UUKV S23. Variants are shown as the percentage of the total clones analyzed.

## Results

We took advantage of early studies on UUKV M segment and on RVFV reverse genetics system to develop our system, which relies on the cellular polymerase I (pol I) promoter<sup>70,72,242</sup>. Viral RNA was extracted from purified stock of UUKV and reverse transcribed using specific primers for each segment (**table 16**). After amplification, the anti-genomic full-length segments S, M, and L from UUKV were cloned into the vector pRF108, which contains the murine pol I promoter and terminator and allows the synthesis of viral transcripts (**figure 14**). From the plasmids coding for the genome of UUKV, it was possible to obtain all the segments encoding the original UUKV S23 with only one point mutation (G2386A in the M segment). This reversion leads to the addition of an arginine instead of a glutamine at position 276 in the sequence of the glycoprotein G<sub>C</sub>. Hereafter, UUKV refers to our laboratory strain, as described above.

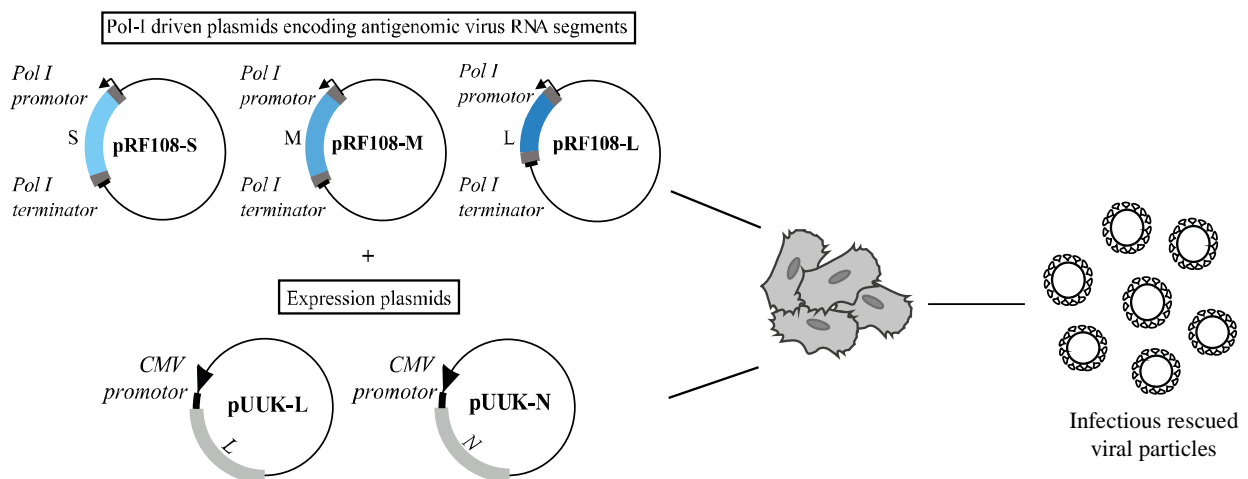


**Figure 14: Schematic representation of the polymerase I driven reverse genetics used to rescue UUKV from plasmids.**

Antigenomic full length segments were cloned into pRF180 vector and were co-transfected in BHK-21 cells, together with two expression plasmids, to allow transcription and replication.

The plasmids that are delivered into the BHK-21 cells code for double stranded DNA fragments, which correspond to the antigenomic, positive-sense RNA sequences of UUKV. Thus, the viral polymerase is required to initiate replication and produce genomic, negative-sense RNA as well as to instigate transcription. The N protein is also required to protect the viral genome. As it would not yet be synthesized, the nucleotide sequences encoding for the N and L proteins were

cloned into an expression plasmid under the cytomegalovirus (CMV) promoter and co-transfected in BHK-21 cells. The complete system is depicted in **figure 14**.

#### **b. The recovery viruses from Pol-I driven plasmid DNA**

As there was no evidence that tick cells would support transfection and murine Pol I activity, viruses were first rescued in BHK-21 cells that are highly permissive to most bunyaviruses. We first attempted to rescue UUKV and UUKV S23, referred as rUUKV and rUUKV S23, respectively, from plasmid DNA. These two viruses differ by a single nucleotide that we used as a genetic marker to confirm the specificity of the rescued viruses with our RGS. The pRF108-S, pRF108-M or pRF108-MS23, pRF108-L, pUUK-N, and pUUK-L were all transfected together in BHK-21 cells (**figure 14**). A sample of the supernatant was harvested every day until cytopathic effects (CPE) were observed, typically five days post transfection. Supernatants were titrated using a foci-forming assay (FFA). Infectious particles were detected for both rUUKV and rUUKV S23. The focus formation as well as the shape of the foci were similar to those of UUKV, as shown in **figure 15A**. Whereas no infectious progeny was detectable after transfection (D0), the titer increased for both rUUKV S23 and rUUKV after 5 days, to a thousand or a hundred thousand focus forming units (FFU) per milliliter, respectively (**figure 15B**). These results indicated that viruses can be recovered from plasmid DNA in BHK-21 cells.

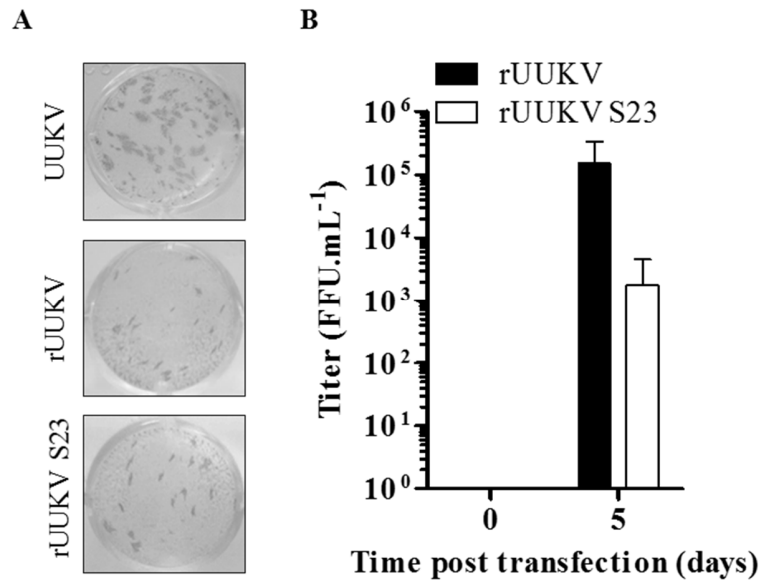


**Figure 15: Recovery of UUKV from plasmid DNA.**

(A) Titration of UUKV lab strain, rUUKV, and rUUKV S23 after five passages in BHK-21 cells by focus-forming assay (FFA). BHK-21 cells were infected with 0.8% CMC (similar to agar) for 3 days at 37°C and foci were immunostained with the rabbit polyclonal antibody U2. (B) rUUKV and rUUKV S23 production five days post transfection of BHK-21 cells with the plasmids expressing the S, M or M S23, and L segment under the control of the Pol I promoter, together with the pUUK-L and pUUK-N that express the N and L proteins of UUKV.

### c. rUUKV and rUUKV S23 characterization

The genetic marker of our system (A2386G substitution) was then used to assess the genome stability of rescued viruses, and therefore, to demonstrate the reliability of our reverse genetics system after passaging viruses in BHK-21 cells multiple times. To this end, supernatant of transfected cells (passage 0 = P0) was used to infect BHK-21 cells at an MOI of 0.01. The supernatant of infected cells (passage 1 = P1) was harvested when CPE was observed. The supernatant was next cleared and titrated by FFA. The P1 supernatant was used to infect BHK-21 cells again, and the process was repeated 5 times, until passage 5 (P5) was achieved. Both rUUKV and rUUKV S23 produce thousands of infectious particles after transfection (P0), but titers significantly increased after two passages to reach a production plateau of 10<sup>7</sup> FFU.mL<sup>-1</sup> (figure 16A), which is typical for UUKV<sup>79,100</sup>.

Using the genetic marker, sequences of rUUKV and rUUKV S23 were aligned. Total mRNA was extracted from purified viruses, passage 4 and 5, through a 25% sucrose cushion. The M segment was reverse transcribed using the specific primer RT-M-segment (**table 16**). A 391 bp DNA fragment was amplified by PCR using primers that flank the reversion site, and was sequenced and aligned. Aligned sequences, as seen in **figure 16B**, showed that after the fifth passage, rUUKV has a G nucleotide at position 2386, whereas rUUKV S23 has an A nucleotide. This sequence matches the sequence of our UUKV lab strain and the prototype UUKV S23, respectively. These results show that our reverse genetics system is reliable and can be used to rescue UUKV. Additionally, it shows that rescued UUKV and UUKV S23 are genetically stable in BHK-21 cells after 5 passages.

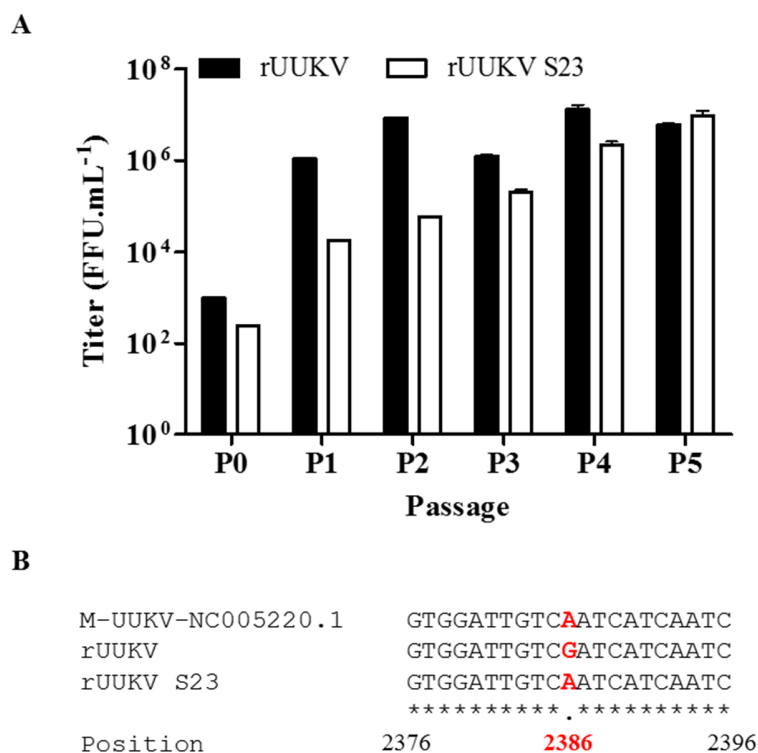


**Figure 16: Genetic stability of rescued viruses.**

(A) Titration of supernatant of transfected (passage 0 = P0) or infected BHK-21 cells after several passages (Px = passage x) with rUUKV or rUUKV S23 using FFA, as described in figure 15. (B) Sequence alignment of rUUKV S23 M segment compared to that of rUUKV and the reference strain UUKV S23 (NC005220.1 accession number). Total RNA was extracted from purified viruses through a 25% sucrose cushion after five passages in BHK-21 cells and reverse transcribed before amplification of a 391 bp using primers spanning the reversion site (bold, red).

#### d. rUUKV behave like UUKV in mammalian cells

The BHK-21 cells allowed the replication and production of viruses recovered from plasmid DNA. However, these results raised some questions: are the replication, the production, and the viral proteins of rUUKV and rUUKV S23 similar to those of UUKV? To answer these questions, I performed kinetics of replication and production and further analyzed viral proteins by immunoblotting.

Rescued viruses were purified through a 25% sucrose cushion and were subjected to SDS-PAGE under non-reducing conditions and Western blot analysis with the rabbit polyclonal antibodies U2. These antibodies recognize all three major structural proteins, namely N, G<sub>N</sub>, and G<sub>C</sub>. As shown in **figure 17A**, three structural proteins are observed at the same molecular weight for both rUUKV and UUKV. Specific mouse monoclonal antibodies against N, G<sub>N</sub>, and G<sub>C</sub> were then used to confirm the specificity of each protein. As indicated in **figure 17B**, these viral proteins were observed for both rUUKV and UUKV at the same molecular weight. These results show that three of the four structural proteins of the rescued viruses seem to be similar in terms of molecular weight and antigenicity. The viral RNA-dependent RNA polymerase L is poorly immunogenic and no antibodies are available, and thus was not detected in this experiment.

We next studied viral infection using the same mouse monoclonal antibodies in a flow cytometry based assay. The three structural proteins described before were detectable for both viruses after 24 hours of infection (**figure 17C**). The N protein was the most abundant viral protein in infected cells. Consequently, it was then used as a readout to analyze viral replication in BHK-21 cells. To this end, cells were infected at MOIs from 0.1 to 10, harvested at different time points, and immunostained for the N protein after permeabilization of the cell membranes. The kinetics are presented in **figure 17D**. As expected, rUUKV and UUKV replications are similar, and independent on the MOI. A plateau is reached after 18 hours for the higher MOI and after 48 hours for the lowest MOI. At an MOI of 0.1, 50% of cells were infected after 24 hours, whereas at an MOI of 10, 6 hours are needed. Input virus was removed after exposure to the cells, and the proportion of infected cells over time increased, which emphasized that viral replication was quantifiable.

To monitor production of viral particles, BHK-21 cells were infected at an MOI of 0.1 for one hour. The medium was then replaced by fresh medium to allow the quantification of newly synthesized infectious particles. After 24 hours, about  $10^4$  FFU per milliliter were produced for both UUKV and rUUKV, and increased significantly to reach a plateau of  $10^7$  FFU.mL<sup>-1</sup> at 48 hours post infection. The titers underwent a further 10-fold increase from 48 to 72 hours post-infection, correlating with a strong CPE (**figure 17E**). These results show that UUKV and rUUKV present a similar production kinetic.

Altogether, these results indicate that the rescued viruses in mammalian cells behave similarly to the lab strain in terms of infection, replication, and progeny production. The reverse genetics system we implemented for UUKV can be confidently use to assess the viral life cycle of tick-borne phleboviruses in vector tick cells.

## Results

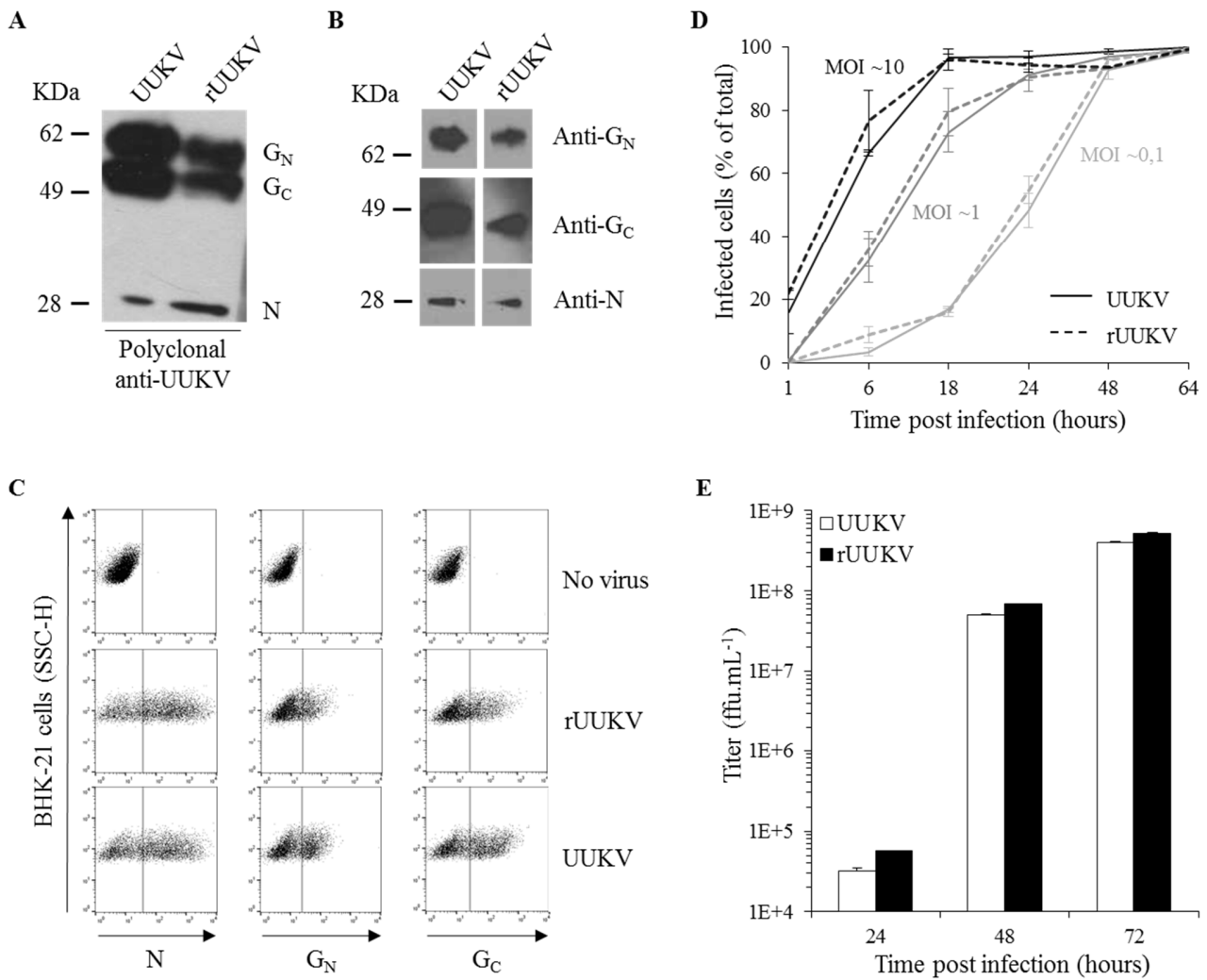


**Figure 17: Characterization of UUKV rescued from plasmids.**

The UUKV lab strain and rUUKV were analyzed by SDS-PAGE and Western blot under (A) reducing conditions using the rabbit polyclonal antibody U2 against the three structural viral proteins N,  $G_N$ , and  $G_C$ , or (B) under non-reducing conditions with the mouse monoclonal antibodies 8B11A3, 6G9E5, and 3D8B3 that recognize each of the structural proteins N,  $G_N$ , and  $G_C$ , respectively. (C) BHK-21 cells were exposed to the UUKV lab strain or rUUKV at a MOI of 0.1 for 24 hours. After fixation and permeabilization, infected cells were immuno-stained for N,  $G_N$ , and  $G_C$  with the mouse monoclonal antibodies 8B11A3, 6G9E5, and 3D8B3, respectively, and analyzed by flow cytometry. (D) Infection of BHK-21 cells by UUKV and rUUKV was monitored over 64 hours using the flow cytometry-based assay used in C. Infection is given as the percentage of N protein-positive cells. (E) Supernatants collected from cells infected at a MOI of 0.1 at indicated times were assessed for the production of infectious viral progeny by focus-forming assay.

## 2. Tick cell lines IRE/CTVM19 and IRE/CTVM20: the proof of concept

This part of the work is focused on the characterization of UUK viral particles produced from vector tick cells with the ultimate goal to recapitulate the host switch transition.

### a. Tick cells are persistently infected

We characterized tick cell-derived rUUKV S23 because we wanted to mimic what naturally happens when the virus is transmitted from the ticks to mammals with a virus that is genetically closer to those circulating. This ensures we are as close as possible to the natural life cycle of a tick-borne phleboviruses.

IRE/CTVM19 and IRE/CTVM20<sup>243</sup> were obtained from the Tick Cell Biobank at the Pirbright Institute, United Kingdom. They are non-clonal cells produced from crushed embryos of *I. ricinus* ticks, the species from which UUKV strain 23 was first isolated. First, we assessed whether tick cells support infection. To this end, they were infected with the BHK-derived rUUKV S23 for 48 hours at various MOIs. After immunostaining with mouse monoclonal antibodies against the N protein of UUKV, infected cells were analyzed by flow cytometry. Independent of the tick cell line, nearly 50% of the cells were infected at an MOI of 5, and about 20% at the lowest MOI (1.25), as indicated in **figure 18A**. Following a similar method, tick cells were infected with rUUKV S23 on poly-L lysine coated coverslips for 24 hours and immunostained for newly synthesized N protein. The number of infected cells increased accordingly to the MOI, although no quantification was performed. The newly synthesized N protein is present in the cytoplasm, which is expected for bunyaviruses that have a cytoplasmic life cycle (**figure 18B**). Using these two techniques, we showed that tick cells were susceptible to mammalian cell-derived virus infection.

To gain more insight into the production of virions in the tick cells, both cell lines were infected with either rUUKV or rUUKV S23 in 10 glass tubes of 3 mL, as the cells do not grow in standard plastic dishes (**figure 44**). Supernatant was harvested at different time points and titrated. The production of both rUUKV S23 (**figure 18C**) and rUUKV (**figure 18D**) increased rapidly over the first 10 days, and reached a plateau after 30 days. Tick cells were persistently infected after 3

## Results

months without any sign of CPE, and the infected cells grew similar to non-infected cells (data not shown). The arrows in **figures 18C** and **18D** indicate sub-culturing of cells at day 34, 54, and 74 post-infection. For this, half of the cell suspension was removed and fresh culture medium was added. The sub-culture did not affect the production nonetheless the dilution is low. 74 days post-infection, supernatant of infected cells was harvested and total RNA extracted. RNA of the M segment was reverse transcribed and amplified to sequence a 391 bp fragment that contains the genetic marker of the RGS. The sequence results showed that the reversion G/A introduced at position 2386 in the M segment was still present in the genome of rUUKV S23 but not in that of rUUKV (**table 2**). Tick cells can, therefore, be confidently used to study the UUKV life cycle in its vector, meaning that we successfully developed a system to study tick-borne viruses in vector cell line.

Altogether these results show that both cell lines derived from *I. ricinus* support a persistent mammalian cell-derived rUUKV S23 infection. It then raised the question whether or not rUUKV S23 derived from tick cells was able to infect mammalian cells. To answer this question, BHK-21 cells were exposed to viral progeny produced in IRE/CTVM19 cells. After 18 hours of infection, mammalian cells were stained for the N, G<sub>N</sub>, and G<sub>C</sub> proteins using mouse monoclonal antibodies and analyzed by flow cytometry. More than 50% of the cells were positive for the viral N protein and about 60% were positive for G<sub>N</sub> or G<sub>C</sub>, suggesting viral replication from tick cell-derived virions into mammalian cells (**figure 19**). Therefore, the tick cell system that I developed enables to reproduce the host switch *in vitro*, and appears as an excellent model to study the natural vector-host alternation of tick-borne phleboviruses.

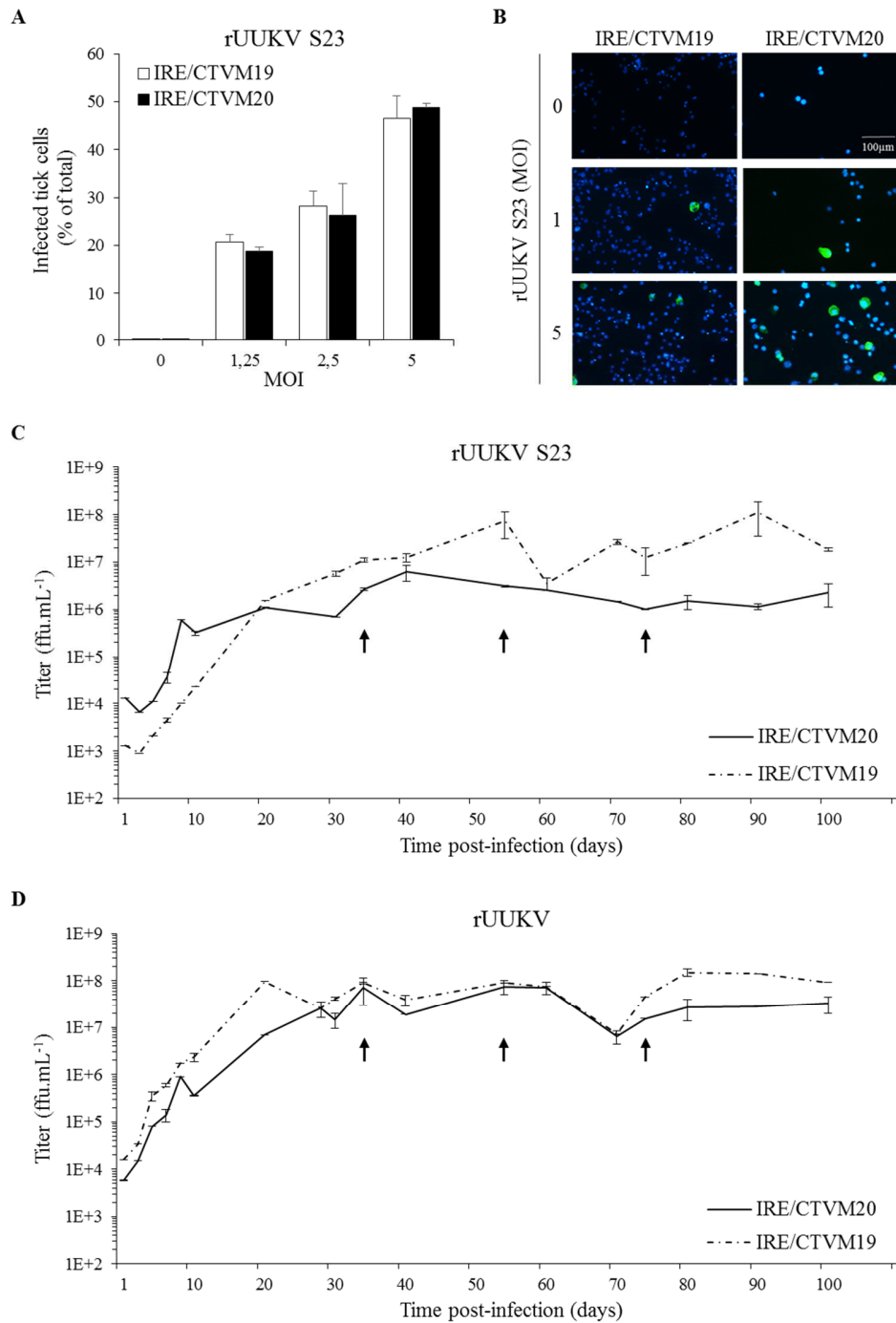


**Figure 18: Infection of IRE/CTVM19 cells by rUUKV and rUUKV S23 is persistent.**

(A) Tick cell lines IRE/CTVM19 and IRE/CTVM20 were exposed to BHK-21 cell-derived rUUKV S23 at the indicated MOIs for 48 hours. Infection was analyzed by flow cytometry after immuno-staining against the nucleoprotein N. (B) IRE/CTVM19 and IRE/CTVM20 cells were exposed to various MOIs of rUUKV S23 derived from BHK-21 cells. The next day, infected cells were immuno-stained for the intracellular UUKV nucleoprotein N using the anti-N primary mouse monoclonal antibody 8B11A3 and an AF488-coupled anti-mouse secondary monoclonal antibody (green). Nuclei were stained with Hoescht (blue) and samples analyzed by wide-field microscopy. (C) and (D) IRE/CTVM19 and IRE/CTVM20 cells were exposed to rUUKV S23 (C) and rUUKV (D). 200  $\mu$ L of supernatant of infected cells was harvested daily during the first ten days, and every ten days thereafter. The

## Results

production of infectious viral particles in the supernatant was determined by focus-forming assays. The cells were subcultured in fresh complete medium (1:1) after sampling of the parent cells on days 34, 54, and 74 (black arrows) <sup>242</sup>.

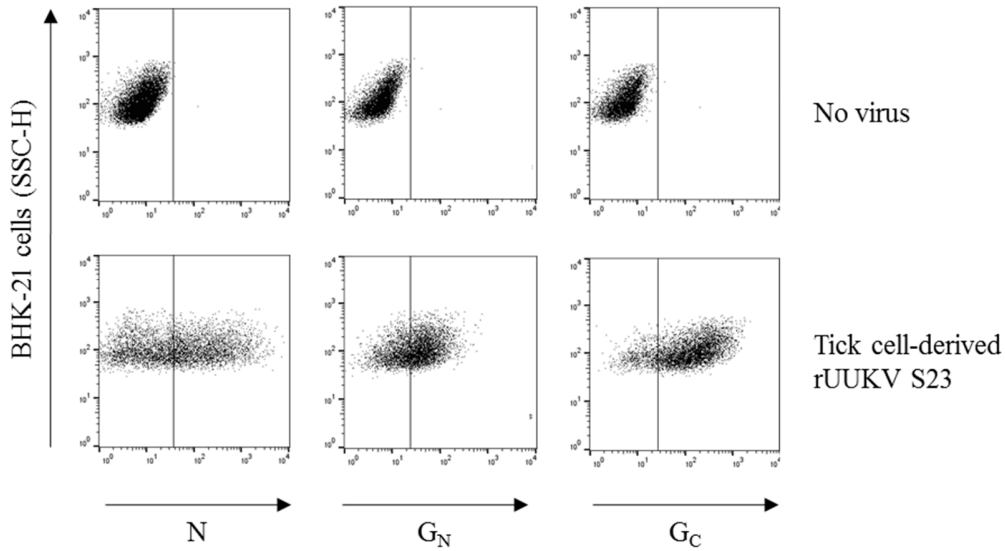


**Figure 19: Tick-cell derived rUUKV S23 infect BHK-21 cells.**

Mammalian cells were infected with supernatant of IRE/CTVM19 cells infected cells for one hour. Supernatant was removed and fresh medium without FBS added. After 18 hours of infection, BHK-21 cells were fixed, permeabilized, and immunostained for the N, G<sub>N</sub>, or G<sub>C</sub> proteins using monoclonal antibodies 8B11A3, 6G9E5, and 3D8B3, respectively.

**Table 2: Sequences of tick cell-derived rescued viruses.**

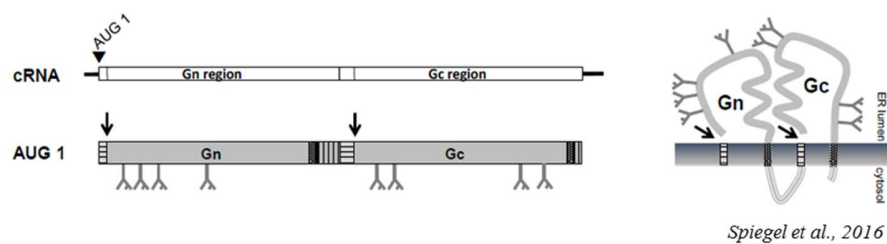
Virus	Cell type (day)	Sequence <sup>a</sup>
rUUKV	BHK-21	TGGATTGTC <b>G</b> ATCATCAATCATAGATCCC
M-UUKV-NC005220.1	BHK-21	TGGATTGTCAATCATCAATCATAGATCCC
rUUKV	IRE/CTVM19 (74)	TGGATTGTC <b>G</b> ATCATCAATCATAGATCCC
rUUKV	IRE/CTVM20 (74)	TGGATTGTC <b>G</b> ATCATCAATCATAGATCCC
rUUKVS23	IRE/CTVM19 (74)	TGGATTGTCAATCATCAATCATAGATCCC
rUUKVS23	IRE/CTVM20 (74)	TGGATTGTCAATCATCAATCATAGATCCC

<sup>a</sup> red bold letters indicate the reversion A/G in the M segment at the position 2386 compared to the prototype strain UUKV S23 (NC005220.1 accession number)

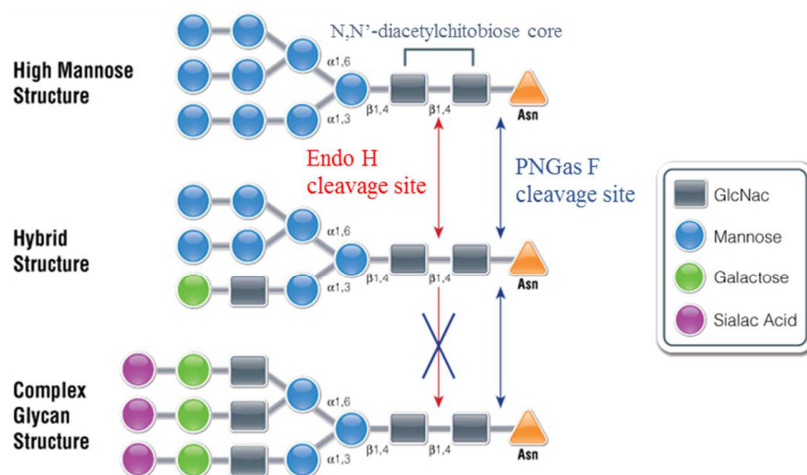
### b. The glycosylation profile of tick cell-derived rUUKV S23 is unique

Glycoproteins are essential for triggering attachment to the receptor via the glycosylation. UUKV has four sites of *N*-glycosylation on both envelope glycoproteins (**figure 20A**). To gain further insight into the *N*-glycosylation pattern of tick cell derived virus, the glycoproteins G<sub>N</sub> and G<sub>C</sub> of rUUKV S23 were treated with different glycosidases. Viruses purified through 25% sucrose cushions were treated with the peptide *N*-glycosidase (PNGase F) under denaturing conditions before SDS-PAGE and Western blot analysis. Proteins were denatured, and thus conformational epitopes were damaged, meaning that monoclonal antibodies could not be used. Instead the polyclonal antibody U2 was used for immunostaining. The PNGase F cleaves *N* linked glycans independent on the nature of glycans (**figure 20B**).

A



B



PNGase F : Peptide-N-glycosidase F ; Endo H: Endoglucosaminidase

Adapted from Promega

## Results

### Figure 20: *N*-linked glycosylation on UUKV glycoproteins.

(A) M segment of UUKV is translated as a precursor protein that is cleaved (arrows) into two glycoproteins ( $G_N$  and  $G_C$ ). *N*-linked glycans on  $G_N$  and  $G_C$  are depicted underneath the precursor. This has been adapted from Spiegel et al.<sup>76</sup>. (B) Cleavage site of the endoglycosidase H (Endo H) and the peptide-*N*-glycosidase F (PNGase F). This has been adapted from Promega.

While the four sites of *N*-glycosylation of the  $G_N$  protein are cleaved for rUUKV S23 produced in BHK-21 cells, only one seems to be digested for the tick cell-derived virus (**figure 21A**). In contrast, both mammalian and tick cell-derived  $G_C$  proteins are entirely sensitive to PNGase F (**figure 21B**). Glycoproteins  $G_N$  and  $G_C$  of the mammalian-derived UUKV are known to be sensitive to PNGase F; the enzyme digests all four sites of *N*-glycosylation of  $G_N$  and  $G_C$ . To further examine *N*-glycans, the glycoproteins were subjected to endoglycosidase H (Endo H), which specifically digests glycans that display high mannose structure but not complex glycans (**figure 20B**). Glycoproteins processed in mammalian systems undergo maturation and folding in the ER and Golgi complexes. During these processes, they acquire different types of glycans. Bunyaviruses bud in the Golgi, thus preventing the full maturation of glycans on glycoproteins. As expected for the mammalian derived rUUKV S23 (Lozach, 2011), glycoprotein  $G_N$  is partially sensitive to Endo H and exhibits several types of glycans, namely complex, non-digested forms and high mannose structures (**figure 21C**). On the other hand, glycoprotein  $G_C$  is mainly sensitive to Endo H, suggesting that  $G_C$  carries high mannose *N*-glycans (**figure 21D**). When rUUKV S23 is produced in IRE/CTVM19, both  $G_N$  (**figure 21A & C**, right panels) and  $G_C$  (**figure 21B & D**, right panels) show sensitivity for Endo H with a profile identical to that of PNGase F. These results show that tick cell-derived rUUKV glycoproteins have *N*-linked glycans with high mannose structure only. It also highlights that there is a difference in maturation of glycoproteins between mammalian and vector tick cell system.

The glycoprotein  $G_N$  of rUUKV S23 produced in IRE/CTVM19, as compared to BHK-21 cells, exhibits a different pattern, and therefore, other glycosidases were tested to investigate the glycosylation profile in more detail.  $G_N$  was then exposed to Neuraminidase,  $\beta$ -1,4-galactosidase and  $\beta$ -*N*-acetylglucosaminidase. As shown in **figure 22A**, Neuraminidase cleaves and releases neuraminic acids residues and  $\beta$ -1,4 linked galactose from oligosaccharides while  $\beta$ -1,4-galactosidase and  $\beta$ -*N*-acetylglucosaminidase digest  $\beta$ -linked *N*-acetylglucosamine and *N*-

acetylgalactosamine, respectively. We found that only the glycoprotein N derived from tick cells was sensitive to  $\beta$ -N acetylglucosaminidase (**figure 22B**).

Altogether, these results suggest a distinct pattern for the glycoprotein N of rUUKV S23 when produced in the vector tick cells.

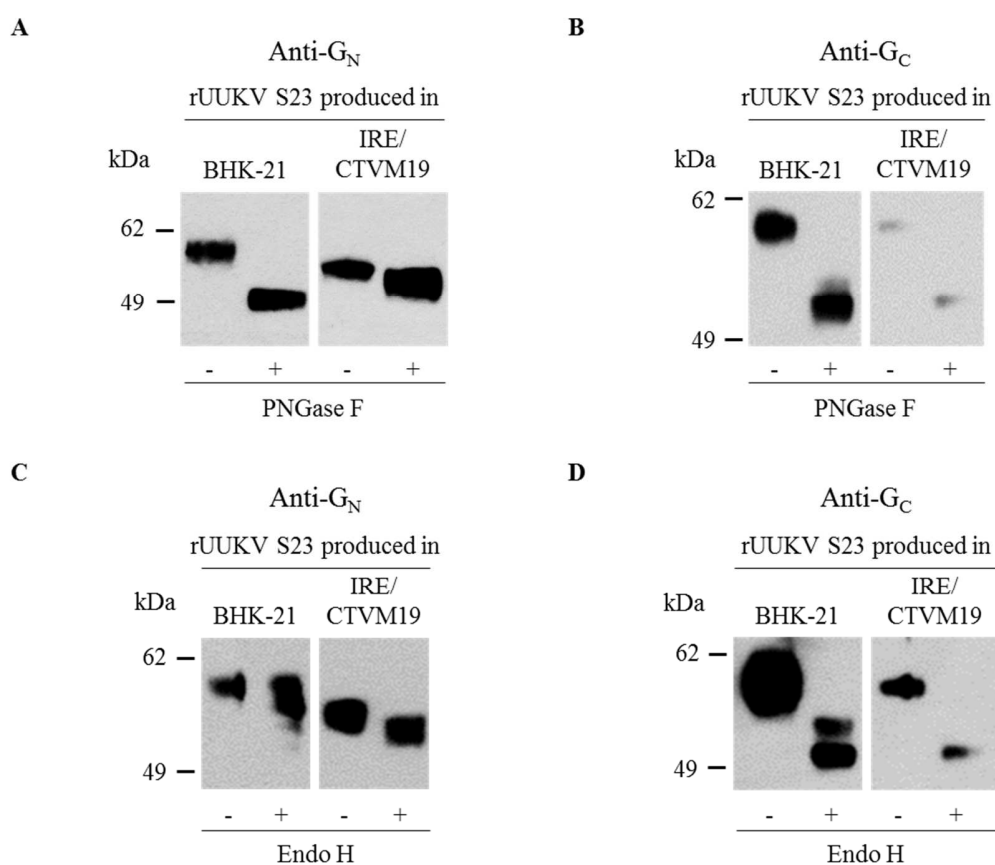
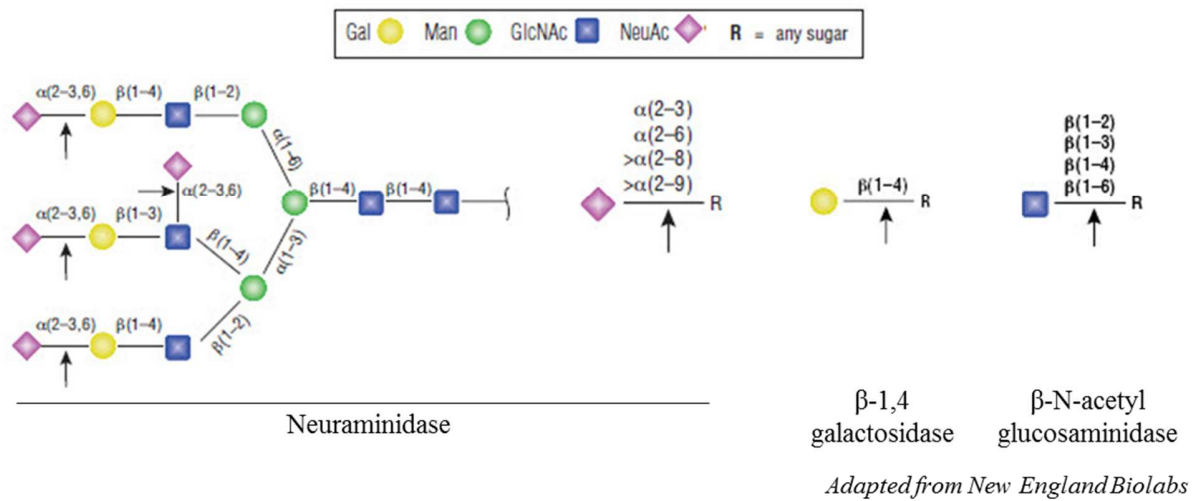


**Figure 21: N-linked glycosylation harbored by the envelop proteins  $G_N$  and  $G_C$  on virions produced in tick or mammalian cells.**

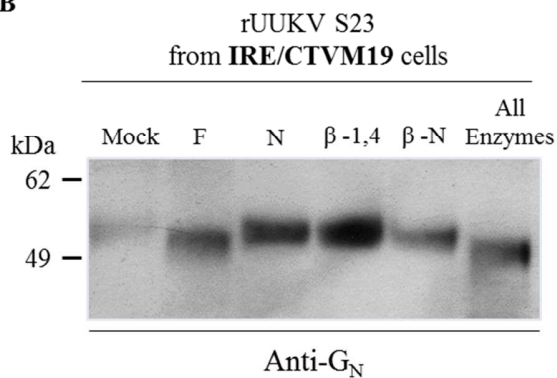
IRE/CTVM19 or BHK-21 cell-derived rUUKV S23 purified through a 25% sucrose cushion was reduced and denatured before digestion by PNGase F (A, B) or Endo H (C, D). Proteins were analyzed by SDS-PAGE and Western blot using polyclonal antibodies K1224 or K5 against the glycoprotein  $G_N$  (A, C) or  $G_C$  (B, D), respectively.

## Results

A



B



C

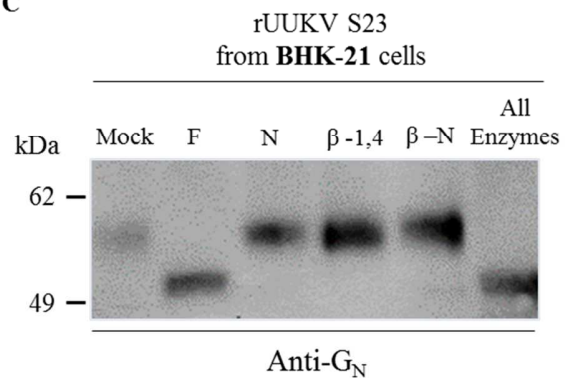


**Figure 22: Glycosylation specificity of tick-cell derived rUUKV S23.**

(A) Scheme adapted from the New England Biolab. The black arrow shows digestion sites by the neuraminidase (purple),  $\beta$ -1,4-galactosidase (yellow), and  $\beta$ -N-acetylglucosaminidase (blue). rUUKV S23 produced in IRE/CTVM19 (B) or BHK-21 (C) cells and purified through a 25% sucrose cushion was reduced and denatured before digestion by PNGase F (F), neuraminidase (N),  $\beta$ -1,4-galactosidase ( $\beta$ -1,4), or  $\beta$ -N-acetylglucosaminidase ( $\beta$ -N). Proteins were analyzed by SDS-PAGE and Western blot using polyclonal antibody K1224 against the glycoprotein  $G_N$ .

### c. A distinct pattern for the tick cell-derived $G_N$

The previous results highlight differences of glycosylation pattern. In addition, SDS-PAGE analysis showed that  $G_N$  does not have the same molecular weight when originating from tick cells or mammalian cells (figure 21A, untreated samples). The difference in the size of the protein could either be due to the glycosylation pattern or to structural differences. To further assess the potential conformational differences of the glycoprotein N when produced in tick cells, viruses purified

through a 25% sucrose cushion were subjected to SDS-PAGE under non-reducing conditions before staining with mouse monoclonal antibodies that recognize conformational epitopes. Interestingly, the mobility of  $G_N$  on tick cell derived rUUKV S23 also appears to be faster than that of mammalian cell-derived proteins (**figure 23A**). The mobility of  $G_C$  is similar for both tick and mammalian background (**figure 23B**). Afterwards, virions were exposed to  $\beta$ -mercaptoethanol to denature proteins and to assess the cleavage of disulfide bonds in  $G_N$ . When viruses are produced in BHK-21 cells, the mobility of reduced  $G_N$  proteins was slower than the non-reduced proteins, suggesting that disulfide bonds were cleaved (**figure 23C**). This is not observed for the proteins that originated from tick cells, suggesting that there are less or no disulfide bonds cleaved.

To understand whether this discrepancy could be due to a deletion in the nucleotide sequence, I sequenced the full-length M segment of rUUKV and rUUKV S23 derived from IRE/CTVM19. The complete nucleotide sequences were those published and expected (data not shown). There was no deletion in the M segment that could explain the lower molecular weight of the glycoprotein  $G_N$  when coming from tick cells. Moreover, we also analyzed the amino acid sequences by mass spectrometry to investigate the possibility of an alternative ORF. Although the sequences obtained were not complete, it is unlikely that there is a difference between mammalian and tick cell-derived glycoproteins at the amino acid level (**supplementary material 1**).

Together, these findings suggest that the number of disulfide bonds differs whether the virus is produced in tick or mammalian system. The results presented here show that the glycoprotein  $G_N$  may undergo a distinct maturation and folding process when the virus is produced in tick cells. This might have consequences for the global structure of the particles and their interaction with the first target cells in mammalian host skin dermis.

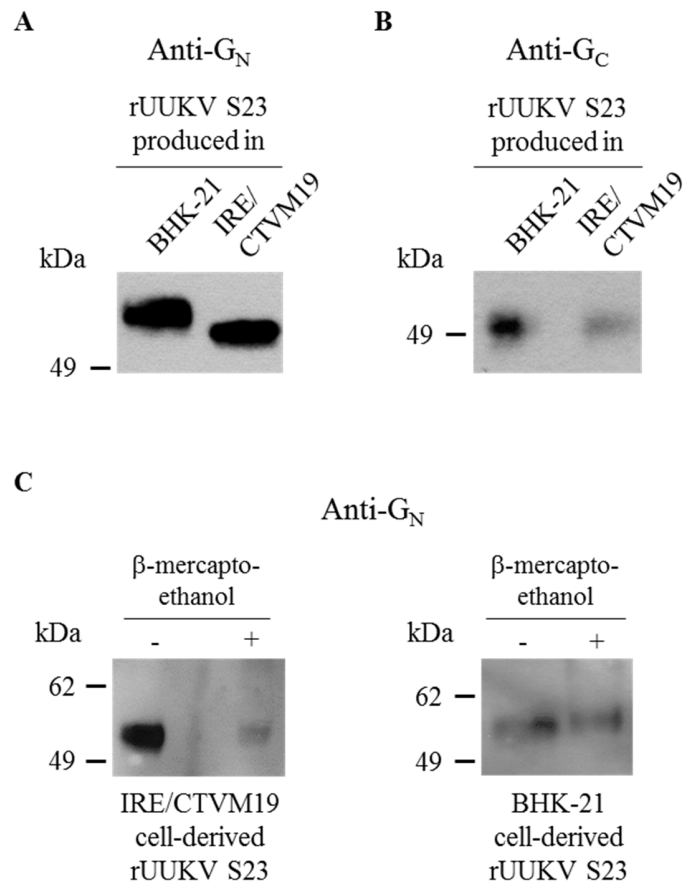


**Figure 23: rUUKV S23 glycoproteins  $G_N$  and  $G_C$  from IRE/CTVM19 and BHK-21 cells.**

BHK-21 or IRE/CTVM19-derived viruses were purified through a 25% sucrose cushion and analyzed by SDS-PAGE and Western blot under non-reducing conditions using monoclonal antibodies 6G9E5 and 3D8B3 that recognize conformation epitopes in  $G_N$  (A) and  $G_C$  (B), respectively. (C) Purified BHK-21 or IRE/CTVM19-derived rUUKV S23 were analyzed by SDS-PAGE and Western blot under non-reducing (-) or reducing (+) conditions, using the rabbit polyclonal antibody K1224 for the detection of  $G_N$ .

#### **d. Tick cell-derived rUUKV S23 is more infectious than mammalian cell-derived rUUKV S23**

I first investigated whether the differences in glycan composition and folding of the viral glycoprotein  $G_N$  may affect the infectivity. To this end, the same amount of infectious units produced either in tick cells (IRE/TCVM19 or IRE/CTVM20) or in BHK-21 cells was analyzed by SDS-PAGE and Western blot using the polyclonal antibodies U2 against UUKV to visualize all three major structural proteins (N,  $G_N$ , and  $G_C$ ). Viral particles produced in either tick cells or mammalian cells were titrated in BHK-21 cells after purification through a 25% sucrose cushion.

For  $10^5$  FFU, the amount of N,  $G_N$ , and  $G_C$  differs from tick versus mammalian cell-derived viruses (**figure 24A**). The difference was also visible when mouse monoclonal antibodies were used to detect the glycoproteins. While the amount of proteins  $G_N$  and  $G_C$  from virions produced in BHK-21 cells appeared to be high (although no quantification being possible), that of glycoproteins on tick cell-derived viruses were barely or not detectable (**figure 24B**). Antibodies used in the laboratory were produced in either rabbit or mice with mammalian virus stocks. Thus, these antibodies recognize specific antigens from the mammalian cell-derived viruses and could not recognize antigens from tick cell-derived viruses.

To exclude this possibility, IRE/CTVM19 and mammalian derived rUUKV were purified through a 25% sucrose cushion and analyzed by Coomassie staining. For a similar amount of infectious units, the N protein of mammalian cell-derived viruses is more abundant than that of tick cell-derived viruses (**figure 24C**). To confirm this result, multiple infectious units of rUUKV S23 were analyzed using an Odyssey imaging system that allows quantitative Western blot analysis. Interestingly, the amount of glycoproteins was higher in tick cell-derived viral particles than in mammalian cell-derived particles, while the N protein was remarkably more expressed when virions were produced in mammalian cells (**figure 24D**). The ratio of the amount of N protein per viral infectious unit is significantly lower for tick cell-derived virus (**figure 25**), while the ratio of the amount of glycoproteins per FFU is higher (**figure 25B**). The N protein is also expressed in a linear range in the tick cell system, compared to the mammalian system, suggesting that more viral particles are infectious when produced in tick cells. It also appears that the ratios of glycoproteins per N protein and of FFU per N protein are higher on IRE/CTVM19-derived viruses (**figure 25C & D**). The N protein surrounds viral genome required for infection inside the particles. With different amounts of N and glycoproteins per infectious units, these results suggest a difference in the overall structural organization that depends on whether virions are produced in tick cells or mammalian cells.

## Results

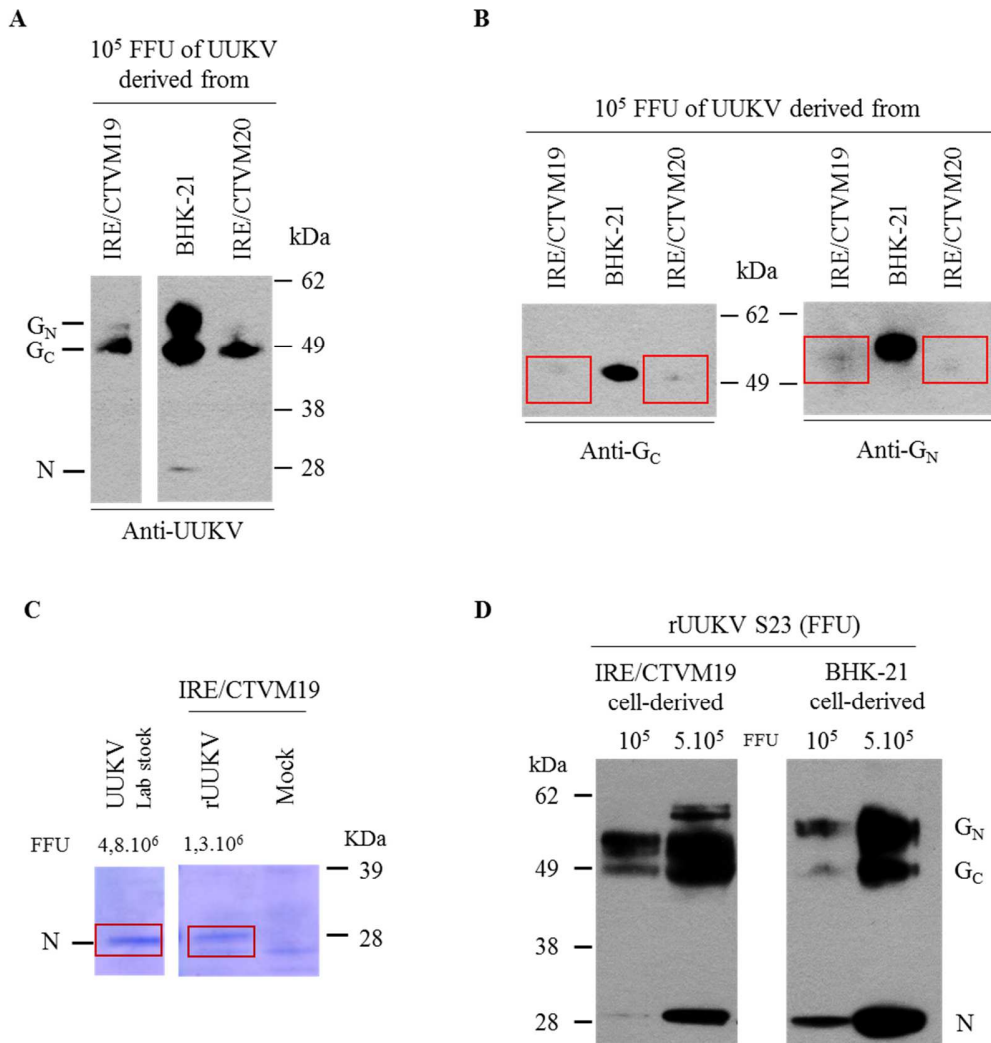


**Figure 24: Tick and mammalian cell-derived structural viral proteins.**

Tick or mammalian cell-derived semi-purified UUKV (A, B) were analyzed under non-reducing SDS-PAGE and Western blot analysis using polyclonal antibodies against UUKV (A) or monoclonal antibodies against G<sub>C</sub> or G<sub>N</sub> (B). Red boxes indicate where the glycoproteins should migrate. (C) UUKV from lab strain stocks produced in BHK-21 cells or rUUKV produced in IRE/CTVM19 cells, both semi purified through a 25% sucrose cushion, were analyzed by SDS-PAGE and Coomassie staining. The N, G<sub>N</sub>, and G<sub>C</sub> proteins of UUKV lab strain stock were detected and the N protein of both viruses was highlighted in red. Focus forming units (FFU) are indicated on top of the gel. (D) The amount of viral G<sub>N</sub>, G<sub>C</sub>, and N for 10<sup>4</sup>, 10<sup>5</sup>, and 5x10<sup>5</sup> FFU of semi-purified rUUKV S23, either produced in tick cells or mammalian cells, were analyzed by SDS-PAGE and Western blot using the rabbit polyclonal antibodies against UUKV.

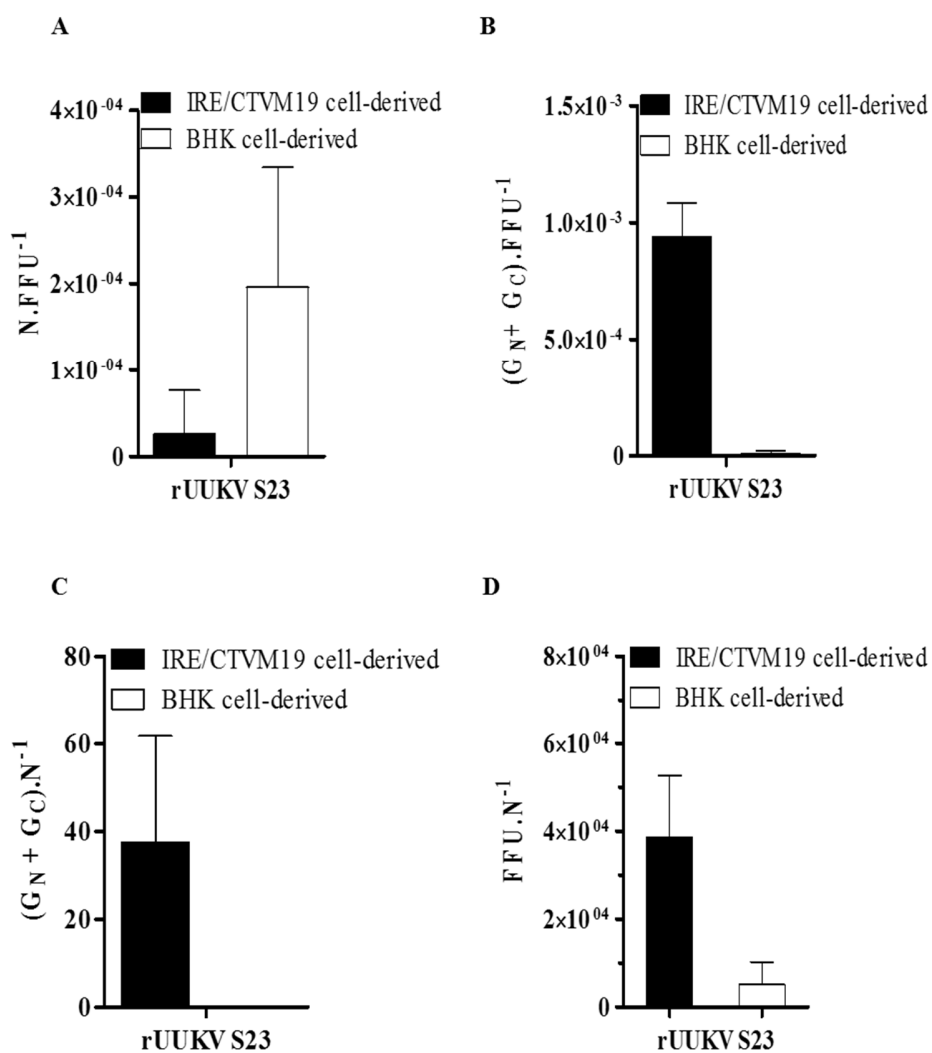


**Figure 25: Quantification of the structural rUUKV S23 proteins G<sub>N</sub>, G<sub>C</sub>, and N in infectious viral particles.**

Tick or mammalian cell-derived rUUKV S23 was purified through a 25% sucrose cushion and were analyzed under non-reducing SDS-PAGE and Western blot using polyclonal anti-UUKV antibody U2 and an anti-rabbit infrared fluorescence secondary antibody. The amount of viral proteins for identical purified infectious rUUKV S23 was determined by quantitative Western blot analysis (Odyssey Imaging System). Ratios of the amount of N protein (A) or glycoproteins (B) per FFU and ratios of glycoproteins (C) or FFU (D) per relative unit of N protein are shown.

### e. Genetic evolution of wild-type UUKV originating from Swedish ticks

UUKV strain 23 was isolated in 1959, but the viral genome sequences were only available in the 1980s for viruses adapted in mammalian cell culture. Compared to those sequences, our laboratory strain showed few mutations in the M and L segments nucleotide sequences (**figure 13**). Because ARN viruses are known to rapidly evolve genetically, we determined whether the wild-

## Results

type UUKV that circulates in tick populations nowadays showed genetic differences with our lab strain and rescued viruses. The ultimate goal was to demonstrate that UUVK produced in tick cells can be used as a tick-borne virus model that is representative of the circulating virus. Through our collaborators, Janne Chirico and Sara Moutailler, we analyzed 16 pools of 25 nymphs of the ticks *I. ricinus* that have been collected in Ramsvik and Hindens Rev regions (Sweden, 2013). Total RNA was extracted from nymphal homogenates with a magnetic bead-based protocol<sup>153</sup> and reverse transcribed to obtain cDNA corresponding to the M segment. The full-length M segment was synthesized by a single PCR and sequenced. 4 homogenates out of 16 were positive, and it was possible to obtain the full-length M sequences for both of them, one pool came from Ramsvik and one from Hindsen Rev region. Hence isolates were named RVS (Ramsyik Sweden) and HRS (Hindsen Rev Sweden). They are now referenced in GenBank as KX219593 and KX219594, respectively. Nucleotide sequence analysis showed identity greater than 93% between the UUKV S23 and the strains circulating currently (data not shown). At the amino acid level, we showed that the percentage of identity was greater than 97%. Also, the intergenic region of RSV was conserved and G<sub>C</sub> was the less affected by the evolution with a minimum of 99.2% identity corresponding to 2 (RVS) to 4 (HRS) variations (**table 3**). G<sub>N</sub> showed 7 (RVS) to 11 (HRS) amino acid variations with 5 positive substitutions for both RVS and HRS (**table 3**). Together, these results demonstrate that the M segment of UUKV has not significantly changed over the past 20 years.

**Table 3: Analysis of the M amino acid sequence from UUKV-infected field *I. ricinus* ticks.**

Region (aa) <sup>a</sup>	Isolate	Identity (%) <sup>b</sup>	Positive sequence (%) <sup>c</sup>	Substitution(s) relative to the UUKV S23 polypeptide precursor <sup>d</sup>
G <sub>N</sub> (18-496)	RSV	98.5	99.6	<b>L8I, L29I, S124T, T167S, L207V</b> , A219T, T237A
	HRS	97.6	98.7	<b>L29I, T44A, S124T, T167S, L207V</b> , A219T, <b>S282T</b> , T287A, N476K, N477Q, A479C
Intraregion (497-513)	RSV	100	100	
	HRS	97.1	97.1	A508T
G <sub>C</sub> (514-1008)	RSV	99.6	100	<b>S695T, Q790R</b>
	HRS	99.2	99.8	<b>K577R, Q790R, T841S</b> , L1003F

<sup>a</sup> Amino acid (aa) position. <sup>b</sup> Percent identity relative to the sequence of the precursor peptide.

<sup>c</sup> Values represent the percent identity of the sequence of interest augmented by the substitutions shown in boldface relative to the sequence of the precursor peptide. <sup>d</sup> Total RNA was extracted from 16 pools of 25 nymphs collected in the region of Ramsvik and Hindens Rev, Sweden. RNA corresponding to the M segment was reverse transcribed and cDNA amplified as a single PCR. Four samples were positive, one could not be sequenced, one was partially sequenced, and two others were sequenced entirely. The list shows amino acids found to be mutated in the full length amino acid sequences of isolate RVS and HRS (GenBank accession number KX219593 and KX219394, respectively) relative to the sequence of the polypeptide precursor of the glycoproteins G<sub>N</sub> and G<sub>C</sub> of UKV S23 (GenBank accession number NC\_005220.1). The point mutations in boldface indicate positive substitutions.

### 3. Towards the characterization of tick cell-derived UUKV viral particles

#### a. *Ixodes scapularis* cell lines are persistently infected by UUKV

The RGS was developed to recover infectious UUK viral particles and to infect tick cells. The tick cell line IRE/CTVM19 has been used as a model to characterize virions, but production had to be done in small glass tubes. Therefore, the volume of infectious supernatant was too small and did not allow for proper purification. This prevented a deep characterization of viral particles using, for instance, electron microscopy or mass spectrometry. With a concern towards continuous improvement, other methods of rUUKV production and purification were developed to produce tick cell-derived virus stocks highly purified and concentrated. They are described in the following sections.

## Results

IDE8 and ISE18 cells were both derived from crushed embryos of *Ixodes scapularis*. UUKV has not been yet reported to be isolated from this species of hard ticks. Since rUUKV S23 refers to the strain 23 that was isolated from the ticks *I. ricinus*, we used rUUKV to develop a new tick cell culture model. In contrast to IRE/CTVM19 and IRE/CTVM20 cells, the genomes of *I. scapularis* (strain Wikel – vectorbase.org) had been sequenced and lately partially annotated<sup>171</sup>. This represents an advantage to investigate the UUKV life cycle in tick cells.

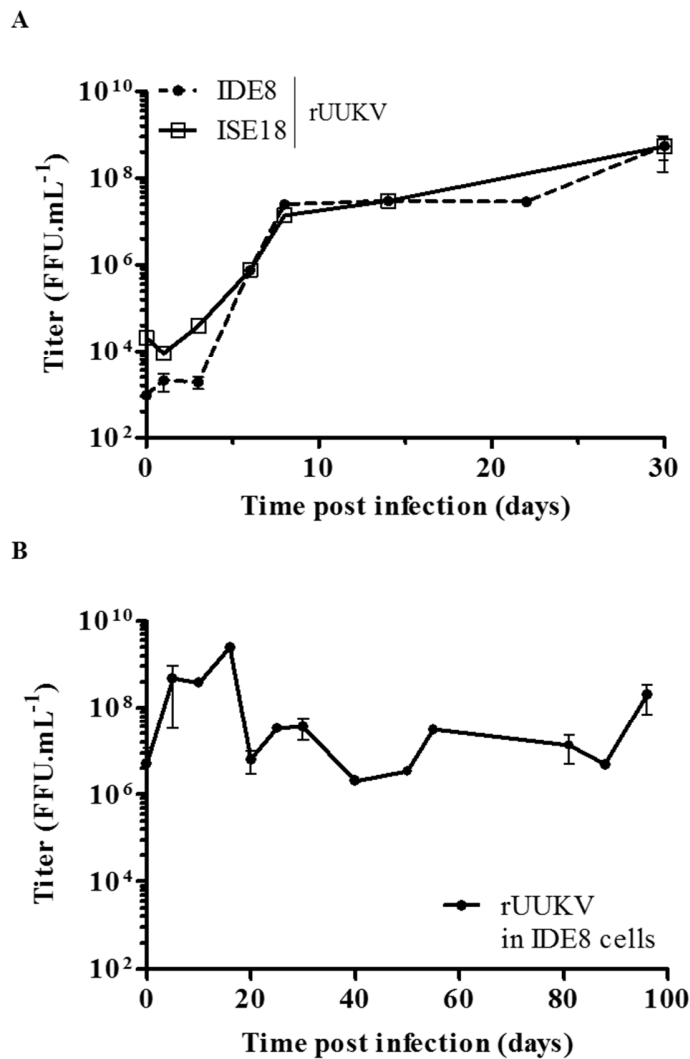


**Figure 26: *I. scapularis* cell lines are persistently infected by rUUKV.**

ISE18 cells (A) or IDE8 cells (A, B) were exposed to rUUKV for 2 hours at 28°C. Supernatant of infected cells were harvested at different times post infection and titrated by focus-forming assay.

### b. IDE8 cells as tick cell culture model

IDE8 and ISE18 are mainly adherent cells, but also grow in suspension when they are over confluent. Compared to IRE/CTVM cells, they are easier to handle. IDE8 and ISE18 cells were infected with rUUKV in small glass tubes. After 24 hours, the viral supernatant was removed and exchanged with fresh medium to analyze viral production. Over the 30 days of experimentation, titers slowly increased from  $10^4$  to  $10^8$  infectious units per milliliter, suggesting that both cell lines supported rUUKV infection (**figure 26A**). IDE8 cells grow faster than ISE18 (subculture 1:5 possible instead of 1:2 every 14 days). For these reasons, an improved production system was developed based on the use of IDE8 cells.

First, a medium scale production of rUUKV in IDE8 cells was evaluated. Cells were seeded in T75 flasks and infected with rUUKV derived from IDE8 (from the production in small glass tube). As shown in **figure 26B**, IDE8 tick cells were able to produce rUUKV for more than 3 months at a high titer. The drop of the titer 20 days post-infection most probably resulted from changing medium. Afterwards, the titer remained nearly stable for 60 days and increased significantly in the last 20 days. Moreover, no CPE was observed in infected cells. They were sub-cultured or the medium was changed every week, just as the non-infected stocks of cells. The cells (infected or non-infected) attached on the plastic dish very well. No difference of growth properties was observed, although cells tended to elongate at a low confluence for both infected and mock infected cells.

To then stretch the limits of the IDE8 production system, the cells were grown without FBS for a week in order to plan a large scale production and to more easily purify viral particles. The cells did not show any difficulties in growing, nor did they change their morphology, but they did require a high density (data not shown). In regard to this, a production of rUUKV in IDE8 with no FBS was tested. Surprisingly, the cells produced a high titrated rUUKV after one month in culture (**figure 27A**). The drop from  $10^7$  to  $10^5$  of the titer (day 15) is due to an exchange of the viral supernatant. The removal of the supernatant was recovered in few days, which indicates that IDE8 cells can produce new virions, at a high titer, in a medium that do not contain FBS (**figure 27A**). Furthermore, more than 80% of the cells were infected after 22 days post-infection when stained for the intracellular N protein, showing that IDE8 are persistently infected (**figure 27B**).

## Results

Each of the results presented here is made of a single experiment. However, these results were a major progress that moved the project forward and opened new perspectives for the characterization of tick cell-derived viral particles. Indeed, to elucidate the shape, size, glycosylation pattern, or the lipid composition of the particles, a high amount and highly purified material was required. As a consequence, a high scale production process was engineered.

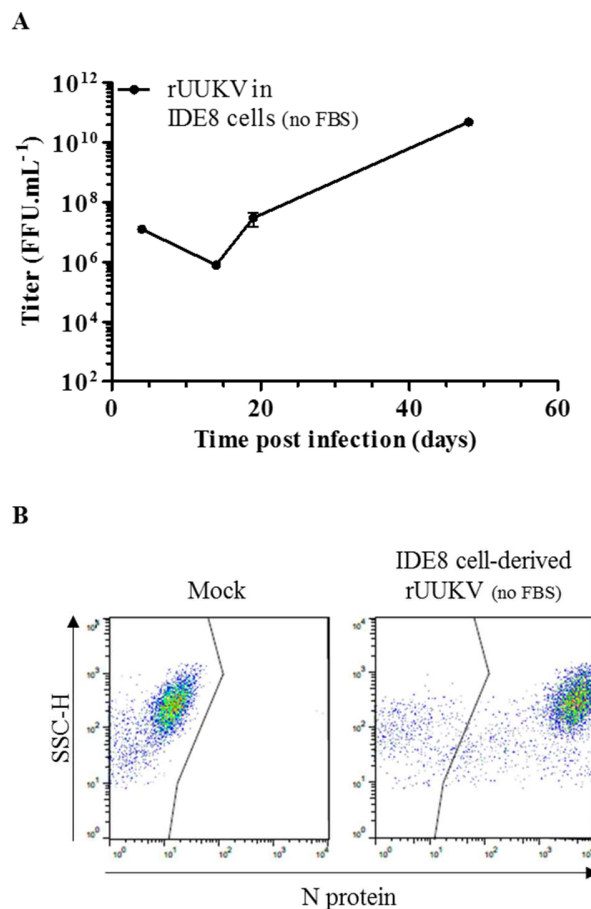


**Figure 27: rUUKV production in IDE8 cells without FBS.**

(A) IDE8 cells were infected with rUUKV in the absence of serum for 2 hours at 28°C. Medium was harvested at different time points to titrate infectious viral particles by focus-forming assay. (B) Infected cells were analyzed by flow cytometry after immunostaining of the intracellular N protein after 22 days of infection.

### c. Development of a high scale virus production in IDE8 cells and purification

Based on the hypothesis that IDE8 cells can grow in any kind of plastic dish that are sealed, tolerate the absence of serum for viral production, but need time to produce rUUKV, the protocol

used for the production of UUKV in BHK-21 cells was thus tested with IDE8 tick cells. Instead of 3 mL glass tubes, 175 cm<sup>2</sup> flasks were seeded with IDE8 cells in the presence of FBS to allow cells to adhere. The day after, cells were washed to remove FBS prior to infection with rUUKV at an MOI of 0.01 and maintained in medium free of FBS. Virus supernatant was removed and 30 mL of completed medium without FBS was added per flask. Production of virions was monitored by FFA at days 10 and 15 post-infection. We observed in the previous experiment (**figure 26A & B** and **figure 27A**) that 20 days was sufficient to produce a high amount of infectious particles. Therefore, the medium was harvested 20 days post-infection, and was cleared before purification procedure.

The purification steps were improved using a protocol previously established to characterize lipids composition of HIV-1 particles<sup>244</sup>. Briefly, rescued virus from BHK cells was semi-purified through a 30% sucrose cushion, and was loaded on top of an OptiPrep Gradient. A band was seen after centrifugation between the steps 18 and 30% of OptiPrep. After collecting the virus band, particles were pelleted by ultracentrifugation in PBS and analyzed by SDS-PAGE and silver staining (detailed protocols in **supplementary material 2**). BHK-derived rUUKV was successfully purified and the N, G<sub>N</sub>, and G<sub>C</sub> proteins were detected (**figure 28A**). Using the virus production in mammalian cells as a control, the same method was then applied to tick cells. Purified IDE8-derived rUUKV remained mainly in fractions 7 and 8, whereas mammalian cell derived-viruses were found in fraction 8 (**figure 28B**, lines 1 to 8 right and left panel). Unfortunately, the majority of tick cell-derived viruses was lost during the last step of purification, whereas mammalian cell-derived viruses were pelleted in PBS (**figure 28B**, line 9 right panel). Nevertheless, titers were determined by FFA for both viral productions and reached 6.4x10<sup>5</sup> FFU.mL<sup>-1</sup> for the tick cell production and 1.2x10<sup>8</sup> FFU.mL<sup>-1</sup> for the mammalian production.

Based on these results, it can be concluded that the protocol developed for the high scale production from tick cells is now working, although there is still place for improvement (**figure 29**, flowchart). To our knowledge, this is the first time that such a high viral production is reached

## Results

for tick cells. This could have a large impact on the production of tick-borne viruses and could lead to faster characterization and understanding of these viruses.

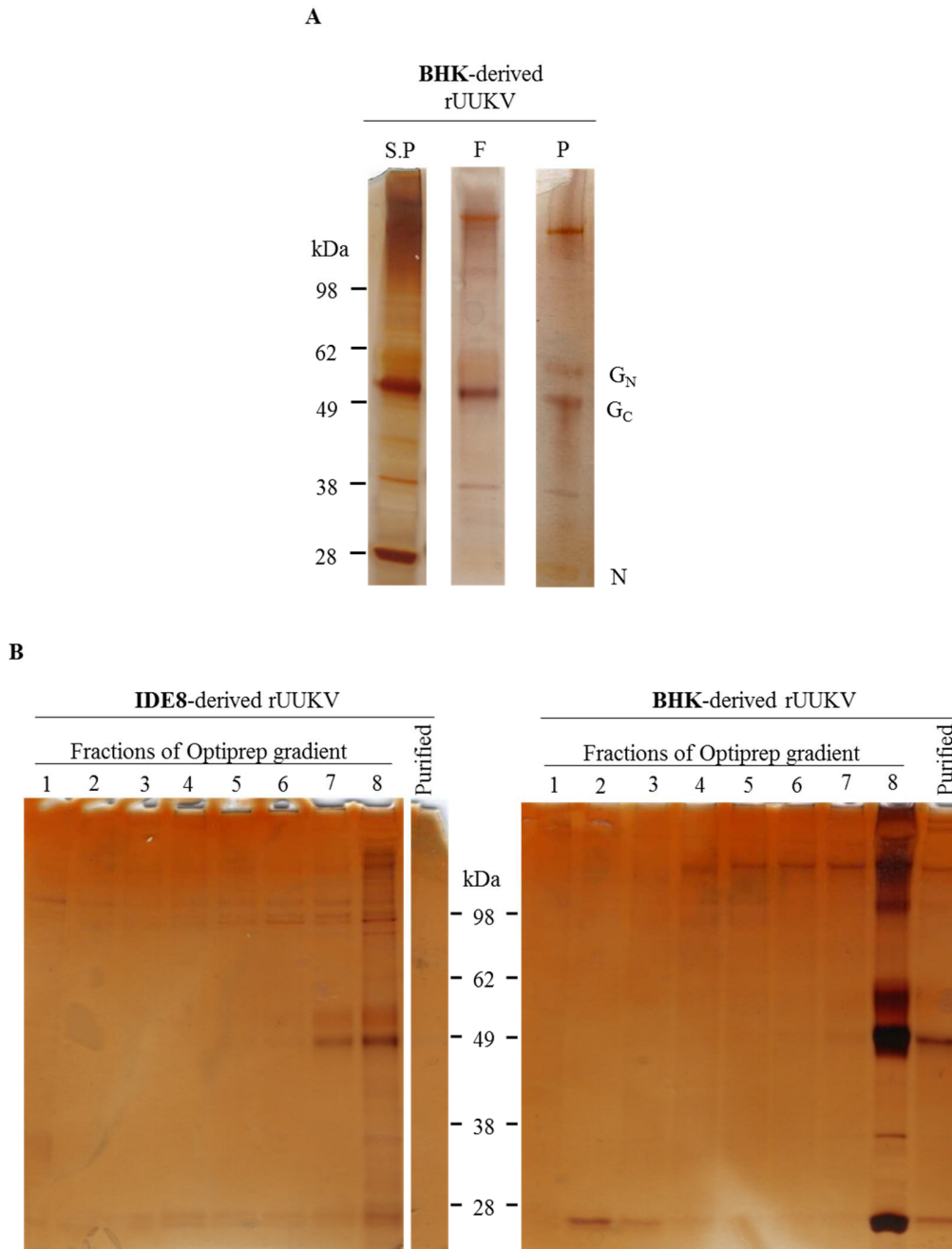


**Figure 28: Purification of viral particles through an Optiprep gradient.**

(A) rUUKV produced in BHK-21 cells was semi purified (S.P) through a 30% sucrose cushion and loaded on top of an Optiprep gradient. Fraction (F) of the gradient that contained rUUKV and the purified (P) viruses were analyzed by SDS-PAGE and silver staining. (B) rUUKV was produced either in IDE8 (left panel) or BHK (right panel) cells for 20 days or 48 hours, respectively. Supernatant was cleared, semi purified through a 30% sucrose cushion, and loaded on an Optiprep gradient. Fractions (columns 1 to 8) of the gradient and purified viruses were analyzed by SDS-PAGE and silver staining.

The flowchart, **figure 29**, represents the procedure implemented that will now be used in our laboratory, although an upgrade is required for the purification steps. Essentially, a supernatant titration (before purification) lower than  $10^7$  infectious particles per milliliter at day 15 post-tick cell infection will lead to a failed procedure (NO), as well as a titration lower than  $10^5$  after purification. Indeed, a high titer is required because a large fraction of viruses is lost during the purification procedure.

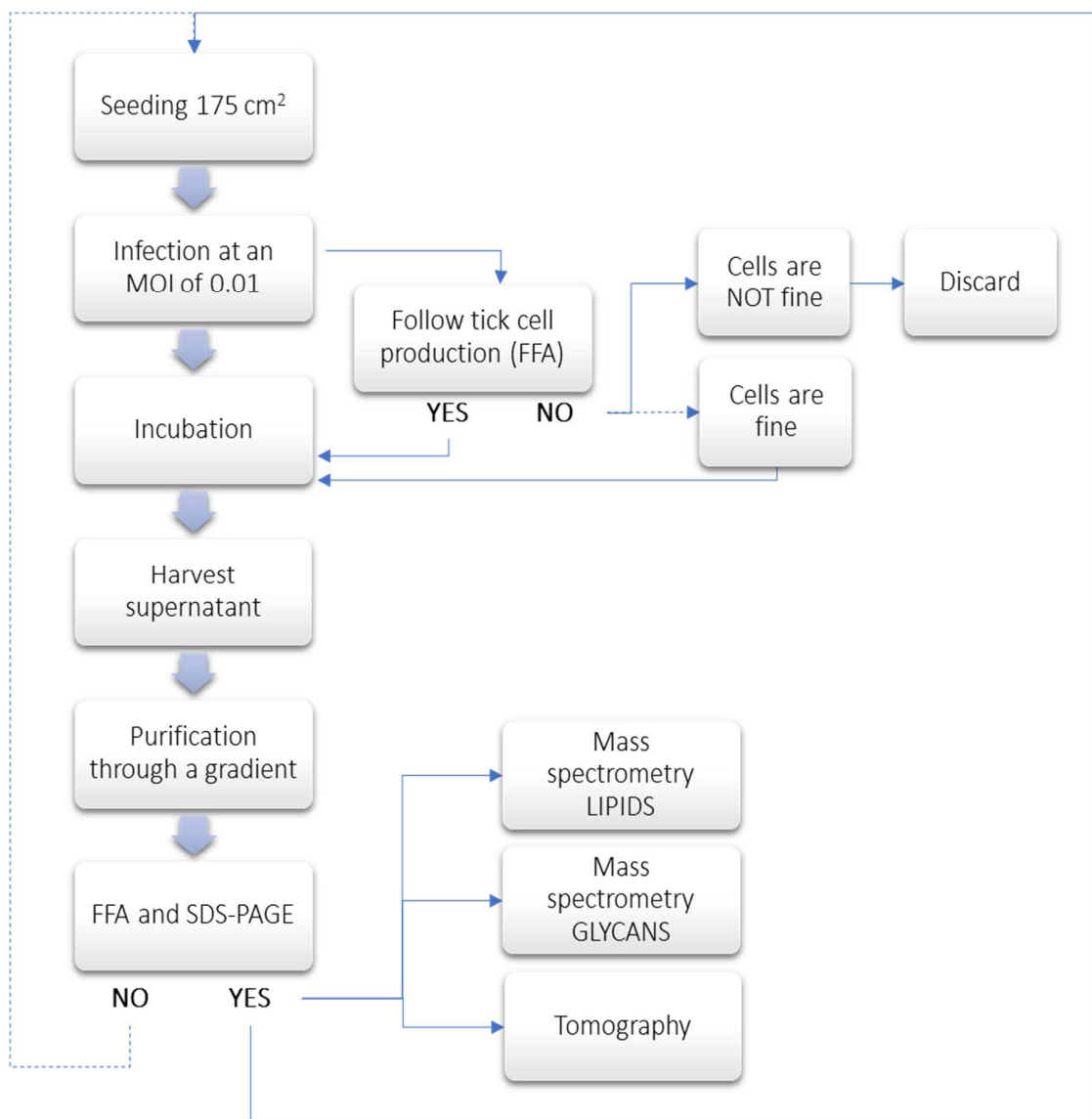


**Figure 29: High scale production of rUUKV in vector tick cells.**

The flowchart represents the protocol to follow for infection, purification, and characterization of viral particles. Two check points provide quality insurance, one before harvesting the supernatant to follow the production tick-cell derived viruses and one after purification. If the titer is high (YES), supernatant will be harvested at day 20 post-infection. If

it is not high enough (NO), cells are either incubated longer or discarded, depending on their shape. When the production passes the last check point (YES), viral particles can be analyzed or used to infect cells for a new production. Whenever the last check point is not successful, a new production is required.

### **d. Tick cell-derived rUUKV: a unique fingerprint**

Tick cell biology is poorly understood, although it plays a central role in the life cycle of the virus. Indeed, the virus will acquire features that are specific from these cells. In particular, during budding events, viral particles are formed with the membrane of the host cells, and are composed of different lipids. Therefore, we further investigate the lipid composition of the viral particles. IRE/CTVM19 derived rUUKV or mock-infected cells were purified through a 25% sucrose cushion, and were lysed in methanol prior to mass spectrometry analysis (in collaboration with Prof. Dr. Britta Brügger, BZH, University Heidelberg). The preliminary results showed that viral particles from the tick IRE/CTVM19 cells are rich in cholesterol (Chol) with 5.66  $\mu\text{M}$  (**figure 30A**) or 24.36 mol% (**figure 30B**) of lipids. Virions also seemed to be enriched in acyl-linked phosphatidyl choline (aPC), sphingomyelin (SM), and acyl-linked phosphoester (aPE) with 3.81, 2.81 and 3.25  $\mu\text{M}$ , respectively (**figure 30A**). They represent more than 30% of lipids measured (**figure 30B**).

The mass spectrometry of the BHK-21 cell-derived viruses were analyzed in an independent experiment. Mammalian cells were infected with rUUKV. After 48 hours, supernatants of infected and mock infected cells were purified through an OptiPrep gradient and the cells, infected or mock infected, were lysed. The viral particles and cell lysates were subjected to lipidomic analysis by mass spectrometry. The major lipid found in the mammalian cell-derived viral particles are the diacylglycerol (DAG), the cholesterol, the phosphatidylserine (PS), the ceramide (Cer), the SM and the aPC (**figure 31A**). Interestingly, it appears that the molecular ratio of lipids changed upon rUUKV infection. Indeed, the ratio of aPC and triacylglycerol (TAG) slightly decreased in the lysate of infected cells compared to the lysate of uninfected cells (**figure 31B**). Interestingly, the mol % of Hexosyl Ceramide (HexCer), but not the mol % of Ceramide (Cer) and Hexosyl 2 ceramide (Hex2Cer), significantly increased in BHK-21 infected cells (**figure 31B**). Together, this suggests that the envelope membrane of viruses derived from tick cells have a specific lipid composition, different from that of particles produced in mammalian cells.

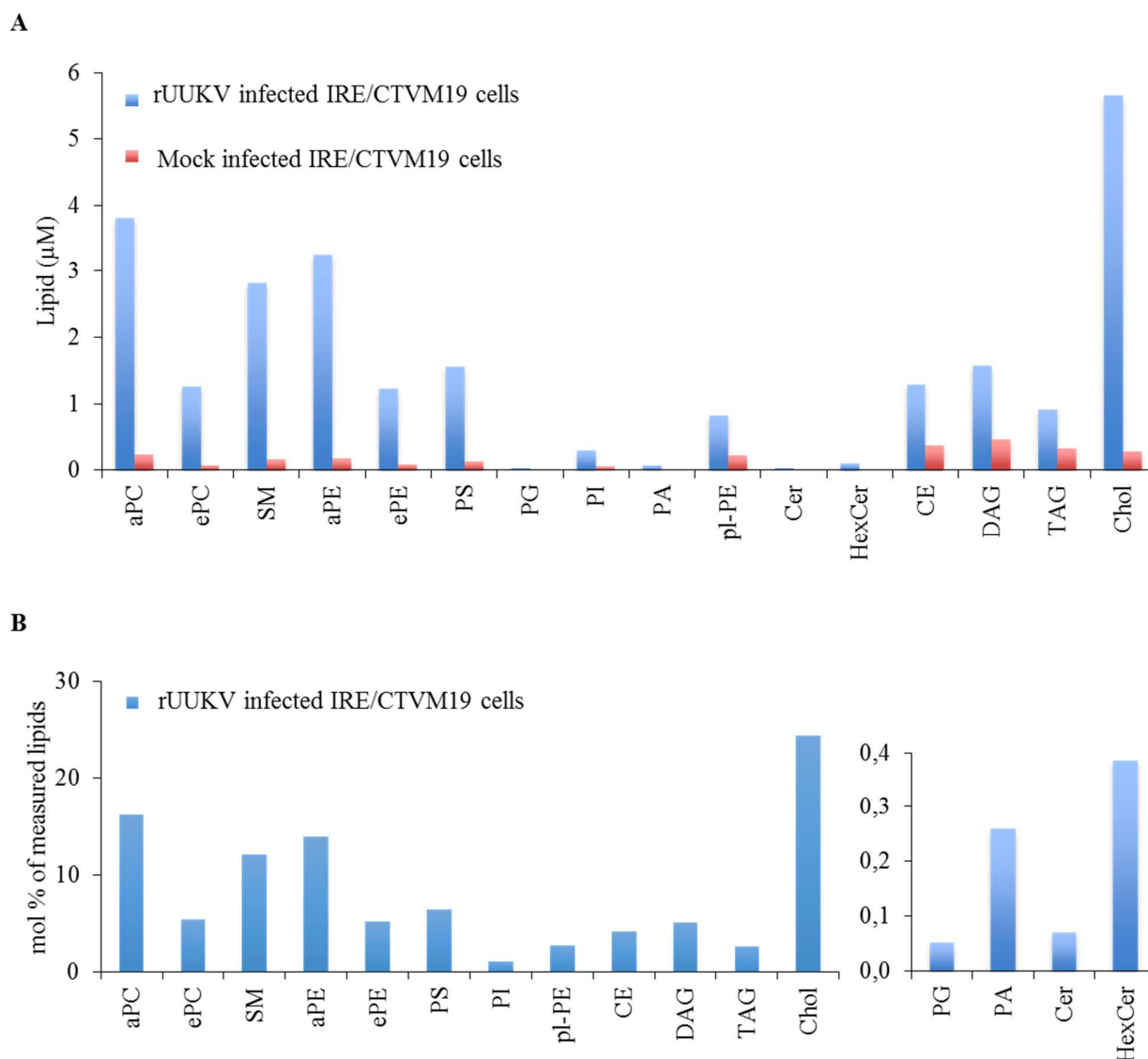


**Figure 30: Lipid composition of IRE/CTVM19-derived Uukuniemi viral particles.**

IRE/CTVM19 cells were mock infected or infected with rUUKV and supernatant was semi purified via a 25% sucrose cushion. Viral particles (blue) and mock infected supernatant (red) were analyzed by mass spectrometry. (A) The concentration of respective lipids are expressed in  $\mu\text{mol}\cdot\text{L}^{-1}$ . (B) Molecular percentage of a lipid specie (relative to the total known lipids). These data represent a single analyze. aPC, acyl-linked phosphatidylcholine; ePC, ether-linked phosphatidylcholine; SM, sphingomyelin; aPE, acyl-linked phosphatidylethanolamine; ePE, ether-linked phosphatidylethanolamine; PS, phosphatidylserine; PG, phosphatidylglycerol; PI, phosphatidylinositol; PA, phosphatidic acid; pl-PE, plasmalogen PE; Cer, ceramide; HexCer, hexosylceramide; CE, cholesteryl ester; DAG, diacylglycerol; TAG, triacylglycerol; Chol, cholesterol.

## Results

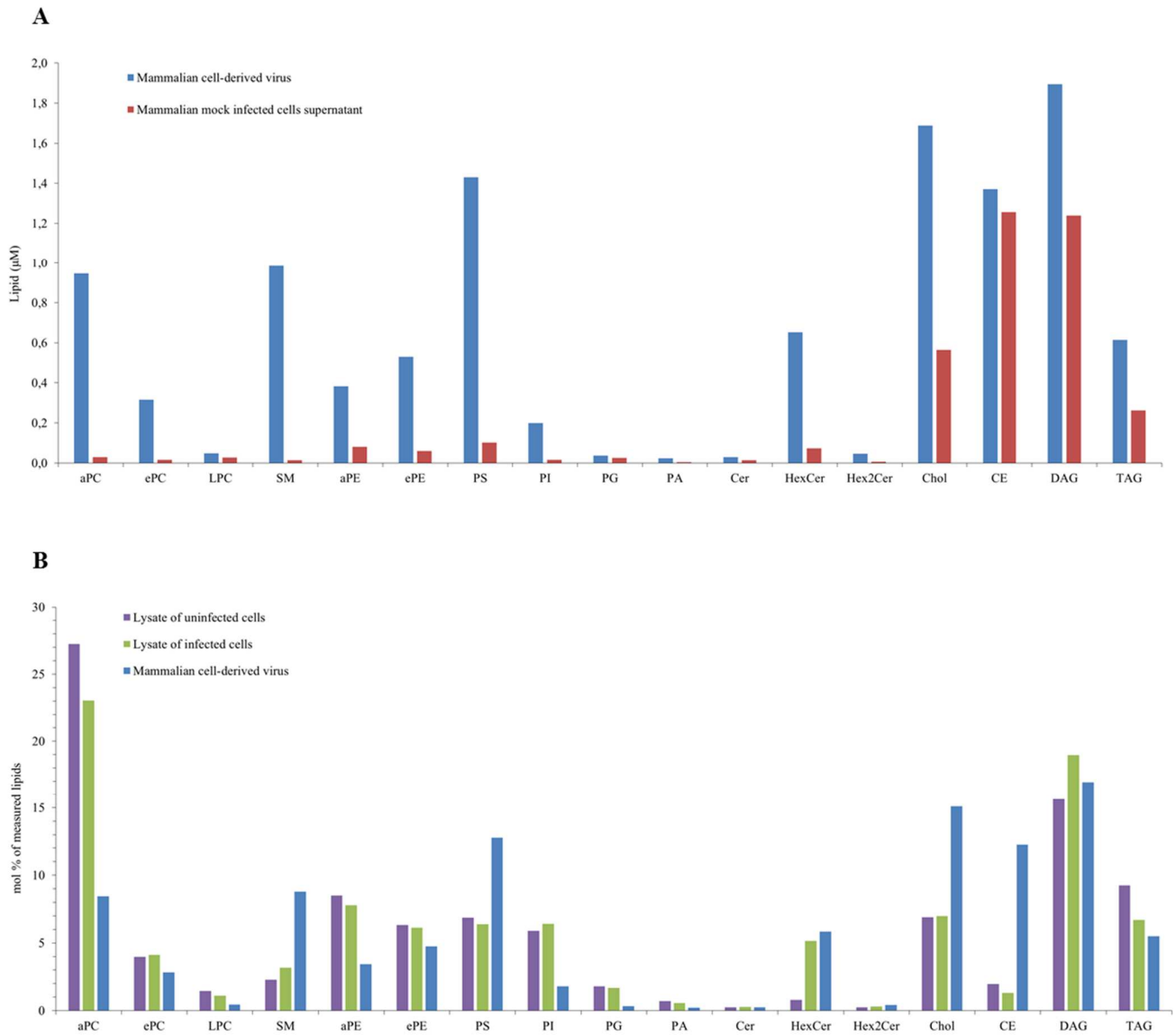


**Figure 31: Lipid composition of mammalian cell-derived Uukuniemi viral particles.**

BHK-21 cells were infected with rUUKV for 48 hours. **(A)** Supernatant was purified via an OptiPrep gradient and viral particles analyzed by mass spectrometry. Viral particles (blue) and mock infected supernatant (red) are represented as a concentration of lipids. **(B)** BHK-21 cells were lysed and analyzed by mass spectrometry. The molecular percentage of a lipid species are shown. These data represent a single analysis. aPC, acyl-linked phosphatidylcholine; ePC, ether-linked phosphatidylcholine; LPC, lysophosphatidylcholine; SM, sphingomyelin; aPE, acyl-linked phosphatidylethanolamine; ePE, ether-linked phosphatidylethanolamine; PS, phosphatidylserine; PI, phosphatidylinositol; PG, phosphatidylglycerol; PA, phosphatidic acid; Cer, ceramide; HexCer, hexosylceramide; Chol, cholesterol; CE, cholesteryl ester; DAG, diacylglycerol; TAG, triacylglycerol;

The tick cell-derived rUUKV present specific biochemical and biophysical features, i.e. glycosylation pattern and folding of the glycoprotein N (**figures 21-23**), ratio of infectivity higher than mammalian cell-derived viral particles (**figure 25**), and lipid composition (**figure 30**). We make the hypothesis that all of these characteristics most likely impact the overall structure of viral particles. Thus, we next aimed to analyze the size and the shape of mammalian and tick cell-derived viral particles by electron microscopy and tomography.

Bunyaviruses are known to be pleomorphic, and UUKV produced in mammalian cells was shown to have a diameter between 100 and 130 nm<sup>61,119</sup>. Whether the size and/or the shape of tick cell-derived particles are the same as mammalian cell-derived particles is unknown. To analyze the size of the tick cell-derived viral particles, rUUKV was produced in either BHK-21 cells or IDE8 cells, purified through a step gradient of OptiPrep, fixed on carbon grids, and stained with uranyl acetate for electron microscopy. Viral particles were imaged by the Electron Microscopy Core Facility (EMCF) at Heidelberg University using a JEOL JEM 1400 microscope. As expected, mammalian cell-derived viral particles are pleomorphic, with some particles spherical and others more elongated (**figure 32A**, left panel). Interestingly, tick cell-derived viral particles were more homogeneous in shape (**figure 32A**, right panel). However, some particles were large (white arrow), some were surrounded by a halo (yellow arrow). In addition small and electron dense spots were visible in the background (**figure 32A**). We cannot exclude that these vesicles are not all viral particles. They could be cellular vesicles with lower density that co-sediment in the OptiPrep gradient. To circumvent this issue, I intend to increase the number of steps in the OptiPrep gradient, i.e. the gradient will thus present a higher resolution and should allow for a better separation of the virus from the other vesicles.

While no structures could be distinguished in mammalian cell-derived viruses, pentons of glycoproteins were visible on IDE8-derived rUUKV particles (**figure 32B & C**). The size of the particles were directly analyzed by the software EMMenue 4 (TVIPS, Gauting, Germany) or using Fiji. The size of mammalian cell-derived viral particles look slightly bigger than those of tick cell-derived viruses. Notably, the biggest particles are more often found for mammalian cell-derived viral particles (**figure 32D**).

## Results

Meanwhile, IDE8-derived viruses were purified through a 25% sucrose cushion and sent to our collaborators at Oxford University, Division of Structural Biology, to assess the viral particles by cryo-EM. Interestingly, our collaborators found a mixed population of particles with different sizes (**figure 33A**). White arrows show the smallest particles (around 60 nm in diameter) that are fairly spherical and regular. The black arrows show bigger particles that seem to have a lipid bilayer and spikes on the surface, but are very heterogeneous in both size and shape (**figure 33A**). Lastly, the yellow arrow indicates particles that seem quite electron dense and have a large size distribution. According to our collaborators, this type of particles is the most abundant. The particles highlighted in white were imaged separately (**figure 33B & C**). These particles harbor spikes inserted in the membrane bilayer and are electron dense, revealing the RNP density. They most likely represent rUUKV particles from vector tick cells, although the diameter is lower than the expected size of mammalian-derived UUKV when looking at the scale bar.

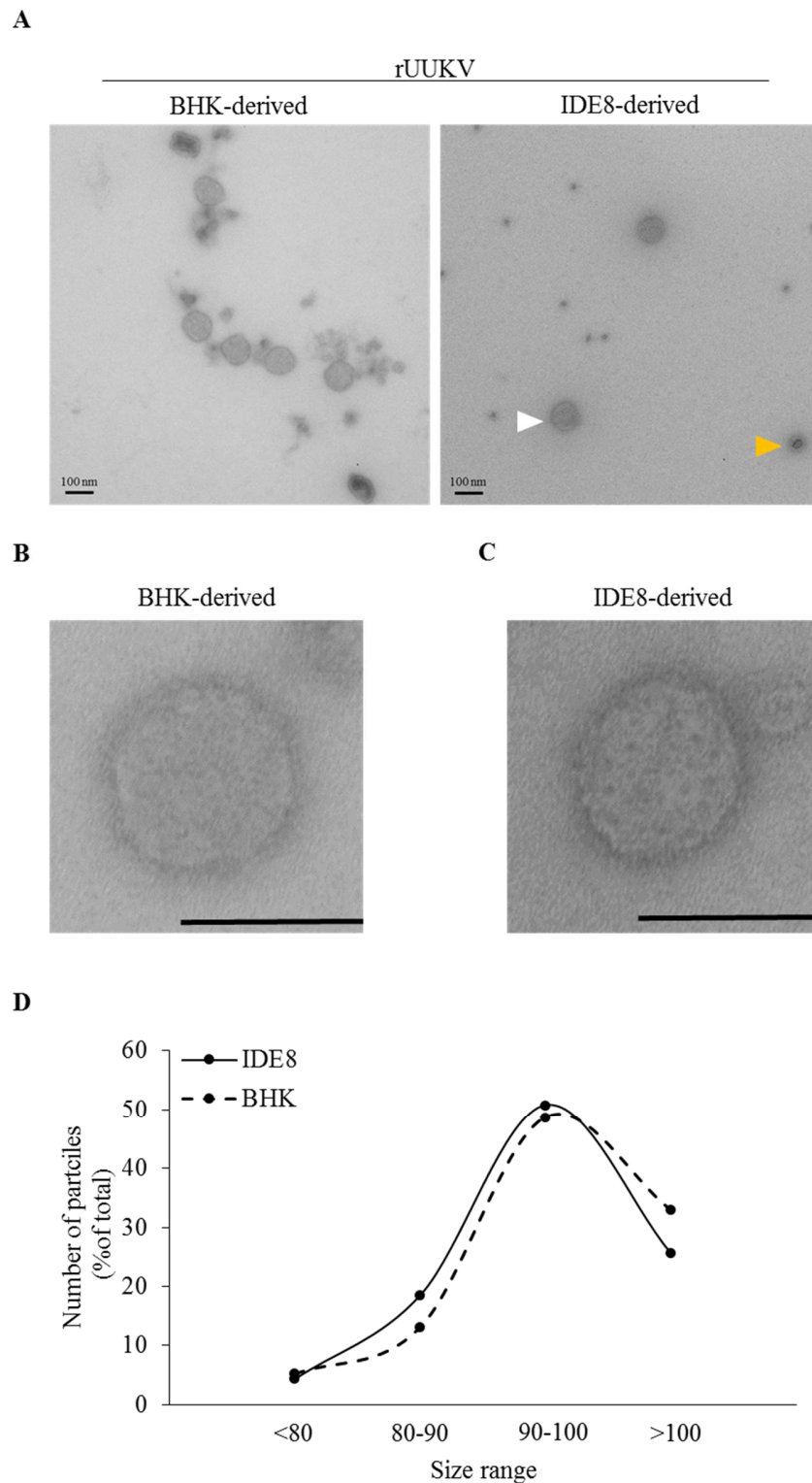


**Figure 32: Size of tick or mammalian cell-derived rUUKV.**

BHK-21 and IDE8 cells were infected with rUUKV at an MOI of 0.01 for 1 or 2 hours, respectively. Supernatant of infected BHK-21 or IDE8 cells was harvested after 48 hours or 20 days, respectively, and purified by OptiPrep gradient. Viruses were then fixed on carbon grids for 1 hour followed by uranyl acetate staining. Images of BHK-21

## Results

cell-derived viral particles (**A**, left panel) and IDE8 cell-derived particles (**A**, right panel) were taken with a JEOL JEM1400 microscope at the EMCF Heidelberg. The white arrow shows big particles of rUUKV and the yellow arrow shows medium size particle of not-yet described structure for phelboviruses. rUUKV derived from BHK-21 cells (**B**) or IDE8 cells (**C**) at a higher magnification. Pictures were acquired with EM10 microscope, scale bar 100 nm. (**D**) Diameters of purified particles were acquired with the JEOL JEM1400 microscope at the EMCF Heidelberg and analyzed with EMMenue 4 or Fiji.

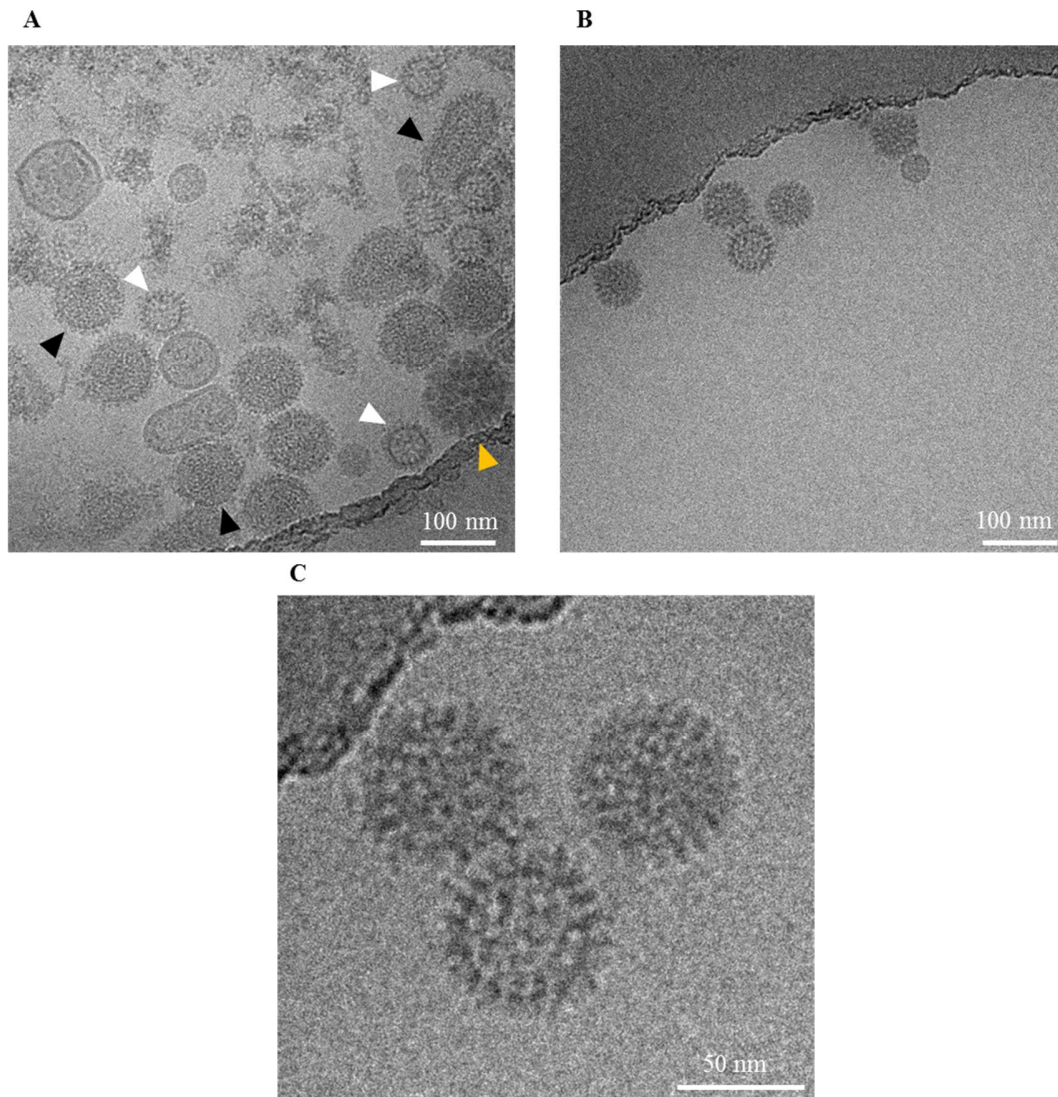


**Figure 33: Tick cell-derived viral particle morphology.**

Electron cryomicroscopy images of semi-purified rUUKV produced in IDE8 cells. Images show an area of a grid of carbon support film with 2 micrometer holes. (**A**) Mixed population of particles: white and black arrows show particles with membrane bilayer and spikes that are either spherical (white) or heterogenous in size (black). The yellow arrow points out a third type of particles that are electron dense but without viral structures. (**B**) Image of the particles highlighted in white in A. Scale bars represent 100 nm. (**C**) Zoom in of the particles from B. Scale bar 50 nm.

#### 4. Early steps of UUKV infection

UUKV has been shown to bind the C-type lectin DC-SIGN before internalization by endocytosis<sup>79</sup>. Moreover, after internalization, UUKV has been shown to require endosomal acidification to infect host cells<sup>100</sup>. The high mannose *N*-glycans of the viral glycoproteins are recognized by the carbohydrate recognition domain of DC-SIGN, allowing binding of the virus<sup>245</sup>. The characterization of UUKV entry was done in various mammalian cells, including human, rodent, or monkey cell lines, with virus stocks produced in mammalian cells (rodent). So far, such characterizations are missing for virus stocks produced in tick cells, and in tick cells. The different glycosylation pattern observed previously with tick cell-derived viral glycoprotein N could change the binding process of tick cell-derived viruses. To address these points, the dependency of rUUKV produced in tick cells on DC-SIGN and a low pH were investigated.

##### a. DC-SIGN mediates infection by tick cell derived rUUKV S23

As shown previously, BHK-21 cells are sensitive to tick cell-derived viruses. However, in a physiological context, dendritic cells are believed to be the first target of arboviruses after introduction in the host skin dermis<sup>21</sup>. Present at the bite site, they are indeed one of the first cells to encounter the incoming viral particles<sup>21,185</sup>. They are believed to participate to the spread of the virus throughout the organism.

To investigate whether the tick cell-derived rUUKV S23 can bind to the receptor DC-SIGN, human B cells (raji) or epithelial cells (HeLa) that stably express the human C-type lectin DC-SIGN (Raji DC-SIGN and HeLa DC-SIGN)<sup>82</sup> were exposed to rUUKV S23 produced in IRE/CTVM19. Raji and HeLa cells are not sensitive to UUKV infection. As expected, at an MOI as high as 5, both raji and HeLa cells are not infected by the tick cell-derived rUUKV S23 (**figure 34A**). However, upon expression of DC-SIGN, 40% of raji are positive for the viral N protein at an MOI of 1. Fluorescent immunostaining against the N protein of rUUKV S23 showed that 50% of HeLa DC-SIGN are infected at an MOI of 5 (**figure 34B & C**). To confirm that the infection was due to DC-SIGN, a mouse monoclonal antibody that specifically blocks the lectin was used (mAbs 1621). After treatment of raji DC-SIGN, infection is inhibited by 90% (**figure 34D**). When using EDTA, which binds calcium and therefore prevents good activity of the lectin, infection is

## Results

also reduced by more than 80%. Similar results were obtained with HeLa DC-SIGN cells; the lectin is inhibited by the mAbs 1621, and the number of infected cells decreases significantly (**figure 34E**).

Altogether, the results show that tick cell-derived rUUKV can also use the receptor DC-SIGN for entry. More specifically, it implies that rUUKV S23 produced in vector tick cells has also, at least in part, high mannose *N*-glycans on its glycoproteins that are recognized by the lectin.

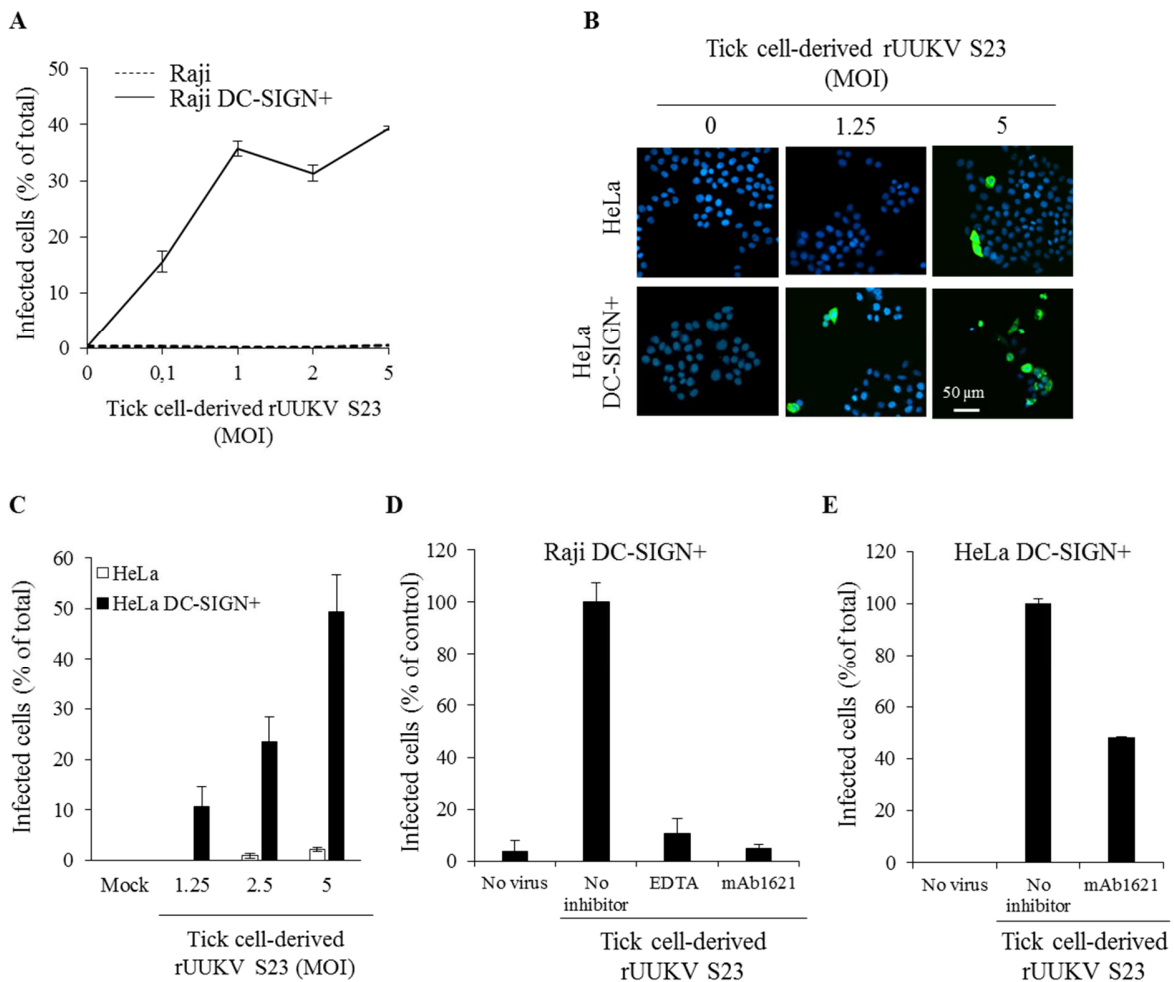


**Figure 34: DC-SIGN is required for the tick cell-derived rUUKV S23 infection.**

(A) BHK-21 cells were infected at an MOI of 0.1 with IRE/CTVM19-derived rUUKV S23 for 18 hours. Cells were immunostained for N, G<sub>N</sub>, G<sub>C</sub> proteins prior to flow cytometry analysis. (B) Parental and DC-SIGN-expressing Raji cells (Raji and Raji DC-SIGN+) were infected with IRE/CTVM19 cell-derived rUUKV S23 for 16 hours. Cells were immunostained for the N protein and analyzed by flow cytometry. (C) Parental and DC-SIGN-expressing HeLa cells (HeLa and HeLa DC-SIGN+) were exposed to various MOIs of IRE/CTVM19 cell-derived rUUKV S23. 24 hours

later, infected cells were immuno-stained for the intracellular virus nucleoprotein N using the anti-N primary mouse monoclonal antibody 8B11A3 and an AF488-coupled anti-mouse secondary monoclonal antibody (green). Nuclei were stained with Hoescht (blue) and samples analyzed by wide-field microscopy. **(D)** More than 100 infected or non-infected cells described in **(C)** were counted in at least three different fields. **(E)** Raji DC-SIGN<sup>+</sup> cells were exposed to IRE/CTVM19 cell-derived rUUKV S23 (MOI ~1) in the presence of inhibitors blocking DC-SIGN, namely EDTA (5 mM) or the neutralizing mouse monoclonal antibody mAb1621 (25  $\mu\text{g}\cdot\text{mL}^{-1}$ ). Intracellular viral antigens were detected by immuno-staining with an anti-UUKV rabbit polyclonal antibody followed by incubation with AF647-conjugated secondary antibodies. Infection was analyzed by flow-cytometry after 18 hours and normalized to infection of DC-SIGN-expressing Raji cells in the absence of inhibitor (% of control).

### **b. pH dependency**

To determine whether tick cell-derived viruses also depend on endosomal acidification for infection, we assess the effect of ammonium chloride ( $\text{NH}_4\text{Cl}$ ) on infection.  $\text{NH}_4\text{Cl}$  is a lysomotropic weak base that neutralizes the pH in all endosomal compartments, instantaneously after addition to the cells <sup>246</sup>. Neutralization of endosomal pH results in an inhibition of infection by viruses that rely on endosomal acidification for penetration.

rUUKV S23 produced in IRE/CTVM19 cells was used to infect human cells (either raji or HeLa cells) expressing DC-SIGN. The cells were treated with  $\text{NH}_4\text{Cl}$  30 minutes before infection and the drug remains during the incubation time (16 hours). Cells were analyzed by flow cytometry after immunostaining of the UUKV protein N. The lysomotropic weak base induced a dose dependent inhibition of infection in both human cell lines (**figure 35A & B**). Similar results were obtained when IRE/CTVM19 or IRE/CTVM20 were infected with rUUKV S23 derived from BHK-21 cells (**figure 35C & D**). Similar results were obtained with chloroquine, another weak base (**figure 35E & F**). To conclude, these results show that UUKV remains dependent on vacuolar acidification to trigger viral fusion, regardless of the host cell origin and the targeted cell type.

## Results

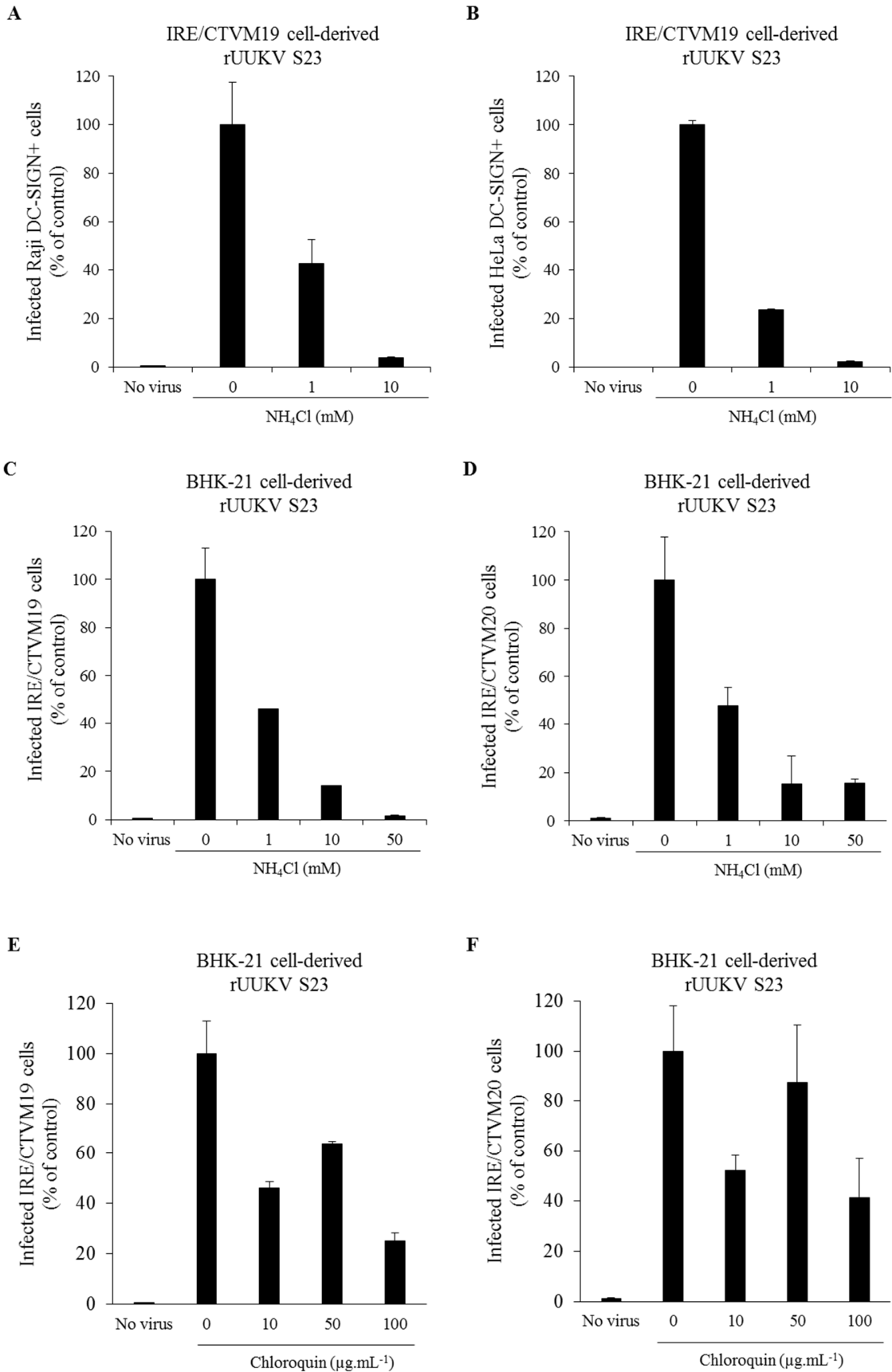


**Figure 35: rUUKV S23 requires low pH for infection.**

Raji (A) and HeLa (B) cells that stably express DC-SIGN were pre-treated with  $\text{NH}_4\text{Cl}$ , a weak base that neutralizes the endosomal pH, and then exposed to IRE/CTVM19 cell-derived rUUKV S23 (MOI ~5) in the continuous presence of the inhibitor. Infected cells were harvested 16 hours later and immuno-stained for the UUKV nucleoprotein N. Infection was analyzed by (A) flow cytometry or (B) wide-field microscopy, counting at least 200 cells in more than three independent fields. Data were normalized to DC-SIGN-expressing cells infected in the absence of inhibitor (% of control). IRE/CTVM19 (C, E) and IRE/CTVM20 (D, F) cells were infected with BHK-21 cell-derived rUUKV S23 at a MOI of 5 for 36 hours in the continuous presence of  $\text{NH}_4\text{Cl}$  (C, D) or chloroquine (E, F). Infection was analyzed by flow cytometry and normalized against data obtained in the absence of inhibitor (% of control).

## 5. Replication of rUUKV: the role of the nonstructural protein NSs

The nonstructural protein NSs is the main virulent factor of RVFV. It counteracts the general transcription of the host cells, including the interferon  $\beta$  response<sup>209–211</sup>. Recently, it has been suggested that UUKV NSs protein could be an IFN antagonist, however with a much lower extent<sup>205</sup>. Not much is known about the role of UUKV NSs, neither in mammalian cells nor tick cells. To define the role of NSs in the replication cycle of UUKV, I took advantage of our RGS<sup>242</sup> to generate recombinant viruses that lack the nonstructural protein.

### a. Generation of recombinant viruses

To visualize and monitor UUKV infection, I engineered S segments with sequences coding for different reporter genes. As all the viral structural proteins are critical for the production of infectious particles, I replaced the sequence encoding NSs by one coding for either the enhancer green fluorescent protein (eGFP), the renilla luciferase (Ren), or the Gaussia luciferase (Gau). This approach has been proved successful for RVFV<sup>72</sup>, although the growth of the recombinant viruses was slightly attenuated compared to the wild-type virus. I also generated recombinant viruses depleted from the sequence encoding the nonstructural protein NSs, which will be designated as UUKV  $\Delta$ NSs. The recombinant UUKV were named as follow and indicated in the **figure 36**:

rUUKV  $\Delta$ NSs is the rescue virus that lacks the NSs ORF

rUUKV eGFP is the rescue virus that lacks the NSs ORF but codes for the eGFP protein instead

rUUKV Ren is the rescue virus that lacks the NSs sequence and encodes the Renilla luciferase protein

## Results

rUUKV Gau is the rescue virus that lacks the NSs ORF but encodes the Gaussia luciferase protein.

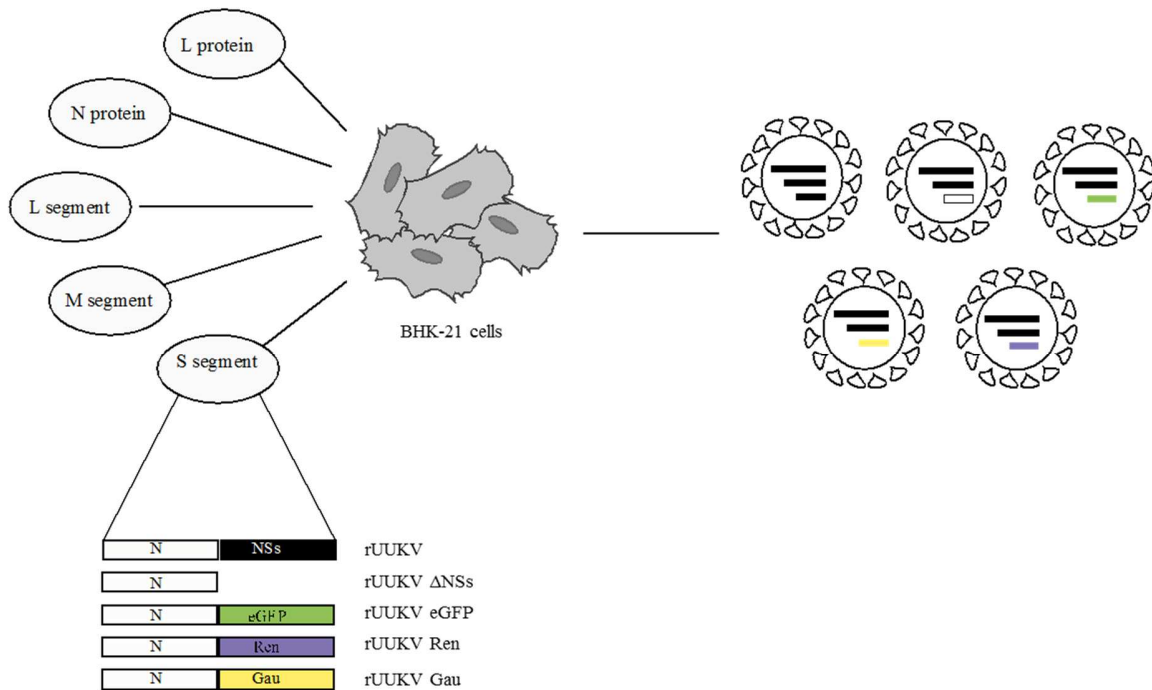


**Figure 36: Schematic representation of the recovery of recombinant UUKV.**

S, M and L segments cloned into the pRF108 were transfected into BHK-21 cells with the pUUK-L and pUUK-N. The S segment has been engineered to express the protein N and different reporter proteins. This includes the enhancer green fluorescent protein (eGFP, green), the renilla luciferase (Ren, blue), or the gaussia luciferase (Gau, yellow). Rescue of UUKV mutants were done by Julia Wegner, a rotation student under my supervision.

As previously described, rUUKV ΔNSs, rUUKV eGFP, rUUKV Ren, and rUUKV Gau were recovered from plasmid DNA after transfection of BHK-21 cells. rUUKV was included in the experiment as a positive control. The shape of foci from rUUKV ΔNSs, rUUKV eGFP, and rUUKV Ren were similar to those of rUUKV (**figure 37A**). As expected, no foci were detected when BHK-21 cells were transfected without the pUUK-N and pUUK-L (data not shown). Starting from day 2 post-transfection, the titer of rUUKV increased over time from a hundred to a hundred thousand FFU per milliliter (**figure 37B**). Similar results were obtained for rUUKV ΔNSs, while infectious progenies of rUUKV Ren and rUUKV Gau were detected at day 3 post-transfection. Moreover, titers for these recombinant viruses were lower, reaching only a thousand FFU per milliliter. rUUKV eGFP was the last to be detected and had significantly lower titer than others

(**figure 37B**). BHK-21 cells that were transfected with the plasmids to recover rUUKV eGFP were monitored under a wide-field microscope to visualize the fluorescence associated with the viral replication. As shown in **figure 37C**, the number of cells that express eGFP increased after 48 hours, indicating an efficient replication and transcription of the S segment. Since the medium is changed after 24 hours, the newly expressing eGFP cells at 48 hours are undoubtedly cells that were infected by neighboring cells rather than transfected cells with a slower expression of the trans gene. Starting 4 days post-transfection, the number of cells that express the eGFP decreased while the number of cells dying increased (data not shown). These results showed, first, that the N and L proteins encoded by the pUUK vectors are essential for the recovery of the virus. Second, our RGS allows for the successful recovery of infectious recombinant UUKV viral particles expressing different reporter genes. Together, these new tools will open the possibility to monitor infection and replication of UUKV and ultimately those of the other tick-borne phleboviruses.

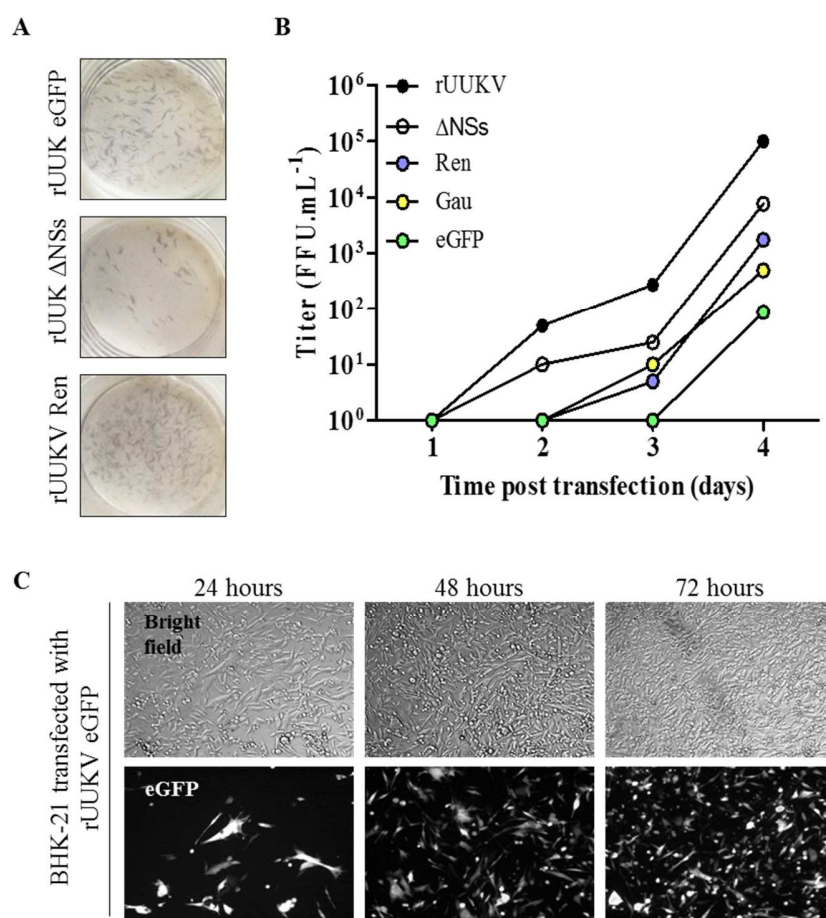


### Figure 37: Recovery of recombinant viruses.

(A) Foci formed in BHK-21 cells by rUUKV Ren, rUUKV  $\Delta$ NSs, and rUUKV eGFP, as described in figure 15. (B) BHK-21 cells were transfected with plasmids encoding UUKV segments M and L in addition to recombinant S segments, together with helper plasmids coding for the N and RdRp proteins. The growth kinetic of rescued viruses rUUKV  $\Delta$ NSs, rUUKV Ren, rUUKV Gau, and rUUKV eGFP were monitored over four days using FFA. (C) BHK-21 cells were transfected to recover rUUKV eGFP and visualized under wide-field microscope 24, 48, or 72 hours post-transfection.

### b. Stability of recombinant viruses

Before using the recombinant viruses to work with, we first assess their stability after several passages in BHK-21 cells. rUUKV eGFP was passaged 5 times in BHK-21 cells, using rUUKV as a control (**figure 38A**). The titers were lower than  $1.10^3$  FFU.mL<sup>-1</sup> for the first four passages. The supernatant was harvested when CPE appeared for rUUKV. After P5, the supernatant was harvested when CPE appeared for the cells infected with rUUKV eGFP instead, which was at days 5 post-infection, significantly later than rUUKV. The titer increased to  $10^5$  FFU.mL<sup>-1</sup>, and almost reached the titer of rUUKV (**figure 38A**). rUUKV eGFP was then passaged five more times and reached a maximum about  $10^5$  FFU.mL<sup>-1</sup> from P5 and higher, which was overall lower than the expected titers for rUUKV (**figure 38A**). The delay in CPE and the lower titers observed raised the question whether the deletion of NSs or most likely the eGFP itself impacts the viral amplification.

To answer this question, we used two other recombinant viruses expressing either the reporter gene luciferase renilla or gaussia. Again rUUKV  $\Delta$ NSs and rUUKV served as controls. Recombinant viruses were passaged only three times in BHK-21 cells. The titers of rUUKV Ren remained stable over the three passages, although they were ten to a hundred times lower than rUUKV (**figure 38B**); nevertheless, the virus seems to infect and propagate after several rounds of infection in BHK-21 cells. However, from the results depicted in **figure 38B**, it is obvious that rUUKV Gau was not able to infect cells after several rounds of infection, suggesting that this recombinant virus was not stable in BHK-21 cells.

Interestingly, the titer of rUUKV  $\Delta$ NSs was 10 times lower than rUUKV at P0, but reached a plateau of  $10^5$  infectious particles produced per milliliters after P1, which is similar to that of

rUUKV (**figure 38B**). The titers at P2 and P3 remained similar to those of rUUKV. From these experiments, we concluded that rUUKV  $\Delta$ NSs and rUUKV Ren seem to be stable in mammalian cells. Moreover, the NSs protein seems to be dispensable for virus production, and thus for the replication and assembly of virions in BHK-21 cells. However, the difference in titers between recombinant viruses and rUUKV shows that manipulation of the genome most likely interferes with the replication and/or production of recombinant viruses.

As these results were intriguing, we then focused on rUUKV  $\Delta$ NSs to better understand the role of NSs in UUKV replication. rUUKV  $\Delta$ NSs, which was passaged independently 5 times in BHK-21 cells, was able to infect the cells after several rounds of infection at a high titers, above  $10^6$  FFU.mL<sup>-1</sup> from P3 (**figure 38C**). This confirmed the previous results and showed that rUUKV  $\Delta$ NSs was stable in mammalian cells. Altogether these results indicate that NSs is dispensable for UUKV propagation, similarly to observations made for RVFV whose some reporter genes interfere with the virus cycle<sup>72</sup>.

### c. Further characterization of recombinant viruses

#### 1-rUUKV Ren

The luciferase that is expressed by the cells was measured after the first passage. The renilla luciferase is not secreted in the supernatant. Therefore, the infected cells were lysed and the level of renilla was measured with a luminometer (see methods). The renilla was detected for the rescue virus rUUKV Ren and to a lesser extend for rUUKV Gau (**figure 39A**).

#### 2-rUUKV $\Delta$ NSs

The titers observed for rUUKV  $\Delta$ NSs and the other recombinant viruses expressing the different reporter genes show that recombinant viruses could be passaged several times in mammalian cells. I then controlled the expression of the NSs protein by immunoblotting. As shown in **figure 39B**, the NSs protein is expressed only in cells infected by rUUKV but not the other viruses, which are all lacking the NSs ORF. The eGFP protein, was also only detected for the rUUKV eGFP, confirming that the protein is expressed (**supplementary material 3**).

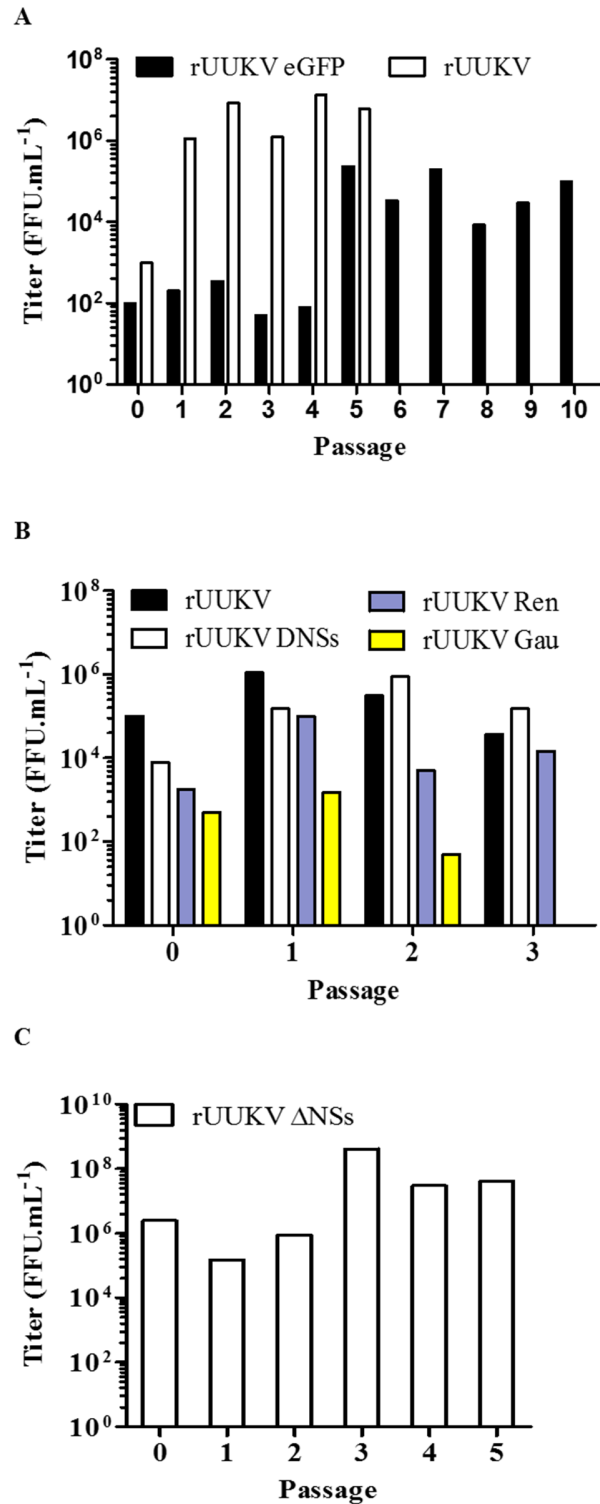


**Figure 38: Passaging of recombinant viruses in BHK-21 cells.**

(A) Titters of recombinant rUUKV eGFP obtained by transfection (passage 0) of BHK-21 cells with our five plasmid system. Supernatant of transfected cells was used to subsequently infect BHK-21 cells, passage 1 (P1) and the process was repeated up to passage 10 (P10). From P5, cells were infected at an MOI of 0.01. Titters were determined using

FFA. **(B)** BHK-21 cells were transfected to rescue rUUKV  $\Delta$ NSs, rUUKV Ren, and rUUKV Gau and supernatant was used to infect BHK-21 cells up to P3. **(C)** BHK-21 cells were transfected to rescue rUUKV  $\Delta$ NSs and supernatant was used to infect BHK-21 cells at an MOI of 0.01 for subsequent passages. Abbreviations: rUUKV Ren, rUUKV expressing renilla luciferase; rUUKV Gau, rUUKV expressing gaussia luciferase; rUUKV eGFP, rUUKV expressing enhancer green fluorescent protein; rUUKV  $\Delta$ NSs, rUUKV lacking the sequence coding for the nonstructural protein

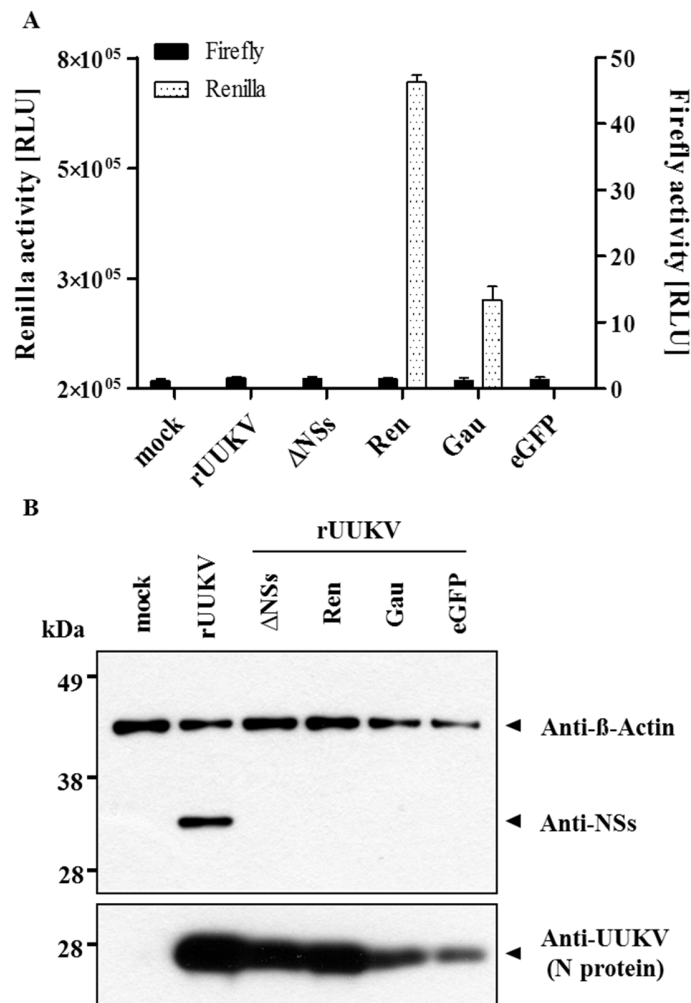


**Figure 39: Characterization of recombinant rescued viruses.**

**(A)** Activity of renilla or firefly luciferase. BHK-21 cells were infected with rUUKV Ren or rUUKV Gau (P1) and lysed. Renilla and firefly activity was measured. RLU, relative light unit. **(B)** Lysates of BHK-21 cells infected with recombinant viruses were analyzed by SDS-PAGE and Western blot under reducing conditions using a polyclonal antibodies against NSs (anti-NSs) or the polyclonal rabbit antibody U2 (anti-UUKV) that recognizes three structural proteins N, G<sub>N</sub>, and G<sub>C</sub>. Here, only the N protein is shown. The mouse monoclonal antibody against  $\beta$ -actin (anti- $\beta$ -actin) was used for normalization. This work was done by Julia Wegner, a bachelor student I supervised.

To conclude, these results demonstrate that the RGS using the murine pol-I promotor allows the recovery of genetically modified UUKV. Some modifications were not always tolerated, e.g.

## Results

the rUUKV Gau, and the titers often lower for recombinant viruses than rUUKV. This suggests that NSs may help for the virus spread, though our results show that virus growth, replication, and propagation can occur in the absence of the nonstructural protein. In addition, the role of NSs in tick cells remains entirely to be discovered.

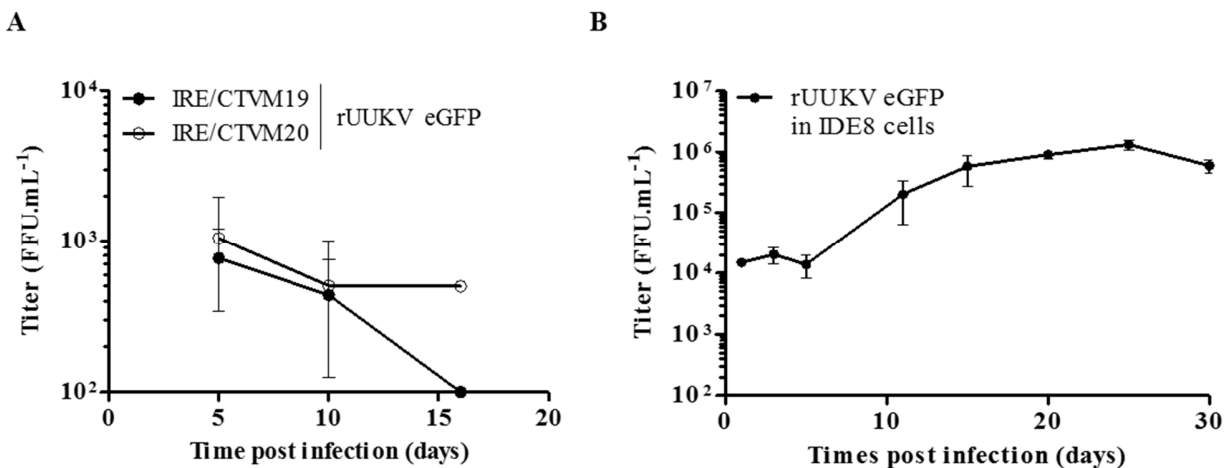


**Figure 40: Infection of tick cells with rUUKV eGFP.**

(A) IRE/CTVM19 or IRE/CTVM20 cells were infected with rUUKV eGFP P6 supernatant. (B) IDE8 cells were infected with rUUKV eGFP (P7 in BHK-21 cells) at an MOI of 0.01. Inoculum was not washed away. Supernatants of infected cells were harvested at various days post-infection. The production of infectious viral particles was determined by a focus-forming assay.

### d. Growth properties of rescued recombinant viruses in tick cells

To determine the role of NSs in UUKV life cycle in arthropod vectors, tick cells IRE/CTVM19 and IRE/TCVM20 were exposed to rUUKV eGFP. After 24 hours of infection, fluorescence was observed but, unfortunately, IRE/CTVM cells had a very high auto-fluorescence background (data not shown). It was, therefore, not possible to follow the EGFP signal in infected tick cells.

To further study the role of NSs in production and persistence of infection in tick cells, supernatants of IRE/CTVM19 and IRE/CTVM20 infected by rUUKV eGFP were tittered over several days. After 15 days, rUUKV eGFP was completely cleared (**figure 40A**). IDE8 are adherent and were shown to produce rUUKV at a high titer, therefore, they were also infected with rUUKV eGFP at an MOI of 0.01. The auto-fluorescence of IDE8 was lower than that of IRE/CTVM cells,

but too high to monitor infection via microscopy. Thus, the replication and production were followed by titration. The inoculum was not removed, but a titration of the supernatant was performed a few hours post-infection and at different time points post-infection.

The titer increased rapidly after day 5 and until day 10 post-infection (from  $1.10^4$  FFU.mL<sup>-1</sup> to  $2.10^5$  FFU.mL<sup>-1</sup>). It reached a plateau after about 20 days post-infection. The growth curve of rUUKV eGFP in IDE8 cells is represented in **figure 40B**. Although, it can be argued that no rUUKV was used as a control for these experiments, the data suggest that rUUKV without the NSs protein does not behave the same in mammalian and tick cells, and it also shows a discrepancy between the two tick species. While UUKV has been isolated from *Ixodes ricinus* ticks, there is no evidence that *Ixodes scapularis* is a vector of UUKV. The loss of the virus in IRE/CTVM cell lines and the low production in IDE8 cells indicates that either the NSs protein is important for UUKV in the vector tick cells or that the eGFP negatively impacts infection.

To further investigate the role of NSs in the infection of tick cells by UUKV, rUUKV  $\Delta$ NSs was then used to infect IRE/CTVM19 and IDE8 cells in 96 well plates and at different MOIs. After 2 hours at 28°C, virus supernatant was removed and cells were incubated for 24 or 48 hours and subjected to flow cytometry analyses after immunostaining against the N protein. It is interesting to note that rUUKV  $\Delta$ NSs does not replicate in IRE/CTM19 cells after 48 hours at an MOI of 5, compared to rUUKV (**figure 41A**). IDE8 cells show a better replication compared to IRE/CTVM19 cells, though low. rUUKV infected more than 80% of the cells after two days at an MOI of 5 (**figure 41B**) and rUUKV  $\Delta$ NSs about 5% of the cells. This might explain why titers of rUUKV eGFP in IDE8 infected cells did not increase during the first 5 days (**figure 40B**). To summarize, within the first two days following infection by rUUKV  $\Delta$ NSs, no or very low infection was detected in tick cells.

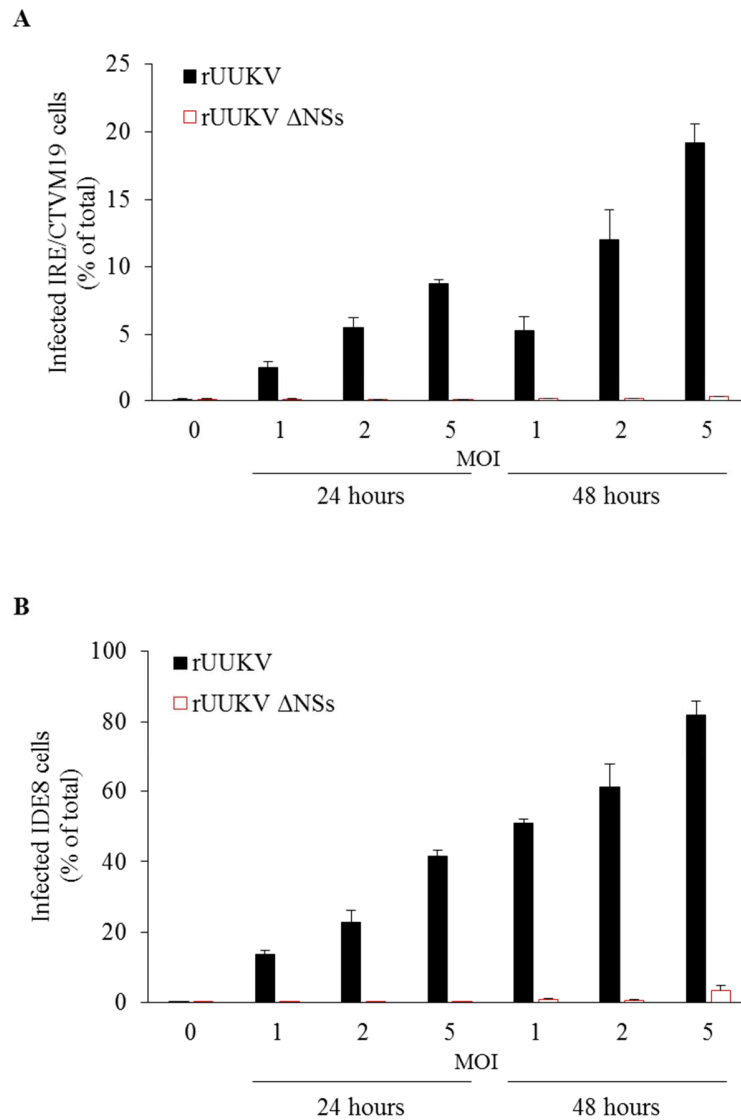


**Figure 41: Early replication of rUUKV  $\Delta$ NSs in tick cells.**

IRE/CTVM19 cells (**A**) and IDE8 cells (**B**) were exposed to rUUKV  $\Delta$ NSs at various MOIs for 24 or 48 hours. Infection was analyzed by flow cytometry after immunostaining against the N protein.

To investigate the involvement of the nonstructural protein in the persistence of infection in vector tick cells, 3 mL glass tubes of IRE/CTVM19 or IDE8 were infected at an MOI of 0.01 with rUUKV  $\Delta$ NSs or rUUKV. Virus supernatant was removed and medium was added into the tubes, which were then incubated for 20 days. Supernatant and cells were harvested at different time points for titration and flow cytometry analyses.

In IRE/CTVM19, the production of rUUKV increased from  $10^3$  to  $10^9$  infectious units per milliliter in 20 days, whereas the production of rUUKV  $\Delta$ NSs increased from  $10^3$  to  $10^4$  infectious units per milliliter, showing a major difference between the two rescued viruses (**figure 42A**). On the contrary, the production of rUUKV  $\Delta$ NSs in IDE8 cells is similar to that of rUUKV (**figure 42B**). These results suggest that the production of viral particles is dependent on NSs in *I. ricinus* cell lines but not in the *I. scapularis* cell line.

To further investigate the replication of the virus in the two different cell species, infection was monitored for 20 days. Cells were harvested and stained for the intracellular N protein at different time points. After more than 10 days of infection, about 50% of *I. ricinus* IRE/CTVM19 cells were infected with rUUKV, whereas rUUKV  $\Delta$ NSs infected only 5% of the cells. After 20 days, 80% of the cells were infected with rUUKV, while the percentage of infected cells slowly increased to 12% with rUUKV  $\Delta$ NSs (**figure 42C**). The picture is totally different when looking at IDE8 infected cells, in which rUUKV and rUUKV  $\Delta$ NSs have similar replication curves. At 6 days post-infection, 20% of the cells were infected, and it increased up to 90% after 20 days for both rescued viruses (**figure 42D**).

To summarize, these data show that NSs seems to be essential for the replication and infection of UUKV in the *I. ricinus* cells, which are the cells from the original host of UUKV. These results also show that NSs could play a role in the production of new virion and might be implicated in the replication of the virus in *I. scapularis* cell lines the first few days of infection, but not after. Altogether, the results presented here point out significant distinctions in UUKV replication dependently on the host cell species.

## Results

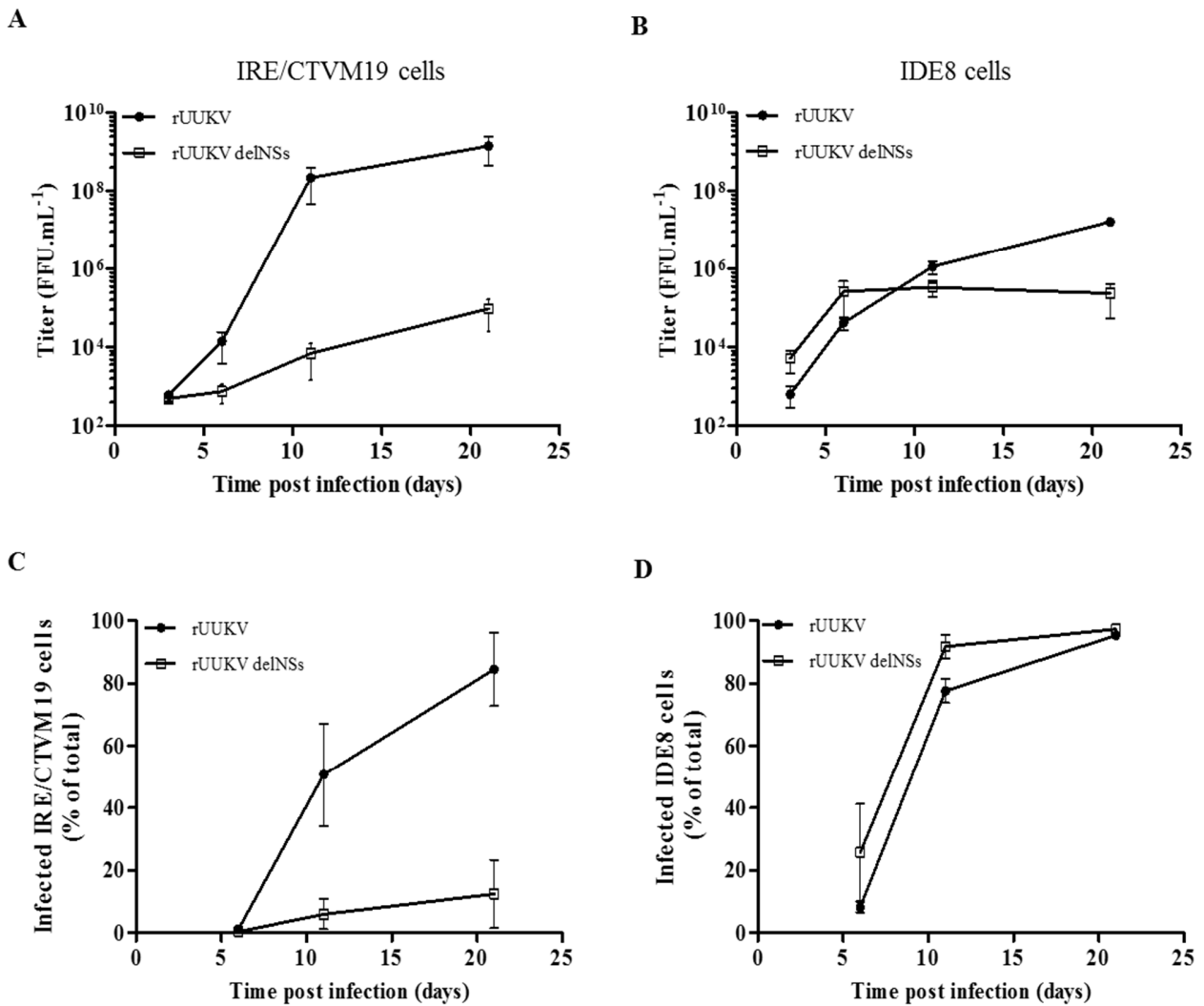


**Figure 42: Production and replication of rUUKV ΔNSs in tick cells.**

IRE/CTVM19 cells (A, C) or IDE8 cells (B, D) were exposed to rUUKV ΔNSs for 2 hours at an MOI of 0.01. Production of viral particles was monitored over 20 days by FFA (A, B) and viral replication in flow cytometry-based assay (C, D) using a monoclonal antibody against N. Infection is given as the percentage of N positive cells.

## Discussion

Ticks parasite a wide variety of vertebrates and are vector of a significant number of pathogens, including bacteria, protozoa, parasites, and viruses worldwide<sup>156</sup>. The diseases they transmit are of huge economic impact for public health and agriculture. An estimation established that approximately 100,000 humans are infected by tick-borne pathogens in the world every year<sup>156</sup>. However, our knowledge on tick molecular and cellular biology is restricted and need to be expanded. During the last decade, new pathogenic tick-borne viruses, such as SFTSV closely related to UUKV, have emerged in different continents<sup>13,14</sup>. This resulted in a renewed interest for UUKV as a tick-borne virus model.

### Implementation of a reverse genetic system for UUKV

The reverse genetic system is a useful tool to study the molecular and cellular biology of viruses in cells. The first RGS developed for bunyaviruses was that of Bunyamwera virus<sup>67,247</sup>. The virus was successfully recovered from plasmid DNAs, and since then other RGS have been developed for members of the family<sup>29,68,69,248,249</sup>. We report here a RGS for UUKV that relies on the pol I promoter, and allows the manipulation of the viral genome. The recovery viruses were infectious in mammalian cells and had features similar to our UUKV lab strain. Moreover, recombinant viruses lacking NSs were successfully recovered from cDNAs. Their full replication characteristic remain to be defined. Another approach, based on the T7 polymerase, was recently used to rescue UUKV<sup>205</sup>. This approach involves the use of the S, M, and L transcripts in an anti-genomic sense. This means that transcripts are directly processed in the cytosol. Consequently, authors did not co-transfect plasmid encoding the RdRp and the N proteins. Under the Pol I promoter regulation, the transcripts follow the mRNA maturation through the nucleus.

UUKV S23 has been isolated in 1959 and adapted to tissue culture prior to sequencing of the genome<sup>250,251</sup>. It was passaged in chicken embryo cells and thereafter in BHK-21 cells<sup>55,250,251</sup>. Surprisingly for a RNA virus the mutation rate was low, and the sequence of our UUKV lab strain did not exhibit major differences compared to that of UUKV S23. A substitution A2386G in UUKV lab strain was found, which is located on the M transcript, in the glycoprotein G<sub>C</sub>. By a single site-directed mutagenesis it was thus possible to obtain the full-length M segment that corresponds to

that of the original strain UUKV S23. This mutation did not show any advantage or disadvantage for the virus life cycle in both mammalian and tick cells in terms of replication and viral production.

In addition, we obtained the full-length M segment for viruses circulating nowadays in tick population in Sweden. We found that the genomic conservation was quite high for RNA viruses, with a sequence identity of amino acids greater than 98% compared to that of UUKV S23. The reversion A2386G was also observed albeit most of the mutations were silent at the amino acid level. Whether these differences show a genetic evolution of UUKV is unknown. The site of collection in Sweden was different from where UUKV S23 was originally isolated, which could also explain the diversity of sequences. Finally, it cannot be excluded that UUKV S23 has adapted to tissue culture, and that the substitution in G<sub>C</sub> is not anymore relevant for circulating UUKV in tick population. Yet, to have a better overview of the RNA mutation rate in UUKV, the S and L segments of these viruses should be also sequenced. To understand whether viruses isolated in Sweden benefit from the non-silent mutations in the M segment, our RGS and tick cell model could be used to investigate the molecular features of the viral particles. It would help us to have a broader overview of the glycoproteins displayed by several of tick-borne UUKV strains.

### **Tick cells are persistently infected with UUKV infection**

Few tick-borne bunyaviruses have been shown to infect tick cells, among them Crimean-Congo hemorrhagic fever virus <sup>252</sup>. During my PhD, I succeeded to infect several tick cell lines with our rescued viruses. Namely, the tick cells IRE/CTVM19 and IRE/CTVM20 originate from embryos of *Ixodes ricinus* ticks, while IDE8 and ISE18 derived from embryos of *Ixodes scapularis* cells. All cell lines supported replication and produced progeny production at a high titer suggesting that the full virus life cycle was accomplished in these cells. That IRE/CTVM cells were infected was rather expected since they derive from the tick species in which UUKV was isolated. Whether *I. scapularis* could be a vector for UUKV remains unclear, although the tick cells IDE8 and ISE18 were sensitive to UUKV infection.

Bunyaviruses are maintained in arthropods and amplified in nonhuman vertebrates. While diseases can occur in vertebrates, there is no evidence for diseases or symptoms in arthropods. This

is also what we observed *in vitro* with infected tick cells: there is no cytopathic effect. This is in line with previous observations made for tick cells infected by CCHFV <sup>252</sup>. Moreover, reports on nonrelated arboviruses TBEV <sup>253</sup> and LGTV have established that tick cells do not present CPE upon infection. Furthermore, tick cells were all persistently infected by UUKV for several weeks in the case of ISE18 cells and even months regarding the IRE/CTVM19, IRE/CTVM20, and IDE8 cells. This reflects the asymptomatic infection of arthropod cells by tick-borne phleboviruses, which contrasts with infection of mammalian cells. Usually, mammalian cells die within 24-48 hours following infection, depending on the viral input load.

### **Characterization of viral particles produced in vector tick and host mammalian cells**

Tick-borne viruses are very often studied with virus stocks produced in mammalian cells. One reason is certainly the difficulty to handle tick cells. As a consequence, little is known about the tick-virus interactions at the molecular and cellular level and viral particles derived from ticks are poorly characterized.

Few years ago, the calcium dependent lectin DC-SIGN has been identified as a true endocytic receptor for UUKV derived from mammalian cells. The lectin recognizes high-mannose residues on the virus glycoproteins  $G_N$  and  $G_C$  and, mediates the internalization and sorting of the virus into the endocytic machinery. We demonstrated in the present work that UUKV derived from vector tick cells can also use DC-SIGN to enter human cells, indicating that glycans on glycoproteins produced in tick cells present, at least in part, high-mannose structures. It was previously shown that BHK-21-derived glycoproteins carried mainly high mannose glycans on the *N*-glycosylation sites of  $G_N$  and  $G_C$  <sup>79,100,254</sup>. Bunyaviruses produced in insect vectors harbor only high mannosylated glycoproteins. In mammalian cells, post-translational modifications, like *N*-glycosylation, occur in the ER and Golgi where glycosylases and glycosyltransferases transform and mature glycoproteins with more complex glycans. It is, thus, not expected that the glycoproteins of BHK-21-derived viruses are highly mannosylated. The reason may be that bunyaviruses bud into the ERGIC or the cis-Golgi and exit cells within vesicles from these compartments, without passing through the normal exocytosis pathway <sup>139</sup>.  $G_N$  and  $G_C$  are then part of viral particles and not accessible anymore to enzymes.

Using semi-purified viral particles through a sucrose cushion and Western blot analysis we demonstrated that glycoprotein G<sub>N</sub> derived from tick cells was much less sensitive to PNGase F and Endo H than the mammalian cell-derived G<sub>N</sub>. Additionally, we showed that the  $\beta$ -N-acetylglucosaminidase recognized glycans on tick-cell derived G<sub>N</sub> but not on mammalian-derived G<sub>N</sub>. It has been postulated that BUNV G<sub>N</sub> would be hidden by G<sub>C</sub> in the heterodimer form, which would inhibit its glycosylation in the Golgi apparatus in mammalian cells<sup>144</sup>. Though the organelles in tick cells like Golgi compartment and ER structures are not characterized, our results tend to indicate that glycosylation acquired in tick cells are different from those acquired in mammalian cells. Moreover, it must be highlighted that maturation and glycan composition of glycoprotein in ticks/tick cells are unknown. The glycosylation metabolism in tick cells is thus virtually completely unknown<sup>255,256</sup>. Senigl et al., postulated that the maturation process of the TBEV envelope and nonstructural protein NS1 was different in mammalian and tick cells when analyzing ultrastructure of ER and membranes in those cells<sup>257</sup> suggesting that vector and host cells have a different biology, which could impact at large the features of the viral particles. It will require further investigations to appreciate the global maturation event of glycoproteins in vector cells and widen our knowledge on tick cell biology.

In the context of virus vector-host switch, the impact of the glycosylation may have a critical importance. Especially, *N*-glycosylation is important for recognition of and attachment to the receptor<sup>258</sup> as illustrated with the phlebovirus-DC-SIGN interactions. The specific type of glycans on tick-derived viruses may increase the diversity of potential receptors in the skin dermis and/or the signalization by the receptors, thus increasing the infectivity of these viruses. It is known that DC-SIGN, according to carbohydrates that are recognized, activates different signalization pathways<sup>93,94</sup>. When UUKV is produced in mammalian cells, the virus is able to use different lectin receptors to enter human cells<sup>90</sup>. It is, therefore, important to elucidate the type of glycan that are synthesized in the vector ticks to understand mechanisms involved in tick-derived virus transmission and early steps of infection in humans. One can easily imagine that tick cell-derived viruses activate different signaling pathways in DCs than those triggered by mammalian cell-derived viruses. Also, it cannot be excluded that different lectin receptors may be recognized by vector cell-derived viruses, which would impact the virus tropism and the identity of first infected cells *in vivo*. In line with this, Shi et al, showed that *N*-glycosylation on BUNV G<sub>C</sub> in mammalian

cells was essential for early steps of viral infection<sup>144</sup>. Glycosylation also determines the glycoprotein folding and trafficking, which consequently allows the maturation and secretion of viruses. For instance, a defect in TBEV *N*-glycosylation has been shown to reduce secretion of viruses in mammalian cells, but not in tick cells<sup>259</sup>.

PNGase F is an enzyme that cleaves *N*-linked glycans independently on their glycan composition. In contrast, Endo H only removes mannose rich structures of *N*-linked glycans. Interestingly, the glycoprotein G<sub>C</sub> from both tick and mammalian cell-derived viruses was sensitive to PNGase F. G<sub>C</sub> on virions derived from tick cells was entirely sensitive to Endo H, which indicates that only mannose decorate the protein. G<sub>C</sub> on virions derived from mammalian cells was partially sensitive, meaning that the glycoprotein harbors hybrid and complex glycans. However, UUKV derived from tick cells can also use DC-SIGN to infect cells. Whether the carbohydrate recognition domain (CRD) of DC-SIGN binds a single mannose residue on G<sub>N</sub> or/and several on G<sub>C</sub> remain to be clarified.

Although both glycoproteins showed differences when expressed from tick cells culture, the glycoprotein G<sub>N</sub> exhibited the most differences between tick and mammalian derived viruses. G<sub>N</sub> produced in tick cells had less *N*-linked glycans and a different type of oligosaccharides. In addition, the apparent molecular weight of G<sub>N</sub> was lower for the protein expressed in both IRE/CTVM and IDE8 tick cells compared to that produced from BHK-21 cells (**figure 21A & C, 23, and 28**). To clarify whether a shorter version of the protein was translated and could explain the difference in molecular weight, the nucleotide sequence of the M segment was sequenced. Neither mutations nor deletions were found. The amino acid sequence of the glycoproteins were then analyzed by mass spectrometry. No alternative open reading frames were found. Though the sequences determined by mass spectrometry were not complete, most likely because some peptide could not be resolved, it is unlikely that there is another ORF that would result in an isoform version of G<sub>N</sub>.

Besides the smaller size of G<sub>N</sub> on viruses derived from tick cells, which might be explained by dissimilar glycosylations or a divergent maturation of the protein, the glycoprotein was not sensitive to  $\beta$ -mercaptoethanol. This suggests that the number of disulfide bonds is not the same

between mammalian host and vector cells. Overall it suggests that the folding of the glycoprotein  $G_N$  is different in mammalian and tick cells. So far, the structure of  $G_N$  is not known, whether it comes from mammalian or tick cells. These information would definitely help to provide new insights into the biochemistry of this glycoprotein.

In this report, we showed that the amount of structural protein N,  $G_N$ , and  $G_C$  varies according the origin of the cells used for virus production, i.e. tick IRE/CTVM19 or BHK-21 cells. Viral particles derived from tick cells carry less nucleoprotein N and more glycoproteins  $G_N$ , and  $G_C$ . The ratio of infectious to noninfectious particles has been shown to be low for UUKV when produced in mammalian cells, estimated to 1:5'000<sup>100</sup>. Here we have showed that the ratio between the number of foci forming units and N protein is higher for tick cell-derived UUKV. This suggests that the number of infectious viral particles produced in tick cells is significantly higher compared to those from mammalian productions. *In fine*, it is reasonable to postulate that the viral particles from vector tick cells are more infectious than viral particles produced in the mammalian host cells.

To confirm our hypothesis, fluorescent labeling and microscopy methods would be helpful. Indeed, by labeling the glycoproteins of UUKV with an Alexa Fluor dye, which form covalent links by reaction with free amine groups (Hoffmann et al., under review), we could count the total number of viral particles under wide field microscope and correlate this number with the number of FFU. Alternatively, we could use light scattering (NanoSight machine) to measure the total concentration of particles and the concentration of fluorescent particles to make a ratio of infectious to noninfectious viral particles. Macrophages and DCs are believed to be critical for the recognition of the virus after a tick bite. It would be interesting to compare their sensitivity to tick and mammalian cell-derived viruses, which could improve our knowledge on the transmission of these viruses to humans. In future perspectives, multiphoton microscopy will be of interest to assess the transmission of arbo-bunyaviruses in live animal imaging. With these different approaches it might be easier to conclude whether or not the tick cell-derived viruses are more infectious than those produced in the mammalian host cells.

Bunyavirus particles do not have any matrix protein nor a capsid, thus the integrity of the overall particle structure relies on RNPs, glycoproteins, and lipid bilayer. Although our results are

preliminary, the lipid composition of viral particles produced in tick cells seems to present a high amount of cholesterol and sphingomyelin (25 mol % Cholesterol and 12 mol % Sphingomyelin). These two lipids are commonly found in lipid raft of ER membrane in eukaryotic cells <sup>260,261</sup> and at the plasma membrane at this molarity <sup>262</sup>. It is then tempting to suggest a budding site from an ER-like membrane in tick cells. Nothing is known about lipid metabolism in such cells and it will require much more work to understand the impact of lipidomics on tick cell-derived viruses in terms of virus structure and infectivity.

Concerning the mammalian cell-derived viruses, we showed that the viral particles were composed of a majority of the gangliosides DAG, Chol, and CE as well as the phospholipid PS, and the sphingolipid SM and HexCer. The lipid of the viral particles produced in mammalian cells are typical of those that constitute the plasma membrane. This, which has never been shown before for bunyaviruses, suggests that UUKV buds from the plasma membrane of mammalian cells. Our results are in agreement with the lipidome of BHK-21-derived vesicular stomatitis virus (VSV) and Semliki Forest virus (SFV) <sup>263</sup>. These two unrelated viruses, *Rhabdoviridae* and *Togaviridae* family respectively, have been shown to present a similar content of lipids found at the plasma membrane of BHK-21 cells <sup>263</sup>. While the viruses in both these families bud from the plasma membrane, it addresses the question about the cellular site used by UUKV for assembly and budding. It may be that UUKV and other phleboviruses create a local lipid environment for budding in ER or Golgi that is similar to that of plasma membrane. Moreover, our lipidomic analysis of uninfected and infected BHK-21 cells revealed that the mol % of DAG, and more importantly HexCer, were enhanced in infected mammalian cells, suggesting a unique lipid biosynthesis rearrangement during infection. Whether this is cell type specific will have to be defined.

Furthermore, we cannot completely exclude that viral particles are enriched in those two lipids simply because the producer cells IRE/CTVM19 are maintained in medium containing 20% FBS. For a more reliable determination of the lipid composition of virus membranes, the viral particles produced in IDE8 as well as in BHK-21 cells without any additional lipids should be analyzed by mass spectrometry. Not only the viral particles but also infected cells should be analyzed. Indeed, the lipid metabolism of infected cells change upon arboviral infection, as shown for flaviviruses infection in both mosquito and mammalian cells <sup>261,264–266</sup>. Finally, the lipidome of

ticks *I. ricinus* and *I. scapularis* at different stages of their animal development (larvae, nymph and adult) should also be analyzed by mass spectrometry to compare with that of the tick cell lines and viruses produced in those cells. This would avoid any problem with the FBS supplementation.

As other phleboviruses, UUKV is known to be pleomorphic in shape and size when produced in mammalian cells<sup>30</sup>. This is also what we observed when analyzing single viral particles from mammalian cells under electron microscopy. However, the viral particles produced in tick cells were found to be more homogeneous in shape when analyzed by EM with a size that appeared to be smaller. When using advanced cryo-EM techniques, we detected heterogeneous particles, those that most likely represent UUKV with a diameter of approximately 60 nm. UUKV, when produced in mammalian cells, has a diameter that varies between 80 to 140 nm<sup>30,61</sup>.

This difference in size may be explained by the results we obtained. We discussed previously the difference in glycosylation, maturation and folding of the glycoproteins G<sub>N</sub>. Western blot analysis and the ratio we presented indicate that the amount of glycoproteins is higher on tick cell-derived viral particles than that of mammalian cell-derived particles. The amount of N protein is also lower in tick cell-derived viral particles. In addition, the lipidome of viral particles differs whether they are produced in tick or mammalian cells. Taken altogether, it is tempting to postulate that arthropod vector-derived viruses packaged less genomic material and express more glycoproteins with a more efficient distribution on the surface of the particles, most likely because of the high amount of cholesterol in the viral envelope allows for a higher lipid bilayer curvature. In turn, the overall structural organization of tick cell-derived viruses, which arguably differs from that of the mammalian cell-derived particles, would make viral particles more stable and infectious.

Together my results participate to improve our understanding of the molecular features and organization of tick-borne viral particles and their impact on virus transmission and entry in humans. Based on the sum of my data presented here, I propose a model of tick-borne viral particles that differs from that of mammalian-derived viral particles (**figure 43**).

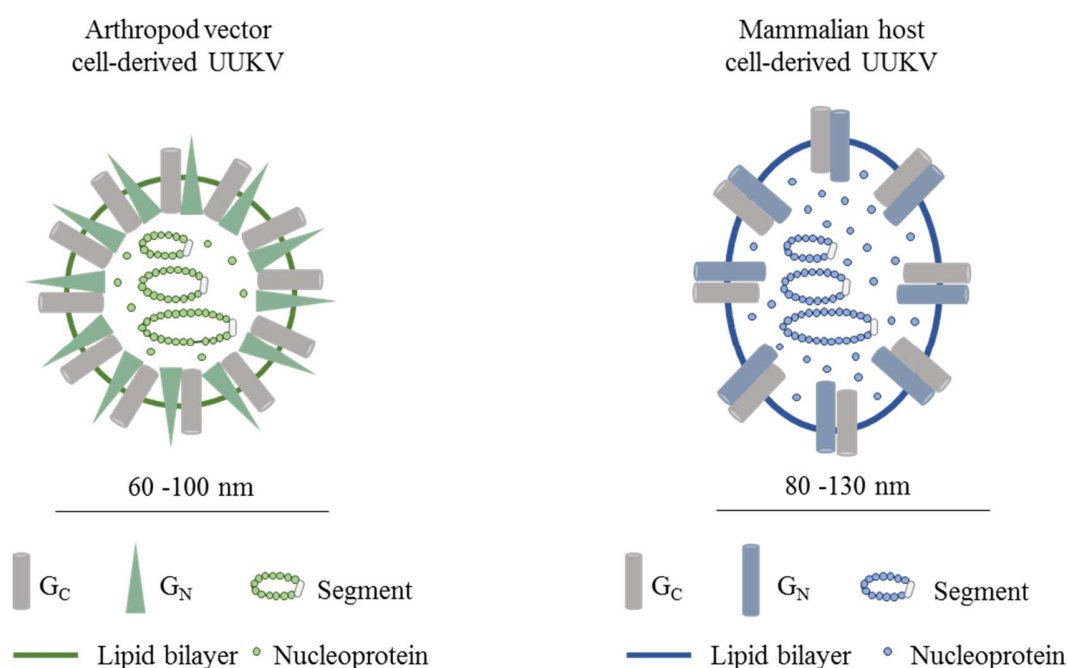


**Figure 43: Proposed model of viral particles coming from vector tick cells and host mammalian cells.**

Tick cell-derived viruses (green) are smaller and more spherical than mammalian cell-derived viruses (blue). Viruses produced in tick cells are composed of less viral nucleoproteins and more glycoproteins. In addition these viruses have an envelope with a specific composition in lipids and a glycoprotein  $G_N$  with an original glycosylation pattern and a reduced number of disulfide bonds.

The procedure of virus purification through OptiPrep gradient can still be improved. This would allow us to exclude that exosomes, for instance, contaminate our virus stocks for mass spec analysis. Their size and density are similar to those of viruses<sup>267</sup>. It would be interesting to know whether tick cells produce such vesicles. To complete the set of our data, cryo-EM analysis of the mammalian cell-derived viruses will reveal the ultrastructure and organization of viral particles that may explain the higher infectivity observed for viruses derived from arthropods.

Like other bunyaviruses, tick-borne viruses are late penetrating viruses. They require endosomal acidification to infect mammalian cells<sup>21,89,98,102</sup>. The weak base  $NH_4Cl$  that neutralizes the pH was found to inhibit infection of human DC-SIGN-expressing cells by tick cell-derived UUKV. Furthermore, IRE/CTVM19 and IRE/CTVM20 cells were not infected by mammalian-derived viruses when treated with either  $NH_4Cl$  or bafilomycine A1, another component that neutralizes the pH. In conclusion, UUKV depends on low pH for infection, regardless of the cell type it infects and from which it originates. While the pH drops, the conformation of the

glycoprotein  $G_C$  changes, which results in the fusion between endosome and virus membranes<sup>76,97,113,119</sup>. The role of  $G_N$  in the entry and fusion remains to be elucidated. That  $G_C$  has a critical role in viral genome uncoating may explain in part why  $G_C$  has conserved a similar biochemical pattern between tick and mammalian cell-derived viruses, but also why  $G_C$  on circulating viruses in the wild has nearly not evolved during the 60 last years.

### **The puzzling NSs protein**

It was possible to develop several recombinant viruses deleted in the NSs ORF to study the life cycle of UUKV in both tick and mammalian cells. Unfortunately, the recombinant rUUKV that expresses the gaussia luciferase was not stable in BHK-21 cells, meaning that the virus could not replicate after three successive infection passages in mammalian cells. rUUKV that expresses the renilla luciferase is probably stable though further passages and sequencing are required to confirm the genetic stability of the virus in mammalian cells. The recombinant viruses that encodes the eGFP, rUUKV eGFP, was struggling to obtain because of the longer period of time the virus required to be produced. That rUUKV  $\Delta$ NSs show a similar production than rUUKV and a stability in BHK-21 cells suggest that the reporter gene expression by itself affects the replication or the assembly of UUKV. eGFP is known for its toxicity in cells. Yet, only Rezelj et al. rescued UUKV that encodes GFP protein instead of the NSs protein with a high titer<sup>205</sup>. It is questionable whether this dichotomy comes from the system they used, which do not require the expression of the N and L proteins. The related mosquito-borne RVFV was also shown to replicate without the NSs protein replaced by the GFP protein but not with humanized firefly luciferase reporter gene<sup>72</sup>. The latter work was performed with a RGS similar to the one we developed. Overall, it is noticeable that RGS have still space for improvement in order to allow larger modifications of bunyavirus genomes.

RNA segments of bunyaviruses are flanked by 3' and 5' nontranslated region (NTR) that are important for base pairing<sup>32</sup> and attachment to the RdRp<sup>128</sup>. Therefore, it is possible that the lower titer observed for rUUKV eGFP is due to the genomic sequence of the reporter gene. Indeed, the nucleotide sequence by itself may form secondary structures that are no longer recognized by the N protein resulting in a misfolding RNP complexes, which would hamper the assembly and the

subsequent release of viral particles. Alternatively, during RNP assembly, the N protein interacts with a precise number of nucleotides. This number is different between the NSs, Gaussia luciferase, and eGFP sequences. It is then possible that the association between the recombinant RNA segment S and molecules of protein N is disrupted or inefficient. This would result in a poor efficiency of RNP assembly and virus packaging, and in turn, a lower infectivity.

rUUKV eGFP was engineered to follow the viral life cycle using microscopy. Unfortunately, high auto-fluorescence background in the green coming from tick cells did not allow for monitoring rUUKV eGFP in tick cells. In addition, after a couple of days of infection, no titer was detected, suggesting that either the eGFP protein or the absence of NSs was deleterious in vector tick cells. To test the second assumption, I analyzed the UUKV  $\Delta$ NSs replication in the tick *I. ricinus* cells using our FACS-based infection assay, which is more sensitive than FFA. Indeed, by staining the newly synthesized N protein, we demonstrated that in absence of NSs UUKV did not replicate in IRE/CTVM19 cells, the species from which the virus was originally isolated. In contrast, in *I. scapularis* cells, the absence of NSs did not affect the replication of the virus. In line with these results, the production of UUKV without the nonstructural protein NSs was much lower in *I. ricinus* cells than in *I. scapularis* cells. This is the first time that a tick-borne virus deleted in a nonstructural protein is shown to be unable to replicate in its vector tick cells. Our results support the idea that NSs could play an important role in the host switch and the adaptation of the virus to its tissue environment.

Using our RGS, I have planned to generate new recombinant viruses that encode for a NSs or N protein either tagged with a Flag or tetracysteine peptide. These tags are smaller than reporter genes and may not disturb viral RNA. Therefore, the monitoring of UUKV replication in tick cells and mammalian cells, fixed (Flag tag) or alive (tetracysteine tag) would be possible. Coupled with immunostaining of cellular proteins, this would allow the identification of cellular partners important for the UUKV replication cycle. This would also enable the localization of the site of viral replication in the different tick species. Although UUKV replicates in *I. scapularis* ticks cells, the virus has never been isolated from any other tick species than that of *I. ricinus*. The differences observed between the two cell lines reflect that the virus can adapt to different tick and host cell biology. It is paramount to elucidate the molecular mechanisms behind the adaptation of

these viruses to their host in order to better understand the associated pathogenesis in humans and other mammals.

### **Antiviral immune response in tick cells**

In 2015, Weisheit et al. have shown that infection by LGTV (tick-borne flavivirus) of IRE/CTVM19 (vector cells of LGTV) and IDE8 (not the vector cell of LGTV) cells resulted in an up and downregulation of diverse RNA transcripts and protein expressions<sup>236</sup>. Additionally, when silencing Ago 30 and Dcr 90 proteins, involved in the RNAi antiviral response, LGTV RNA levels and production increased significantly, demonstrating that both cell lines have an RNAi based antiviral response<sup>236</sup>. Recently, IRE/CTVM20 cells were shown to activate innate immune response via the Jak-STAT and toll pathways when infected with TBEV or LIV (tick-borne flaviviruses)<sup>167</sup>. Jak/STAT and toll proteins are part of the innate immune system of *Ixodes scapularis* ticks<sup>268</sup>.

UUKV NSs has never been investigated and characterized deeply, and thus, our knowledge on this protein is very limited. One study suggested that UUKV NSs is a weak IFN antagonist<sup>205</sup>, while NSs of RVFV and SFTSV has been shown to be strong IFN antagonists<sup>198,204,210</sup>. It is thus tempting to postulate that UUKV NSs in its vector IRE/CTVM19 cells inhibits immune response (mainly siRNA pathway) allowing the replication of the virus; whereas without NSs the tick cells activate the mechanisms for immune response that partially inhibits the replication of the virus. Future experiments should consist in silencing proteins involved in the RNAi pathway in IRE/CTVM19 such as Ago, Dcr, and Toll proteins to assess the replication of UUKV and the role of the NSs protein.

IDE8 cells, which has never been described as a tick vector of UUKV, have arguably a specific molecular biology compared to that of IRE/CTVM19 and probably rely on other cellular factors and processes to control infection. It cannot be excluded that endogenous pathogens influence immune response in IDE8 cells in a different manner than in IRE/CTVM cells. The first tick cells that have been shown to be persistently infected with an endogenous virus were IDE2 cells, also from *I. scapularis* ticks<sup>269</sup>. IDE2 cells were infected with St Croix River virus (SCRV).

SCRV is a member of the *Orbivirus* genus, *Reoviridae* family, and is approximately 60 nm in diameter<sup>269</sup>. More recently, a study that investigated endogenous bacteria and viruses in another *I. scapularis* tick cell lines showed that ISE18 were PCR negative for SCR. However, reovirus like particles have been seen by electron tomography in *I. ricinus* IRE/CTVM19 and IRE/CTVM20 cells as well as *I. scapularis* IDE8 and ISE18<sup>270</sup> although these particles were not formally identified. Other endogenous viruses, with diameter between 60 to 80 nm, have been described in IRE/CTVM19 cells and IDE8 cells, such as those we used to produce tick cell-derived UUKV<sup>271,272</sup>. This could also explain the diversity of particles and vesicles observed by EM and cryo-EM. Further investigations will require immunogold labeling approaches to complete EM analysis and confirm that the particles seen on EM pictures are UUKV.

## Conclusion – Perspective

The aim of my PhD project was to recapitulate *in vitro* the tick vector-to-mammalian host transition of tick-borne viruses with the ultimate goal to provide new insights into the early steps of infection by these arboviruses in humans and other mammals.

To this end, we developed and took advantage of a reverse genetics system to recover the original tick-borne UUKV strain 23 from cDNA. The rescued virus was then used to develop a tick cell model in which tick-borne phleboviruses can be studied. This model is based on IRE/CTVM19 and IRE/CTVM20 cells that derived from the tick species *Ixodes ricinus* from which UUKV was originally isolated. IRE/CTVM cells were sensitive to infection and persistently infected for months without apparent cytopathic effect. We demonstrated that the structural, biochemical, and biophysical properties of vector tick-cell viruses show significant distinctions compared to the mammalian host viruses. Moreover, viral progeny produced in tick cells seem to have a higher infectivity than those derived from mammalian cells. These results highlight a possible difference in the cell biology between mammalian host and vector tick cells, which is still largely uncharacterized.

This work has also resulted in the establishment of a new method of virus production from tick cells. Using IDE8 cells, derived from embryos of *I. scapularis* ticks, it was possible to produce large volume of viruses without FBS. This achievement will allow the analysis of viral particles by all the techniques related to electron microscopy and mass spectrometry approaches. This is the first time that such a progress is made in the field. In addition, a new method of virus purification involving the use of OptiPrep gradient was successfully tested. This also improves the quality of samples prior to mass spectrometry analysis for instance. Though this method is still under improvement with respect to the yield and purity of virus stocks, we could already show that viral particles produced from tick cells differ from those derived from mammalian cells. They were smaller, more homogeneous in shape, and more spherical than mammalian cell-derived viruses. Moreover, preliminary results pointed out a high content in cholesterol and sphingomyelin. My results, for the first time, emphasize the importance to work with viruses produced from arthropod vector cells when studying arbovirus transmission to mammals.

Finally, with the advantage of RGS to manipulate the genome, we rescued viruses that lack the nonstructural protein NSs sequence and encode, instead, a reporter gene such as eGFP and the renilla luciferase. The deleted NSs mutant was stable in BHK-21 cells and was used to monitor the replication in tick cells IRE/CTVM19 and IDE8. Though the replication and the production of rUUKV and rUUKV  $\Delta$ NSs were similar in mammalian cells, the replication and the production kinetics were dramatically different between those viruses in IRE/CTVM19. NSs appeared to be essential for the virus life cycle in its vector cells. In contrast, IDE8 did not show dissimilarity between the two viruses, revealing a different response to viral infection.

Our work brought new insights into the molecular and cellular interactions between tick-borne viruses and the vector cells, and also between tick-borne viruses and the host cells. The future perspectives concern different aspects of tick-borne viruses. We will further examine the specificities of viral particles components from vector and host cell types in terms of glycosylation and lipid composition as well as size and shape of the viral particles. The characterization needs to be continued using advanced methods such as mass spectrometry to decipher glycome of viruses produced in tick cells. The lipid composition of tick cell-derived and mammalian cell-derived viruses also has to be further analyzed to have a broad overview of the viral production in the vector tick cells. Finally, the shape and the size of the particles will be analyzed by cryo-EM or tomography to expand our knowledge on glycoproteins' structure. Altogether, the characteristics of arthropod-borne viruses will shed light on the first steps of viral entry into vertebrate hosts. It will be useful to identify the first target cells of tick-borne phleboviruses in the skin dermis and to find new receptors, which could lead to a better explanation of the large tropism of those viruses in mammalian hosts.

With UUKV, this project opened several questions and new avenues to study the life cycle of tick-borne phleboviruses in their vector ticks *in vitro*. The cell biology of tick cells is insufficiently known given the central role it plays on tick-borne diseases. Applying OMICS techniques (lipidomics and glycomics for instance) would give us the opportunity to shed light on the cell biology of the vector tick. The knowledge gained on tick-borne viruses will also be useful to understand other tick-borne pathogens, such as *Borrelia burgdorferi*, the bacteria responsible of Lyme disease.

## Conclusion - Perspective

While few receptors for bunyaviruses, like DC-SIGN, are already known in mammalian cells, none have been described in arthropods cells. The critical role of DCs *in vitro* will have to be confirmed *in vivo* with regards to host-pathogen interactions. Following studies will aim to define the role of DCs or any other cells in the human skin dermis and the first-target cells of tick-borne viruses following transmission. For this particular purpose, live animal imaging represents the future of analysis. Arboviruses usually persist in arthropods but not in humans where the outcome might be fatal. The molecular determinants and processes that drive survival or death outcome of infected cells will also have to be defined.

## Material and Methods

### 1. Material

**Table 4: Chemicals and reagents**

Compounds/ Reagents	Suppliers
<b>3M sodium acetate</b>	Thermo Fisher Scientific
<b>Bovine Serum Albumin</b>	Roth
<b>Chloroquine diphosphate salt</b>	Sigma Aldrich
<b>Coomassie brilliant blue</b>	Biomol
<b>Dithiotreitol (DTT)</b>	Biomol
<b>Endo H</b>	Promega
<b>Hepes 1M</b>	Thermo Fisher Scientific
<b>Hoechst 33258</b>	Thermo Fisher Scientific
<b>Laemli Buffer 4X</b>	Invitrogen
<b>Luciferase</b>	Progema
<b>NH<sub>4</sub>Cl</b>	Sigma
<b>NP-40</b>	Merck Millipore
<b>OptiPrep</b>	Axis shield POC AS
<b>Paraformaldehyde</b>	Merck
<b>Phosphate Buffer Saline (PBS) w/o Ca<sup>2+</sup> w/o Mg<sup>2+</sup></b>	Merck Millipore
<b>Pierce™ 16% Formaldehyde (w/v), Methanol-free</b>	Thermo Fisher Scientific
<b>PNGase F</b>	Promeage
<b>Precast gel 4-12% bis tris</b>	Thermo Fisher Scientific
<b>Precast gel 10% Bis tris</b>	
<b>Prestained protein marker</b>	Thermo Fisher Scientific
<b>Protease inhibitor cocktail</b>	Roche
<b>Saponin from quillaja bark</b>	Sigma
<b>Sucrose</b>	MP biomedical
<b>See Blue Plus strand</b>	Invitrogen
<b>Super signal West Femto Solution kit</b>	Thermo Fisher Scientific
<b>Supersignal West Pico kit</b>	
<b>Peroxidase solution</b>	Thermo Fisher Scientific
<b>Luminol enhancer</b>	
<b>Tween20</b>	Roth
<b>B-mercaptoethanol</b>	Sigma Aldrich

**Table 5: Components used for DNA analysis**

DNA products	Supplier
Cutsmart buffer	NEB
DNA ladder 1kb	NEB
DNA loading buffer 6X	NEB
DNA Restriction enzymes	NEB
dNTPs	NEB
Herculase II polymerase	Agilent
KOD polymerase	Novagen
<i>Pfu</i> polymerase	Promega
RNase OUT	Thermo Fisher Scientific
SuperScript III	Invitrogen
Syber Safe marker	Thermo Fisher Scientific
T4 DNA ligase	Fermentas
Taq polymerase	NEB
TOPO® cloning	Thermo Fisher Scientific
Ultrapure agarose	Thermo Fisher Scientific

**Table 6: Buffers and their composition**

Buffers	Composition
Coomassie staining	50% Methanol - 10% acetic acid - 40% H <sub>2</sub> O - 0.25% coomassie brilliant blue
FACS Permeabilization buffer (FPB)	FCS 2% - EDTA 5mM - NaN <sub>3</sub> 0,02% - saponin 0,1% for 1L PBS 1X
Fixative solution	40% Methanol - 10% acetic acid
Hepes NaCl EDTA (HNE) 10X	Hepes 100mM - NaCl 1M - EDTA 20mM Use 1X
Lysis buffer	TNE - 0,01% Triton 100X - antiproteases
SDS running buffer	NuPage Invitrogen
Sodium dodecylsulfate (SDS)	5% in H <sub>2</sub> O
Sodium phosphate buffer	0,5M in H <sub>2</sub> O
TBS – Tween	TBS 1X - 0,1% Tween20
TBS – Tween- Milk	TBS - Tween - 5% Milk
Tris Acetate EDTA (TAE) 50 X stock solution	2M tris - 1M sodium acetate - 0,1 M EDTA pH 8,3
Tris Buffer Saline (TBS) 1X stock solution	Tris base 24g - NaCl 88g for 1L
Tris NaCl EDTA (TNE)	20mM tris - 50mM NaCl - 2mM EDTA pH 7,5

**Table 7: Commercial kits**

<b>Kit</b>	<b>Supplier</b>
<b>DAB peroxidase substrate kit</b>	Vector Laboratories
<b>Deglycosydases kit</b>	Merck Millipore
<b>Dual-Luciferase® Reporter Assay System</b>	Promega
<b>NucleoBond PC 500</b>	Macherey-Nagel
<b>Nucleospin Gel and PCR clean-up</b>	Macherey-Nagel
<b>QIAamp Viral RNA extraction Mini Kit</b>	Qiagen
<b>QIAprep Spin Miniprep Kit</b>	Qiagen
<b>QIAquick Gel Extraction Kit</b>	Qiagen
<b>QIAquick PCR Purification Kit</b>	Qiagen

**Table 8: Compounds used for cellular culture**

<b>Name</b>	<b>Company</b>
<b>Penicillin (100X stock solution)</b>	Capricorn
<b>Streptomycin (100X stock solution)</b>	Capricorn
<b>Glutamax™</b>	Gibco®
<b>Tryptose phosphate broth</b>	Sigma Aldrich
<b>Fetal bovine serum (FBS)</b>	Gibco® lot 41A0731K
<b>Fetal calf serum (FCS)</b>	Merck lot 1286C
<b>Trypsin/EDTA (0,5%/0,2% -w/v)</b>	Biochrom AG
<b>Poly – L –Lysine (0,01% solution)</b>	Sigma Aldrich
<b>EDTA 0,5M</b>	Thermo Fisher Scientific
<b>Lipofectamine2000</b>	Invitrogen
<b>Lipoprotein Cholesterol concentrate</b>	MP Biomedicals
<b>L-Proline</b>	Sigma Aldrich
<b>D-glucose</b>	Sigma Aldrich
<b>α-ketoglutaric acid</b>	Sigma Aldrich
<b>Aspartic acid</b>	Sigma Aldrich
<b>Glutamic acid</b>	Sigma Aldrich
<b>Glutathione (reduced)</b>	Sigma Aldrich
<b>Ascorbic acid</b>	Sigma Aldrich
<b>aminobenzoic acid</b>	Sigma Aldrich
<b>Cyanocobalamine (B12)</b>	Sigma Aldrich
<b>d- Biotin</b>	Sigma Aldrich
<b>Carboxymethyl cellulose sodium</b>	Sigma Aldrich
<b>Dimethylsulfoxide (DMSO)</b>	Merck Millipore

**Table 9: Media used for mammalian cell culture**

Medium	Supplementation
<b>GMEM (Gibco®)</b> <b>Ref: 11710-035</b>	Glasgow's minimal essential medium supplemented with 10% tryptose phosphate broth 5% FBS 100 units.mL <sup>-1</sup> penicillin and 100 µg.mL <sup>-1</sup> streptomycin
<b>DMEM (Gibco®)</b> <b>Ref: 61965-026</b>	Dulbecco's Modified Eagle's Medium supplemented with 10% FCS 100 units.mL <sup>-1</sup> penicillin and 100 µg.mL <sup>-1</sup> streptomycin
<b>RPMI (Gibco®)</b> <b>Ref: 61870-010</b>	Roswell Park Memorial Institute supplemented with 10% FCS 100 units.mL <sup>-1</sup> penicillin and 100 µg.mL <sup>-1</sup> streptomycin
<b>Opti-MEM®</b> <b>(Gibco®)</b> <b>Ref: 11058-021</b>	Reduced Serum Medium without phenol red No supplementation
<b>Freezing medium</b>	90% (v/v) FBS – 10% DMSO

**Table 10: Media used for tick cell culture**

Medium	Supplementation
<b>L-15 (Gibco®)</b> <b>Ref: 11415-049</b> <b>500 mL</b>	Leibovitz's L-15 Medium supplemented with 10% tryptose phosphate broth 20% FBS 1% GlutaMAX™ 100 units.mL <sup>-1</sup> penicillin and 100 µg.mL <sup>-1</sup> streptomycin. Filtration through 0,22 or 0,33µm
<b>L-15B (Gibco®)</b> <b>Ref: 41300-021</b>	Leibovitz's L-15 Medium powder reconstituted in 1L H <sub>2</sub> O with : aspartic acid 299mg – glutamic acid 500mg – proline 300mg – α ketoglutaric acid 299mg – D-glucose 2239mg – vitamin and mineral stock solutions 1 mL each ( <b>supplementary material 4</b> ). supplemented with: 10% tryptose phosphate broth 5% FBS 1% Lipoprotein Cholesterol concentrate 1% GlutaMAX™ 100 units.mL <sup>-1</sup> penicillin and 100 µg.mL <sup>-1</sup> streptomycin. Filtration with 0,22 or 0,33µM filters
<b>L-15/L-15B</b>	50% L-15 supplemented and filtered – 50% L-15B supplemented and filtered
<b>L-15B300</b>	¼ H <sub>2</sub> O and ¾ of L-15B supplemented and filtered

Fetal bovine and calf serum used for mammalian or tick media were heat inactivated (30 min 56°C) and filtered prior utilization.

**Table 11: Mammalian cell line and seeding**

Cell line	Medium	Seeding	Assay
<b>BHK-21: Baby Hamster Kidney</b>	GMEM	1.10 <sup>5</sup> cells in 24 well-plate	FACS
		1,2.10 <sup>5</sup> cells in 24 well-plate	Titration
		3.10 <sup>5</sup> cells in 6 well-plate	Transfection
		2.10 <sup>6</sup> cells T25 flask 5.10 <sup>6</sup> cells T75 flask 16.10 <sup>6</sup> cells T175 flask	Infection / Production
		3.10 <sup>5</sup> cells in 96 well-plate	Flow cytometry
<b>Human B Raji / Raji DC-SIGN Epithelial HeLa / HeLa DC-SIGN</b>	RPMI	8.10 <sup>4</sup> cells in LabTeck chamber	Immuno- fluorescence

**Table 12: Tick cells**

Cell line	Medium	Seeding	Assay
<b>IRE/CTVM19 from <i>Ixodes ricinus</i></b>	L-15 based medium	3mL glass tube *	Maintenance Infection
<b>IRE/CTVM20 from <i>Ixodes ricinus</i></b>	L-15/L-15B	2.10 <sup>5</sup> cells in 96 well-plate	FACS based assay
		3mL glass tube	Maintenance Infection
<b>IDE8 from <i>Ixodes scapularis</i></b>	L-15B based medium	2.10 <sup>5</sup> cells in 96 well-plate	FACS based assay
		3mL glass tube	Maintenance Infection
<b>ISE18 from <i>Ixodes scapularis</i></b>	L-15B300	2.10 <sup>5</sup> cells in 96 well-plate	FACS based assay
		22.10 <sup>6</sup> cells in T175 flasks 3mL glass tube	Production Maintenance Infection

\* flat-side tubes Nunc ref 156758

**Table 13: Primary antibodies**

Name	Anti	Species	Dilution	Method	Provider
<b>8B11A3</b>	N protein	Mouse monoclonal	1: 400 1: 100	FACS WB	Anna Överby
<b>3D8B3</b>	Glycoprotein C	Mouse monoclonal	1: 100	FACS WB	
<b>6G9E5</b>	Glycoprotein N	Mouse monoclonal	1: 100	FACS WB	
<b>K5</b>	Glycoprotein C	Rabbit polyclonal	1: 100	WB	
<b>K1224</b>	Glycoprotein N	Rabbit polyclonal	1: 100	WB	
<b>NSs</b>	Nonstructural protein	Rabbit polyclonal	1: 100	WB	Pierre-Yves Lozach
<b>U2</b>	UUKV	Rabbit polyclonal	1: 1 000	FFA WB FACS	
<b>mAb1621</b>	DC-SIGN	IgG2a Mouse monoclonal	25 µg.mL <sup>-1</sup>	FACS	
					R&D system

The mouse monoclonal antibodies 8B11A3, 6G9E5 and 3D8B3<sup>133</sup>. The rabbit polyclonal antibodies K1224 and K5<sup>141</sup> were all a kind gift from Anna Överby and the Ludwig Institute for Cancer Research (Stockholm, Sweden). The rabbit polyclonal antibody U2 has been described previously, and recognizes the UUKV proteins N, G<sub>N</sub>, and G<sub>C</sub><sup>79</sup>.

**Table 14: Secondary antibodies**

Name	Species	Dilution	Method	Provider
<b>Anti-rabbit HRP</b>	Goat	1: 10 000	WB	Santa Cruz
<b>Anti-mouse HRP</b>	Goat	1: 10 000	WB	Santa Cruz
<b>Anti-rabbit AF647</b>	Goat	1: 500	FACS	Thermo Fisher Scientific
<b>Anti-mouse AF647</b>	Goat	1: 500	FACS	Thermo Fisher Scientific
<b>Anti- rabbit IRDye® 800</b>	Goat	1: 10 000	WB	Li-cor Odyssey®
<b>Anti-rabbit HRP</b>	Goat	1: 400	FFA	Vector Laboratories

**Table 15: Plasmids list**

Name	Description	Reporter gene	Promotor	Provider
<b>pRF108</b>	Vector	/	Pol I	Pierre-Yves Lozach
<b>pRF108-S</b>	Full S segment of UUKV	/	Pol I	Mazelier et al.,
<b>pRF108-M</b>	Full M segment of UUKV	/	Pol I	Mazelier et al.,
<b>pRF108-MS23</b>	Full M segment of UUKV M S23	/	Pol I	Mazelier et al.,
<b>pRF108-L</b>	Full L segment of UUKV	/	Pol I	Mazelier et al.,
<b>pRF108-eGFP</b>	S segment $\Delta$ NSs	eGFP	Pol I	Pierre-Yves Lozach
<b>pRF108-Ren</b>	S segment $\Delta$ NSs	Renilla luciferase	Pol I	Pierre-Yves Lozach
<b>pRF108-Gau</b>	S segment $\Delta$ NSs	Gaussia Luciferase	Pol I	Pierre-Yves Lozach
<b>pRF108-delNSs</b>	S segment $\Delta$ NSs	/	Pol I	This PhD thesis
<b>pUUK-N</b>	Nucleoprotein of UUKV	/	CMV	A. Överby
<b>pUUK-L</b>	Polymerase of UUKV	/	CMV	A. Överby

All plasmids code for an ampicillin resistance cassette. pRF108 vector backbone is presented in supplementary material 5

**Table 16: Primers used to generate plasmids for the reverse genetics system**

Primer	Sense	Sequence (5' -> 3') <sup>a</sup>	Purpose <sup>b</sup>
<b>RT-S</b>	Forward	<i>acacaaagacctccaacttagctatcg</i>	RT S segment
<b>RT-M</b>	Forward	<i>acacaaagacggctaacatggtaagg</i>	RT M segment
<b>RT-L</b>	Forward	<i>acacaaagacgccaagatgcttttagcg</i>	RT L segment
<b>UUKV-S-5NC</b>	Forward	<i>AATCGTCTCTAGGTacacaaagacctccaacttagctatcg</i>	Cloning S segment into pRF108
<b>UUKV-S-3NC</b>	Reverse	<i>AATCGTCTCTGGGacacaaagaccctec</i>	(pRF108-S)
<b>UUKV-M-5NC</b>	Forward	<i>AATCGTCTCTAGGTacacaaagacggctaacatggtaagg</i>	

## Material and Methods

<b>UUKV-M-3NC</b>	Reverse	AAT <u>CGTCTC</u> GGGG <i>Gacacaaagacacggctacatgg</i>	Cloning M segment into pRF108 (pRF108-M)
<b>UUKV-L-5NC</b>	Forward	AAT <u>CGTCTC</u> TAGGT <i>Tacacaaagacgccaagatgcttttagcg</i>	Cloning L segment into pRF108 (pRF108-L)
<b>UUKV-L-3NC</b>	Reverse	AAT <u>CGTCTC</u> GGGG <i>Gacacaaagtccgccaagatggaagtaaagg</i>	Mutagenesis M segment (G2386A)
<b>Mut-M-S</b>	Forward	<i>caaggattcagtggttgtaaatcatcaatcatagatccca</i>	Mutagenesis M segment (G2386A)
<b>Mut-M-AS</b>	Reverse	<i>tgggatctatgattgatgattgacaatccactgaatccttg</i>	Mutagenesis M segment (G2386A)

*a* The virus RNA sequence that is targeted is in italics, and the sequences introduced for cloning are in capital letters. Underlined nucleotide sequences indicate a BsmBI restriction site. Bold nucleotides are the point mutations introduced in the M segment sequence of the UUKV lab strain.

*b* RT, reverse transcription.

**Table 17: Primers used to sequence the M segment**

Name of primer	Sequence 5' -> 3' antigenomique	Position 5' -> 3' antigenomique
<b>For-98</b>	acacaaagacggctaacaatgg	1-21
<b>Rev-110</b>	gctcatgtcatgtcaatgtagggg	171-195
<b>For-105</b>	gcatctggtctatgacgacgccatttgcc	404-432
<b>For-91</b>	ggagggcagatgttctgg	683-700
<b>Rev-106</b>	ggcagacaggctctcagattcacacttgc	1037-1065
<b>For-111</b>	cctggaagaaggactgaataatgtgg	1397-1422
<b>For-92</b>	ggcatgctgtgtctggc	1524-1540
<b>For-107</b>	ggagttgatggctcagctaggctgg	1901-1925
<b>For-80b*</b>	gggaggatctacacggcacaagttcc	2206-2232
<b>For-86</b>	acggcacaagttccacaca	2218-2237
<b>Rev-112</b>	ccataattttctccaaggtccacaagg	2344-2370
<b>Rev-87</b>	acttggcatctgccacatg	2497-2516
<b>Rev-81b*</b>	gccaagattcttatcattatcagg	2572-2596
<b>For-130</b>	ccataaggacaatgcatttaaagc	2731-2754
<b>For-113</b>	ccctattcccctcccctctacc	3050-3073
<b>Rev-99</b>	gtagccgtgtctttgtg	3194-3218

\* primers used to amplify a 391 DNA fragment that spans the reversion site in the G<sub>C</sub> of UUKV.

**Table 18: primers for S or S-ΔNSs segment amplification**

Name of primer	Sequence 5' -> 3' antigenomique
9	aatcgtctctaggtacacaaagacctccaacttagctatc
10	aatcgtctcggggacacaaagacctccaacattaagc
76	ggactctaaaagggttcggcccaaacagtcttcgaattcgaagactggcttaatggtggagggtctttgtgtcccc gagacgatt

**Table 19: Equipment**

Equipement	Company
<b>Centrifuge Fresco 21</b>	Heraeus - Thermo Fisher Scientific
<b>Centrifuge 5430R</b>	Eppendorf
<b>Ibnot</b>	Invitrogen (Thermo Fisher Scientific)
<b>Incubator tick cell culture 28°C – IF260</b>	Memmert
<b>Incubator mammalian cell culture 37°C – Inkubator C200</b>	Labotect
<b>Ultracentrifuge L8-60M or L8-70M</b>	Beckman
<b>Rotor SW32 or SW60</b>	
<b>J2HS or J2HC Centrifuge</b>	Beckman Coulter
<b>Rotor JA-20 or JA10</b>	
<b>Flow cytometer FACS Calibur</b>	BD Bioscience
<b>Multifuge 3S-R</b>	Heraeus – Thermo Fischer Scientific
<b>Wide-field microscope iX70 or iX81 S1F-3</b>	Olympus
<b>Thermocycler – MultiGene Optimax EM10</b>	Axon Labortechnik
<b>Jeol JEM-1400 transmission electron microscope (TEM)</b>	Zeiss Jeol Ltd., Tokyo, Japan
<b>Safety cabinet NU-543</b>	ibs Tecnomara
<b>Safety cabinet SterilGard III advance</b>	The baker Company
<b>Shaker 37° (bacteria) – Unitron</b>	INFORS HT
<b>Incubator 37°C (bacteria) – B12</b>	Heraeus – Thermo Fischer Scientific
<b>Nanophotometer</b>	Implen

**Viruses.** The prototype UUKV strain 23 (UUKV S23) was originally isolated from the tick *I. ricinus* in the 1960s (i.e. the virus in tick suspension)<sup>250</sup>. The UUKV strain used in this study results from five successive plaque purifications of UUKV S23 in chicken embryo fibroblasts (CEFs) and subsequent passages in BHK-21 cells<sup>55,251</sup>. Virus multiplicity of infection is given according to the titer determined in BHK-21 cells.

## Material and Methods

**Bacteria.** For plasmids production, the chemically competent *E. coli* DH5 $\alpha$  (F<sup>-</sup>  $\Phi$ 80*lacZ* $\Delta$ M15  $\Delta$  (*lacZYA-argF*) U169 *recA1 endA1 hsdR17* ( $r_k^-$ ,  $m_k^+$ ) *phoA supE44 thi-1 gyrA96 relA1  $\lambda^-$* ) were used (homemade).

For cloning procedure, the chemically competent *E. coli* DH10B<sup>TM</sup> from Invitrogen, One Shot<sup>®</sup> TOP10 (F- *mcrA*  $\Delta$  (*mrr-hsdRMS-mcrBC*)  $\Phi$ 80*lacZ* $\Delta$ M15  $\Delta$  *lacX74 recA1 araD139*  $\Delta$  (*araleu*) 7697 *galU galK rpsL* (StrR) *endA1 nupG*) were used.

## 2. Methods

### a. Cellular culture

#### i. Mammalian cell culture

BHK-21 were grown in GMEM supplemented as described in **table 9**<sup>273</sup>. Human B (Raji) and Raji cells that stably express DC-SIGN were cultured according to ATCC recommendations<sup>79,82</sup> and epithelial (HeLa) cells and HeLa cells that stably express DC-SIGN were grown in DMEM supplemented as described in **table 9**. All mammalian cell lines were grown in a humidified atmosphere of 5% CO<sub>2</sub> in air at 37°C. The seeding was done depending on the experiment (**table 11**).

#### ii. Tick cell culture

IRE/CTVM19 and IRE/CTVM20 derived from embryos of *Ixodes ricinus* ticks whereas ISE18 and IDE8 derived from embryos of *Ixodes scapularis*. All tick cell lines were cultured in sealed, flat-side tubes for the maintenance (**figure 44**) and IDE8 cells were adapted to tissue culture dishes during this project, as described in **table 12**. The medium was changed every week the cells were not sub-cultured. For this, tubes are hold on a rack until cells pellet. 1.4 mL of the supernatant is removed and 1.5 mL of fresh medium is added. The cells were sub-cultured half every two weeks maximum when the cells were confluent. They tolerate up to two weeks without sub-culturing or medium change. To subculture the cells, 1.5 mL of medium is removed and 3.7 mL of fresh medium is added. Cells are re-suspended with a 2 mL pipette using a pipette rubber (pipette boy is not strong enough). Then, 2.2 mL of cell suspension is removed.

#### iii. Medium preparation for tick cells

The tick cell lines IRE/CTVM19 and IRE/CTVM20 were cultured in L-15 based medium from liquid commercial medium and IDE8 and ISE18 in L-15B based medium homemade<sup>243</sup>. L-15B powder was resuspended in water, components listed in **table 10** were added and the pH was adjust to a “nice orange color”. After filtration, medium was stored at 4°C. Every week, media were warm to RT and supplemented as indicated in **table 10** prior to culturing.

**iv. Long term storage of cell lines**

Tick cell lines cannot be stored for a long term. Some cell lines can be stored for several weeks at 15°C or 4-6°C<sup>274,275</sup>. Mammalian cell lines were cryopreserved in liquid nitrogen or frozen at -80°C. Cells were washed with PBS 1X once, detached by trypsinization and counted. After five minutes of centrifugation at 1300 rpm they were re-suspended in freezing medium to freeze  $3 \cdot 10^6$  cells per cryotube. They were stored in a box filled with isopropanol for one night at -80°C, then either transferred to liquid nitrogen tank or kept at -80°C (only BHK-21 cells).

To thaw cells, one cryotube is heated in a 37°C water bath and cell suspension is transferred to 5 mL warm complete medium. Cells are pelleted by centrifugation at 1200 rpm for 5 min to remove DMSO. The pellet is resuspended with complete warm medium and transferred in a T-75 flask. When necessary, medium is changed 24 hours later.

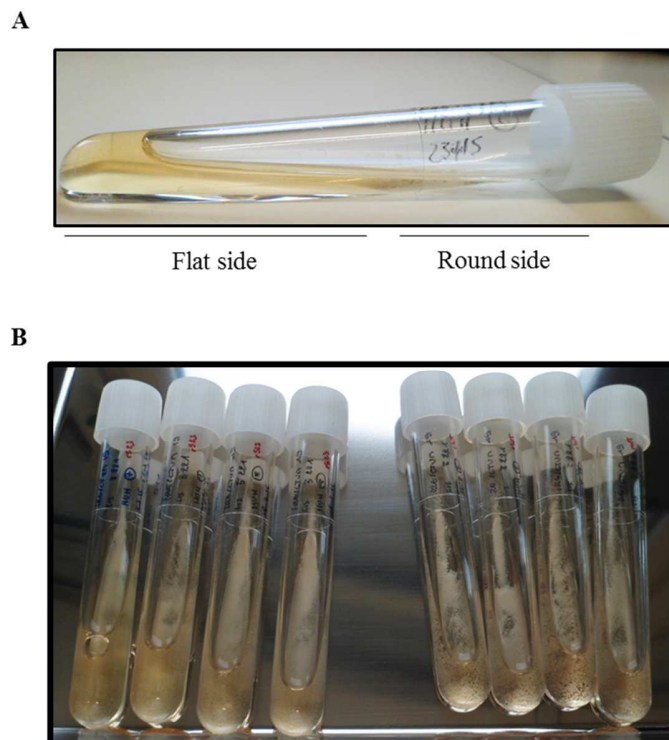


**Figure 44: Culture of tick cells in 3 mL flat glass tubes.**

(A) IRE/CTVM19 cells are cultured in 3 mL glass tubes. They sediment on the flat side of the tube but are poorly adherent and they grow also in suspension in the round part of the tube. Cells remain in the same tube once subcultured (here passage 221), in L-15 based medium supplemented with 20% FBS. Cells pellet on the flat side but are mainly in suspension. They are incubated at 28°C. (B) Cells were infected with rUUKV S23 or rUUKV.

## **b. Molecular biology methods**

### **i. RNA extraction**

Total RNA was extracted either from 140  $\mu$ L of supernatant of infected cells or from 20  $\mu$ L of semi purified virus using the QIAamp Viral RNA extraction Kit following manufacturer's protocol. RNA were eluted in a maximum volume of 40  $\mu$ L H<sub>2</sub>O and stored at -80°C.

### **ii. Reverse Transcription**

Viral RNA (vRNA) was reverse transcribed using specific primers RT-S, RT-M or RT-L for each segment (see **table 16**) and the SuperScript III (SS III) following manufacturer's protocol. Briefly, vRNA was mixed with the specific primer (2  $\mu$ M), dNTPS (10 mM each), and H<sub>2</sub>O. After 5 min in a warm water bath at 65°C, the mix is cool down. Then, 0.1 M DTT, 5X buffer (both from the kit) and RNase OUT are added and heated for 2 min at 42°C (in thermocycler). After addition of the SS III, the following amplification cycle was used: 50 min 42°C, 15 min 70°C.

A very important step after the reverse transcription is the purification of the cDNA with the QIAquick PCR purification Kit.

### **iii. Polymerase chain reaction**

The reversion of the single amino acid (G2386A) in the M segment of the rUUKV was checked by PCR. Amplification of a 391bp fragment in the G<sub>C</sub> nucleotide sequence was performed with the primers 80b and 81b (**table 17**) using the KOD polymerase and following the manufacturer's protocol. Amplification cycles: 95°C 2 min, 30 times 95°C 30 sec – 58°C 30 sec – 70°C 30 sec, 70°C 10 min.

For cloning procedure, DNA of the full-length S segment was synthesized using the KOD polymerase with the primers 9 and 10 and the S $\Delta$ NSs segment was synthesized with the primers 9 and 76 (see **table 18**). Amplification cycles: 95°C 2 min, 30 cycles of 95°C 30 sec - 58°C 45 sec - 70°C 2 min and 70°C 10 min.

## Material and Methods

In order to sequence the full-length M segment from ticks, DNA corresponding to the RNA sequence was synthesized with the *Pfu* polymerase using primers PCR-M-S and PCR-M-AS using the following amplification cycle: 95°C 2 min, 30 cycles of 95°C 30 sec – 60°C 30 sec – 72°C 7 min and 72°C 5 min.

The full length S, M and L segments for the cloning procedure (see below) were synthesized with the Herculanase II fusion polymerase. Amplification cycles:

Segment	PCR amplification program
<b>Segment S</b>	95°C, 1 min 95°C, 20 s 58.1°C, 20 s 68°C, 2 min 68°C, 4 min. } 30cycles
<b>Segment M</b>	95°C, 1 min 95°C, 20 s 55.1°C, 20 s 68°C, 3 min 30 s 68°C, 4 min. } 30cycles
<b>Segment L</b>	95°C, 1min 95°C, 20 s 62°C, 20 s 68°C, 6 min 30 s 68°C, 4 min. } 30cycles

### iv. Gel extraction

After DNA amplification, DNA was loaded on a 1 to 2% agarose gel and observed under UV light after migration. The band that correspond to the size of the expected fragment was cut and DNA was extracted from the gel using the QIAquick Gel Extraction Kit (Qiagen) or the Nucleospin Gel and PCR clean-up (Macherey-Nagel).

### v. Cloning procedure

The expression plasmids pUUK-N and pUUK-L were a kind gift from Anna Överby and code for, respectively, the UUKV nucleoprotein N and polymerase L<sup>55</sup>. The cDNAs corresponding to the S, M, and L segments of UUKV were synthesized by RT-PCR from vRNA extracts of purified-virus stock produced in mammalian cells using the reverse transcriptase Superscript III. Their amplification as a single PCR product was carried out using the Herculase II fusion DNA polymerase. The PCR products were then cloned in the TOPO vector for sequencing and then between the murine Pol I RNA polymerase promoter and terminator sequences in the pRF108 vector, a kind gift from Ramon Flick, Bioprotection Systems Corporation<sup>70</sup>. The resulting Pol I-driven plasmids (pRF108-S, pRF108-M, and pRF108-L) encoded each of the antigenomic UUKV RNA molecules i.e. S, M, and L segments. The point mutation G2386A in the M segment was obtained with the QuikChange XL site-directed mutagenesis kit (Agilent) using the plasmid pRF108-M as a template. The reporter gene enhancer green fluorescent protein (eGFP), renilla luciferase (Ren) or gaussia luciferase (Gau) were amplified by PCR with primers that introduced a BsmBI restriction site. They were ligate to a  $\Delta$ NSs fragment DNA obtained from PCR of N from the TOPO plasmids and cloned into the pRF108 vector. To generate an S segment delta NSs ( $\Delta$ NSs), the nucleotide sequence corresponding to the nucleoprotein N was amplified using the KOD polymerase together with the noncoding 5' and the intergenic regions. The second primer included the 3' noncoding region and a BsmBI restriction site. The resulting fragment was cloned into the pRF108 vector (a kind gift from Ramon Flick, Bioprotection Systems Corporation).

The complete list of primers and restriction enzymes used for cloning and mutagenesis is shown in **table 16**.

### c. Production and purification of plasmids DNA

*E. coli* DH5  $\alpha$  or One shot Top10 competent cells were transformed with 10 to 20 ng of plasmids and incubated for 1 hour at 37°C in LB medium with antibiotic at 150 rpm. 100  $\mu$ L were seeded on LB-agar plate containing antibiotic and incubated overnight at 37°C. In the case of plasmid production, one colony was picked and bacteria were grown overnight in 250 mL LB medium supplemented with ampicillin. After pelleting bacteria for 30 min at 4°C 2500 rpm, plasmid DNA

was purified using Nucleo Bond 500 kit (Machery Nagel). Glycerol stocks of the bacterial culture were stored at -80°C and plasmids at -20°C. In the case of cloning procedure, several colonies were picked and seeded in 5 mL medium with antibiotic. Bacterial DNA was purified using a QIAgen midi kit and sequenced as described below.

### **d. Sequencing**

#### **i. DNA for cloning procedure**

In order to clone the proper DNA sequence in a vector backbone, each purified DNA (from bacterial culture or PCR products) were first sequenced with a capillary sequencer by ABI (Eurofins Scientific).

#### **ii. Full-length S or M segment**

The full-length S segment of UUKV, M segment of rUUKV and rUUKV S23 were sequenced after total RNA extraction, RT-PCR and purification as described above. The DNA was analyzed with a capillary sequencer by ABI (Eurofins Scientific).

#### **iii. Full-length M segment isolated from UUKV-infected ticks**

Questing nymphs of the tick *I. ricinus* were collected in the region of Ramsvik and Hindens Rev (Sweden; 2013). Pools of 25 nymphs were homogenized and the total RNA was extracted with a magnetic bead-based protocol as described elsewhere (kind gift of Janne Chirico, National Veterinary Institute, Uppsala, Sweden, and Sara Moutailler, ANSES, Maisons-Alfort, France)<sup>153</sup>. The DNA corresponding to the M segment of UUKV synthesized by RT-PCR (see above) was analyzed with a capillary sequencer by ABI (Eurofins Scientific). Sequences were aligned using the Clustal-omega website and analyzed with SnapGene viewer software.

All primers used for sequencing are found in **table 17**.

**Nucleotide sequence accession numbers.** The GenBank accession numbers for the nucleotide sequences of the M segments of the tick isolates RVS and HRS are KX219593 and KX219594, respectively.

**e. Virus production and virology assay**

**i. Rescue of UUKV from plasmid DNAs**

UUKV was rescued by transfecting BHK-21 cells ( $0.6 \times 10^6$ ) with the expression plasmids pUUK-L (1  $\mu$ g) and pUUK-N (0.3  $\mu$ g) together with 0.5  $\mu$ g each of pRF108-S, pRF108-M, and pRF108-L. Transfection was performed in the presence of Lipofectamine 2000 (Life Technologies) using a ratio of 3.8  $\mu$ L to 1  $\mu$ g of plasmids in 400  $\mu$ L of OptiMEM (Life Technologies). One hour post-transfection, complete GMEM medium containing 2% FBS was added to the cells. After 4 to 5 days supernatants were collected, clarified, and titrated as described below.

**ii. Passaging of rescued viruses**

Supernatant of transfected BHK-21 cells (named P0) was harvested, cleared and titrated. It was then used to infect BHK-21 cells at a maximum MOI of 0.01. Supernatant of infected cells was collected when cytopathogenic effect (CPE) was observed or at day 5 post infection the latest, cleared and titrated. This supernatant was named P1 and used for a second round on infection in BHK-21 cells, the passage 2 (P2). As for P0 and P1, supernatant P2 was harvested, cleared and titrated and used for the third passage, P3. The passaging process was conducted until P3 for rUUKV Ren and rUUKV Gau; until passage 5(P5) for rUUKV, rUUKV S23, rUUKV delNSs, and until passage10 (P10) for rUUKV eGFP.

**iii. Virus production**

BHK-21 cells were infected with UUKV (laboratory strain) or rescued viruses at an MOI of 0.01 in medium without FBS at 37°C for one hour. Virus supernatant was removed and replaced by medium without FBS. Cells were incubated 48 hours for UUKV lab strain or until CPE was

## Material and Methods

detected. IRE/CTVM19 or IRE/CTVM20 were infected with rescued viruses that was not removed from the culture supernatant. Infection was carried out up to three months with rescued virus in 3 mL glass tubes with complete medium. ISE18 cells and IDE8 cells were, at a first place, infected for 40 days in 3 mL glass tube with complete medium without removing virus. IDE8 were then infected following the same procedure for up to 8 months. Supernatant of infected tick cells were harvested at different time point for titration. Independently, IDE8 were infected with rUUKV in tissue culture dish for two hours at 28°C. Virus supernatant was removed and replace by medium without FBS. Cells were incubated for 20 days without FBS and supernatant was harvested, cleared and buffered with 20 mM hepes before storage at -80°C.

### **iv. Virus purification**

#### Sucrose cushion

A small scale purification in Eppendorf tube was developed for IRE/CTVM-derived viruses. 800 µL of infected IRE/CTVM19 supernatant was loaded on Eppendorf tubes. 600 µL of 25% sucrose cushion was carefully added in the bottom of the tube. Supernatant was centrifuged for 4 hours at 4°C, 14 000 rpm. Supernatant and sucrose cushion were removed with a pipette tip and 50 µL of HNE 1X buffer was added. To allow virus pellet to re-suspend, tubes were incubated on ice for 1h30. Then, pellet was re-suspended and stored at -80°C.

For supernatant of infected BHK-21 or IDE8 cells collected from large flaks, supernatant was collected, cleared by centrifugation at 1300 rpm for 20 min at room temperature (RT) and stored at -80°C with 20 mM hepes. 30 mL was loaded on a tube for SW32 rotor and 3 mL of 25 or 30% sucrose was carefully added on the bottom of the tube to make a cushion. The tubes were centrifuged for 2 hours at 4°C, 27 000 rpm. Supernatant was removed and sides of tube were wiped off. 300µL of HNE 1X was added on the bottom of the tube and let for at least 1 hour on ice. Then, semi purified virus was re-suspended by pipetting, cleared if any clumps was observed, aliquoted and stored at -80°C.

## Gradient

As previously described elsewhere<sup>244</sup>, purified virus through 25% sucrose was added on top of an OptiPrep™ step gradient in an SW60 tube and centrifuged for 1h30 at 32 000 rpm, 4°C. The gradient was composed of fractions containing 6 – 7.2 – 8.4 – 9.6 – 10.8 – 12 – 13.2 – 14.4 – 15.6 – 16.8 – 18 and 35% of OptiPrep™. A ring of viruses was observed between the fractions of 35% and 18% OptiPrep™. Fractions of 540 µL were collected and those containing the virus was pipetted in a new SW60 tube to be pelleted for 45 min at 44 000 rpm, 4°C. Purified virus was resuspended in PBS 1X and stored at -80°C.

UUKV virus lab stock and rescued virus were titrated in BHK-21 cells as described below.

### **f. Virus titration by focus-forming assay**

BHK-21 cells were seeded the day before infection (see **table 11**) and infected with 10-fold dilution of virus in FBS-free medium. After one hour of incubation at 37°C - 5% CO<sub>2</sub> atmosphere, infected cells were grown in the presence of medium containing 5% serum and supplemented with 0.8% carboxymethyl-cellulose (CMC) to prevent virus spread. 3 days post infection, cells were washed with medium to remove the CMC and subsequently with PBS before fixation with a solution of 3.7% paraformaldehyde. To visualize eGFP, a solution of 3.7% formaldehyde methanol free was used. The cells were then permeabilized with a FACS permeabilization buffer. Foci were revealed with a diaminobenzidine solution kit (Vector Laboratories) after a two-step immunostaining with the antibody U2 and an anti-rabbit horseradish peroxidase-conjugated secondary antibodies (see **tables 13 & 14**)<sup>100</sup>.

### **g. Infection assays**

Mammalian cells were infected with virus at different MOIs in medium without FBS at 37°C for one hour. Virus supernatant was then replaced by complete culture medium and cultures were incubated for up to 64 hours before fixation. Tick cells were exposed to viruses at different MOIs in culture medium containing FBS (IRE/CTVM19 and IRE/CTVM20 cells) or without FBS (IDE cells) at 28°C for up to 48 hours. When used for microscopy, IRE/CTVM cells were seeded on

poly-L-Lysin (0.01%)-coated coverslips at 28°C on the day before infection. For inhibition assays, IRE/CTVM cells were pretreated with inhibitors at different concentrations for 30 min and exposed to UUKV in the continuous presence of the inhibitors. The infection was monitored by either wide-field fluorescence microscopy or flow cytometry.

### **h. Biochemistry**

#### **i. Luciferase assay**

Renilla luciferase activity was determined using a Dual-Luciferase Reporter Assay System (Promega) following manufacturer's protocol. The infected or mock infected cell pellets were resuspended in 400  $\mu$ l 1x passive lysis buffer (PLB) and incubated for 30 min at RT. Cell debris were pelleted by centrifugation at 10 000 rpm for 30 min at 4°C and the supernatant was stored at -20°C until the assay was performed. 20  $\mu$ l of lysates were added per well of a white microplate and 20  $\mu$ l of 1x PLB was used for normalization. After addition of 50  $\mu$ l Luciferase Assay Reagent (LAR II), Firefly luciferase activity was measured using a Luminoskan Ascent Microplate Luminometer. For determination of Renilla luciferase activity, 50  $\mu$ l of Stop&Glo Reagent was added on top and bioluminescence was measured.

#### **ii. Deglycosylation**

To assess the glycosylation pattern of the UUKV glycoproteins, virus stocks semi purified through a 25%-sucrose cushion were denatured and exposed to one of the five following treatments: 1,000 units of Endo H (Promega), 40 units of PNGase F (Promega) or 5 units of PNGase F (Merck Millipore), 0.005 units of  $\alpha$ -2(3,6,8,9)-neuraminidase, 0.003 units of  $\beta$ -1,4-galactosidase, 0.05 units of  $\beta$ -N-acetylglucosaminidase (all enzymes from Merck Millipore) according to the manufacturer's recommendations, and then analyzed by SDS-PAGE on a 4-12% or 10% Bis-Tris Nu-PAGE Novex gel (Life Technologies) and Western Blotting.

Enzyme	Manufacturer	Treatment
<b>Endo H</b>	Promega	16 hours 37°C
<b>PNGase F</b>	Promega	3 hours 37°C
<b>PNGase F</b>	Merck Millipore	
<b><math>\alpha</math>-2(3,6,8,9)-neuraminidase</b>	Merck Millipore	4 hours 37°C
<b><math>\beta</math>-1,4-galactosidase</b>	Merck Millipore	
<b><math>\beta</math>-N-acetylglucosaminidase</b>	Merck Millipore	

### iii. Protein analysis by SDS-PAGE

Viral protein extracts from virus stocks purified through a 25% sucrose cushion were analyzed by SDS-PAGE (Nu-PAGE Novex 4-12% Bis-Tris gel or Nu-PAGE Novex 10% Bis-Tris gel) and stained Coomassie. Viral protein extracts from virus purified through an OptiPrep™ step gradient were analyzed by silver staining. After fixation for 1 hour, the sucrose purified proteins were stained with brilliant blue, whereas OptiPrep™ purified proteins were analyzed by silver staining. Basically, after impregnation for 1min, silver staining was performed for 20 min at RT, which is immediately followed by the development to build up the silver metal image.

For western blot analysis, viral proteins were transferred to a Polyvinylidene difluoride (PVDF) membrane using the iBlot system<sup>79,100</sup>. When indicated, purified viruses were pre-treated with glycosidases or  $\beta$ -mercaptoethanol (40%). The PVDF membranes were first saturated in TBS containing 0.1% Tween and 5% milk (TBS- Tween-Milk) for one hour at RT and incubated with primary mouse monoclonal antibodies 8B11A3, 3D8B3 or 6G9E5, or rabbit polyclonal antibodies K5, 1224 or U2, all diluted in TBS-Tween-Milk. After 3 washes of TBS-Tween, PVDF membranes were incubated with an anti-mouse or anti-rabbit horseradish peroxidase-conjugated secondary antibody, respectively. Bound antibodies were detected by exposure to enhanced chemiluminescence reagents (ECL, GE Healthcare or Life Technologies). For quantitative detection of viral proteins, membranes were first incubated with the rabbit polyclonal antibody U2 and then with an anti-rabbit infrared fluorescence (IRDye) secondary antibody and analyzed with the Odyssey Imaging Systems and the software Image Studio (Li-Cor Biosciences).

### **i. Flow cytometry**

The flow cytometry-based infection assay has been described previously<sup>100</sup>. Briefly, after fixation and permeabilization with 0.1% saponin, infected cells were incubated with the mouse monoclonal antibodies 8B11A3, 6G9E5 or 3D8B3 at room temperature for one hour, washed, and subsequently exposed to Alexa Fluor (AF) 647-conjugated secondary anti-mouse antibodies at room temperature for one hour. When the mouse monoclonal antibody 1621 was used in infection assays to neutralize DC-SIGN, UUKV-infected cells were immuno-stained with the rabbit polyclonal antibody U2 and AF647-conjugated secondary anti-rabbit antibody. Flow cytometry-based analysis involved the use of a FACS Calibur cytometer and Flowjo software (Treestar).

### **j. Microscopy**

#### **i. Wide-field fluorescence microscopy.**

Infected cells were fixed and permeabilized with PBS containing 0.1% Triton X-100, incubated with the mouse monoclonal antibody 8B11A3 (1:1,000) at room temperature for one hour, washed, and then exposed to AF488-conjugated secondary anti-mouse (1:800) at room temperature in the dark for one hour. Nuclei were subsequently stained with Hoechst 33258 (0.5  $\mu\text{g}\cdot\text{mL}^{-1}$ ). Infection was quantified by counting cells in three independent fields and cells were imaged with an Olympus IX81 microscope.

#### **ii. Electron Microscopy.**

9  $\mu\text{L}$  of purified virus through 25% sucrose cushion or by gradient were used for negative staining. Virus was loaded on carbon grids and fixed for 1 hour with glutaraldehyde 3% diluted in cacodylate buffer. Virus were stained with 1,8% uranyl acetate – 0,8% CMC for 10 min in the dark at RT, washed in water and dry at RT. The staining and acquisition of pictures were done by the Electron Microscopy Core Facility (EMCF), university Heidelberg. Viruses were imaged with either a Zeiss EM10 or a Jeol JEM-1400 (Jeol Ltd., Tokyo, Japan) and sizes of viral particles acquired either with the EMMenu 4 (TVIPS, Gauting, Germany) or Fiji software.

### iii. Cryo- electron microscopy

Semi purified IDE8-derived rUUKV through 25% sucrose cushion were analyzed by our collaborators, laboratory of Professor Juha T Huiskonen, (Division of structural biology, University of Oxford). Samples were collected on Technai T12 transmission electron microscope equipped with an Eagle CCD camera (FEI, Thermo Fisher Scientific). Images were converted and adjusted using ImageJ.

### k. Mass spectrometry of lipids.

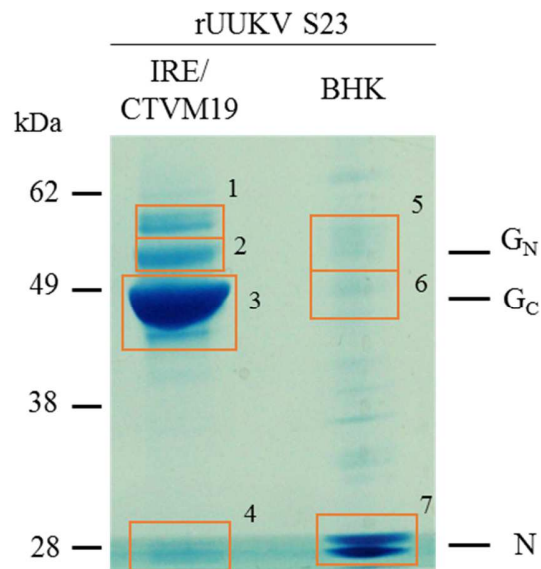
Lipid extractions were performed in the laboratory of Prof. Dr. Britta Brügger (BZH, Haidelberg University) using chloroform:methanol:37% HCl (5:10:0.15, vol:vol:vol,) except for plasmalogens, which were extracted using chloroform/methanol (5:10, vol:vol) as extraction solvent. Lipid extractions were done in 10 ml Wheaton vial with Teflon-screw caps as described<sup>276</sup>. Typically, the following lipid standards were added to the solvent prior to extractions : 50 pmol of PC (13:0/13:0, 14:0/14:0, 20:0/20:0; 21:0/21:0, Avanti Polar Lipids), SM (d18:1 with N-acylated 15:0, 17:0, 25:0, semi-synthesized as described in<sup>276</sup>) and d6Chol (Cambridge Isotope Laboratory), 20 pmol PI (16:0/16:0, 17:0/20:4, Avanti Polar Lipids), 25 pmol PE and PS (14:1/14:1, 20:1/20:1, 22:1/22:1, semi-synthesized as described in<sup>276</sup>, DAG (17:0/17:0, Larodan) and cholesterol ester (CE, 9:0, 19:0, 24:1, Sigma) 40 pmol TAG (D5-TAG-Mix, LM-6000 / D5-TAG 17:0,17:1,17:1 – Avanti Polar Lipids), 5 pmol Cer and GlcCer (d18:1 with N-acylated 15:0, 17:0, 25:0, semi-synthesized as described in<sup>276</sup>), PA (PA 17:0/20:4, Avanti Polar Lipids) and PG (14:1/14:1, 20:1/20:1, 22:1/22:1, semi-synthesized as described in<sup>276</sup>). For lipid analysis, ~30 µL of purified BHK-21 derived virions, 15 µL of purified IDE8-derived virus, 35 µL of mock infected cell supernatant, 15 µL of infected cell lysate and 60 µL of medium in which each cell type was cultured and were subjected to extractions. Mass spectrometric analysis was performed on a QTRAP6500 (ABSciex) coupled to a Triversa NanoMate device (Advion) as described in<sup>276</sup>). Data processing was performed using LipidView (ABSciex) and Microsoft Excel.

### **I. Statistical Analysis.**

The results of electron microscopy and lipidomic analysis are based on a single experiment. The other data shown are representative of at least three independent experiments. Values are given as the mean of at least duplicates  $\pm$  standard deviation (SD).

## Supplementary Material

A



B

	<i>Tick cell-derived virus</i>		<i>Mammalian cell-derived virus</i>	
	Protein extracted from Western blot	% amino acid sequence coverage	Protein extracted from Western blot	% amino acid sequence coverage
<i>Glycoproteins</i>	1	5	5	47
	2	30	6	32
	3	15	-	-
<i>Nucleoprotein</i>	4	48	7	86

**Supplementary material 1: Protein analysis of tick and mammalian cell-derived viruses.** (A) IRE/CTVM19 and BHK-21 cells were infected with rUUKV S23. Supernatants were purified through a 25% sucrose cushion and analyzed by SDS-PAGE and coomassie staining. (B) Each band on the gel were extracted and analyzed by mass spectrometry. Corresponding coverage sequence of the viral proteins were compared to UUKV S23 glycoproteins and nucleoprotein.

### **Uukuniemi viral particles purification**

After the production of Uukuniemi virus in BHK-21 or IDE8 cells, harvest supernatant, centrifuge it for 20 min at 1200 rpm, 4°C. Keep the supernatant with 20 mM hepes at -80°C for long storage or proceed to the purification.

#### **Purification through sucrose cushion**

- Pipet 30 mL of supernatant in SW30 tubes. Add 3 mL of 30% sucrose in the bottom carefully.
- Equilibrate tubes and centrifuge for 2 hours at 28 000 rpm, 4°C.
- Remove quickly the supernatant and wipe the tube carefully
- Add 300 µL of HNE buffer 1X in the tubes, incubate on ice for at least 1 hour (or overnight at 4°C) with parafilm on the top of the tube
- Pipet up and down to resuspend viruses.

Load 2.5 µL of purified virus on gel to stain the N, G<sub>N</sub>, and G<sub>C</sub> proteins with silver staining.

#### **Purification via an OptiPrep gradient**

- Prepare the dilutions and the gradient the day of purification! Dilution are made in filtered PBS.
- The gradient of OptiPrep is prepared in SW60 tubes as follow (from bottom to top):

500 µL 35.0%  
300 µl 18.0%  
300 µl 16.8%  
300 µl 15.6%  
300 µl 14.4%  
300 µl 13.2%  
300 µl 12.0%  
300 µl 10.8%  
300 µl 9.6%  
300 µl 8.4%  
300 µl 7.2%  
430 µl 6.0%

Grey bands should be visible between each fraction of OptiPrep while preparing the gradient.

- Load 300  $\mu$ L of purified virus through 30% sucrose on top of the gradient.
- Centrifuge at 32 000 rpm for 1 hour and 30 min at 4°C. The virus should be visible as a white band between the fraction 35% and 18% of OptiPrep.
- Remove the fractions from 6% to 16.8% and pool the last two fractions in a new SW60 tube. Fill the tube up to 4 mL of PBS.
- Centrifuge for 45 min at 44 000 rpm, 4°C.

If the white band is not visible, pipet fractions of the gradient of 500  $\mu$ L and analyze them via Western blot. Then, pool the fractions that contain viruses in an SW60 tube, fill the tube up to 4 mL and centrifuge as mentioned above.

- After the centrifugation, remove PBS, add 50  $\mu$ L of fresh PBS and let the virus on ice for 1 hour.
- Resuspend the virus, titrate via FFA, and analyze virus proteins by silver staining . Store viruses at -80°C.

### **Silver staining protocol**

#### **Migration**

Load a 10% Bis-Tris precast gel (Thermo Fisher Scientific) with purified virus and 7  $\mu$ L of prestained SeeBlue protein ladder (Thermo Fisher Scientific). Run at 120 V until the 28 kDa from the ladder reach the bottom of the gel.

While the proteins migrate, prepare the solutions for the staining and proceed to the staining as indicated below.

#### **Solutions**

All solutions should be freshly prepared (only Fixation solution could be stored).

Use distilled water for preparing the solutions.

## Supplementary Material

Solutions	Composition	How to prepare it
Fixation	50 % Methanol 12 % acetic acid 0.0185 % Formaldehyde	<u>1 Liter</u> : 500 ml Methanol 120 ml acetic acid 0.5 ml 37 % Formaldehyde
Impregnation	8.6% Sodium Thiosulfate Pentahydrate	<u>100 ml</u> : 150 µl Solution A in 100 ml water
Stain	0.2 % Silver nitrate 0,28 % Formaldehyde	<u>100 ml</u> : 0.2 g silver nitrate 75 µl Formaldehyde
Develop	6 % sodium carbonate 0,185 % Formaldehyde solution A	<u>100 ml</u> : 6 g sodium carbonate 50 µl 37% Formaldehyde 5 µL solution A
Solution A	8.6 % Solution	5 mL: 430 mg sodium thiosulfate pentahydrate in 5 mL water
Ethanol	50% ethanol	100 ml: 50 ml ethanol absolute 50 ml water

### Staining

The staining is done in autoclaved glass becher under shaking.

Fix the gel for 1 hour at RT

Wash 3 times 20 min with 50 % ethanol

Wash 3 times with distilled water

Impregnation for 1 min

Wash 3 times with distilled water

Stain for 20 min with the staining solution

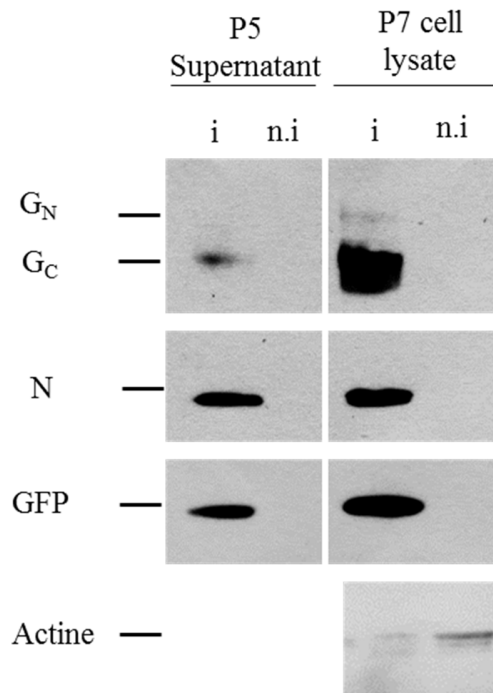
Wash 3 times with distilled water

Develop for 5 to 10 min with the develop solution. Brown bands should appeared.

Wash 3 times with distilled water

To store the gel, keep it in the fixation solution.

**Supplementary material 2: OptiPrep step gradient and silver staining protocols.** Protocols performed for the production and purification of rUUKV in IDE8 and BHK-21 cells. Viral particles were then used for lipidomic and electron microscopy analysis.



**Supplementary material 3: rUUKV eGFP is functional in mammalian cells.** BHK-21 cells were infected with rUUKV eGFP, supernatant was harvested, cleared and purified via a 25% sucrose cushion. Cells were lysed and rUUKV eGFP was analyzed by SDS-PAGE and Western blotting under reducing conditions. The rabbit polyclonal antibody U2 against the three structural viral proteins N, G<sub>N</sub>, and G<sub>C</sub>; the rat polyclonal antibody against the GFP; and the mouse monoclonal antibody against actine were used. Abbreviations: i, infected; n.i, non-infected.

## Supplementary Material

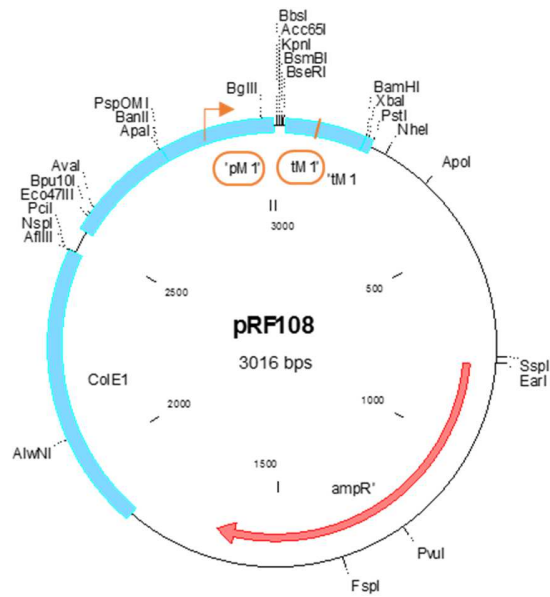
A

<b>Ingredient (for 100 mL)</b>	<b>Weight (mg)</b>	<b>Volume (mL)</b>
<b>Stock solution A</b>		
CoCl · 6H <sub>2</sub> O	20	
CuSO <sub>4</sub> · 5H <sub>2</sub> O	20	
MnSO <sub>4</sub> · H <sub>2</sub> O	160	
Zn SO <sub>4</sub> · 7H <sub>2</sub> O	200	
<b>Stock solution B</b>		
NaMoO <sub>4</sub> · 2H <sub>2</sub> O	20	
<b>Stock solution C</b>		
Na <sub>2</sub> SeO <sub>3</sub>	20	
<b>Stock solution D</b>		
Glutathione (reduced)	1000	
Ascorbic acid	1000	
FeSO <sub>4</sub> · 7H <sub>2</sub> O	50	
Stock solution A		1
Stock solution B		1
Stock solution C		1
<b>Vitamin stock solution</b>		
<i>p</i> -aminobenzoic acid	100	
Cyanocobalamine (B <sub>12</sub> )	50	
d- Biotin	10	

B

<b>Ingredient for 1L of L-15B</b>	<b>Weight (mg)</b>	<b>Volume (mL)</b>
Aspartic acid	299	
Glutamic acid	500	
Proline	300	
α-ketoglutaric acid	299	
D-glucose	2239	
Mineral stock D		1
Vitamin stock		1

**Supplementary material 4: Preparation of L-15B medium for tick cell culture.** (A) Ingredients for the stock solutions should be dissolved in distilled water in the order listed, and the volume of each stock solution brought to 100 ml. Store aliquots of stock solution D and the vitamin stock in 1mL amounts at –20°C. Stock solutions A,B and C can be stored in universals at –20°C. Protocol from Munderloh and Kurtti, <sup>277</sup>. (B) L-15B powder should be dissolve in 1L of distilled water with the components listed. The solution has to be filtered. It can be stored at at 4°C for up to 4 months, or at –20°C.



**Supplementary material 5: pRF108 vector backbone.** Murine polymerase I promoter and terminator are highlighted in orange. Some of the restriction sites are indicated. UUKV segments were inserted using the BsmBI site.

## References

## References

1. Gubler, D. J. & Vasilakis, N. in *Arboviruses: Molecular Biology, Evolution and Control* 1–6 (Caister Academic Press, 2016). doi:10.21775/9781910190210.01
2. Conway, M. J., Colpitts, T. M. & Fikrig, E. Role of the Vector in Arbovirus Transmission. *Annu. Rev. Virol.* **1**, 71–88 (2014).
3. Jupille, H., Vega-Rua, A., Rougeon, F. & Failloux, A.-B. Arboviruses: variations on an ancient theme. *Future Virol.* **9**, 733–751 (2014).
4. Schmaljohn, C. S. & Nichol, S. T. in *Fields Virology* (eds. Knipe, D. M. & Howley, P. M.) 1741–1789 (Lippincott Williams & Wilkins, 2007).
5. Vaheri, A. *et al.* Uncovering the mysteries of hantavirus infections. *Nat. Rev. Microbiol.* **11**, 539–550 (2013).
6. Elliott, R. M. & Brennan, B. Emerging phleboviruses. *Curr. Opin. Virol.* **5**, 50–57 (2014).
7. Elliott, R. M. Orthobunyaviruses: recent genetic and structural insights. *Nat. Rev. Microbiol.* **12**, 673–85 (2014).
8. Lasecka, L. & Baron, M. D. The molecular biology of nairoviruses, an emerging group of tick-borne arboviruses. *Arch. Virol.* **159**, 1249–1265 (2014).
9. Van Poelwijk, F., Prins, M. & Goldbach, R. Completion of the impatiens necrotic spot virus genome sequence and genetic comparison of the L proteins within the family Bunyaviridae. *J. Gen. Virol.* **78**, 543–546 (1997).
10. Elbeaino, T., Digiaro, M. & Martelli, G. P. Complete nucleotide sequence of four RNA segments of fig mosaic virus. *Arch. Virol.* **154**, 1719–1727 (2009).
11. Tokarz, R. *et al.* Virome analysis of *Amblyomma americanum*, *Dermacentor variabilis*, and *Ixodes scapularis* ticks reveals novel highly divergent vertebrate and invertebrate viruses. *J. Virol.* **88**, 11480–92 (2014).
12. Li, C.-X. *et al.* Unprecedented genomic diversity of RNA viruses in arthropods reveals the ancestry of negative-sense RNA viruses. *Elife* **4**, 209–220 (2015).
13. Yu, X. J. *et al.* Fever with Thrombocytopenia Associated with a Novel Bunyavirus in China. *N Engl J Med* 1523–1532 (2011). doi:10.1056/NEJMoa1010095
14. McMullan, L. K. *et al.* A New Phlebovirus associated with severe febrile illness in Missouri. *N. Engl. J. Med.* **367**, 834–841 (2012).
15. Li, D. A highly pathogenic new bunyavirus emerged in China. *Emerg. Microbes Infect.* **2**, e1 (2013).
16. Liu, Q., He, B., Huang, S. Y., Wei, F. & Zhu, X. Q. Severe fever with thrombocytopenia syndrome, an emerging tick-borne zoonosis. *Lancet Infect. Dis.* **14**, 763–772 (2014).
17. Beer, M., Conraths, F. J. & Van Der Poel, W. H. M. ‘Schmallenberg virus’ – a novel orthobunyavirus emerging in Europe. *Epidemiol. Infect.* 1–8 (2012). doi:10.1017/S0950268812002245
18. Doceul, V. *et al.* Epidemiology, molecular virology and diagnostics of Schmallenberg virus, an emerging orthobunyavirus in Europe. *Vet. Res.* **44**, 31 (2013).
19. conraths, F.J. Kämer, D. Teske, K. Hoffmann, B. Mettenleiter, T.C. Beer, M. Reemerging

- Schmallenberg virus infections, Germany, 2012. *Emerging Infectious Diseases* **19**, 513–514 (2013).
20. Elliott, R. M. Emerging viruses: the Bunyaviridae. *Mol. Med.* **3**, 572–577 (1997).
  21. Léger, P. & Lozach, P.-Y. Bunyaviruses: from transmission by arthropods to virus entry into the mammalian host first-target cells. *Future Virol.* **10**, 859–881 (2015).
  22. Horne, K. M. E. & Vanlandingham, D. L. Bunyavirus-vector interactions. *Viruses* **6**, 4373–4397 (2014).
  23. Bente, D. A. *et al.* Crimean-Congo hemorrhagic fever: History, epidemiology, pathogenesis, clinical syndrome and genetic diversity. *Antiviral Res.* **100**, 159–189 (2013).
  24. Pepin, M., Bouloy, M., Bird, B. H., Kemp, A. & Paweska, J. Rift Valley fever virus (Bunyaviridae: Phlebovirus): An update on pathogenesis, molecular epidemiology, vectors, diagnostics and prevention. *Vet. Res.* **41**, (2010).
  25. Bouloy, M. in *Bunyaviridae* (eds. Plyusnin, A. & Elliott, R. M.) 95–128 (Caister Academic Press, 2011).
  26. Xu, B. *et al.* Metagenomic analysis of fever, thrombocytopenia and leukopenia syndrome (ftls) in Henan province, China: Discovery of a new bunyavirus. *PLoS Pathog.* **7**, (2011).
  27. Dilcher, M., Alves, M. J., Finkeisen, D., Hufert, F. & Weidmann, M. Genetic characterization of bhanja virus and palma virus, two tick-borne phleboviruses. *Virus Genes* **45**, 311–315 (2012).
  28. Palacios, G. *et al.* Characterization of the Uukuniemi virus group (Phlebovirus: Bunyaviridae): evidence for seven distinct species. *J. Virol.* **87**, 3187–95 (2013).
  29. Brennan, B. *et al.* Reverse genetics system for severe fever with thrombocytopenia syndrome virus. *J. Virol.* **89**, 3026–37 (2015).
  30. Overby, A. K., Pettersson, R. F., Grünewald, K. & Huisken, J. T. Insights into bunyavirus architecture from electron cryotomography of Uukuniemi virus. *Proc. Natl. Acad. Sci. U. S. A.* **105**, 2375–9 (2008).
  31. Reguera, J., Weber, F., Cusack, S., Shimizu, T. & Minaka, N. Bunyaviridae RNA Polymerases (L-Protein) Have an N-Terminal, Influenza-Like Endonuclease Domain, Essential for Viral Cap-Dependent Transcription. *PLoS Pathog.* **6**, e1001101 (2010).
  32. Barr, J. N. & Wertz, G. W. Bunyamwera bunyavirus RNA synthesis requires cooperation of 3'- and 5'-terminal sequences. *J. Virol.* **78**, 1129–38 (2004).
  33. Won, S., Ikegami, T., Peters, C. J. & Makino, S. NSm and 78-kilodalton proteins of Rift Valley fever virus are nonessential for viral replication in cell culture. *J. Virol.* **80**, 8274–8 (2006).
  34. Won, S., Ikegami, T., Peters, C. J. & Makino, S. NSm protein of Rift Valley fever virus suppresses virus-induced apoptosis. *J. Virol.* **81**, 13335–45 (2007).
  35. Bergeron, E., Vincent, M. J. & Nichol, S. T. Crimean-Congo hemorrhagic fever virus glycoprotein processing by the endoprotease SKI-1/S1P is critical for virus infectivity. *J. Virol.* **81**, 13271–6 (2007).
  36. Altamura, L. A. *et al.* Identification of a novel C-terminal cleavage of Crimean-Congo hemorrhagic fever virus PreGN that leads to generation of an NSM protein. *J. Virol.* **81**, 6632–42 (2007).
  37. Watret, G. E. & Elliott, R. M. The proteins and RNAs specified by Clo Mor virus, a Scottish naivovirus. *J. Gen. Virol.* **66**, 2513–2516 (1985).

## References

38. Foulke, R. S., Rosato, R. R. & French, G. R. Structural polypeptides of Hazara virus. *J. Gen. Virol.* **53**, 169–172 (1981).
39. Le May, N. & Gauthier, N. The N Terminus of Rift Valley Fever Virus Nucleoprotein Is Essential for Dimerization. *J. Virol.* **79**, 11974–11980 (2005).
40. Walter, C. T. & Barr, J. N. Recent advances in the molecular and cellular biology of bunyaviruses. *J. Gen. Virol.* **92**, 2467–84 (2011).
41. Alborno, A., Hoffmann, A. B., Lozach, P. Y. & Tischler, N. D. Early bunyavirus-host cell interactions. *Viruses* **8**, (2016).
42. Jääskeläinen, K. M. *et al.* Tula and Puumala hantavirus NSs ORFs are functional and the products inhibit activation of the interferon-beta promoter. *J. Med. Virol.* **79**, 1527–1536 (2007).
43. Eifan, S., Schnettler, E., Dietrich, I., Kohl, A. & Blomström, A. L. Non-structural proteins of arthropod-borne bunyaviruses: Roles and functions. *Viruses* **5**, 2447–2468 (2013).
44. Wu, X. *et al.* Roles of viroplasm-like structures formed by nonstructural protein NSs in infection with severe fever with thrombocytopenia syndrome virus. *FASEB J.* **28**, 2504–2516 (2014).
45. Qu, B. *et al.* Suppression of the interferon and NF- $\kappa$ B responses by severe fever with thrombocytopenia syndrome virus. *J. Virol.* **86**, 8388–401 (2012).
46. Chen, X. *et al.* Severe fever with thrombocytopenia syndrome virus inhibits exogenous Type I IFN signaling pathway through its NSs in vitro. *PLoS One* **12**, 1–12 (2017).
47. Barr, J. N. & Wertz, G. W. Role of the conserved nucleotide mismatch within 3'- and 5'-terminal regions of Bunyamwera virus in signaling transcription. *J. Virol.* **79**, 3586–94 (2005).
48. Kohl, A., Dunn, E. F., Lowen, A. C. & Elliott, R. M. Complementarity, sequence and structural elements within the 3' and 5' non-coding regions of the Bunyamwera orthobunyavirus S segment determine promoter strength. *J. Gen. Virol.* **85**, 3269–3278 (2004).
49. Elliott, R. M. *et al.* Nucleotide sequence and coding strategy of the Uukuniemi virus L RNA segment The complete nucleotide sequence of the L RNA segment of Uukuniemi virus has been determined from length, and is of negative polarity. The viral-complementary RNA contains 1745–1752 (1992).
50. Pettersson, R. F. & Von Bonsdorff, C.-H. Ribonucleoproteins of Uukuniemi Virus are Circular. *J. Virol.* **15**, 386–392 (1975).
51. Hewlett, M. J., Pettersson, R. F. & Baltimore, D. Circular forms of Uukuniemi virion RNA: an electron microscopic study. *J. Virol.* **21**, 1085–1093 (1977).
52. Gerlach, P., Malet, H., Cusack, S. & Reguera, J. Structural insights into bunyavirus replication and its regulation by the vRNA promoter. *Cell* **161**, 1267–1279 (2015).
53. Reguera, J., Cusack, S. & Kolakofsky, D. Segmented negative strand RNA virus nucleoprotein structure. *Curr. Opin. Virol.* **5**, 7–15 (2014).
54. Kuismanen, E., Bang, B., Hurme, M. & Pettersson, R. F. Uukuniemi virus maturation: Immunofluorescence Microscopy with Monoclonal Glycoprotein-Specific Antibodies. *J. Virol.* **51**, 137–146 (1984).
55. Overby, A. K., Popov, V., Neve, E. P. A. & Pettersson, R. F. Generation and analysis of infectious virus-like particles of uukuniemi virus (bunyaviridae): a useful system for studying bunyaviral

- packaging and budding. *J. Virol.* **80**, 10428–35 (2006).
56. Overby, A. K., Pettersson, R. F. & Neve, E. P. A. The glycoprotein cytoplasmic tail of Uukuniemi virus (Bunyaviridae) interacts with ribonucleoproteins and is critical for genome packaging. *J. Virol.* **81**, 3198–205 (2007).
  57. Overby, A. K., Popov, V. L., Pettersson, R. F. & Neve, E. P. A. The cytoplasmic tails of Uukuniemi Virus (Bunyaviridae) GN and GC glycoproteins are important for intracellular targeting and the budding of virus-like particles. *J. Virol.* **81**, 11381–91 (2007).
  58. Wichgers Schreur, P. J. & Kortekaas, J. Single-Molecule FISH Reveals Non-selective Packaging of Rift Valley Fever Virus Genome Segments. *PLOS Pathog.* **12**, 1–21 (2016).
  59. Freiberg, A. N., Sherman, M. B., Morais, M. C., Holbrook, M. R. & Watowich, S. J. Three-dimensional organization of Rift Valley fever virus revealed by cryoelectron tomography. *J. Virol.* **82**, 10341–10348 (2008).
  60. Talmon, Y. *et al.* Electron microscopy of vitrified-hydrated La Crosse virus. *J. Virol.* **61**, 2319–2321 (1987).
  61. Huisken, J. T., Overby, A. K., Weber, F. & Grünewald, K. Electron cryo-microscopy and single-particle averaging of Rift Valley fever virus: evidence for GN-GC glycoprotein heterodimers. *J. Virol.* **83**, 3762–9 (2009).
  62. Bowden, T. A. *et al.* Orthobunyavirus Ultrastructure and the Curious Tripodal Glycoprotein Spike. *PLoS Pathog.* **9**, e1003374 (2013).
  63. Enamit, M., Luytjes, W., Krystal, M. & Palese, P. Introduction of site-specific mutations into the genome of influenza virus. *Proc Natl Acad Sci U S A* **87**, 3802–3805 (1990).
  64. Neumann, G. *et al.* Generation of influenza A viruses entirely from cloned cDNAs. *Microbiology* **96**, 9345–9350 (1999).
  65. Garcia-Sastre, A. & Palese, P. Annu. Rev. Microbio.-1993-Garcia-Sastre. *Annu. Rev. Microbiol.* **47**, 765–90 (1993).
  66. Walpita, P. & Flick, R. Reverse genetics of negative-stranded RNA viruses: A global perspective. *FEMS Microbiol. Lett.* **244**, 9–18 (2005).
  67. Bridgen, A. & Elliott, R. M. Rescue of a segmented negative-strand RNA virus entirely from cloned complementary DNAs. *Microbiology* **93**, 15400–15404 (1996).
  68. Blakqori, G. & Weber, F. Efficient cDNA-based rescue of La Crosse bunyaviruses expressing or lacking the nonstructural protein NSs. *J. Virol.* **79**, 10420–8 (2005).
  69. Elliott, R. M. *et al.* Establishment of a reverse genetics system for Schmallenberg virus, a newly emerged orthobunyavirus in Europe. *J. Gen. Virol.* **94**, 851–9 (2013).
  70. Flick, R. & Pettersson, R. F. Reverse genetics system for Uukuniemi virus (Bunyaviridae): RNA polymerase I-catalyzed expression of chimeric viral RNAs. *J. Virol.* **75**, 1643–1655 (2001).
  71. Fodor, E. *et al.* Rescue of Influenza A Virus from Recombinant DNA. *J. Virol.* **73**, 9679–9682 (1999).
  72. Billecocq, A. *et al.* RNA polymerase I-mediated expression of viral RNA for the rescue of infectious virulent and avirulent Rift Valley fever viruses. *Virology* **378**, 377–384 (2008).
  73. de Boer, S. M. *et al.* Heparan sulfate facilitates Rift Valley fever virus entry into the cell. *J. Virol.*

## References

- 86**, 13767–71 (2012).
74. Riblett, A. M. *et al.* A Haploid Genetic Screen Identifies Heparan Sulfate Proteoglycans Supporting Rift Valley Fever Virus Infection. *J. Virol.* **90**, 1414–23 (2015).
  75. Pietrantoni, A., Fortuna, C., Remoli, M., Ciufolini, M. & Superti, F. Bovine Lactoferrin Inhibits Toscana Virus Infection by Binding to Heparan Sulphate. *Viruses* **7**, 480–495 (2015).
  76. Spiegel, M., Plegge, T. & Pöhlmann, S. The role of phlebovirus glycoproteins in viral entry, assembly and release. *Viruses* **8**, (2016).
  77. Sun, Y. *et al.* Nonmuscle myosin heavy chain IIA is a critical factor contributing to the efficiency of early infection of severe fever with thrombocytopenia syndrome virus. *J. Virol.* **88**, 237–48 (2014).
  78. Xiao, X., Feng, Y., Zhu, Z. & Dimitrov, D. S. Identification of a putative Crimean-Congo hemorrhagic fever virus entry factor. *Biochem. Biophys. Res. Commun.* **411**, 253–258 (2011).
  79. Lozach, P.-Y. *et al.* DC-SIGN as a receptor for phleboviruses. *Cell Host Microbe* **10**, 75–88 (2011).
  80. Curtis, B. M., Scharnowske, S. & Watson, A. J. Sequence and expression of a membrane-associated C-type lectin that exhibits CD4-independent binding of human immunodeficiency virus envelope glycoprotein gp120 (virus receptor/type UImembrane protein/mannose binding). *Med. Sci.* **89**, 8356–8360 (1992).
  81. van Kooyk, Y. C-type lectins on dendritic cells: key modulators for the induction of immune responses. *Biochem. Soc. Trans.* **36**, 1478–1481 (2008).
  82. Lozach, P.-Y. *et al.* Dendritic cell-specific intercellular adhesion molecule 3-grabbing non-integrin (DC-SIGN)-mediated enhancement of dengue virus infection is independent of DC-SIGN internalization signals. *J. Biol. Chem.* **280**, 23698–708 (2005).
  83. Davis, C. W. *et al.* The location of asparagine-linked glycans on West Nile virions controls their interactions with CD209 (dendritic cell-specific ICAM-3 grabbing nonintegrin). *J. Biol. Chem.* **281**, 37183–94 (2006).
  84. Martina, B. E. E. *et al.* DC-SIGN enhances infection of cells with glycosylated West Nile virus in vitro and virus replication in human dendritic cells induces production of IFN- $\alpha$  and TNF $\alpha$ . *Virus Res.* **135**, 64–71 (2008).
  85. Shimojima, M., Takenouchi, A., Shimoda, H., Kimura, N. & Maeda, K. Distinct usage of three C-type lectins by Japanese encephalitis virus: DC-SIGN, DC-SIGNR, and LSECtin. *Arch. Virol.* **159**, 2023–2031 (2014).
  86. Wang, P. *et al.* DC-SIGN as an attachment factor mediates Japanese encephalitis virus infection of human dendritic cells via interaction with a single high-mannose residue of viral E glycoprotein. *Virology* **488**, 108–119 (2016).
  87. Švajger, U., Anderluh, M., Jeras, M. & Obermajer, N. C-type lectin DC-SIGN: An adhesion, signalling and antigen-uptake molecule that guides dendritic cells in immunity. *Cell. Signal.* **22**, 1397–1405 (2010).
  88. Garcia-Vallejo, J. J. & van Kooyk, Y. The physiological role of DC-SIGN: A tale of mice and men. *Trends Immunol.* **34**, 482–486 (2013).
  89. Hofmann, H. *et al.* Severe fever with thrombocytopenia virus glycoproteins are targeted by neutralizing antibodies and can use DC-SIGN as a receptor for pH-dependent entry into human and animal cell lines. *J. Virol.* **87**, 4384–94 (2013).

90. Léger, P. *et al.* Differential Use of the C-Type Lectins L-SIGN and DC-SIGN for Phlebovirus Endocytosis. *Traffic* **17**, 639–656 (2016).
91. Boulant, S., Stanifer, M. & Lozach, P. Y. Dynamics of virus-receptor interactions in virus binding, signaling, and endocytosis. *Viruses* **7**, 2794–2815 (2015).
92. Goncalves, A.-R. *et al.* Role of DC-SIGN in Lassa virus entry into human dendritic cells. *J. Virol.* **87**, 11504–15 (2013).
93. Gringhuis, S. I. *et al.* C-Type Lectin DC-SIGN Modulates Toll-like Receptor Signaling via Raf-1 Kinase-Dependent Acetylation of Transcription Factor NF- $\kappa$ B. *Immunity* **26**, 605–616 (2007).
94. Gringhuis, S. I., den Dunnen, J., Litjens, M., van der Vlist, M. & H Geijtenbeek, T. B. Carbohydrate-specific signaling through the DC-SIGN signalosome tailors immunity to *Mycobacterium tuberculosis*, HIV-1 and *Helicobacter pylori*. *Nat. Immunol.* **10**, 0–8 (2009).
95. Schelhaas, M. Come in and take your coat off - how host cells provide endocytosis for virus entry. *Cell. Microbiol.* **12**, 1378–1388 (2010).
96. Harmon, B. *et al.* Rift Valley fever virus strain MP-12 enters mammalian host cells via caveola-mediated endocytosis. *J. Virol.* **86**, 12954–70 (2012).
97. de Boer, S. M. *et al.* Acid-activated structural reorganization of the Rift Valley fever virus Gc fusion protein. *J. Virol.* **86**, 13642–52 (2012).
98. Garrison, A. R. *et al.* Crimean-Congo hemorrhagic fever virus utilizes a clathrin- and early endosome-dependent entry pathway. *Virology* **444**, 45–54 (2013).
99. Hollidge, B. S. *et al.* Orthobunyavirus entry into neurons and other mammalian cells occurs via clathrin-mediated endocytosis and requires trafficking into early endosomes. *J. Virol.* **86**, 7988–8001 (2012).
100. Lozach, P.-Y. *et al.* Entry of bunyaviruses into mammalian cells. *Cell Host Microbe* **7**, 488–99 (2010).
101. Shtanko, O., Nikitina, R. A., Altuntas, C. Z., Chepurnov, A. A. & Davey, R. A. Crimean-Congo Hemorrhagic Fever Virus Entry into Host Cells Occurs through the Multivesicular Body and Requires ESCRT Regulators. *PLoS Pathog.* **10**, (2014).
102. Lozach, P. Y., Huotari, J. & Helenius, A. Late-penetrating viruses. *Curr. Opin. Virol.* **1**, 35–43 (2011).
103. Liu, L., Celma, C. C. P. & Roy, P. Rift Valley fever virus structural proteins: expression, characterization and assembly of recombinant proteins. *Virol. J.* **5**, 82 (2008).
104. Wang, D. & Hiesinger, P. R. The vesicular ATPase: A missing link between acidification and exocytosis. *J. Cell Biol.* **203**, 171–173 (2013).
105. Tani, H. *et al.* Characterization of severe fever with thrombocytopenia syndrome virus glycoprotein-mediated entry. *J. Virol.* **90**, 5292–5301 (2016).
106. Guardado-Calvo, P. & Rey, F. A. in *Advances in Virus Research* **98**, 83–118 (2017).
107. Harrison, S. C. Viral membrane fusion. *Virology* **479–480**, 498–507 (2015).
108. Weissenhorn, W., Hinz, A. & Gaudin, Y. Virus membrane fusion. *FEBS Lett.* **581**, 2150–2155 (2007).

## References

109. Kielian, M. Mechanisms of Virus Membrane Fusion Proteins. *Annu. Rev. Virol* **1**, 171–89 (2014).
110. Garry, C. E. & Garry, R. F. Proteomics computational analyses suggest that the carboxyl terminal glycoproteins of Bunyaviruses are class II viral fusion protein (beta-penetrenes). *Theor. Biol. Med. Model.* **1**, 10 (2004).
111. Rusu, M. *et al.* An Assembly Model of Rift Valley Fever Virus. *Front. Microbiol.* **3**, 254 (2012).
112. Dessau, M. & Modis, Y. Crystal structure of glycoprotein C from Rift Valley fever virus. **2012**, (2013).
113. Halldorsson, S. *et al.* Structure of a phleboviral envelope glycoprotein reveals a consolidated model of membrane fusion. *Proc. Natl. Acad. Sci.* **113**, 7154–7159 (2016).
114. Liao, M. & Kielian, M. Domain III from class II fusion proteins functions as a dominant-negative inhibitor of virus membrane fusion. *J. Cell Biol.* **171**, 111–120 (2005).
115. Schmidt, A. G., Yang, P. L., Harrison, S. C., Brandt, W. & Ma, N. Peptide Inhibitors of Dengue-Virus Entry Target a Late-Stage Fusion Intermediate. *PLoS Pathog.* **6**, 1–11 (2010).
116. Koehler, J. W. *et al.* A Fusion-Inhibiting Peptide against Rift Valley Fever Virus Inhibits Multiple, Diverse Viruses. *PLoS Negl. Trop. Dis.* **7**, 1–11 (2013).
117. Fritz, R., Stiasny, K. & Heinz, F. X. Identification of specific histidines as pH sensors in flavivirus membrane fusion. *J. Cell Biol.* **183**, 353–361 (2008).
118. Qin, Z.-L., Zheng, Y. & Kielian, M. Role of conserved histidine residues in the low-pH dependence of the Semliki Forest virus fusion protein. *J. Virol.* **83**, 4670–7 (2009).
119. Bitto, D., Halldorsson, S., Caputo, A. & Huiskonen, J. T. Low pH and anionic lipid-dependent fusion of uukuniemi phlebovirus to liposomes. *J. Biol. Chem.* **291**, 6412–6422 (2016).
120. Bishop, D. H. L., Matsuo, Y. & Yamazaki, T. Nonviral heterogeneous sequences are present at the 5' ends of one species of snowshoes hare bunyavirus S complementary RNA. *Nucleic Acids Res.* **11**, 1–2 (1983).
121. Plotch, S. J., Bouloy, M., Ulmanen, I. & Krug, R. M. A unique cap(m7GpppXm)-dependent influenza virion endonuclease cleaves capped RNAs to generate the primers that initiate viral RNA transcription. *Cell* **23**, 847–58 (1981).
122. Reich, S. *et al.* Structural insight into cap-snatching and RNA synthesis by influenza polymerase. *Nature* **516**, 361–366 (2014).
123. Jin, H. & Elliott, R. M. Characterization of Bunyamwera virus S RNA that is transcribed and replicated by the L protein expressed from recombinant vaccinia Characterization of Bunyamwera Virus S RNA That Is Transcribed and Replicated by the L Protein Expressed from Recombinant Va. **67**, 1396–1404 (1993).
124. Ikegami, T., Won, S., Peters, C. J. & Makino, S. Rift Valley fever virus NSs mRNA is transcribed from an incoming anti-viral-sense S RNA segment. *J. Virol.* **79**, 12106–11 (2005).
125. Patterson, J. L. & Kolakofsky, D. Characterization of La Crosse virus small-genome transcripts. *J. Virol.* **49**, 680–5 (1984).
126. Barr, J. N. Bunyavirus mRNA synthesis is coupled to translation to prevent premature transcription termination. *RNA* **13**, 731–6 (2007).
127. Elliott, R. M. *The Bunyaviridae.* (1996).

128. Ferron, F., Weber, F., de la Torre, J. C. & Reguera, J. Transcription and replication mechanisms of Bunyaviridae and Arenaviridae L proteins. *Virus Res.* (2017). doi:10.1016/j.virusres.2017.01.018
129. Ulmanen, I., Seppälä, P. & Pettersson, R. F. In vitro translation of Uukuniemi virus-specific RNAs: identification of a nonstructural protein and a precursor to the membrane glycoproteins. *J. Virol.* **37**, 72–79 (1981).
130. Kuismanen, E. Posttranslational processing of Uukuniemi virus glycoproteins G1 and G2. *J. Virol.* **51**, 806–812 (1984).
131. Andersson, a M. *et al.* Processing and membrane topology of the spike proteins G1 and G2 of Uukuniemi virus. *J. Virol.* **71**, 218–225 (1997).
132. Gerrard, S. R. & Nichol, S. T. Synthesis, proteolytic processing and complex formation of N-terminally nested precursor proteins of the Rift Valley fever virus glycoproteins. *Virology* **357**, 124–133 (2007).
133. Persson, R. & Pettersson, R. F. Formation and Intracellular Transport of a Heterodimeric Viral Spike Protein Complex. *J. Cell Biol.* **112**, 257–266 (1991).
134. Andersson, a M., Melin, L., Bean, a & Pettersson, R. F. A retention signal necessary and sufficient for Golgi localization maps to the cytoplasmic tail of a Bunyaviridae (Uukuniemi virus) membrane glycoprotein. *J. Virol.* **71**, 4717–4727 (1997).
135. Andersson, A. M. & Pettersson, R. F. Targeting of a short peptide derived from the cytoplasmic tail of the G1 membrane glycoprotein of Uukuniemi virus (Bunyaviridae) to the Golgi complex. *J. Virol.* **72**, 9585–96 (1998).
136. Melin, L. *et al.* The membrane glycoprotein G1 of Uukuniemi virus contains a signal for localization to the Golgi complex. *Virus Res.* **39**, 49–66 (1995).
137. Matsuoka, Y., Chen, S. Y. & Compans, R. W. A signal for Golgi retention in the bunyavirus G1 glycoprotein. *J. Biol. Chem.* **269**, 22565–22573 (1994).
138. Gerrard, S. R. & Nichol, S. T. Characterization of the Golgi retention motif of Rift Valley fever virus G(N) glycoprotein. *J. Virol.* **76**, 12200–10 (2002).
139. Kuismanen, E., Hedman, K., Saraste, J. & Pettersson, R. F. Uukuniemi virus maturation: accumulation of virus particles and viral antigens in the Golgi complex. *Mol. Cell. Biol.* **2**, 1444–58 (1982).
140. Salanueva, I. J. *et al.* Polymorphism and structural maturation of bunyamwera virus in Golgi and post-Golgi compartments. *J. Virol.* **77**, 1368–81 (2003).
141. Veijola, J. & Pettersson, R. F. Transient association of calnexin and calreticulin with newly synthesized G1 and G2 glycoproteins of uukuniemi virus (family Bunyaviridae). *J. Virol.* **73**, 6123–7 (1999).
142. Schwarz, F. & Aebi, M. Mechanisms and principles of N-linked protein glycosylation. *Curr. Opin. Struct. Biol.* **21**, 576–582 (2011).
143. Chen, S. Y., Matsuoka, Y. & Compans, R. W. Assembly of G1 and G2 glycoprotein oligomers in Punta Toro virus-infected cells. *Virus Res.* **22**, 215–25 (1992).
144. Shi, X., Brauburger, K. & Elliott, R. M. Role of N-Linked Glycans on Bunyamwera Virus Glycoproteins in Intracellular Trafficking , Protein Folding , and Virus Infectivity. *J. Virol.* **79**, 13725–13734 (2005).

## References

145. Erickson, B. R., Deyde, V., Sanchez, A. J., Vincent, M. J. & Nichol, S. T. N-linked glycosylation of Gn (but not Gc) is important for Crimean Congo hemorrhagic fever virus glycoprotein localization and transport. *Virology* **361**, 348–355 (2007).
146. Rönnholm, R. & Pettersson, R. F. Complete nucleotide sequence of the M RNA segment of Uukuniemi virus encoding the membrane glycoproteins G1 and G2. *Virology* **160**, 191–202 (1987).
147. Zivcec, M., Scholte, F., Spiropoulou, C., Spengler, J. & Bergeron, É. Molecular Insights into Crimean-Congo Hemorrhagic Fever Virus. *Viruses* **8**, 106 (2016).
148. Brites-Neto, J., Duarte Roncato, K. M. & Martins, T. F. Tick-borne infections in human and animal population worldwide. *Vet. World* **8**, 301–315 (2015).
149. Labuda, M. & Nuttall, P. A. Tick-borne viruses. *Parasitology* **129**, S221–S245 (2004).
150. Nuttall, P. A. Molecular characterization of tick-virus interactions. 2466–2483 (2009).
151. Brackney, D. E. & Armstrong, P. M. Transmission and evolution of tick-borne viruses. *Curr. Opin. Virol.* **21**, 67–74 (2016).
152. Estrada-Peña, A. & de la Fuente, J. The ecology of ticks and epidemiology of tick-borne viral diseases. *Antiviral Res.* **108**, 104–128 (2014).
153. Moutailler, S., Popovici, I., Devillers, E., Vayssier-Taussat, M. & Eloit, M. Diversity of viruses in *Ixodes ricinus*, and characterization of a neurotropic strain of Eyach virus. *New Microbes New Infect.* **11**, 71–81 (2016).
154. Kocan, K. M., de la Fuente, J. & Coburn, L. A. Insights into the development of *Ixodes scapularis*: a resource for research on a medically important tick species. *Parasit. Vectors* **8**, 592 (2015).
155. Parola, P. & Raoult, D. Ticks and Tickborne Bacterial Diseases in Humans: An Emerging Infectious Threat. *Clin. Infect. Dis.* **32**, 897–928 (2001).
156. de la Fuente, J., Estrada-Peña, A., Venzal, J. M., Kocan, K. M. & Sonenshine, D. E. Ticks as vectors of pathogens that cause diseases in humans and animals. *Front. Biosci.* **13**, 6938–6946 (2008).
157. de la Fuente, J. *et al.* Tick-Pathogen Interactions and Vector Competence: Identification of Molecular Drivers for Tick-Borne Diseases. *Front. Cell. Infect. Microbiol.* **7**, 114 (2017).
158. Alberdi, P. *et al.* Infection of *Ixodes* spp. tick cells with different *Anaplasma phagocytophilum* isolates induces the inhibition of apoptotic cell death. *Ticks Tick. Borne. Dis.* **6**, 758–767 (2015).
159. Applegren, N. D. & Kraus, C. K. Lyme Disease: Emergency Department Considerations. *J. Emerg. Med.* 1–10 (2017). doi:10.1016/j.jemermed.2017.01.022
160. McCoy, K. D., Léger, E. & Dietrich, M. Host specialization in ticks and transmission of tick-borne diseases: a review. *Front. Cell. Infect. Microbiol.* **3**, 57 (2013).
161. Karbowiak, G. & Biernat, B. The role of particular tick developmental stages in the circulation of tick-borne pathogens affecting humans in Central Europe . 2 . Tick-borne encephalitis virus . **62**, 3–9 (2016).
162. Mardani, M., Keshtkar-Jahromi, M., Ataie, B. & Adibi, P. Short report: Crimean-Congo hemorrhagic fever virus as a nosocomial pathogen in Iran. *Am. J. Trop. Med. Hyg.* **81**, 675–678 (2009).
163. Tang, X. *et al.* Human-to-Human Transmission of Severe Fever With Thrombocytopenia Syndrome Bunyavirus Through Contact With Infectious Blood. *J. Infect. Dis.* **207**, 736–739 (2013).

164. Jiang, X. L. *et al.* A cluster of person-to-person transmission cases caused by SFTS virus in Penglai, China. *Clin. Microbiol. Infect.* **21**, 274–279 (2014).
165. Gong, Z. *et al.* Probable aerosol transmission of severe fever with thrombocytopenia syndrome virus in southeastern China. *Clin. Microbiol. Infect.* **21**, 1115–1120 (2015).
166. Ayllón, N. *et al.* Systems Biology of Tissue-Specific Response to *Anaplasma phagocytophilum* Reveals Differentiated Apoptosis in the Tick Vector *Ixodes scapularis*. *PLoS Genet.* **11**, e1005120 (2015).
167. Mansfield, K. L. *et al.* Tick-borne pathogens induce differential expression of genes promoting cell survival and host resistance in *Ixodes ricinus* cells. *Parasit. Vectors* **10**, 81 (2017).
168. Platt, K. B. *et al.* Impact of Dengue Virus Infection on Feeding Behavior of *Aedes aegypti*. *Am. J. Trop. Med. Hyg.* **57**, 119–125 (1997).
169. Lima-Camara, T. N. *et al.* Dengue Infection Increases the Locomotor Activity of *Aedes aegypti* Females. *PLoS One* **6**, e17690 (2011).
170. Dickson, D. L. & Turell, M. J. Replication and tissue tropisms of Crimean-Congo hemorrhagic fever virus in experimentally infected adult *Hyalomma truncatum* (Acari: Ixodidae). *J. Med. Entomol.* **29**, 767–73 (1992).
171. Gulia-Nuss, M. *et al.* Genomic insights into the *Ixodes scapularis* tick vector of Lyme disease. *Nat. Commun.* **7**, 10507 (2016).
172. Dejnirattisai, W. *et al.* Lectin Switching During Dengue Virus Infection. *J. Infect. Dis.* **203**, 1775–1783 (2011).
173. Richter, D., Matuschka, F., Spielman, A. & Mahadevan, L. How ticks get under your skin : insertion mechanics of the feeding apparatus of *Ixodes ricinus* ticks. *Proc. R. Soc. Biol. Sci.* **280**, (2013).
174. Francischetti, I. M. B., Sa-Nunes, A., Mans, B. J., Santos, I. M. & Ribeiro, J. M. C. The role of saliva in tick feeding. *Front. Biosci. (Landmark Ed.)* **14**, 2051–88 (2009).
175. Hovius, J. W. R., Levi, M. & Fikrig, E. Salivating for knowledge: Potential pharmacological agents in tick saliva. *PLoS Med.* **5**, 0202–0208 (2008).
176. Kotál, J. *et al.* Modulation of host immunity by tick saliva. *J. Proteomics* **128**, 58–68 (2015).
177. Urioste, B. S., Hall, L. R., Sam, P., Iii, T. & Titus, R. G. Saliva of the Lyme disease vector, *Ixodes dammini*, blocks cell activation by nonprostaglandin E2-dependent mechanism. *J. Exp. Med.* **180**, (1994).
178. Skallová, A., Iezzi, G., Ampenberger, F., Kopf, M. & Kopecky, J. Tick saliva inhibits dendritic cell migration, maturation, and function while promoting development of Th2 responses. *J. Immunol.* **180**, 6186–6192 (2008).
179. Kubes, M. *et al.* Heterogeneity in the effect of different ixodid tick species on human natural killer cell activity . *Parasite Immunol* **24**, 23–28 (2002).
180. Ferreira, B. R. & Silva, J. S. Saliva of *Rhipicephalus sanguineus* tick impairs T cell proliferation and IFN- $\gamma$ -induced macrophage microbicidal activity. *Vet. Immunol. Immunopathol.* **64**, 279–293 (1998).
181. Flores-Romo, L. In vivo maturation and migration of dendritic cells. *Immunology* **102**, 255–262 (2001).

## References

182. Hotchkiss, R. S., Monneret, G. & Payen, D. Sepsis-induced immunosuppression: from cellular dysfunctions to immunotherapy. *Nat. Rev. Immunol.* **13**, 862–74 (2013).
183. Alekseev, A. N., Burenkova, L. A., Vasilieva, I. S., Dubinina, H. V & Chunikhin, S. P. Preliminary studies on virus and spirochete accumulation in the cement plug of ixodid ticks. *Exp. Appl. Acarol.* **20**, 713–23 (1996).
184. Hermance, M. E. & Thangamani, S. Tick Saliva Enhances Powassan Virus Transmission to the Host, Influencing Its Dissemination and the Course of Disease. *J. Virol.* **89**, 7852–60 (2015).
185. Heath, W. R. & Carbone, F. R. The skin-resident and migratory immune system in steady state and memory: innate lymphocytes, dendritic cells and T cells. *Nat. Immunol.* **14**, 978–85 (2013).
186. Peyrefitte, C. N. *et al.* Differential activation profiles of Crimean-Congo hemorrhagic fever virus- and Dugbe virus-infected antigen-presenting cells. *J. Gen. Virol.* **91**, 189–198 (2010).
187. Connolly-Andersen, A.-M., Douagi, I., Kraus, A. a & Mirazimi, A. Crimean Congo hemorrhagic fever virus infects human monocyte-derived dendritic cells. *Virology* **390**, 157–162 (2009).
188. Hofmann, H. & Pöhlmann, S. DC-SIGN: Access portal for sweet viral killers. *Cell Host Microbe* **10**, 5–7 (2011).
189. Nfon, C. K., Marszal, P., Zhang, S., Weingartl, H. M. & Glatzer, T. Innate Immune Response to Rift Valley Fever Virus in Goats. *PLoS Negl. Trop. Dis.* **6**, e1623 (2012).
190. Gommel, C. *et al.* Tissue tropism and target cells of NSs-deleted rift valley fever virus in live immunodeficient mice. *PLoS Negl. Trop. Dis.* **5**, (2011).
191. Fernandez-Garcia, M. D., Mazzon, M., Jacobs, M. & Amara, A. Pathogenesis of Flavivirus Infections: Using and Abusing the Host Cell. *Cell Host Microbe* **5**, 318–328 (2009).
192. Wu, X. *et al.* Evasion of antiviral immunity through sequestering of TBK1/IKKε/IRF3 into viral inclusion bodies. *J. Virol.* **88**, 3067–76 (2014).
193. Weber, F., Dunn, E. F., Bridgen, a & Elliott, R. M. The Bunyamwera virus nonstructural protein NSs inhibits viral RNA synthesis in a minireplicon system. *Virology* **281**, 67–74 (2001).
194. Léger, P. *et al.* Dicer-2- and Piwi-Mediated RNA Interference in Rift Valley Fever Virus-Infected Mosquito Cells. *J. Virol.* **87**, 1631–1648 (2013).
195. Ly, H. J. *et al.* Rift Valley fever virus NSs protein functions and the similarity to other bunyavirus NSs proteins. *Virol. J.* **13**, 118 (2016).
196. Xu, F., Chen, H., Travassos da Rosa, A. P. A., Tesh, R. B. & Xiao, S. Y. Phylogenetic relationships among sandfly fever group viruses (Phlebovirus: Bunyaviridae) based on the small genome segment. *J. Gen. Virol.* **88**, 2312–2319 (2007).
197. Perry, A. & *et al.* The host type I interferon response to viral and bacterial infections. *Cell Res.* **15**, 407–422 (2005).
198. Wuerth, J. & Weber, F. Phleboviruses and the Type I Interferon Response. *Viruses* **8**, 174 (2016).
199. Qu, B. *et al.* Suppression of the interferon and NF-κB responses by severe fever with thrombocytopenia syndrome virus. *J. Virol.* **86**, 8388–401 (2012).
200. Pichlmair, A. *et al.* Activation of MDA5 requires higher-order RNA structures generated during virus infection. *J. Virol.* **83**, 10761–9 (2009).

201. Flint, S. J., Enquist, L. W., Racaniello, V. R. & Skalka, A. M. in *Principles of virology - 3rd ed. - volume II* 53–84 (2009).
202. Ning, Y.-J. *et al.* Viral suppression of innate immunity via spatial isolation of TBK1/IKK from mitochondrial antiviral platform. *J. Mol. Cell Biol.* **6**, 324–337 (2014).
203. Santiago, F. W. *et al.* Hijacking of RIG-I signaling proteins into virus-induced cytoplasmic structures correlates with the inhibition of type I interferon responses. *J. Virol.* **88**, 4572–85 (2014).
204. Ning, Y.-J. *et al.* Disruption of type I interferon signaling by the nonstructural protein of severe fever with thrombocytopenia syndrome virus via the hijacking of STAT2 and STAT1 into inclusion bodies. *J. Virol.* **89**, 4227–36 (2015).
205. Rezelj, V. V., Överby, A. K. & Elliott, R. M. Generation of mutant Uukuniemi viruses lacking the nonstructural protein NSs by reverse genetics indicates that NSs is a weak interferon antagonist. *J. Virol.* **89**, 4849–56 (2015).
206. Lihoradova, O. A. *et al.* Characterization of Rift Valley Fever Virus MP-12 Strain Encoding NSs of Punta Toro Virus or Sandfly Fever Sicilian Virus. *PLoS Negl. Trop. Dis.* **7**, 1–15 (2013).
207. Habjan, M. *et al.* NSs protein of rift valley fever virus induces the specific degradation of the double-stranded RNA-dependent protein kinase. *J. Virol.* **83**, 4365–75 (2009).
208. Kainulainen, M., Lau, S., Samuel, C. E., Hornung, V. & Weber, F. NSs Virulence Factor of Rift Valley Fever Virus Engages the F-Box Proteins FBXW11 and  $\beta$ -TRCP1 To Degrade the Antiviral Protein Kinase PKR. *J. Virol.* **90**, 6140–7 (2016).
209. Bouloy, L. E. *et al.* Genetic Evidence for an Interferon-Antagonistic Function of Rift Valley Fever Virus Nonstructural Protein NSs. *J. Virol.* **75**, 1371–1377 (2001).
210. Billecocq, A. *et al.* NSs Protein of Rift Valley Fever Virus Blocks Interferon Production by Inhibiting Host Gene Transcription NSs Protein of Rift Valley Fever Virus Blocks Interferon Production by Inhibiting Host Gene Transcription. **78**, 9798–9806 (2004).
211. Vialat, P., Billecocq, A., Kohl, A. & Bouloy, M. The S segment of rift valley fever phlebovirus (Bunyaviridae) carries determinants for attenuation and virulence in mice. *J. Virol.* **74**, 1538–43 (2000).
212. Le May, N. *et al.* TFIIF Transcription Factor, a Target for the Rift Valley Hemorrhagic Fever Virus. *Cell* **116**, 541–550 (2004).
213. Kalveram, B., Lihoradova, O. & Ikegami, T. NSs protein of rift valley fever virus promotes posttranslational downregulation of the TFIIF subunit p62. *J. Virol.* **85**, 6234–43 (2011).
214. Kainulainen, M. *et al.* Virulence factor NSs of rift valley fever virus recruits the F-box protein FBXO3 to degrade subunit p62 of general transcription factor TFIIF. *J. Virol.* **88**, 3464–73 (2014).
215. Cyr, N. *et al.* A  $\Omega$ XaV motif in the Rift Valley fever virus NSs protein is essential for degrading p62, forming nuclear filaments and virulence. *Proc. Natl. Acad. Sci. U. S. A.* **112**, 6021–6 (2015).
216. Le May, N. *et al.* A SAP30 Complex Inhibits IFN- $\beta$  Expression in Rift Valley Fever Virus Infected Cells. *PLoS Pathog.* **4**, e13 (2008).
217. Kalveram, B. & Ikegami, T. Toscana Virus NSs Protein Promotes Degradation of Double-Stranded RNA-Dependent Protein Kinase. *J. Virol.* **87**, 3710–8 (2013).
218. Gori-Savellini, G., Valentini, M. & Cusi, M. G. Toscana virus NSs protein inhibits the induction of

## References

- type I interferon by interacting with RIG-I. *J. Virol.* **87**, 6660–7 (2013).
219. Blair, C. D. Mosquito RNAi is the major innate immune pathway controlling arbovirus infection and transmission. *Future Microbiol.* **6**, 265–277 (2011).
220. Hedil, M. & Kormelink, R. Viral RNA Silencing Suppression: The Enigma of Bunyavirus NSs Proteins. *Viruses* **8**, 208 (2016).
221. Mussabekova, A., Daeffler, L. & Imler, J.-L. Innate and intrinsic antiviral immunity in *Drosophila*. *Cell. Mol. Life Sci.* 1–16 (2017). doi:10.1016/j.jdermsci.2014.05.004
222. Blair, C. D. & Olson, K. E. The role of RNA interference (RNAi) in arbovirus-vector interactions. *Viruses* **7**, 820–843 (2015).
223. Ding, S.-W. RNA-based antiviral immunity. *Nat. Rev. Immunol.* **10**, 632–44 (2010).
224. Donald, C. L., Kohl, A. & Schnettler, E. New Insights into Control of Arbovirus Replication and Spread by Insect RNA Interference Pathways. *Insects* **3**, 511–531 (2012).
225. Schnettler, E. *et al.* Knockdown of piRNA pathway proteins results in enhanced semliki forest virus production in mosquito cells. *J. Gen. Virol.* **94**, 1680–1689 (2013).
226. Cirimotich, C. M., Scott, J. C., Phillips, A. T., Geiss, B. J. & Olson, K. E. Suppression of RNA interference increases alphavirus replication and virus-associated mortality in *Aedes aegypti* mosquitoes. *BMC Microbiol.* **9**, 49 (2009).
227. Schnettler, E. *et al.* Induction and suppression of tick cell antiviral RNAi responses by tick-borne flaviviruses. *Nucleic Acids Res.* **42**, 9436–9446 (2014).
228. Garcia, S. *et al.* Nairovirus RNA Sequences Expressed by a Semliki Forest Virus Replicon Induce RNA Interference in Tick Cells Nairovirus RNA Sequences Expressed by a Semliki Forest Virus Replicon Induce RNA Interference in Tick Cells. (2005). doi:10.1128/JVI.79.14.8942
229. Kurscheid, S. *et al.* Evidence of a tick RNAi pathway by comparative genomics and reverse genetics screen of targets with known loss-of-function phenotypes in *Drosophila*. *BMC Mol Biol* **10**, 26 (2009).
230. de la Fuente, J., Kocan, K. M., Almazán, C. & Blouin, E. F. RNA interference for the study and genetic manipulation of ticks. *Trends Parasitol.* **23**, 427–433 (2007).
231. Brackney, D. E. *et al.* C6/36 *Aedes albopictus* Cells Have a Dysfunctional Antiviral RNA Interference Response. *PLoS Negl. Trop. Dis.* **4**, e856 (2010).
232. Dietrich, I. *et al.* The Antiviral RNAi Response in Vector and Non-vector Cells against Orthobunyaviruses. *PLoS Negl. Trop. Dis.* **11**, e0005272 (2017).
233. Tong, M. & Jiang, Y. FK506-Binding Proteins and Their Diverse Functions. *Curr. Mol. Pharmacol.* 48–65 (2015).
234. Dunys, J., Duplan, E. & Checler, F. The transcription factor X-box binding protein-1 in neurodegenerative diseases. *Mol. Neurodegener.* **9**, 35 (2014).
235. He, Y. *et al.* Emerging roles for XBP1, a sUPeR transcription factor. *Gene Expr.* **15**, 13–25 (2010).
236. Weisheit, S. *et al.* *Ixodes scapularis* and *Ixodes ricinus* tick cell lines respond to infection with tick-borne encephalitis virus: transcriptomic and proteomic analysis. *Parasit. Vectors* **8**, 599 (2015).
237. Grabowski, J. M., Gulia-Nuss, M., Kuhn, R. J. & Hill, C. A. RNAi reveals proteins for metabolism

- and protein processing associated with Langkat virus infection in *Ixodes scapularis* (black-legged tick) ISE6 cells. *Parasit. Vectors* **10**, 24 (2017).
238. Barnard, A. C., Nijhof, A. M., Fick, W., Stutzer, C. & Maritz-Olivier, C. RNAi in arthropods: Insight into the machinery and applications for understanding the pathogen-vector interface. *Genes (Basel)*. **3**, 702–741 (2012).
  239. Pettersson, Ralf F. Kääriäinen, L. von Bonsdorff, C-H. Oker-Blom, N. Structural Components of Uukuniemi virus, a noncubical tick-borne arbovirus. **729**, 1–8 (1971).
  240. Surface structure of Uukuniemi Surface Structure of Uukuniemi Virus. **16**, (1975).
  241. Simons, J. A. N. F., Hellman, U. L. F. & Pettersson, R. F. coding strategy , packaging of complementary Uukuniemi Virus S RNA Segment : Ambisense Coding Strategy , Packaging of Complementary Strands into Virions , and Homology to Members of the Genus Phlebovirus. *J. Virol.* (1990).
  242. Mazelier, M. *et al.* Uukuniemi virus as a tick-borne virus model. *J. Virol.* **90**, 6784–6798 (2016).
  243. Bell-Sakyi, L., Zweygarth, E., Blouin, E. F., Gould, E. A. & Jongejan, F. Tick cell lines: tools for tick and tick-borne disease research. *Trends Parasitol.* **23**, 450–457 (2007).
  244. Brügger, B. *et al.* The HIV lipidome: A raft with an unusual composition. *Proc Natl Acad Sci U S A* **103**, 2641–2646 (2006).
  245. van Kooyk, Y., Unger, W. W. J., Fehres, C. M., Kalay, H. & García-Vallejo, J. J. Glycan-based DC-SIGN targeting vaccines to enhance antigen cross-presentation. *Mol. Immunol.* **55**, 143–145 (2013).
  246. Mercer, J., Schelhaas, M. & Helenius, A. Virus Entry by Endocytosis. *Annu. Rev. Biochem.* **79**, 803–833 (2010).
  247. Lowen, A. C., Noonan, C., McLees, A. & Elliott, R. M. Efficient bunyavirus rescue from cloned cDNA. *Virology* **330**, 493–500 (2004).
  248. Ikegami, T., Won, S., Peters, C. J. & Makino, S. Rescue of Infectious Rift Valley Fever Virus Entirely from cDNA , Analysis of Virus Lacking the NSs Gene , and Expression of a Foreign Gene Rescue of Infectious Rift Valley Fever Virus Entirely from cDNA , Analysis of Virus Lacking the NSs Gene , and Expr. **80**, 2933–2940 (2006).
  249. Bergeron, É. *et al.* Recovery of Recombinant Crimean Congo Hemorrhagic Fever Virus Reveals a Function for Non-structural Glycoproteins Cleavage by Furin. *PLoS Pathog.* **11**, 1–19 (2015).
  250. Oker-Blom, N., Salminen, A., Brummer-Korvenkontio, M., Kaeaeriaeinen, L. & Weckstroem, P. Isolation of some viruses other than typical tick-borne encephalitis viruses from *Ixodes ricinus* ticks in Finland. *Ann. Med. Exp. Biol. Fenn.* **42**, 109–12 (1964).
  251. Pettersson, R. & Kääriäinen, L. The ribonucleic acids of Uukuniemi virus, a noncubical tick-borne arbovirus. *Virology* **56**, 608–19 (1973).
  252. Bell-Sakyi, L., Kohl, A., Bente, D. A. & Fazakerley, J. K. Tick cell lines for study of Crimean-Congo hemorrhagic fever virus and other arboviruses. *Vector Borne Zoonotic Dis.* **12**, 769–81 (2012).
  253. Růžek, D., Bell-Sakyi, L., Kopecký, J. & Grubhoffer, L. Growth of tick-borne encephalitis virus (European subtype) in cell lines from vector and non-vector ticks. *Virus Res.* **137**, 142–146 (2008).
  254. Crispin, M. *et al.* Uukuniemi phlebovirus assembly and secretion leaves a functional imprint on the virion glycome. *J. Virol.* **88**, 10244–10251 (2014).

## References

255. Man, P. *et al.* Deciphering Dorin M glycosylation by mass spectrometry. *Eur. J. Mass Spectrom. (Chichester, Eng)*. **14**, 345–354 (2008).
256. Sterba, J., Vancova, M., Sterbova, J., Bell-Sakyi, L. & Grubhoffer, L. The majority of sialylated glycoproteins in adult *Ixodes ricinus* ticks originate in the host, not the tick. *Carbohydr. Res.* **389**, 93–99 (2014).
257. Senigl, F., Grubhoffer, L. & Kopecky, J. Differences in maturation of tick-borne encephalitis virus in mammalian and tick cell line. *Intervirology* **49**, 239–48 (2006).
258. Vigerust, D. J. & Shepherd, V. L. Virus glycosylation: role in virulence and immune interactions. *Trends Microbiol.* **15**, 211–218 (2007).
259. Yoshii, K., Yanagihara, N., Ishizuka, M., Sakai, M. & Kariwa, H. N-linked glycan in tick-borne encephalitis virus envelope protein affects viral secretion in mammalian cells, but not in tick cells. *J. Gen. Virol.* **94**, 2249–58 (2013).
260. Sezgin, E., Levental, I., Mayor, S. & Eggeling, C. The mystery of membrane organization: composition, regulation and roles of lipid rafts. *Nat. Rev. Mol. Cell Biol.* (2017). doi:10.1038/nrm.2017.16
261. Martín-Acebes, M. A., Vazquez-Calvo, angela & Saiz, J. C. Lipids and flaviviruses, present and future perspectives for the control of dengue, Zika, and West Nile viruses. *Prog. Lipid Res.* **64**, 123–137 (2016).
262. Subczynski, W. K., Pasenkiewicz-Gierula, M., Widomska, J., Mainali, L. & Raguz, M. High Cholesterol/Low Cholesterol: Effects in Biological Membranes Review. *Cell Biochem. Biophys.* 1–17 (2017). doi:10.1007/s12013-017-0792-7
263. Kalvodova, L. *et al.* The lipidomes of vesicular stomatitis virus, semliki forest virus, and the host plasma membrane analyzed by quantitative shotgun mass spectrometry. *J Virol* **83**, 7996–8003 (2009).
264. Perera, R. *et al.* Dengue virus infection perturbs lipid homeostasis in infected mosquito cells. *PLoS Pathog.* **8**, (2012).
265. Martín-Acebes, M. A. *et al.* The composition of West Nile virus lipid envelope unveils a role of sphingolipid metabolism in flavivirus biogenesis. *J. Virol.* **88**, 12041–54 (2014).
266. Melo, C. F. O. R. *et al.* A lipidomics approach in the characterization of zika-infected mosquito cells: Potential targets for breaking the transmission cycle. *PLoS One* **11**, 1–15 (2016).
267. Chahar, H. S., Bao, X. & Casola, A. Exosomes and their role in the life cycle and pathogenesis of RNA viruses. *Viruses* **7**, 3204–3225 (2015).
268. Smith, A. A. & Pal, U. Immunity-related genes in *Ixodes scapularis*--perspectives from genome information. *Front. Cell. Infect. Microbiol.* **4**, 116 (2014).
269. Attoui, H. *et al.* Complete sequence characterization of the genome of the St Croix River virus, a new orbivirus isolated from cells of *Ixodes scapularis*. *J. Gen. Virol.* **82**, 795–804 (2001).
270. Alberdi, M. P. *et al.* Detection and identification of putative bacterial endosymbionts and endogenous viruses in tick cell lines. *Ticks Tick. Borne. Dis.* **3**, 137–146 (2012).
271. Bell-Sakyi, L. & Attoui, H. Endogenous tick viruses and modulation of tick-borne pathogen growth. *Front. Cell. Infect. Microbiol.* **3**, 25 (2013).

## References

272. Bell-Sakyi, L. & Attoui, H. Virus discovery using tick cell lines. *Evol. Bioinforma.* **12**, 31–34 (2016).
273. Lozach, P. Y. *et al.* DC-SIGN and L-SIGN are high affinity binding receptors for hepatitis C virus glycoprotein E2. *J. Biol. Chem.* **278**, 20358–20366 (2003).
274. Bastos, C. V., das Vasconcelos, M. M. C., Ribeiro, M. F. B. & Passos, L. M. F. Use of Refrigeration as a Practical means to Preserve Viability of in Vitro-Cultured IDE8 Tick Cells. *Exp. Appl. Acarol.* **39**, 347–352 (2006).
275. Lallinger, G., Zweygarth, E., Bell-Sakyi, L. & Passos, L. M. Cold storage and cryopreservation of tick cell lines. *Parasit. Vectors* **3**, 37 (2010).
276. Özbacı, C., Sachsenheimer, T. & Brügger, B. in *Methods in molecular biology (Clifton, N.J.)* **1033**, 3–20 (2013).
277. Munderloh, U. G. & Kurtti, T. J. Formulation of medium for tick cell culture. *Exp. Appl. Acarol.* **7**, 219–29 (1989).



## Scientific Knowledge Dissemination

### Publications

First author:

Uukuniemi virus as a tick-borne virus model. Journal of virology. 90, 6784-6798 (2016). Mazelier Magalie, Ronan Rouxel, Zumstein Michael, Mancini Roberta, Bell-Sakyi Lesley and Lozach Pierre-Yves

Co-author:

High-throughput small interfering RNA screens: when small interfering RNAs behave like microRNA. Médecine sciences 2015 ; 31 : 233-59 (French). Roger Meier, Magalie Mazelier, Pierre-Yves Lozach.

Deciphering virus entry with fluorescently-labeled viral particles. Methods in molecular biology. 2017. Anja B. Hoffmann, Magalie Mazelier, Psylvia Léger, and Pierre-Yves Lozach.

### Oral presentations

27<sup>th</sup> Annual Meeting of the Society for Virology – Marburg, Germany 22-25/04/2017

Uukuniemi virus as a tick-borne virus model. Mazelier Magalie, Bell-Sakyi Lesley, and Lozach Pierre-Yves

26<sup>th</sup> Annual Meeting of the Society for Virology – Münster, Germany 06-09/04/2016

Glycoprotein G<sub>N</sub> of Uukuniemi virus differences between tick vector and mammalian host cells. Mazelier Magalie, Ronan Rouxel, Zumstein Michael, Mancini Roberta, Bell-Sakyi Lesley, and Lozach Pierre-Yves

International Meeting on Arboviruses and their Vectors – Glasgow, United Kingdom 7-8/09/2015

DC-SIGN enhances tick cell-derived Uukuniemi Virus infection. Mazelier Magalie, Ronan Rouxel, Zumstein Michael, Mancini Roberta, Bell-Sakyi Lesley, and Lozach Pierre-Yves

**Travel Award** from the Society for General Microbiology

13<sup>th</sup> Workshop "Cell Biology of Viral Infections" of the Society for Virology (GfV) - Schöntal, Germany 19-21/11/2014

Uukuniemi Virus: a model for tick-borne bunyaviruses. Mazelier Magalie, Ronan Rouxel, Zumstein Michael, Mancini Roberta, Bell-Sakyi Lesley, and Lozach Pierre-Yves

## Poster presentations

16<sup>th</sup> Negative Strand RNA virus meeting – Sienna, Italy 14-19/06/2015

DC-SIGN enhances tick cell-derived Uukuniemi Virus infection. Mazelier Magalie, Ronan Rouxel, Zumstein Michael, Mancini Roberta, Bell-Sakyi Lesley, and Lozach Pierre-Yves

34<sup>th</sup> annual meeting: American Society for Virology symposia – London, Canada 11-15/07/2015

DC-SIGN enhances tick cell-derived Uukuniemi Virus infection. Mazelier Magalie, Ronan Rouxel, Zumstein Michael, Mancini Roberta, Bell-Sakyi Lesley, and Lozach Pierre-Yves